

Oceanography of the New Zealand subantarctic region

Aitana Forcén-Vázquez

A thesis submitted to Victoria University of Wellington
in fulfilment of the requirements for the degree of
Doctor of Philosophy in Geophysics

School of Geography, Environment and Earth Sciences
Victoria University of Wellington
Wellington, New Zealand

March, 2015

Abstract

Subantarctic New Zealand is an oceanographically dynamic region with the Subtropical Front (STF) to the north and the Subantarctic Front (SAF) to the south. This thesis investigates the ocean structure of the Campbell Plateau and the surrounding New Zealand subantarctic, including the spatial, seasonal, interannual and longer term variability over the ocean properties, and their connection to atmospheric variability using a combination of *in-situ* oceanographic measurements and remote sensing data.

The spatial and seasonal oceanographic structure in the New Zealand subantarctic region was investigated by analysing ten high resolution Conductivity Temperature and Depth (CTD) datasets, sampled during oceanographic cruises from May 1998 to February 2013. Position of fronts, water mass structure and changes over the seasons show a complex structure around the Campbell Plateau combining the influence of subtropical and subantarctic waters.

The spatial and interannual variability on the Campbell Plateau was described by analysing approximately 70 low resolution CTD profiles collected each year in December between 2002 and 2009. Conservative temperature and absolute salinity profiles reveal high variability in the upper 200 m of the water column and a homogeneous water column from 200 to 600 m depth. Temperature variability of about 0.7 °C, on occasions between consecutive years, is observed down to 900 m depth. The presence of Subantarctic Mode Water (SAMW) on the Campbell Plateau is confirmed and Antarctic Intermediate Water (AAIW) reported for the first time in the deeper regions around the edges of the plateau.

Long-term trends and variability over the Campbell Plateau were investigated by analysing satellite derived Sea Level Anomalies (SLA) and Sea Surface Temperature (SST) time series. Links to large scale atmospheric processes are also explored through correlation with the Southern Oscillation Index (SOI) and Southern Annular Mode (SAM). SST shows a strong seasonality and interannual variability which is linked to local winds, but no significant trend is found. The SLA over the Campbell Plateau has increased at a rate

of $5.2 \text{ cm decade}^{-1}$ in the last two decades. The strong positive trend in SLA appears to be a combination of the response of the ocean to wind stress curl (Ekman pumping), thermal expansion and ocean mass redistribution via advection amongst others.

These results suggest that the variability on the Campbell Plateau is influenced by the interaction of the STF and the SAF. The STF influence reaches the limit of the SAF over the western Campbell Plateau and the SAF influence extends all around the plateau. Results also suggest different connections between the plateau with the surrounding oceans, e.g., along the northern edge with the Bounty Trough and via the southwest edge with the SAF. A significant correlation with SOI and little correlation with SAM suggest a stronger response to tropically driven processes in the long-term variability on the Campbell Plateau.

The results of this thesis provide a new definitive assessment of the circulation, water masses and variability of the Campbell Plateau on mean, annual, and interannual time scales which will support research in other disciplines such as palaeoceanography, fisheries management and climate.

Acknowledgements

My sincere thanks go to my supervisors, Dr. Mike Williams, Dr. Melissa Bowen and Professor Lionel Carter for their support, patience and faith. With his positivism, Mike always makes me think that it can be done, his sharp comments always give to my ideas a new exciting point of view and his generosity with his time has no limits. Thank you Mike for taking me to the South. Melissa Bowen, her questions about how the ocean works always make me want to know more, to study more, to go further. Lionel Carter, thank you, your enthusiasm and faith has always encouraged me to keep going and to believe, when I lose hope. I feel incredible lucky to have worked under their supervision.

Thanks to Victoria University of Wellington for the financial support through my Victoria Doctoral Scholarship. To the Antarctic Research Center (ARC) for selecting me as a recipient of the Endowed Development Fund.

Special thanks go to the RV TANGAROA crew and its Captain, and all the staff members and research leaders who have been involved in collecting the high resolution data along the last 15 years. Also, for taking me onboard and showing me the beauty of the Southern Ocean.

Thanks to the Ministry for Primary Industries (MPI) for the access to the low resolution data set.

The Argo data were collected and made freely available by the International Argo Program and the national programs that contribute to it. (<http://www.argo.ucsd.edu>, <http://argo.jcommops.org>). The Argo Program is part of the Global Ocean Observing System. The altimeter products were produced by Ssalto/Duacs and distributed by AVISO with support from Cnes. Ocean mass data was provided by GRACE and processed by Don P. Chambers, supported by the NASA MEaSUREs Program, and are available at <http://grace.jpl.nasa.gov>. NCEP Reanalysis data was provided by the NOAA/OAR/ESRL and are available at <http://www.esrl.noaa.gov/psd>.

It has been a pleasure to work at NIWA, thank you for the support and the productive environment. Big thanks to the Marine Physics Department, it is very inspiring to work with so many talented people. Thank you to Craig Stevens for the sharing and the creativity encouragement. Thank you to Helen Bostock for the enthusiasm and energy (and the wool!).

I have to thank Professor Dean Roemmich and Dr Phil Sutton for productive ideas and useful conversations.

I am going to miss the crazy conversations at coffee break, it has been a pleasure to share time and laughs with you guys, thank you to Andy, Caroline, Graham, James, Jim, Kath, Mike, Rachel, Sadie, Tim, Vidette, Yana.

Special thanks go to my PhD battle friends. Dr Tim Divett, for his energy and his kindness, (and for being the first one!!). Stefan Jendersie, I could not have had a better office mate, thank you for the coffees@1630h, the MatLab knowledge, the numbers, the unconditional support and an endless list. Denise Fernandez, what can I say? gracias!, you are an inspiration for me.

Special thanks go to Charlie, thank you for the support, for the patience and for showing me the way back to the Ocean.

I also have to thank the ones in the other side. Gracias Ana and Chicho, for always being in the other side of the screen, for the faith, for making me feel home so far away from home.

And finally thank you to my family, my parents, Emilio and Melania, and my sisters, Eneida and Isadora. Gracias, for the support, the strength and the love from the other side of the world.

Contents

| | |
|--|------------|
| Abstract | iii |
| Acknowledgements | v |
| List of Figures | xi |
| 1 Overview and motivation | 1 |
| 2 Literature review | 7 |
| 2.1 The Campbell Plateau | 7 |
| 2.1.1 Introduction | 7 |
| 2.1.2 Oceanographic settings | 10 |
| 2.2 Previous findings in the Campbell Plateau | 18 |
| 2.2.1 Campbell Plateau in a global context | 22 |
| 3 Oceanography of the Campbell Plateau | 25 |
| 3.1 Data and Methods | 26 |
| 3.1.1 Front and water mass identification criteria | 29 |
| 3.2 Results | 31 |
| 3.2.1 Horizontal sections | 32 |
| 3.2.2 Water mass analysis | 60 |
| 3.2.3 Geostrophic velocities (general flow) | 68 |
| 3.3 Discussion | 72 |
| 3.3.1 Fronts | 72 |
| 3.3.2 Water masses | 73 |

| | | |
|----------|---|------------|
| 3.3.3 | Circulation | 77 |
| 3.4 | Summary of the chapter | 79 |
| 4 | Interannual variability of the Campbell Plateau | 83 |
| 4.1 | Data and methods | 83 |
| 4.1.1 | Low resolution data processing | 86 |
| 4.1.2 | Water mass identification criteria | 90 |
| 4.2 | Results | 91 |
| 4.2.1 | Spatial variability over the Campbell Plateau | 91 |
| 4.2.2 | Vertical variability over the Campbell Plateau | 94 |
| 4.2.3 | Water mass variability | 97 |
| 4.2.4 | Interannual variability on the Campbell Plateau | 98 |
| 4.2.5 | Steric height | 109 |
| 4.3 | Discussion | 112 |
| 4.3.1 | Water masses | 112 |
| 4.3.2 | Circulation | 115 |
| 4.3.3 | Spatial and interannual variability | 116 |
| 4.4 | Summary of the Chapter | 117 |
| 5 | Long-term variability on the Campbell Plateau | 119 |
| 5.1 | Data and Methods | 120 |
| 5.1.1 | Time series processing methods | 120 |
| 5.1.2 | Statistical methods | 121 |
| 5.1.3 | Maps of Sea Level Anomalies | 124 |
| 5.1.4 | Sea Surface Temperature | 127 |
| 5.1.5 | Climate Indices | 130 |
| 5.1.6 | Steric Height | 131 |
| 5.1.7 | Ocean mass | 131 |
| 5.1.8 | Wind | 133 |
| 5.2 | Results | 136 |
| 5.2.1 | Sea Level Anomaly | 136 |
| 5.2.2 | Sea Surface Temperature | 139 |

| | | |
|----------|--|------------|
| 5.2.3 | Sea Surface Temperature vs Sea Level Anomalies | 143 |
| 5.2.4 | Campbell Plateau sea level budget | 144 |
| 5.3 | Discussion | 150 |
| 5.3.1 | Sea surface temperature | 150 |
| 5.3.2 | Sea level anomalies | 153 |
| 5.4 | Summary of the Chapter | 162 |
| 6 | Conclusions | 165 |
| | Bibliography | 169 |
| A | The International Thermodynamic Equation of Seawater - 2010 (TEOS-10) | 185 |

List of Figures

| | | |
|------|---|----|
| 1.1 | Southwest Pacific region | 2 |
| 2.1 | Southern Ocean wind stress | 9 |
| 2.2 | New Zealand subantarctic region and Campbell Plateau | 10 |
| 2.3 | Fronts positions | 13 |
| 2.4 | Surface geostrophic currents over the New Zealand subantarctic region | 15 |
| 2.5 | Θ - S_A diagram for New Zealand subantarctic region | 16 |
| 2.6 | Moorings positions over the Campbell Plateau | 21 |
| 2.7 | Campbell Plateau mean currents paths | 22 |
| 2.8 | South Pacific mechanisms | 23 |
| 3.1 | High resolution transects | 26 |
| 3.2 | Southern Ocean section | 31 |
| 3.3 | Hydrographic stations for the Tasman Sea transect. | 32 |
| 3.4 | Conservative temperature section along the Tasman transect | 33 |
| 3.5 | Absolute salinity section along the Tasman transect | 33 |
| 3.6 | Hydrographic stations for the Macquarie Ridge transects. | 34 |
| 3.7 | Conservative temperature sections along Macquarie Ridge. | 36 |
| 3.8 | Absolute Salinity sections along Macquarie Ridge. | 37 |
| 3.9 | Hydrographic stations for the Solander Trough transects. | 38 |
| 3.10 | Conservative temperature sections along Solander Trough. | 39 |
| 3.11 | Absolute salinity sections along Solander Trough. | 40 |
| 3.12 | Hydrographic stations east of Macquarie Ridge. | 41 |
| 3.13 | Conservative temperature sections east of Macquarie Ridge. | 42 |

| | | |
|------|---|-----|
| 3.14 | Absolute salinity sections east of Macquarie Ridge. | 43 |
| 3.15 | Hydrographic stations crossing the Snares Depression | 44 |
| 3.16 | Conservative temperature section across Snares Depression. | 45 |
| 3.17 | Absolute salinity section across Snares Depression. | 46 |
| 3.18 | Hydrographic stations for the Campbell Plateau transects. | 47 |
| 3.19 | Conservative temperature section over the Campbell Plateau. | 51 |
| 3.20 | Absolute salinity section over the Campbell Plateau. | 53 |
| 3.21 | Hydrographic stations (blue) along the Pukaki Saddle. | 54 |
| 3.22 | Conservative temperature section across the Pukaki Saddle. | 55 |
| 3.23 | Absolute Salinity section across the Pukaki Saddle. | 55 |
| 3.24 | Hydrographic stations for the Bounty Trough transects. | 57 |
| 3.25 | Conservative temperature sections over the Bounty Trough. | 58 |
| 3.26 | Absolute salinity sections over the Bounty Trough. | 59 |
| 3.27 | Θ - S_A diagrams for Macquarie Ridge. | 61 |
| 3.28 | Θ - S_A diagrams. | 64 |
| 3.29 | Θ - S_A diagrams. | 67 |
| 3.30 | Geostrophic velocity transects | 68 |
| 3.31 | Geostrophic velocities sections. | 71 |
| 3.32 | Subantarctic water masses | 75 |
| 3.33 | Front and currents summary | 78 |
| 4.1 | Low resolution stations distribution | 85 |
| 4.2 | Missing low resolution Stations | 88 |
| 4.3 | Low resolution interpolation | 89 |
| 4.4 | Low resolution TS | 91 |
| 4.5 | Mean temperature and salinity maps | 93 |
| 4.6 | Mean vertical profiles | 96 |
| 4.7 | Mean Θ - S_A (2002-2009) | 98 |
| 4.8 | Surface anomalies | 103 |
| 4.9 | 200 m anomalies | 105 |
| 4.10 | Variability at 450 m | 107 |

| | |
|--|-----|
| 4.11 Θ - S_A diagrams (2002-2009) | 108 |
| 4.12 Mean Steric height | 110 |
| 4.13 Steric height interannual variability | 111 |
| 4.14 AAIW position | 113 |
| 4.15 AAIW transects. | 115 |
| | |
| 5.1 Auto-correlation function for SST and for SOI. | 123 |
| 5.2 Bathymetric masks | 125 |
| 5.3 SLA time series | 126 |
| 5.4 SST anomalies time series | 129 |
| 5.5 Steric height anomalies time series | 132 |
| 5.6 Ocean mass anomalies time series | 133 |
| 5.7 Anomalies of the wind stress magnitude time series | 134 |
| 5.8 Wind stress anomalies time series, two components | 135 |
| 5.9 Wind stress anomalies seasonal cycle | 136 |
| 5.10 SLA and SOI time series | 137 |
| 5.11 SLA, SAM and wind time series | 138 |
| 5.12 SST seasonal structure over the Campbell Plateau | 140 |
| 5.13 SST standard deviation | 141 |
| 5.14 SST anomalies, SOI and SAM time series | 142 |
| 5.15 Wind stress and SST anomalies time series | 143 |
| 5.16 SST anomalies and SLA time series | 144 |
| 5.17 Seasonal mass balance over the Campbell Plateau | 147 |
| 5.18 Sea level budget seasonality | 148 |
| 5.19 Sea level budget no season | 149 |
| 5.20 Sea level budget no trend | 150 |
| 5.21 SST vs temperature observations | 152 |
| 5.22 Ekman pumping vs SLA | 155 |
| 5.23 Sea level budget | 156 |
| 5.24 Off Plateau SH map | 158 |
| 5.25 Steric height and SSH in box 1 | 159 |

| | |
|---|-----|
| 5.26 Steric height and SSH in box 2 | 160 |
| 5.27 Steric height and SSH in box 3 | 161 |

Chapter 1

Overview and motivation

The New Zealand subantarctic region is a zone of uniform water properties in the Southern Ocean between two strong large scale features (Tomczak and Godfrey, 2001). To the north lies the Subtropical Front (STF) and to the south lies the Subantarctic Front (SAF) (Figure 1.1). The STF is almost continuous around the Southern Hemisphere and separates the cold and fresh Subantarctic Water (SAW) from the warm and salty Subtropical Water (STW) transported by the subtropical gyres (e.g., Deacon, 1982; Belkin and Gordon, 1996). The SAF, a circumpolar feature that isolates the southern polar regimes, marks the northern limit of the Antarctic Circumpolar Current (ACC) (e.g., Orsi et al., 1995; Belkin and Gordon, 1996).

Within the New Zealand subantarctic region lies the Campbell Plateau to the southeast of New Zealand's South Island. It is a large fragment of submerged continental crust most of which is shallower than 1000 m. The Campbell Plateau can be categorized as a mix between continental margin seas and a fully open ocean setting (Simpson and Sharples, 2012). In that context, the plateau is influenced by the different water masses and currents at its margins and with more localised processes over the plateau interior.

The Campbell Plateau is important for local climate, fisheries and marine mammal populations. The oceanic variability over the Campbell Plateau influences New Zealand's climate by affecting the local oceanography southeast of the South Island (e.g., Hopkins

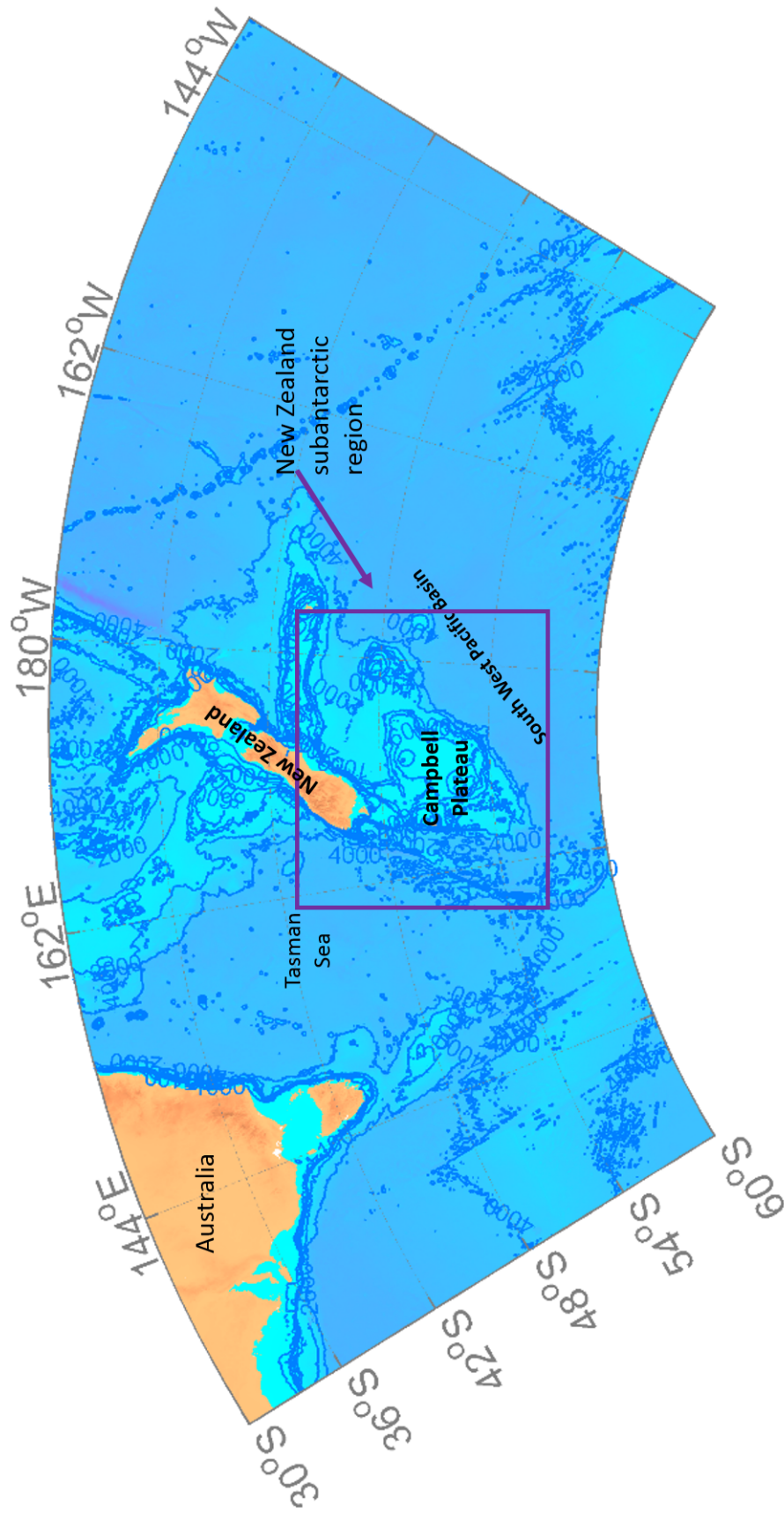


Figure 1.1: Southwest Pacific region showing location of the New Zealand sub-antarctic and the Campbell Plateau.

et al., 2010). The Campbell Plateau supports fisheries of economic importance reflecting the productivity associated with the fronts, especially the STF (Butler and Butt, 1992; Murphy et al., 2001; Bradford-Grieve et al., 2003; Hanchet and Bradford, 2002). The New Zealand subantarctic islands also support a variety of marine mammals and sea-birds whose populations are regulated by oceanographic climatic factors as well as human activities (Robertson and Chilvers, 2011; Bradford-Grieve et al., 2003). Finally, a more modern assessment of the plateau oceanography is relevant to paleoceanography studies by providing knowledge of the processes that influence the ocean environment (Cortese et al., 2013).

From a global perspective it is important as a region of carbon dioxide uptake into the oceans (Currie and Hunter, 1998; Currie et al., 2011). Together with the Macquaire Ridge, the Campbell Plateau is a major constriction of the ACC modifying not only its flow, but also the orientation and latitudinal position of the Southern Ocean fronts (Deacon, 1982; Tomczak and Godfrey, 2001; Gille, 2003; Sokolov and Rintoul, 2007a; Talley et al., 2011).

As noted earlier, the oceanic circulation and distribution of fronts are strongly constrained by the complex bathymetry of the region (e.g., Gordon, 1975; Heath, 1981; Williams, 2004). Because of this, the Campbell Plateau has been considered as a system without long-term variability in the positions of the fronts (Heath, 1981). The general ocean circulation over the plateau, north of the SAF and southeast of the STF, was described as a persistent weak anticyclonic and cyclonic flow (Morris et al., 2001). However, the inhospitable nature of this area has made it difficult to develop a complete record of observations to give a precise idea of the oceanographic regime, its variability and any long-term changes (Morris et al., 2001).

The complexity of the oceanographic boundaries of the Campbell Plateau and the complexity of the Campbell Plateau itself makes it an ideal location to study the different interactions between the subtropical and subantarctic fronts, and an interesting piece of the puzzle for the New Zealand local climate and marine life populations.

It is also a key area to investigate the interaction of subtropical-subpolar water as the Campbell Plateau may be influenced by both the STF and the ACC system. To find the link between the Campbell Plateau and large scale atmospheric processes, climate indices, such as Southern Oscillation Index (SOI) and Southern Annular Mode (SAM), are used. By studying the relation that the Campbell Plateau variability has with those climate indices, the influence of variations in the equatorial region (SOI) or in the mid-latitudes (SAM) can be inferred.

One of the main reasons why knowledge of the Campbell Plateau oceanography and forcing mechanisms is limited is due to the lack of detailed spatial and temporal data. In this thesis, seven different data sets, including remote sensing and new subsurface data, gathered over the last two decades (Table 1.1) provide the opportunity for a new investigation of the Campbell Plateau from several different perspectives and time scales.

Questions to be explored over the Campbell Plateau that motivated this thesis, include:

1. What is the oceanographic structure of the New Zealand subantarctic region and the Campbell Plateau?
2. What is the seasonal, interannual and long-term variability of the ocean properties on the Campbell Plateau?
3. What physical mechanisms, local or large scale, are driving these changes?

These questions will be examined in this thesis. The methods used for analysing each data set are different and specific to each data set so are described in the beginning of each chapter. This format, which is similar to that of a science journal, leads to some repetition of the methods and the background for each individual chapter, but this allows each chapter to be developed logically and consistently.

Thesis outline

Chapter 2 sets the background for this study. It summarizes the relevant literature and describes the regional geography and oceanography of the Campbell Plateau.

In Chapter 3 a synthesis of the plateau oceanography based on ten research voyages over the last two decades is presented. High resolution Conductivity Temperature and Depth (CTD) transects across the Campbell Plateau are analysed to determine the water mass structure, geostrophic flows, and general circulation over the 15 years that these records encompass. The transects were carried out in different years and seasons, but with some repeated sections. Nevertheless, they provide a new oceanographic perspective of the Campbell Plateau, in particular the relative influences and pathways of the subtropical and subantarctic exchanges.

Chapter 4 explores the interannual variability over the Campbell Plateau based on the low resolution CTD data set. Eight years of hydrographic casts have been collected each December between 2002 and 2009. These are used to define the interannual variability. Spatial variability is also explored to investigate how the surroundings fronts, the STF and the SAF, might influence the Campbell Plateau variability. Steric height is calculated from the hydrographic profiles to determine the mean circulation and its variability.

In Chapter 5 the focus is on remotely sensed long-term time series to describe the seasonal and interannual variability. For this, data such as Sea Surface Height (SSH) and Sea Surface Temperature (SST) are used. Interactions with global climate indices will be investigated. Ocean mass data along with steric height data from Argo floats are analysed to investigate the seasonal and interannual sea level budget over the Campbell Plateau.

Chapter 6 summarizes the analyses and draws a number of conclusions ending with suggestions for future research.

Chapter 2

Literature review

This chapter sets the background for this thesis by describing the oceanographic features as understood from previous studies of the region. It also gives the context for this study and the origins of the problems being examined.

2.1 The Campbell Plateau

2.1.1 Introduction

The Southern Ocean plays an important role in the global climate. It is a key place for anthropogenic carbon dioxide and heat uptake from the atmosphere (Gnanadesikan and Hallberg, 2000; Sokolov and Rintoul, 2002; Morrison et al., 2011; Currie et al., 2011; Schulz et al., 2012). The Antarctic Circumpolar Current (ACC) in its flow around Antarctica, carries heat, salt, nutrients and gases between the Pacific, Atlantic and Indian Oceans, which helps to ventilate the intermediate and abyssal waters of the world ocean (Rintoul and Bullister, 1999; Sokolov and Rintoul, 2007a; Gille, 2003; Tomczak and Liefvink, 2005; Hasson et al., 2011).

The Southern Ocean wind regime is dominated by strong and persistent westerlies in the latitudinal band 40° to 60°S (Orsi et al., 1995; Tomczak and Godfrey, 2001) (Figure 2.1). The wind stress combined with the Coriolis force drives an Ekman current northward at the surface (Talley et al., 2011). The ocean circulation is dominated by

the eastward-flowing ACC (e.g., Carter et al., 2008; Marshall and Speer, 2012), the largest and strongest ocean current that extends unbroken around the planet (Orsi et al., 1995).

Subantarctic New Zealand sits in the Southern Ocean and encompasses the Macquarie Ridge, Emerald Basin, Campbell Plateau and Bounty Trough (Figure 2.2), (e.g., Morris et al., 2001; Williams, 2004). It is a complex oceanographic system with three distinct oceanographic regions: north of the Subtropical Front (STF), the region is defined by the presence of warm and salty Subtropical Water (STW); the subantarctic zone (SAZ) lies between the STF and the SAF, and is characterised by cooler and fresher Subantarctic Water (SAW); and south of the SAF where there are colder and fresher polar waters.

Ocean circulation and the distribution of the fronts are strongly constrained by the complex bathymetry in this area (e.g., Gordon, 1975; Heath, 1981; Williams, 2004). Studies derived from *in situ* hydrographic data suggest that bathymetry not only strongly influences the latitude and orientation of the fronts in the ACC but also influences its flow (Deacon, 1982; Gille, 2003; Sokolov and Rintoul, 2007a). In that way, the Macquarie Ridge creates a natural barrier to the ACC and the Campbell Plateau acts as a boundary steering the flow of the SAF northwards (Tomczak and Godfrey, 2001; Stanton and Morris, 2004; Talley et al., 2011).

Campbell Plateau

The Campbell Plateau is an extension of the New Zealand continental shelf and extends ~1000 km southeast from the South Island, New Zealand. It occupies an important position in the southwest Pacific sector of the Southern Ocean (Neil et al., 2004), with most depths shallower than 1000 m but extending in parts to 2000 m. Its boundaries are well defined, with a steep continental slope that descends sharply to 4000 m. Several subantarctic islands and bathymetric features, such as the Auckland Islands and Campbell Island, make the regional topography very complex (Heath, 1985; Neil et al., 2004; Mitchell et al., 2012).

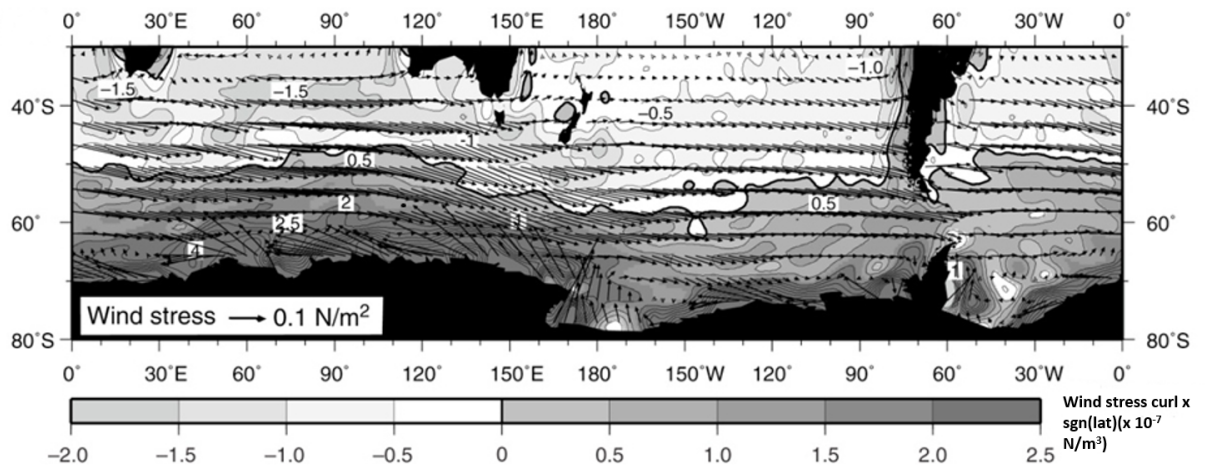


Figure 2.1: Annual average wind stress N/m^2 (vectors) and wind stress curl 10^{-7}N/m^3 (shading) multiplied by -1 in the Southern Hemisphere so that positive values (dark greys) indicate Ekman upwelling, from Talley et al. (2011) from the NCEP reanalysis 1968-1996 (Kalnay and Kanamitsu, 1996)

Several studies have focused on the position and variability in the fronts around the Campbell Plateau, but little is known about the Campbell Plateau itself. Attempts to understand the oceanography of the New Zealand subantarctic region go back to Burling (1961) on his trips from New Zealand to Antarctic waters near Scott Island in December 1956 and January 1957. Before that, a number of studies along the Southern Ocean had been carried out as part of the R.R.S. Discovery voyages starting in 1929 (e.g., Deacon, 1937). In continuing this research, a number of voyages from New Zealand and Australia to Antarctica have been carried out describing the circulation, defining water masses and identifying the position and variability of the fronts in an effort to understand the oceanography of this part of the Southern Ocean (Garner, 1959; Gordon, 1966, 1972, 1975; McCartney, 1977; Olson and Emery, 1978).

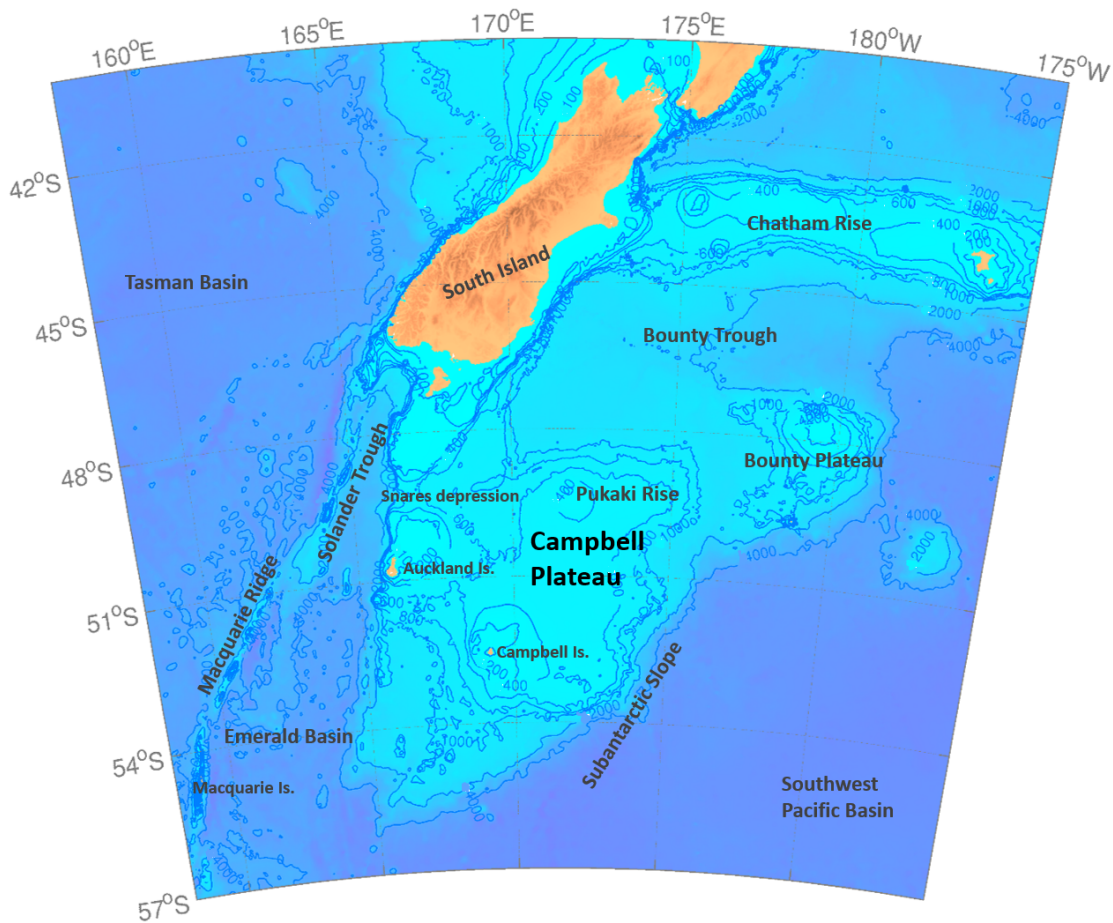


Figure 2.2: New Zealand subantarctic region and Campbell Plateau

2.1.2 Oceanographic settings

An oceanographic front is a region of strong horizontal gradients in water mass properties such as temperature, salinity and usually density (e.g., Belkin and Gordon, 1996; Orsi et al., 1995; Sokolov and Rintoul, 2002). These gradients allow frontal positions to be located with hydrographic data (Heath, 1985; Orsi et al., 1995). Some fronts, such as those within the ACC in the Southern Ocean, are also regions of enhanced gradients in Sea Surface Height (SSH) and maxima in geostrophic flow derived from strong gradients in density (Sokolov and Rintoul, 2007b, 2009a). In some places, the fronts are also areas of high primary production, which comes from the complimentary mixing of nutrients from different water masses, e.g., SAW high-nutrient low-chlorophyll (HNLC) with micro-nutrient rich (especially iron) STW (Moore and Abbott, 2000; Sutton, 2001;

Murphy et al., 2001; Sokolov and Rintoul, 2002). As a general rule, the fronts are not a single static entity but have multiple branches or filaments that change in position and intensity on different scales (Moore et al., 1999). However, the main structure of the fronts have consistent streamlines (e.g., Sokolov and Rintoul, 2002, 2007a, 2009a).

Off southern New Zealand, the main fronts can be seen in the mean Sea Surface Temperature (SST) (Figure 2.3a) and SSH (Figure 2.3b). The STF has a strong surface gradient in the mean SST south of the South Island, approximately following the 11 °C isotherm (Butler and Butt, 1992). The positions of the fronts for the STF are from (Smith et al., 2013) and Southland Current from (Sutton, 2003). The different branches of the SAF and the Polar Front are better identified by the signal in SSH. The positions of the SAF and the Polar Front are from (Sokolov and Rintoul, 2007a).

Subtropical Front

The STF is an almost global oceanographic feature that sits within 35° to 45°S, with the exception of a region in the Pacific Ocean west of South America which breaks the front's continuity (e.g., Deacon, 1982; Belkin and Gordon, 1996). It can be identified by its strong gradients in temperature, salinity, oxygen and primary productivity (Butler and Butt, 1992; Orsi et al., 1995; Belkin and Gordon, 1996). The STF is considered the northern limit of the subantarctic waters (Deacon, 1982; Orsi et al., 1995) and also the southern boundary of the subtropical gyres (e.g., Smith et al., 2013). It is a shallow front, typically extending between 200 to 300 m depth. In some places, it is a density compensated front, i.e., there is little or no change in density across the front resulting in little or no SSH signature. Instead it is better recognized by changes in SST or by hydrographic profiles showing changes in the vertical structure of the front (Sokolov and Rintoul, 2007a, 2009b; Smith et al., 2013). However, the latest studies suggest that the density compensated STF and the non-density compensated STF are different, not connected, and forced by different mechanisms. Hence they should not be considered as two branches of the STF (Graham and De Boer, 2013). In their study, Graham and De Boer (2013) identify the STFZ as a region of strong SST, but weak SSH gradients (density compensated) while the Dynamical STF is associated with strong SST and SSH gradi-

ents (weakly density compensated) and is found only on the western sides of the basins where it is an extension of the western boundary current of each basin. Although in the SW Pacific region, the changes in temperature and salinity are nearly density compensated, around southern New Zealand the South-STF (S-STF) is weakly compensated and hence easier to recognize from its SST signature (Rintoul and Bullister, 1999; Sokolov and Rintoul, 2002; Smith et al., 2013). In their study, Smith et al. (2013) showed that the New Zealand STF is strongly located by the topography and is a well defined feature.

Off the southeast coast of the South Island, the STF density gradient becomes higher and is locally known as the Southland Front (e.g., Chiswell, 1996; Sutton, 2003). Although the Southland Current, the flow associated with the Southland Front, is well defined flowing northeast along the 200 m isobath, it has some variation on seasonal time scales (e.g., Jillett, 1969; Butler and Butt, 1992; Chiswell, 1996; Currie and Hunter, 1999). The temperature gradients within the Southland Front also vary interannually, and are correlated with El Niño-Southern Oscillation (ENSO), decreasing with El Niño and increasing with La Niña events (Hopkins et al., 2010). The Southland Current transports SAW close to New Zealand (Sutton, 2003), influencing the local climate on the South Island (e.g., Heath, 1972; Hopkins et al., 2010). It is also a place of high productivity which supports different fishing stocks (Hopkins et al., 2010).

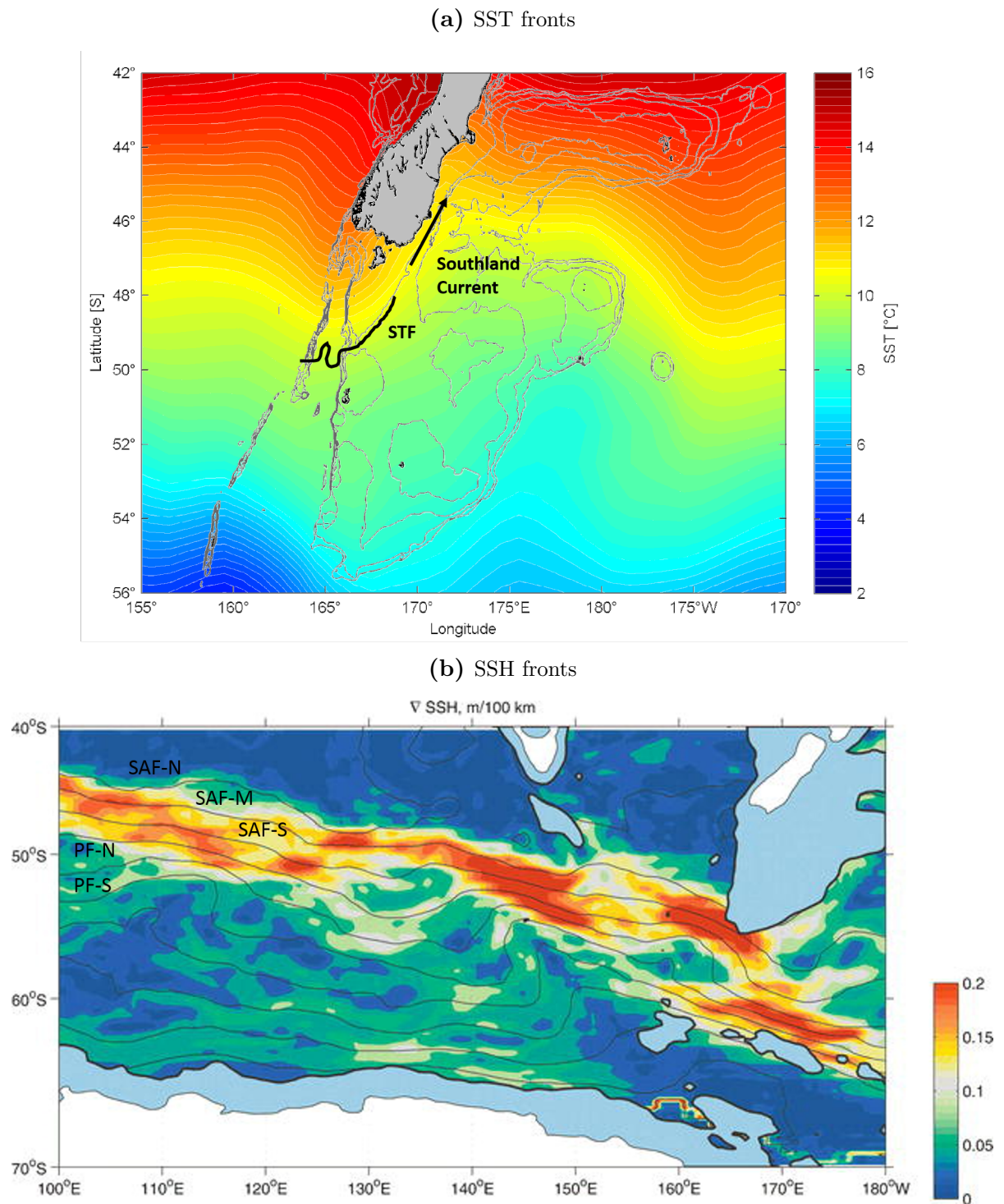


Figure 2.3: Fronts position in the New Zealand subantarctic region, (a) STF from (Smith et al., 2013) and Southland Current from (Sutton, 2003) over mean SST colourmap. SST data for the period 1982-2013 were retrieved from the National Oceanic and Atmospheric Administration (NOAA), Optimum Interpolation (OI) SST version 2 (V2); <http://www.esrl.noaa.gov/psd/>. Gray lines show bathymetry. (b) Gradient of mean SSH [$\text{m}(100 \text{ km}^{-1})$] overlaid with the mean position of the Southern Ocean fronts. Depths shallower than 2500 m are shaded, from (Sokolov and Rintoul, 2007a)

Subantarctic Front

The SAF is the northern boundary of the ACC, and the maximum transport of the ACC (Gille, 2003; Sokolov and Rintoul, 2007a). The SAF consists of three branches that extend from the sea surface to the deep ocean (e.g., Orsi et al., 1995; Rintoul and Bullister, 1999; Rintoul and Trull, 2001; Sokolov and Rintoul, 2007a, 2009b). For this reason it is not always easy to identify its position and there has been some confusion and disagreement in the literature (Sokolov and Rintoul, 2007a). This confusion also comes from the different criteria and methods for identifying the fronts, either identified via water mass properties or inferred from SSH signals (Sokolov and Rintoul, 2002, 2009a). However, Sokolov and Rintoul (2009a) demonstrated that both ways of identifying the front position agree for the whole Southern Ocean, so can be used together.

The three branches of the SAF are modified by bathymetry in the New Zealand sub-antarctic region. Branches are merged where the SAF is forced to pass south of the Campbell Plateau. Downstream, the flow divides into two branches, the northern one following the plateau bathymetry and the middle and southern ones turning sharply to the south east at 164°E (Orsi et al., 1995; Belkin and Gordon, 1996; Gille, 2003; Stanton and Morris, 2004; Sokolov and Rintoul, 2007a). Possible explanations for the northward turn of the flow are the steering by topography (Pickard and Emery, 1990) or wind forcing across the South Pacific (LaCasce and Isachsen, 2010).

Absolute geostrophic velocities computed from absolute topography confirm the main surface currents described in the previous section (Figure 2.4): the eastward ACC flow is forced to pass through the topographic gaps in the Macquarie Ridge before encountering the Campbell Plateau; the SAF is deflected to the north following the western boundary presented by the Campbell Plateau; some of the SAF leaks north-westward through the Pukaki Saddle; and the remaining flow continues north before turning eastward at around 164°E to continue its way into the Pacific. The Southland Current flowing along the southeast coast of New Zealand can also be seen.

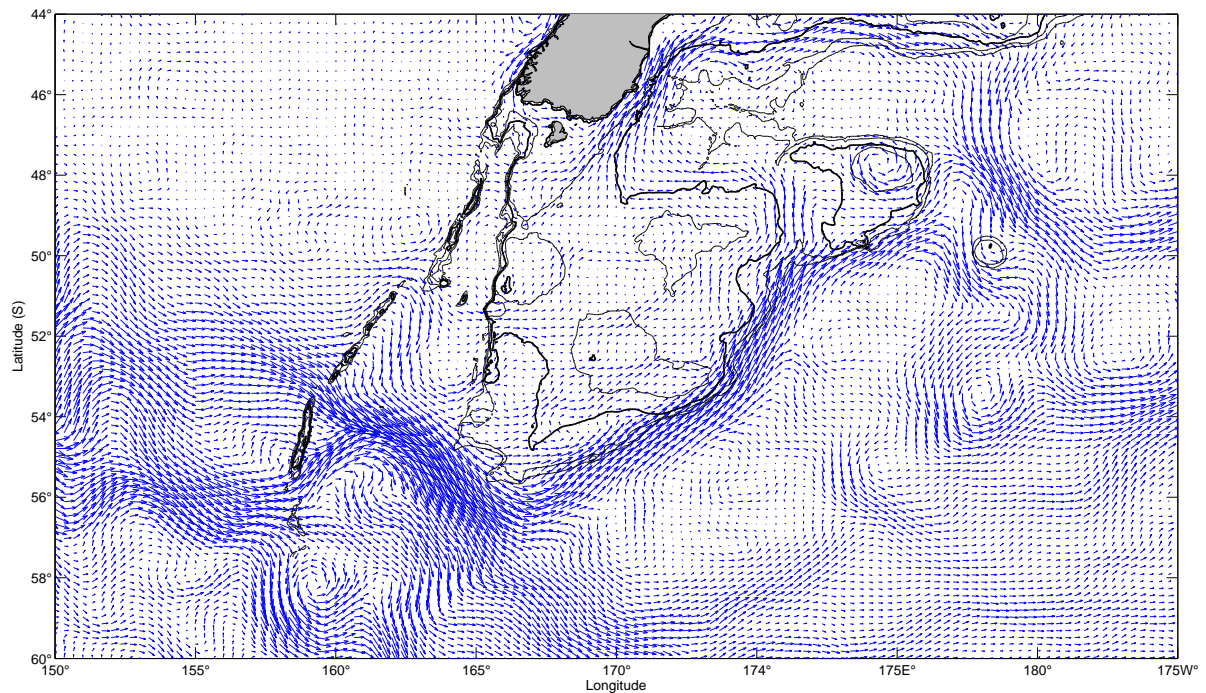


Figure 2.4: Mean surface geostrophic currents over the New Zealand subantarctic region. Data were retrieved from the AVISO (Archiving, Validation and Interpretation of Satellite data in Oceanography; <http://www.aviso.oceanobs.com/en/>) and was averaged over the whole period (January 1993 to December 2012). Thick black line shows the 1000 m isobath.

Water masses

A water mass is a body of water that has a common formation process. Normally, a water mass is formed in a specific place by surface processes. These processes leave their signature on the temperature and salinity properties of the water mass. Because temperature and salinity are effectively conserved once it leaves the surface, the water mass keeps its combination of properties thus providing an identifying signature. The water mass can be identified by its properties and from them, the process and place of formation can be investigated (e.g., Tomczak and Godfrey, 2001; Brown et al., 2001; Talley et al., 2011). However, care is needed in the identification of water masses, as different types of the same water mass with slightly different properties can be found depending on the place where the water masses are identified.

Within the literature, different water masses have been identified in the New Zealand subantarctic region. The water masses used in this thesis are presented in Table 3.2. Conductivity Temperature and Depth (CTD) stations from the high resolution data set that will be investigated in Chapter 3 are used as a reference for the water masses in the New Zealand subantarctic region and their different properties (Figure 2.5).

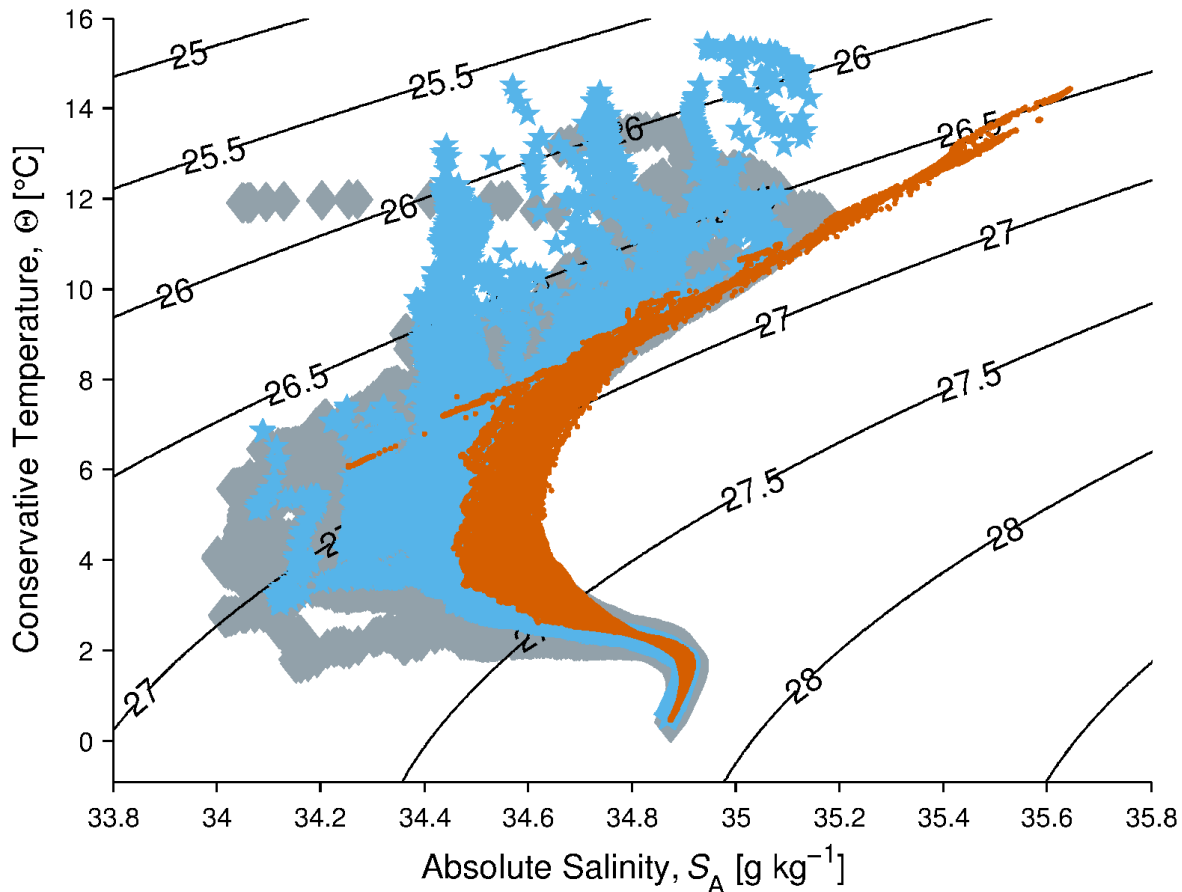


Figure 2.5: Conservative temperature [$^{\circ}\text{C}$] versus absolute salinity [g kg^{-1}] for the New Zealand subantarctic region. Colours indicate different voyages. Contours are potential density referenced to 0 dbar.

Subantarctic Mode Water and Antarctic Intermediate Water.

Subantarctic Mode Water (SAMW) and Antarctic Intermediate Water (AAIW) occupy the surface and intermediate waters of the SAZ (Talley et al., 2011). SAMW, a thick layer of uniform properties, minimum vertical temperature gradient and weak stratifica-

tion is found as deep as 600 m (e.g., McCartney, 1977; Heath, 1981; Rintoul and Trull, 2001). AAIW, a water mass characterized by a salinity minimum is found between 600 and 1100 m underneath the SAMW (e.g., Hanawa and Talley, 2001; Sloyan and Rintoul, 2001; Hartin et al., 2011).

SAMW is formed by deep mixing of the upper ocean on the equatorward side of the SAF (e.g., McCartney, 1977). The properties of the water are modified during winter when convection creates a deep surface layer with water of uniform temperature and salinity in a region of usually strong horizontal and vertical gradients (McCartney, 1977; Rintoul and Bullister, 1999; Morris et al., 2001). However, different modes of SAMW can be found in the South Pacific, changing characteristics and circulation from west to east (Rintoul and Bullister, 1999; Herraiz-Borreguero and Rintoul, 2011). Different combinations of temperature and salinity conform to different modes of SAMW. For example, SAMW with temperature ranges of 8.8 °C to 9.5 °C and salinities of 34.73 to 34.58 g kg⁻¹ are found south of Australia, while the mode water found south of New Zealand is cooler and fresher (<8 °C, <34.45 g kg⁻¹). The formation process of SAMW provides it with another property that can be used as a dynamical tracer, namely a minimum in potential vorticity. Because potential vorticity is a conservative property it can be traced when it is moved away from the source of formation (McCartney, 1977, 1982; Rintoul and Bullister, 1999; Sloyan and Rintoul, 2001).

AAIW is not a single homogeneous water mass. Bostock et al. (2013) reported four different types of AAIW with different temperature and salinity combinations. In their work, they identified the Southern Ocean type as the AAIW with a temperature between 4 and 8 °C, a salinity between 34.45 and 34.57 g kg⁻¹ and a density anomaly of 27.1 kg m⁻³. South of Australia, Rintoul and Bullister (1999) also found different types of AAIW, colder and fresher (3.7 °C to 4.5 °C; <34.51 g kg⁻¹) and warmer and saltier (4.3 °C to 5.1 °C; 34.55 g kg⁻¹) both lying within the range of the Southern Ocean type. Formation processes of the AAIW are still under study, with some theories suggesting SAMW may be the origin of AAIW (e.g., McCartney, 1977; Hartin et al., 2011) and others suggesting ASW is the source for AAIW, through air-sea fluxes in the equatorward

side of the Polar Front (Naveira-Garabato et al., 2009).

SAMW and AAIW play a major role in the modulation of global climate variations. The formation of SAMW and AAIW is a primary mechanism for sequestering and storing anthropogenic CO₂ and chlorofluorocarbons (CFCs) within the oceans (McCartney, 1982; Sabine et al., 2002; Hartin et al., 2011; Hasson et al., 2011; Holte et al., 2012). They are both part of the global overturning circulation. They export heat, salt and nutrients into the Southern Hemisphere basin-wide gyre circulation at depths isolated from the atmosphere (e.g., Herraiz-Borreguero and Rintoul, 2011; Hasson et al., 2011), ventilating the lower thermocline of the southern hemisphere subtropical gyres (e.g., McCartney, 1977; Rintoul and Bullister, 1999; Sloyan and Rintoul, 2001; Morris et al., 2001).

2.2 Previous findings in the Campbell Plateau

Although from the beginning of the 1980s some studies were carried out in the subantarctic region, it was not until the late 1990s that a number of voyages were specifically designed to evaluate the New Zealand subantarctic region. This coincided with the beginning of the satellite era, which also increased the tools for studying this area.

The first studies that specifically mentioned the Campbell Plateau were carried out by Heath (e.g., 1981, 1985). In those studies, the main oceanographic features such as fronts and water mass structure were described. It was also suggested that SAMW was being formed at the SAF during the whole year instead of only in winter. The complexity of the area was stated but its variability was unclear.

The STF entering the western Campbell Plateau was described by Butler and Butt (1992). They described STW locked to the 200 m isobath and apparently mixed with freshwater run-off from the South Island. Although their study was carried out on the plateau margin, two interesting features were pointed out that are useful in this thesis: i) the variability of the SST over the Snares Shelf may be transferred to the whole water column through wind forcing, ii) the idea of Solander Trough and Puysegur Trench as

areas where mixing of subtropical, subantarctic and freshwater occurs. Also noticed was the subsurface high-salinity tongue around 150m depth close to the coast. This marks the southern limit of the Subtropical Frontal Zone (STFZ) and suggests that it could extend up to half-way across the SAZ. This result is consistent with later studies such as Morris et al. (2001) and Smith et al. (2013). However, the position of the front does not agree with that found by Smith et al. (2013), who found it to be further south around 49.6°S, the most southern position in the Southern Hemisphere. Smith et al. (2013) found that the STF south of New Zealand is well defined and located by the bathymetry.

East of the South Island, the front is directed northwards where the Southland Current flows northeast steered by the topography (e.g., Chiswell, 1996; Sutton, 2003; Hopkins et al., 2010). Further north, the STF is diverted eastwards along the Chatham Rise and keeps its flow into the Pacific Ocean (Sutton, 2001; Hopkins et al., 2010).

Morris et al. (2001) investigated a series of CTD profiles to determine the variability of the New Zealand subantarctic region, if SAMW was present, and the position of the SAF. Their results show the difference between the STW found south of New Zealand close to the coast in the Solander Trough transect, and the strongly modified water mass found east of New Zealand. This result agreed with the findings of Butler and Butt (1992) and suggest that southernmost New Zealand is a mixing place for STW and SAW. Morris et al. (2001) also reported the change in density properties of the STF, which is strongly density compensated south of New Zealand, and becomes weakly compensated once it reaches the eastern continental margin of the South Island as also noted by Smith et al. (2013).

In their work, Morris et al. (2001) found SAMW between 200m and the bottom over the Campbell Plateau with a surface layer responding to seasonal atmospheric changes. The type of SAMW found in the Campbell Plateau is colder and fresher than the variety of SAMW found in the Tasman Sea. It has been suggested by several studies that the Tasman Sea SAMW cannot be tracked further east than 164°E, as the Campbell Plateau seems to act like an eastern boundary blocking the access of this water to the

southwest Pacific (McCartney, 1977; Rintoul and Bullister, 1999; Morris et al., 2001). The origin of the differences between both water masses has been previously debated. For example, Sloyan and Rintoul (2001) suggested that the two types of SAMW are independent pools. They also proposed that this sharp change in properties is not a result of intense sea-air interactions, but is instead due to a change in the dominance of the colder and fresher SAMW east of the Campbell Plateau, likely caused by the path restriction of the bathymetry, an idea that was also supported by Rintoul and Bullister (1999). However, SAMW formation and location south of New Zealand is a discussion that has been around for decades. Heath (1981, 1985) suggested SAMW is formed over the plateau by deep vertical mixing. Morris et al. (2001) suggested that the water over the plateau is made lighter and not denser, hence SAMW could not be formed over the plateau. They proposed that the plateau's SAMW is replenished by an inflow of dense water from the edges of the plateau, implying that SAMW is formed on the equatorward side of the SAF. This idea was first suggested by McCartney (1977) and Butler and Butt (1992), and has been supported by other authors lately such as Hasson et al. (2011).

Other types of SAMW were previously reported in the Campbell Plateau. Griffith et al. (2010) noticed two variations of SAMW on the east corner of the Campbell Plateau: one SAMW was saltier and warmer and found over the Pukaki Rise; the other was fresher and colder and found in the Pukaki Saddle. Fresher AAIW flowing through the Pukaki Saddle was previously reported by Bostock et al. (2013). The question arises: are there two different SAMW's or are they SAMW and AAIW?

Stanton and Morris (2004) described the variability over the Campbell Plateau and along the Subantarctic Slope from mooring data (Figure 2.6) and confirmed the mean weak circulation suggested by Morris et al. (2001). These currents had peaks of 16 cm s^{-1} , but despite the high variability the mean flow was near zero. In their study, Mooring number 3, at 1000 m depth on the Subantarctic Slope, showed stronger currents than those on the plateau, suggesting that this location was already being influenced by the SAF. The core of the SAF was identified between moorings 4 and 5, confirming that SAF follows the bathymetry, leaving Mooring 6 south of the ACC influence. Links with

local winds were made by suggesting that stronger currents were found in winter, maybe due to strengthening of winter winds and eddy activity.

However, some of the variability seen in this region may be associated with the eddies embedded in the SAF. The Campbell Plateau region is associated with high eddy activity, some of the largest observed around the world (e.g., Morrow et al., 1994; Morris et al., 2001; Stanton and Morris, 2004). This eddy activity may also influence SAMW formation as well as its properties, as it is very close to the source of formation. These influences may be related to changes in stratification, mixing and circulation in the Southern Ocean. AAIW would be less influenced as it is formed further south (e.g., Sallée et al., 2008; Hartin et al., 2011).

Long term mean currents show a strong steering by the bathymetry through the depths selected (Figure 2.7). Mid depth currents use gaps in the bathymetry to continue with their flow. The paths seem to be consistent with the literature with inflow of water through the Pukaki Saddle, Campbell Rise, and Pukaki Rise, the current following the 500 m depth isobath into the Southland Current, and deep currents following the Campbell Plateau edge.

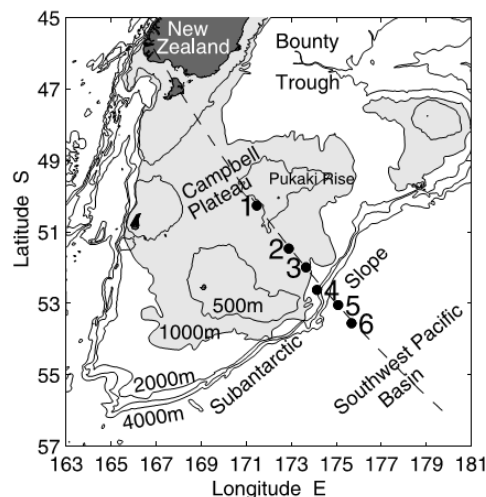


Figure 2.6: Moorings positions deployed over the Campbell Plateau and Subantarctic Slope from Stanton and Morris (2004)

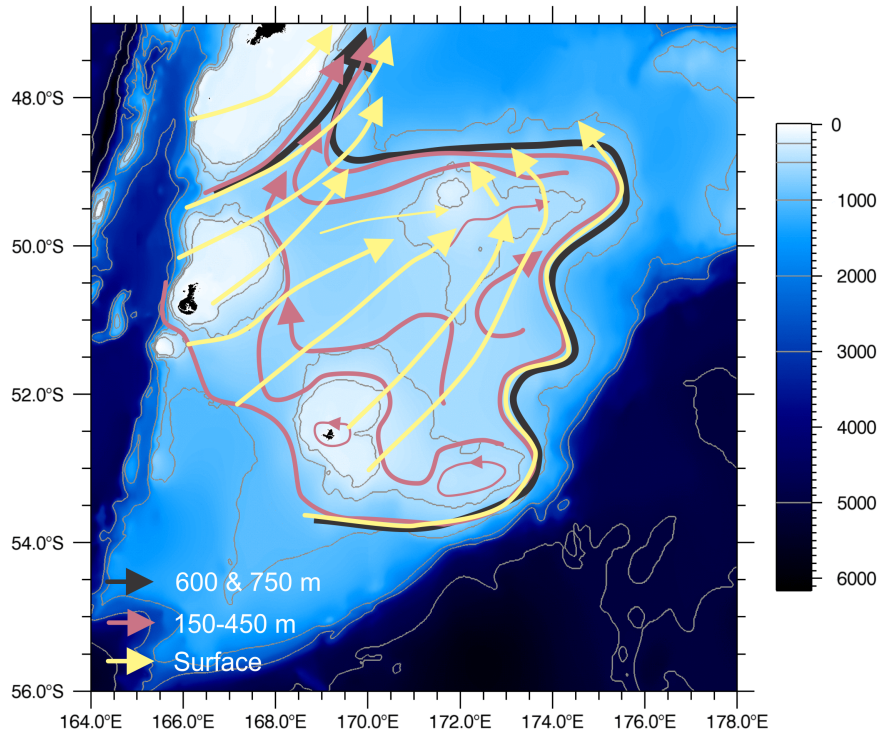


Figure 2.7: Campbell Plateau mean currents paths. Interpolated by Mike Williams from model data from Mark Hadfield.

2.2.1 Campbell Plateau in a global context

Another step forward in understanding the ocean variability and structure of the Campbell Plateau is to consider the position of the Campbell Plateau on a global scale. While it might be reasonable to think that direct influence on the Campbell Plateau will come from the STF and SAF, larger scale driving mechanisms have to be included in the big picture.

The New Zealand land mass is in between the South Pacific Subtropical Gyre and the Tasman Sea (e.g., Sutton et al., 2005). The southern limit of STW is marked by the STF that is found around southern New Zealand as previously described. East to the Campbell Plateau, flows from the South Pacific Subtropical Gyre and the ACC meet

in a confluence region described in Fernandez et al. (2014). Changes in wind forcing in the South Pacific might be influencing the variability in the Campbell Plateau through this complex set of currents that surround it. For example, Hill et al. (2010) suggested several types of waves communicating changes in wind between the South Pacific and the East Australian Current (EAC) (Figure 2.8). In a previous work, they suggested that changes in the EAC extension at Maria Island were linked to changes in wind stress curl in the South Pacific (Hill et al., 2008).

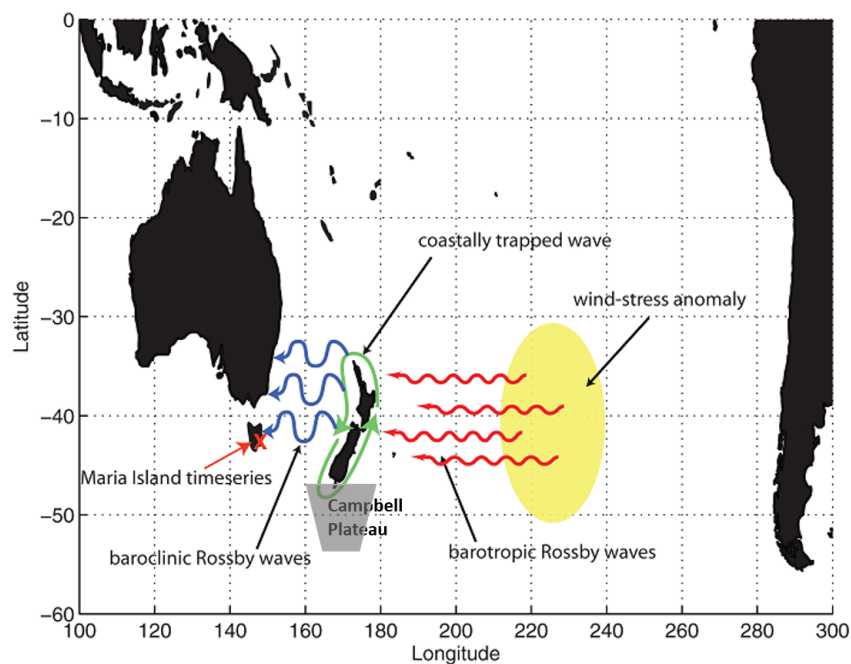


Figure 2.8: Mechanism by which changes in the winds in the South Pacific can be communicated to the East Australian current. Modified from Hill et al. (2010).

Qiu and Chen (2006) also show that the South Pacific has had the largest positive trend in SSH in the last decade, with the largest trend east of New Zealand. They suggest the increase in SSH is due to changes in wind stress curl by Ekman pumping and the propagation of Rossby waves. Thus, sea level variations are likely a variation of local and remote responses to winds.

These studies suggest that the ocean properties and currents of the New Zealand sub-antarctic region and the Campbell Plateau may respond to a complex set of dynamics. Several questions will be posed and addressed in this thesis, other questions will arise in the process, and some will remain for future investigation.

Chapter 3

Oceanography of the Campbell Plateau

Until this study, the most comprehensive analysis of the physical oceanography of the Campbell Plateau came from Morris et al. (2001). This chapter provides new data that, when integrated with the data used by Morris et al. (2001), gives new insights into the ocean's regional variability and seasonality. The dataset consists of hydrographic transects carried out in recent decades covering both the Campbell Plateau and the surrounding area. The transects will be discussed from west to east, from the Tasman Sea, across the topographically rugged Macquarie Ridge and Solander Trough, onto Campbell Plateau itself and finishing with the Bounty Trough (Figure 3.1). Shorter transects through Snares Depression and Pukaki Saddle are also shown to complete the description.

The positions in space and time of the ocean fronts and water masses are investigated, Θ - S_A (conservative temperature-absolute salinity) diagrams evaluated and the general geostrophic circulation described. This allows variability over the last two decades to be investigated through high resolution snap shots of the subantarctic region. Some of the transects were repeated in different voyages, allowing seasonal variability to be assessed. Variables such as conservative temperature, absolute salinity and geostrophic velocities are explained in detail to provide a regional view of the New Zealand subantarctic region and how it interacts with the Campbell Plateau.

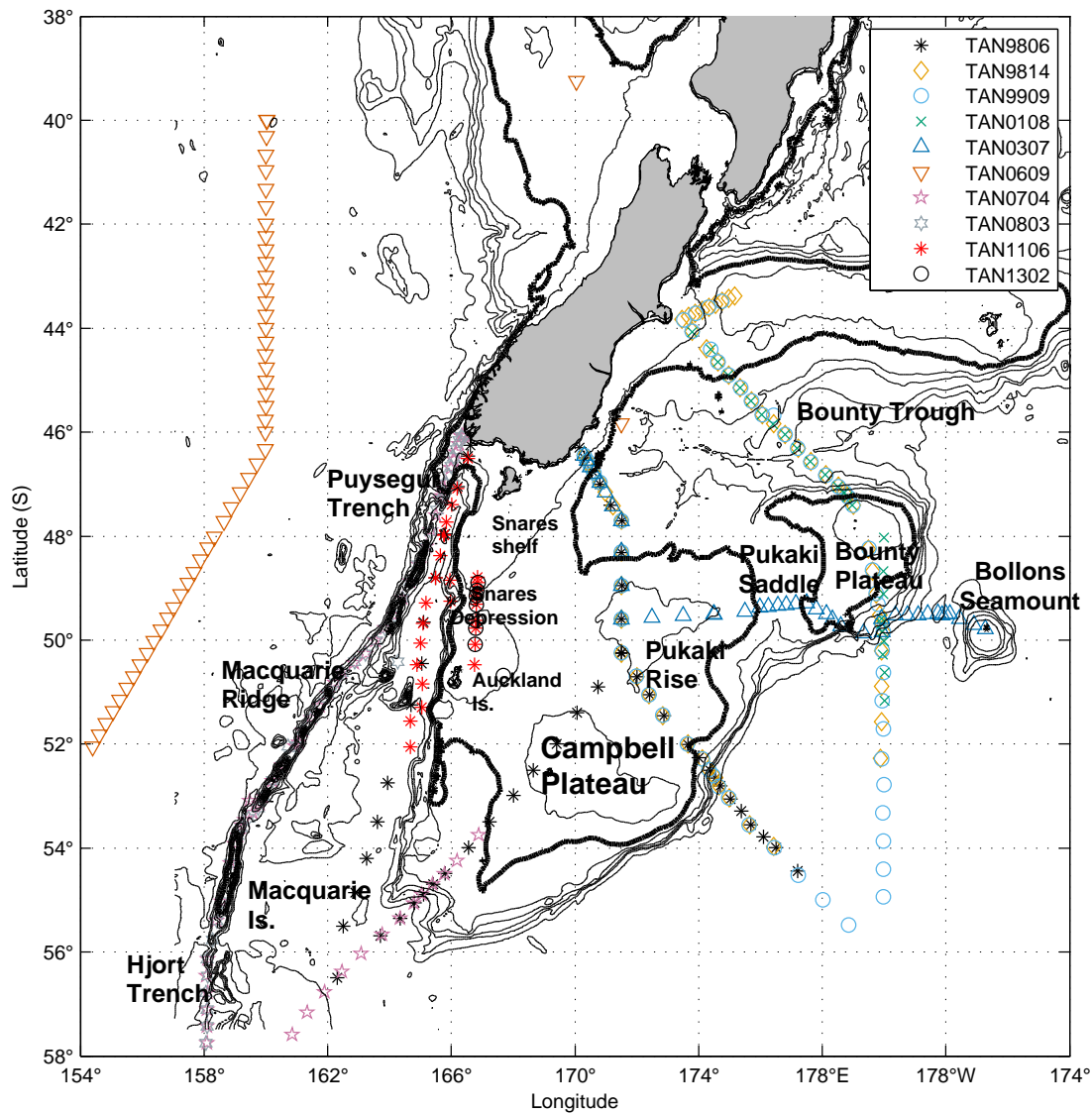


Figure 3.1: High resolution hydrographic profile positions. Bathymetry details related with transects. Contours every 500 m, bold contour show 1000 m isobath.

3.1 Data and Methods

Nine oceanographic cruises were carried out from 1998 to 2013. On each cruise high resolution Conductivity, Temperature and Depth (CTD) profiles were obtained in different parts of the New Zealand subantarctic region (Figure 3.1). Details of the voyages are presented in Table 3.1. Each voyage consists of several transects crossing significant oceanographic features in the subantarctic region.

Table 3.1: High resolution details

| Year | Month | Number of casts | Positions | Cruise name | Voyage report |
|------|-----------|-----------------|--|--------------------|-----------------------------|
| 1998 | May & Dec | 68 & 59 | Solander Trough Campbell Plateau Bounty Trough | TAN9806 TAN9814 | (Stanton, 1998; Neil, 1998) |
| 1999 | Aug | 69 | Campbell Plateau Bounty Trough | TAN9909 | (Grieg, 1999) |
| 2001 | Jun | 60 | Bounty Trough | TAN0108 | (Neil, 2001) |
| 2003 | May | 57 | Campbell Plateau | TAN0307 | (Neil, 2003) |
| 2006 | Jul | 51 | Tasman Sea | TAN0609 | (Sutton, 2006) |
| 2007 | Mar | 74 | Solander Trough Macquarie Ridge | TAN0704 | (Williams, 2007) |
| 2008 | Apr | 59 | Solander Trough Macquarie Ridge | TAN0803 | (Rowden, 2008) |
| 2011 | Apr | 56 | Solander Trough | TAN1106 | (Bostock, 2011) |
| 2013 | Feb/Mar | 86 | Mertz Polynya Snares Depression | TAN1302 | (Williams, 2013) |

The data at each CTD station on each voyage were binned into 2 dbar vertical regular matrix. For each voyage, the stations are evenly distributed along the transects, however, stations were closer when crossing major oceanographic features to better resolve them. The International Thermodynamic Equation of Seawater-2010, TEOS-10 (Appendix A) was used to calculate the derived variables, conservative temperature and absolute salinity. No interpolation was used to fill in the missing data, which were minimal and left all the important features remain clear.

Positions of the ocean fronts can be identified by the change in horizontal structure and strong properties gradients (e.g., Belkin and Gordon, 1996), in particular conservative temperature and absolute salinity. Horizontal transects are drawn for front and water mass identification. The repeated transects also help with the identification of the seasonality.

To describe the ocean currents, geostrophic velocities were calculated from the density gradients using the geostrophic method. This method assumes that the ocean is in

geostrophic balance when the horizontal dimensions are larger than 50 km and the time scales greater than a few days (e.g., Stewart, 2008). This means that the balance of forces in the horizontal is between the pressure force (horizontal pressure gradient) and the Coriolis acceleration. The pressure gradient force vector points from high to low pressure, the Coriolis force exactly opposes the pressure gradient force. Once the forces are balanced the parcel of water moves perpendicular to both, the pressure gradient force and the Coriolis force (e.g., Pickard and Emery, 1990; Talley et al., 2011). To calculate the pressure gradient, density is first calculated using an empirical equation of state of sea water (TEOS-10) from measurements of temperature and salinity as functions of depth between two CTD stations. The computed density represents the distribution of mass in the ocean which creates gradients of pressure (e.g., Pickard and Emery, 1990). To calculate geostrophic velocities, the absolute horizontal pressure difference between two stations is needed. However, only the density distribution is known, and hence only the geostrophic velocity shear through the water column can be calculated. This is orthogonal to each pair of stations (e.g., Sutton, 2003). The relation between the geostrophic velocity shear and the horizontal density gradient is called the thermal wind relation (Equation 3.1), and are used to calculate the vertical shear (e.g., Pickard and Emery, 1990; Stewart, 2008; Cushman-Roisin and Beckers, 2011):

$$\left. \begin{aligned} \frac{\partial v}{\partial z} &= -\frac{g}{\rho_0 f} \frac{\partial \rho}{\partial x} \\ \frac{\partial u}{\partial z} &= \frac{g}{\rho_0 f} \frac{\partial \rho}{\partial y} \end{aligned} \right\} \quad \text{thermal wind equations} \quad (3.1)$$

where ρ is the sea water density, (kg m^{-3}); ρ_0 is reference density of sea water, (1028 kg m^{-3}); p is pressure, (dbar); u and v are the velocity components in the x and y -directions, (m s^{-1}); z is depth, (m); f is the Coriolis parameter, (s^{-1}), given by $f = 2\Omega \sin \varphi$, where Ω is the angular velocity vector of Earth, ($7.29 \times 10^{-5} \text{ s}^{-1}$) and φ is the latitude.

To convert relative currents to absolute currents a known velocity at some level is needed, i.e., a reference level (e.g., Talley et al., 2011). In this thesis, the calculations are referenced to a reference level called the “level of no motion” where the velocity is assumed to be zero. The sea floor was chosen as a “level of no motion”, in accord with other

studies (Stanton and Morris, 2004; Sutton, 2003; Morris et al., 2001). Then the currents are integrated up to the surface.

3.1.1 Front and water mass identification criteria

Front and water mass identification has many challenges as the definition of such features changes with time, place and method of identification. Under TEOS-10, absolute salinity is the variable used for the description of water masses and fronts. Absolute salinity is, as a general rule, about 0.17 g kg^{-1} saltier than practical salinity. For that reason, and to be consistent with the literature, salinity measurements reported in the literature have been adjusted to absolute salinity. Conservative temperature does not need adjustment as values are the same as the potential temperature previously reported in the literature.

Water mass identification follows Table 3.2. Although the scope of this work is focused north of the SAF, all the listed water masses are important when defining the general picture of the Southern Ocean water masses frontal structure. A reference transect of the Southern Ocean with the main water masses and fronts is presented in Figure 3.2.

Front identification criteria are used as follows below:

The STF in the south Tasman Sea is identified by its double structure, the North Subtropical Front (N-STF) and the South Subtropical Front (S-STF) that encompass an eddy-rich zone with little frontal structure with the entire STF being around 300 km wide (Hamilton, 2006; Smith et al., 2013). The S-STF in the New Zealand region is found where the temperature decreases from 12°C to 10°C at a depth of 100 to 200 m. The front is also characterized by a high salinity tongue, with a range of 34.77 g kg^{-1} to 35.17 g kg^{-1} . The STF is limited to the upper 500 m of the water column (Belkin and Gordon, 1996; Sokolov and Rintoul, 2002; Smith et al., 2013).

The SAF can be identified by strong gradients in properties that extend from the sea surface to the sea floor. It has three different branches each of which correspond to a

Table 3.2: Subantarctic region water masses, compiled from ¹ McCartney (1977),² Pickard and Emery (1990), ³ Morris et al. (2001), ⁴ (Tomczak and Godfrey, 2001), ⁵ Sokolov and Rintoul (2002), ⁶ Carter et al. (2008), and ⁷ Talley et al. (2011). The acronyms in the table are: Antarctic Intermediate Water (AAIW); Antarctic Surface Water (AASW); Circumpolar Surface Water (CSW); Lower Circumpolar Deep Water (LCDW); North Atlantic Deep Water (NADW); Subantarctic Mode Water (SAMW); Subantarctic Water (SAW); Subtropical Water (STW); Upper Circumpolar Deep Water (UCDW).

| | Temperature [C] | Absolute salinity | Density [kg m-3] | Depth [m] | Oxygen [mL L-1] | Other features |
|---------------------|------------------------------|------------------------------------|-------------------------|--|-----------------|---|
| AAIW ⁵ | 4-5 | 34.46-34.66 | 27.1-27.3 | 600-1200 | | Salinity minimum core |
| AASW ⁷ | -1.9-1 winter -1-4 summer | 33.16-34.66 | | less than 50m thickness in the summer | | south of the SAF |
| CSW ^{3,6} | 5-8 | 34.66 | | | | Salinity drop |
| LCDW ^{5,7} | | 34.88 | 28.27 lower boundary | 2500-3000 | | salinity maximum derived from NADW |
| NADW ² | 2-3 | 34.86-35.06 | | 1500-3000 | 4-5 | |
| SAMW ^{1,4} | 7 over the plateau | 34.51-34.66 over the plateau | | 200-500 over the plateau | | weak stratification minimum in potential vorticity |
| SAW ⁷ | 4-10 winter 14 summer | 34.06-34.16 summer 33.16 winter | | up to 500m | | north of SAF |
| STW ⁵ | | high salinity core | | 0-200 | | north of 45S |
| UCDW ^{5,7} | 2-2.5 | >34.86 | | 1500 | Oxygen minimum | below ASW and AAIW |

maxima in properties. The northern branch (SAF-N) can be identified as a decrease from $>8^{\circ}\text{C}$ to $<6^{\circ}\text{C}$ at a depth of 300 to 400 m and a salinity of 34.37 g kg^{-1} to 34.77 g kg^{-1} . The middle branch (SAF-M) is characterised by temperatures of $>6^{\circ}\text{C}$ to $<5^{\circ}\text{C}$ and the southern branch (SAF-S) is where the temperature decreases from $>5^{\circ}\text{C}$ to $<3^{\circ}\text{C}$ at the same depths. However, branches are forced by bathymetry, such as the Campbell Plateau, to merge and divert making hydrographic identification a difficult task (Sokolov and Rintoul, 2002, 2007a).

The northern reach of the Polar Front Zone (PFZ) was crossed by some of the transects included in this work. Sokolov and Rintoul (2002) identified the PFZ as a double front structure in SR3 (140°E). In their work, the northern branch of the PFZ is a steady feature found between 53.0° and 54.3°S , and it can be identified by its subsurface temperature minimum signature, approximately the 2°C isotherm at around 200 m (Belkin and Gordon, 1996; Sokolov and Rintoul, 2009a).

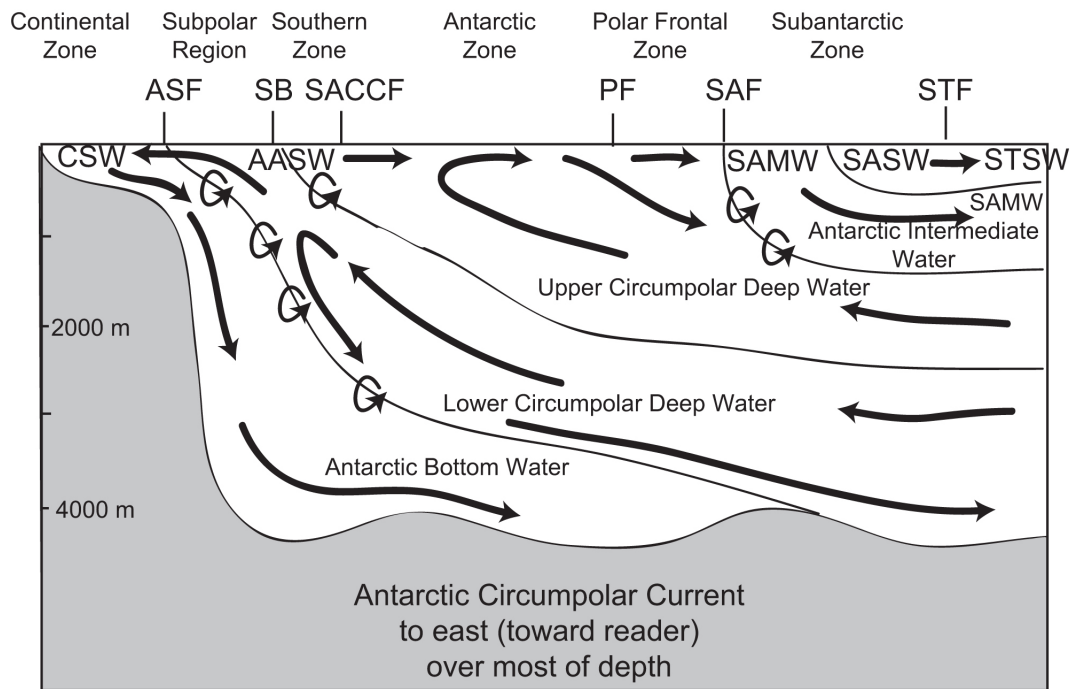


Figure 3.2: Schematic Southern Ocean section with the main water masses and fronts positions. Continental Shelf Water (CSW), Antarctic Surface Water (AASW), Subantarctic Mode Water (SAMW), Subantarctic Surface Water (SASW), Subtropical Surface Water (STSW), Antarctic Slope Front (ASF), Southern Boundary (SB), Southern ACC Front (SACCF), Polar Front (PF), Subantarctic Front (SAF), and Subtropical Front (STF). From Talley et al. (2011) after Speer et al. (2000).

3.2 Results

The results presented here are organized from west to east, starting with the Tasman Sea, the Macquarie Ridge and the Solander Trough transects, a transect across the Snares Depression, the Campbell Plateau transects, a longitudinal transect across the Pukaki Saddle and finishing with the Bounty Trough transects (Figure 3.1). Conservative temperature and absolute salinity transects are described, comparing similar transects when possible. Θ - S_A diagrams are shown for some transects to identify common water masses and transitions between water masses. Finally, geostrophic velocity transects are shown to describe the general flow around the Campbell Plateau.

3.2.1 Horizontal sections

Tasman transect

The stations of the Tasman transect, from 40°S to 52°S, were occupied in July 2006 (winter) (Figure 3.3).

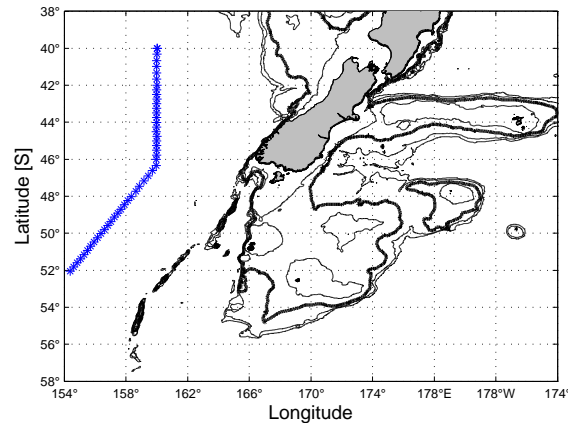


Figure 3.3: Hydrographic stations (blue) for the Tasman Sea transect, TAN0609. Contours every 500 m, bold contour show 1000 m isobath.

The STF can be identified between Stations 20 and 23 (Figure 3.4) as a change in temperature from 11 °C to 10 °C around 45.6°S. A tongue of Subtropical Lower Water (SLW) that extends poleward is associated with it. This position is consistent with a salinity tongue protruding poleward to around Stations 20 to 22 (Figure 3.5). The tongue evolves into a uniform body with a weakly stratified layer in the upper 500 m layer which has a temperature between 7 °C and 9 °C lying between 47°S and 52°S. This appears to be Subantarctic Mode Water (SAMW). Further south, the isotherms tilt approaching the SAF. From 500 m to 1500 m there is a stratified layer and below this the temperature decreases uniformly. Salinity shows a fresher tongue of water coming from the south sitting between 500 m and 1250 m which has the characteristics of Antarctic Intermediate Water (AAIW), i.e., a temperature between 4 and 5 °C and a salinity minimum core <34.66 g kg⁻¹. Below that layer, the salinity is uniform along the transect.

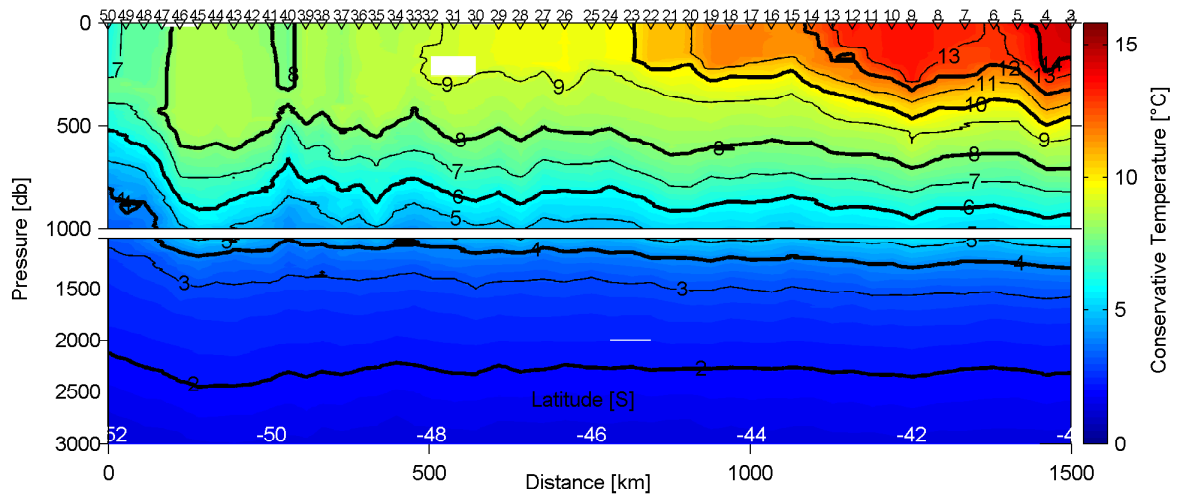


Figure 3.4: Conservative temperature section along the Tasman transect. North to the right side of the figure. Contour interval is $1\text{ }^{\circ}\text{C}$, with bold contours every $2\text{ }^{\circ}\text{C}$. Station positions are marked on the top of the figure. Top panel shows top 1000 m of the water column and bottom panel from 1000 to 3000 m. Blank patches show missing data.

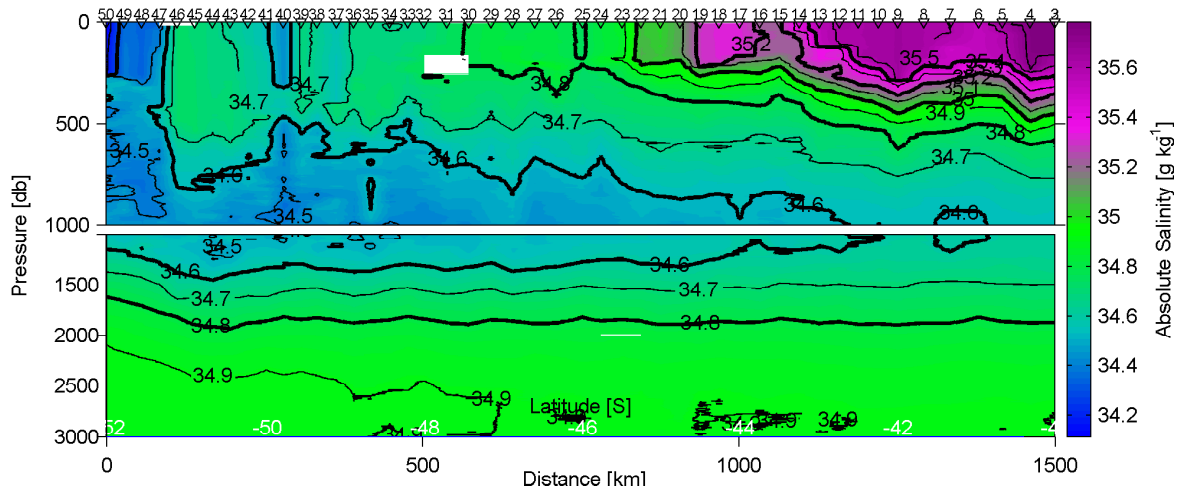


Figure 3.5: Absolute salinity section along the Tasman transect. North to the right side of the figure. Contour interval is 0.1 g kg^{-1} , with bold contours every 0.2 g kg^{-1} . Station positions are marked on the top of the figure. Top panel shows top 1000 m of the water column and bottom panel from 1000 to 3000 m. Blank patches show missing data.

Macquarie Ridge transects

The Macquarie Ridge transects start at the southern tip of the South Island and follow the Macquarie Ridge system, here taken to include Puysegur Trench, Macquarie Ridge and Hjort Trench to 60°S (Figure 3.6). The Macquarie Ridge rises to 1000 m along most of its length and forms a bathymetric wall for the ACC, excluding narrow gaps that act as natural gates for the ACC (Rintoul et al., 2014). These transects were sampled in March 2007 and April 2008, i.e., consecutive years at the end of the summer.

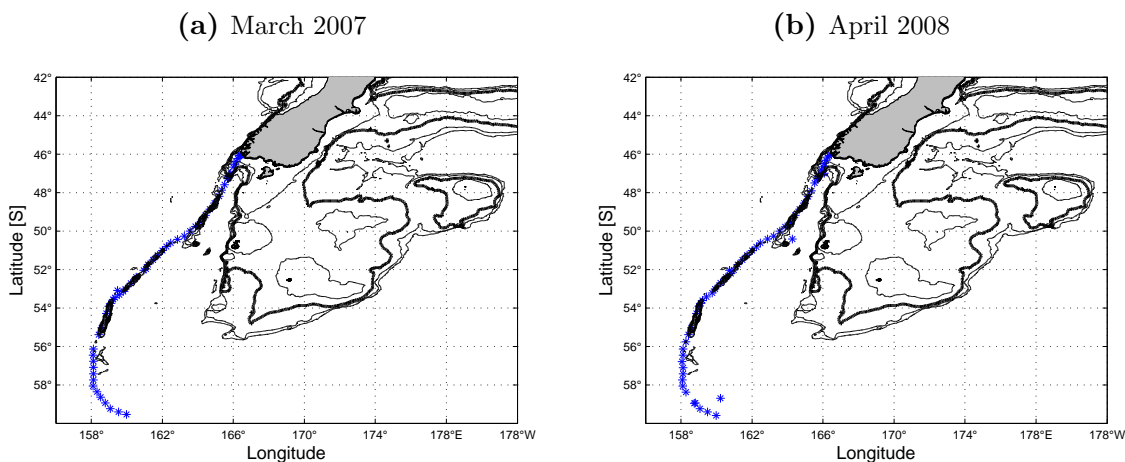


Figure 3.6: Hydrographic stations (blue) for the Macquarie Ridge transects, (a) TAN0704 and (b) TAN0803. Contours every 500 m, bold contour show 1000 m isobath.

The northern part of the transects is dominated by the STF and the southern end by the SAF. During the March transect, the S-STF was crossed between Stations 19 and 20, at approximately 49.6°S (Figure 3.7a). During the April transect the S-STF was crossed between Stations 17 and 18 almost in the same position as the previous year (Figure 3.7a). The temperature is consistent in the salinity transects which shows a high salinity tongue at the northern end of the transect and a similar frontal location (Figure 3.8a and Figure 3.8b). The northern part of the transects was previously presented by Smith et al. (2013) who provided a complete description of the behaviour of the STF. Here the focus is south of the STF.

Along Macquarie Ridge, the different branches of the SAF have been identified with mean positions, the SAF-N at 50.5°S and 52.1°S, the SAF-M at 53.3°S and a combined SAF-S and Polar Front at approximately 55°S (Sokolov and Rintoul, 2007a; Rintoul et al., 2014).

Three branches of the SAF were crossed in both transects. During March 2007, the SAF-N was crossed at around 50.8°S at Station 26, the SAF-M was crossed at 53.3°S between Stations 39 and 40 and the SAF-S appears to be combined with the Polar Front, at around 55.8°S. This combination of the two fronts has been previously reported in other locations by Sokolov and Rintoul (2007a); Rintoul et al. (2014). In the April 2008 transect, the northern branch appears to be merged with the middle branch, almost at the same position where the SAF-M was crossed the previous year, between Stations 37 and 40 and the SAF-S is not so well defined being crossed around 56°S between Stations 45 and 47.

The northern branch of the Polar Front was crossed in March 2007 at 55.8°S near Station 46, and was identified by a subsurface temperature minimum of 2°C at 200 m depth. In April 2008, the northern Polar Front was crossed approximately 1° further south, at 57°S (Station 49). The salinity signal also follows this pattern with the deepening of the isohalines delimiting the front.

The relative fresh surface layer of water south of 53°S is the Antarctic Surface Water (AASW). The cold and salty water that can be seen south of 56°S below 1000 m is Circumpolar Deep Water (CDW), which is formed by Upper Circumpolar Deep Water (UCDW) and Lower Circumpolar Deep Water (LCDW) identified by a salinity maximum.

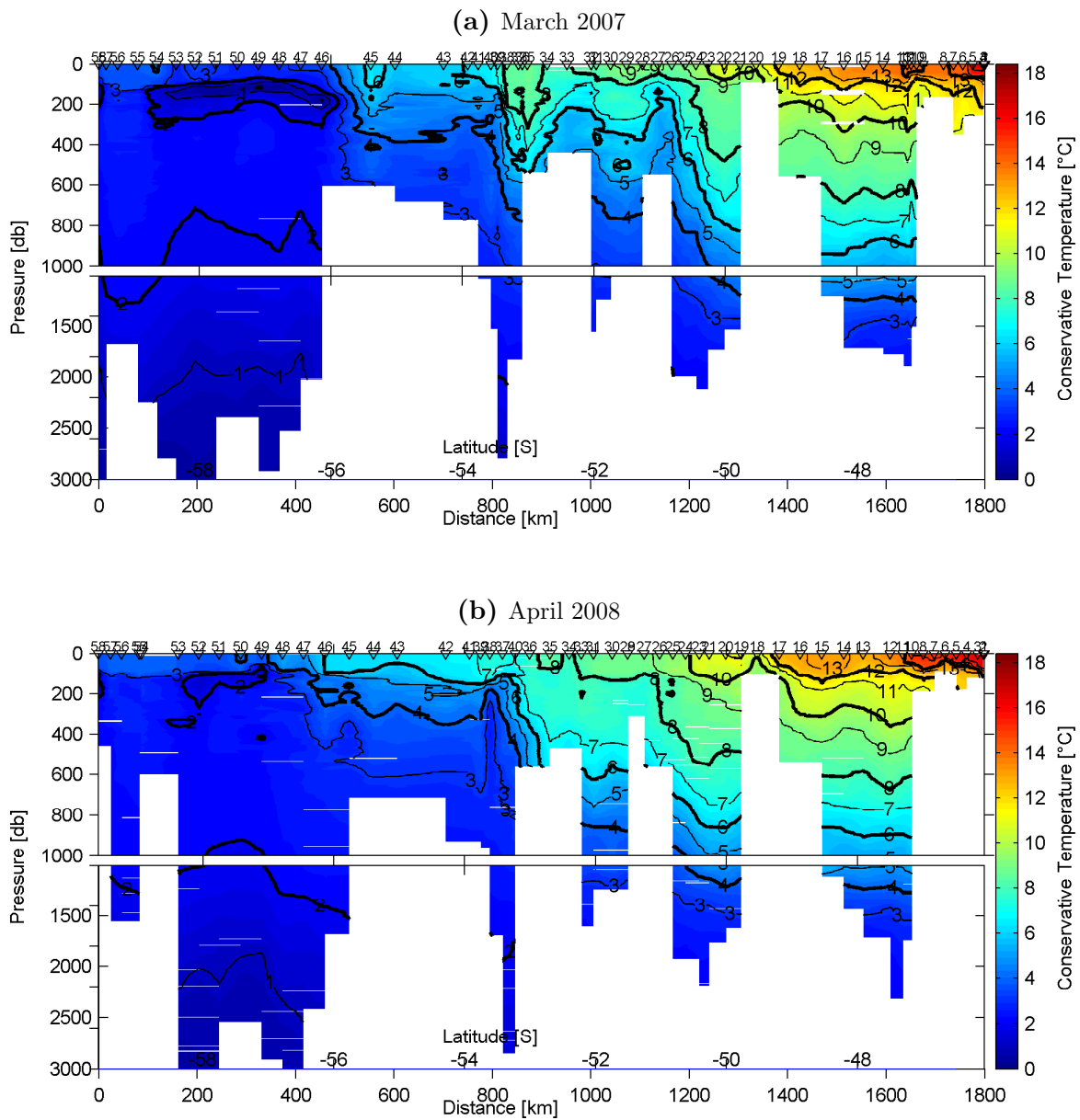


Figure 3.7: Conservative temperature sections along the Macquarie Ridge. Labels are above each figure. North to the right side of the figure. Contour interval is 1 °C, with bold contours every 2 °C. Positions of the stations are marked on the top of the figure. Top panel shows top 1000 m of the water column and bottom panel from 1000 to 3000 m. Temperature scale is the same for both panels.

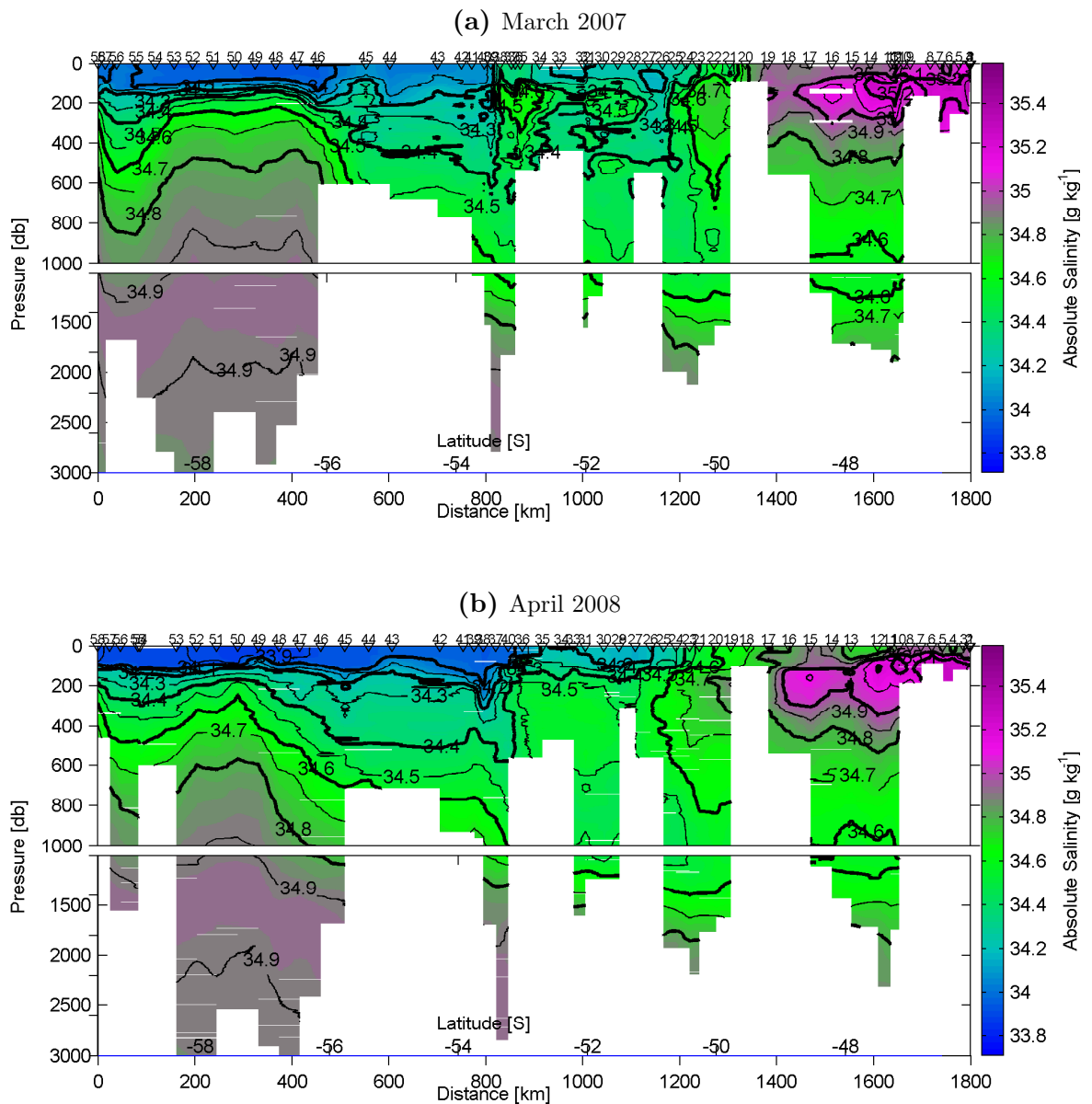


Figure 3.8: Absolute Salinity sections along the Macquarie Ridge. Labels are above each figure. North to the right side of the figure. Contour interval is 0.1 g kg^{-1} , with bold contours every 0.2 g kg^{-1} . Positions of the stations are marked on the top of the figure. Top panel shows top 1000 m of the water column and bottom panel from 1000 to 3000 m. Salinity scale is the same for both panels.

Solander Trough transects

The Solander Trough transects were carried out in May 1998 and May 2011. Both go along the Solander Trough, an elongated depression between the Macquarie Ridge and Campbell Plateau. Figure 3.9 shows the locations of the stations in both sections.

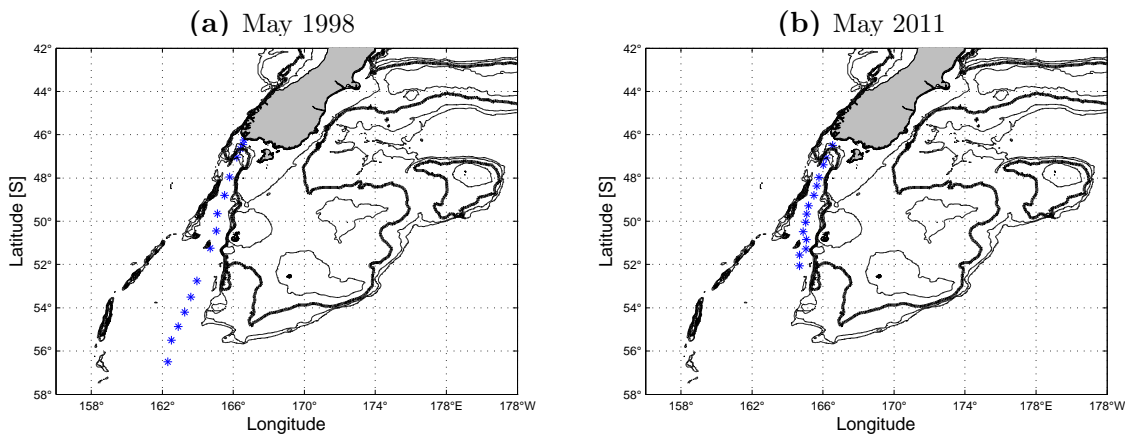


Figure 3.9: Hydrographic stations (blue) for the Solander Trough transects, (a) TAN9814 and (b) TAN1106. Contours every 500 m, bold contour show 1000 m isobath.

The STF was crossed in May 1998 at 49.52°S, between Stations 63 and 60 (Figure 3.10a), this is shown by the subsurface high salinity tongue ($>34.8 \text{ g kg}^{-1}$) protruding south (Figure 3.11a). In the May 2011 transect the STF is less clear as it is crossed several times between Stations 21 and 24. Temperatures are higher in the coastal side (northern side of the transect) of the May 2011 transect by 2 °C, with a low salinity value ($<34.6 \text{ g kg}^{-1}$) that may be due to the higher input of terrestrial freshwater run-off (Figure 3.11b).

The branches of the SAF were crossed in May 1998 further south than over the Macquarie Ridge and are closer together, probably due to the forcing of the bathymetry. The SAF-N is crossed at 54.1°S, followed by the SAF-M at 54.2°S and the SAF-S at around 56°S. The SAF was not crossed in May 2011. Cool, fresh Subantarctic Surface Water (SASW) was encountered south of the SAF in the May 1998 transect. Mixed layer depths typically reached 50 m to 150 m (increasing southward), with the base of the thermocline at 750 m to 1000 m. AAIW is present between 900 m and 1200 m in both

transects, with CDW also present in both transects from 1200 m, the limit of the AAIW, to the bottom of the water column.

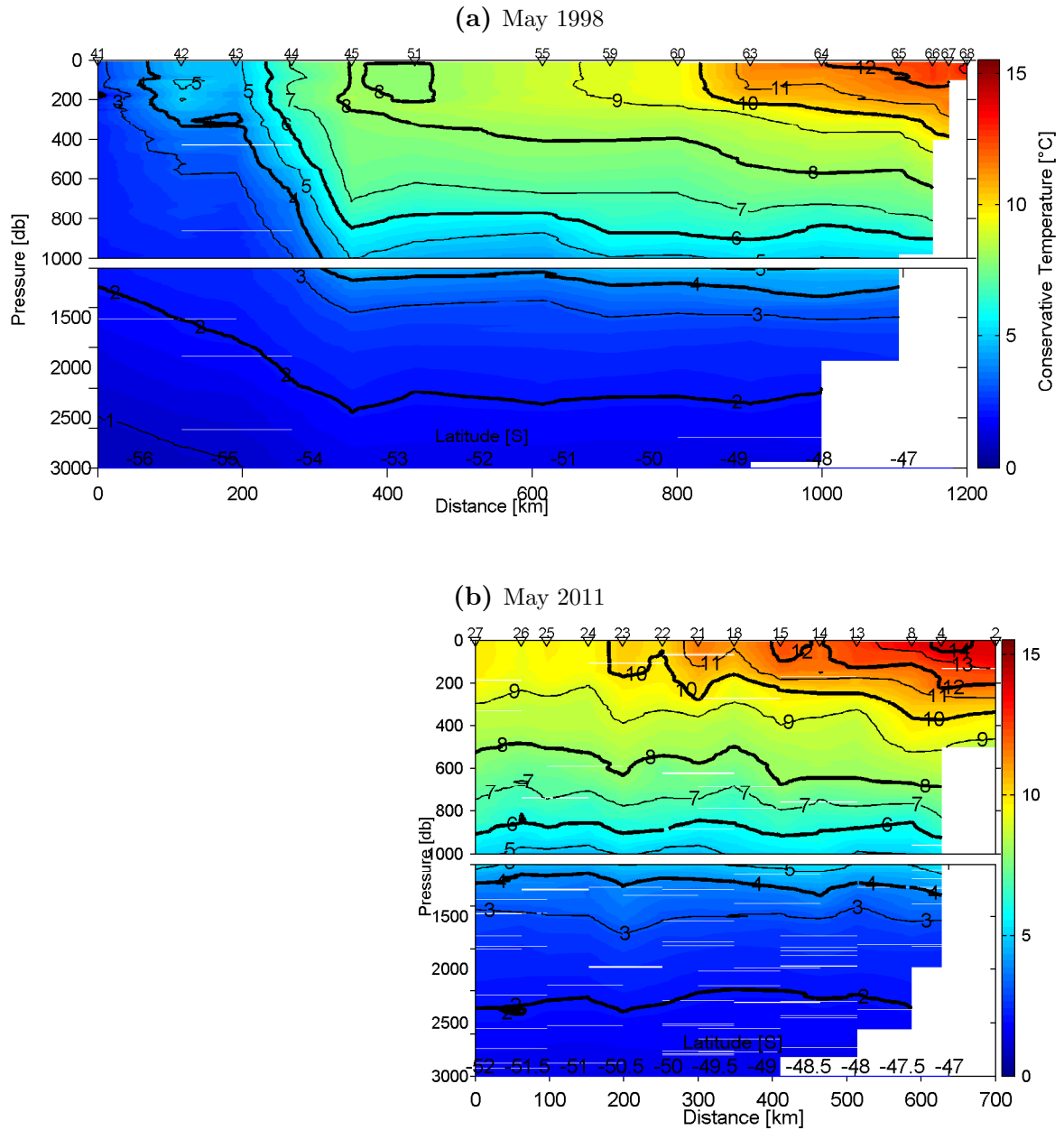


Figure 3.10: Conservative temperature sections along the Solander Trough. Labels are above each figure. North to the right side of the figure. Contour interval is 1°C, with bold contours every 2°C. Positions of the stations are marked on the top of the figure. Top panel shows top 1000 m of the water column and bottom panel from 1000 to 3000 m. Temperature scale is the same for both panels.

west edge of the plateau, and ii) the behaviour of the SAF in response to the Campbell Plateau bathymetry.

The distinction of the northern, middle and southern branch of the SAF are unclear in these transects, as the different branches are merged due to the bathymetry of the Campbell Plateau, forming a strong gradient with the isotherms outcropping at the surface. During March 2007 the SAF-N was crossed at approximately 55.3°S , between Stations 68 and 69, followed by the SAF-M at 55.45°S between Stations 67 and 68, then the SAF-S at 55.9°S followed by the Polar Front crossed at 56°S . In the May 1998 transect, the fronts were more separated, although still close together, the SAF-N was crossed at 55.2°S near Station 38, the SAF-M at 55.4°S south to Station 39. However, the SAF-S and Polar Front were both found further south, the SAF-S at 55.9°S south to Station 40 and the Polar Front at approximately 56.5°S .

The surface layer in the northern edge of the March 2007 transect is warmer and more stratified than May 1998, due to the greater insolation at the beginning of Autumn and less cooling to the atmosphere in May. There is a well developed mixed layer from the surface to approximately 500 m. At the southern edge of both transects a surface layer of cold and fresh AASW is sitting above a layer of AAIW. Below there is a layer of CDW to the bottom of the water column.

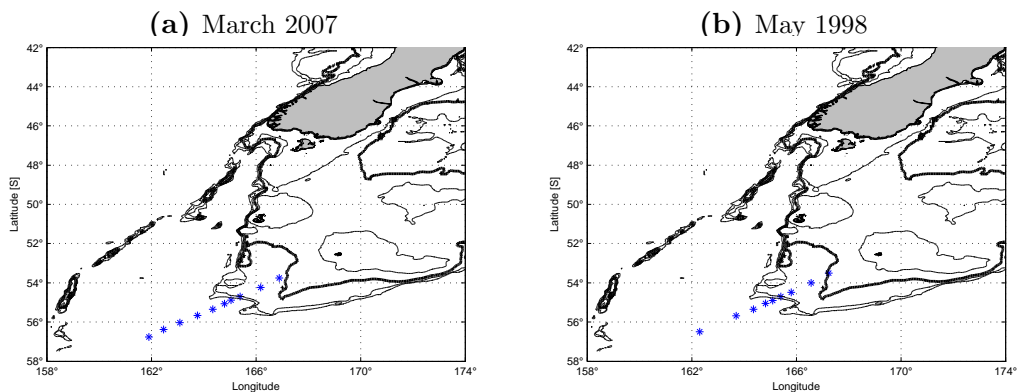


Figure 3.12: Hydrographic stations (blue) east of Macquarie Ridge transects, (a) TAN0708 and (b) TAN9806. Contours every 500 m, bold contour show 1000 m isobath.

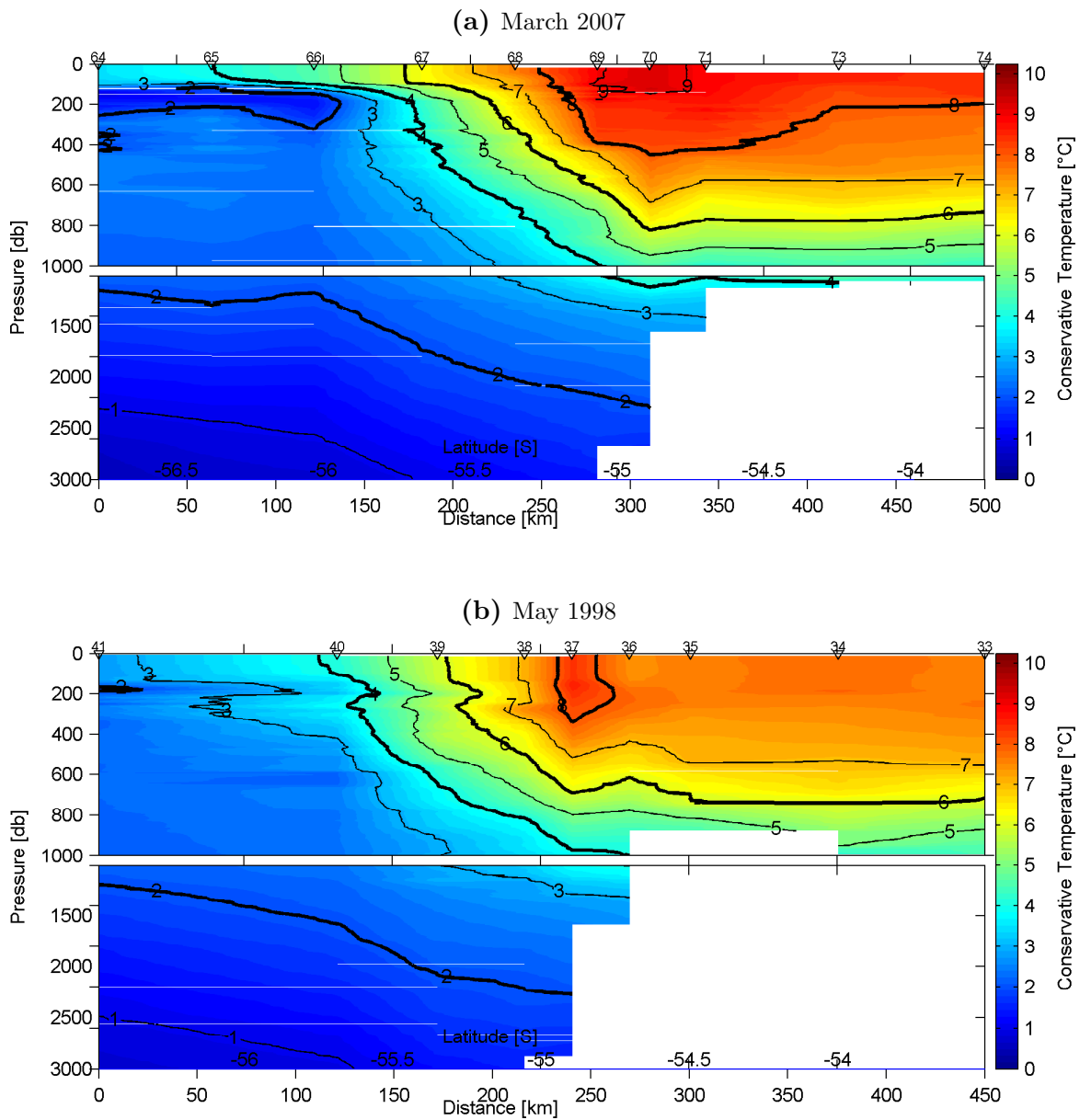


Figure 3.13: Conservative temperature sections east of Macquarie Ridge. Labels are above each figure. North to the right side of the figure. Contour interval is 1 °C, with bold contours every 2 °C. Positions of the stations are marked on the top of the figure. Top panel shows top 1000 m of the water column and bottom panel from 1000 to 3000 m. Temperature scale is the same for all the panels.

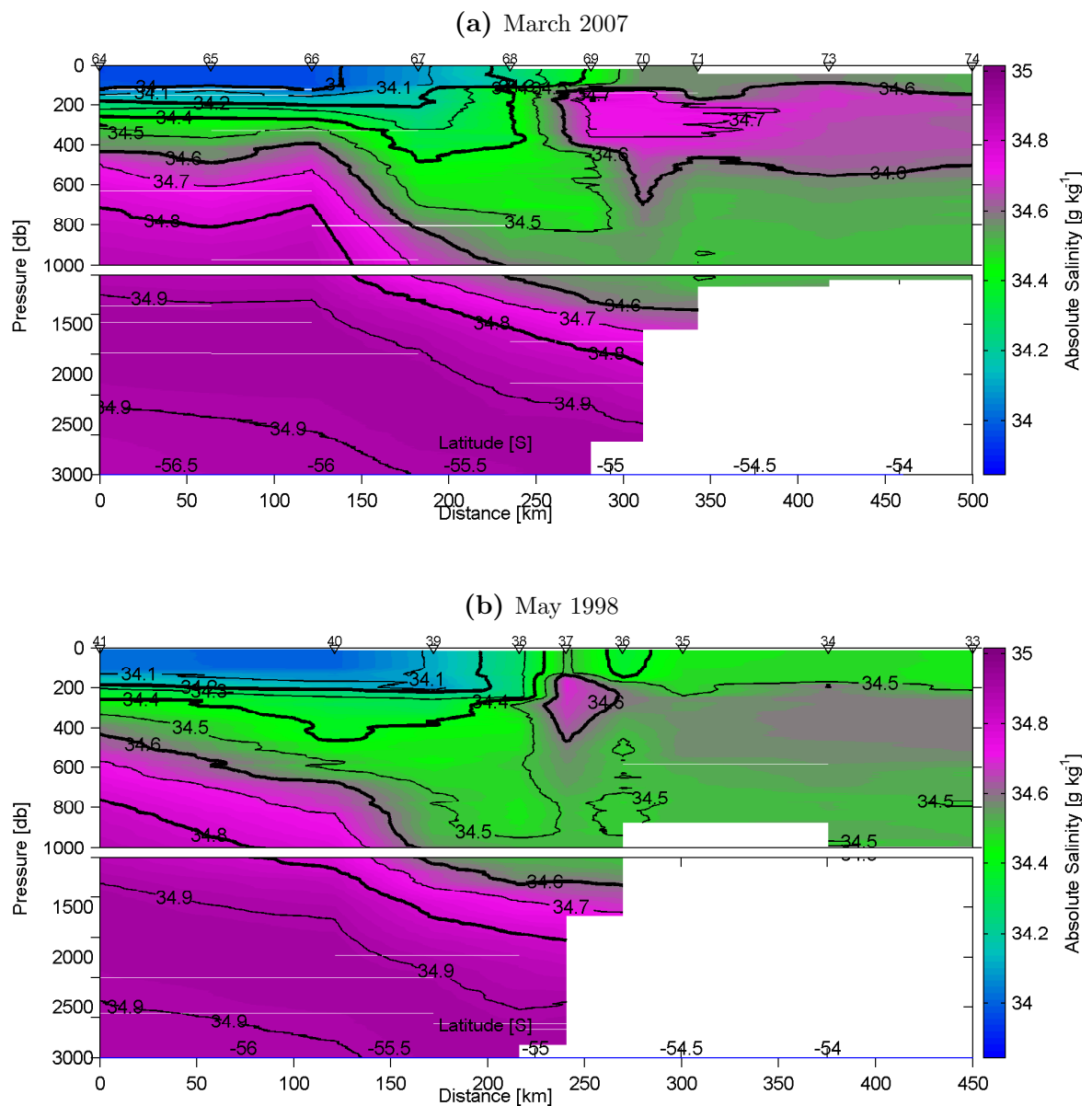


Figure 3.14: Absolute salinity sections east of Macquarie Ridge. Labels are above each figure. North to the right side of the figure. Contour interval is 0.1 g kg^{-1} , with bold contours every 0.2 g kg^{-1} . Positions of the stations are marked on the top of the figure. Top panel shows top 1000m of the water column and bottom panel from 1000 to 3000 m. Salinity scale is the same for all the panels.

Snares Depression transects

The Snares Depression transects were carried out in Autumn, during April 2011 and March 2013, from north of the Auckland Islands through the Snares Depression to the Snares shelf (Figure 3.15). The April 2011 transect was previously presented in Smith et al. (2013), however, it is shown here for completeness. The S-STF was crossed in the March 2013 transect at the same position as reported by Smith et al. (2013) in April 2011, that is at approximately 49.2°S, between Stations 83 and 84. This is clear in both temperature and salinity transects (Figure 3.16b and Figure 3.17b). The surface layer is warmer in the March transect presumably because it is earlier in the season compared to the April counterpart, however, the subsurface layer (from 150 to 600 m depth) is colder in March 2013 than in April 2011. This is also seen in the salinity transects where there is a fresh body of water between Stations 81 and 83 (Figure 3.17b). The high salinity core of STW identified by Smith et al. (2013) (Figure 3.17a) is also seen for the March 2013 transect but with a stronger gradient. The gradients for the S-STF in these transects are strong, with the isolines outcropping at the surface.

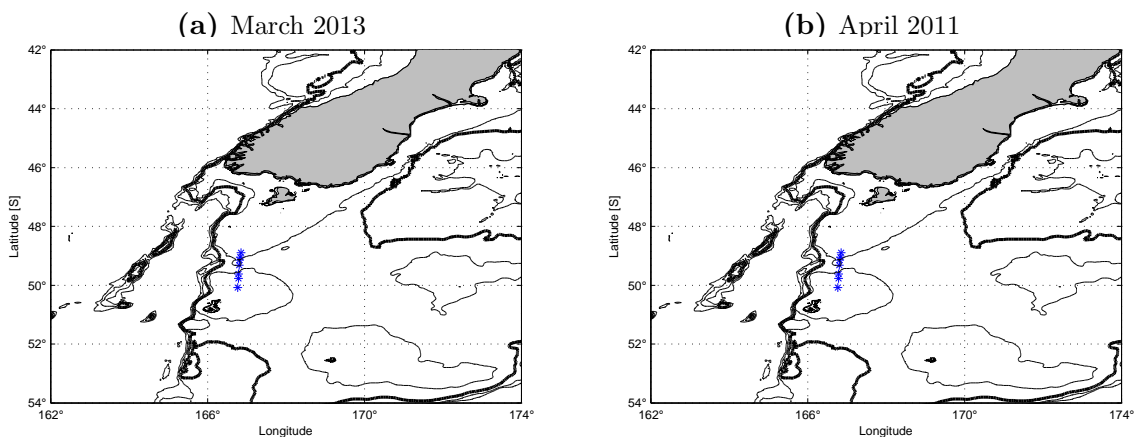


Figure 3.15: Hydrographic stations (blue) crossing the Snares Depression, (a) TAN1302 and (b) TAN1106. Contours every 500 m, bold contour show 1000 m isobath.

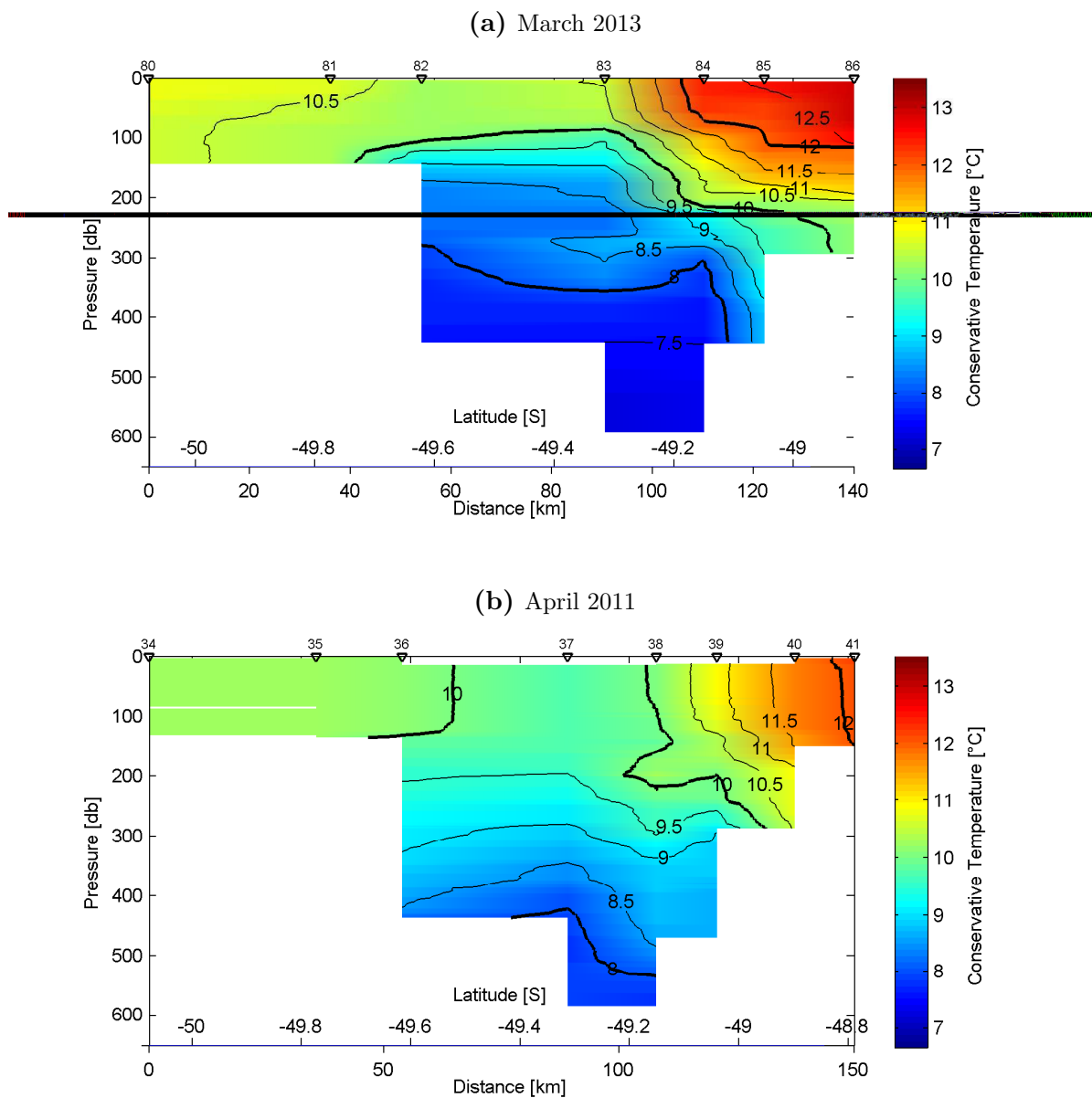


Figure 3.16: Conservative temperature sections across Snares Depression. Labels are above each figure. North to the right side of the figure. Contour interval is 0.5°C , with bold contours every 2°C . Positions of the stations are marked on the top of the figure. Temperature scale is the same for all the panels.

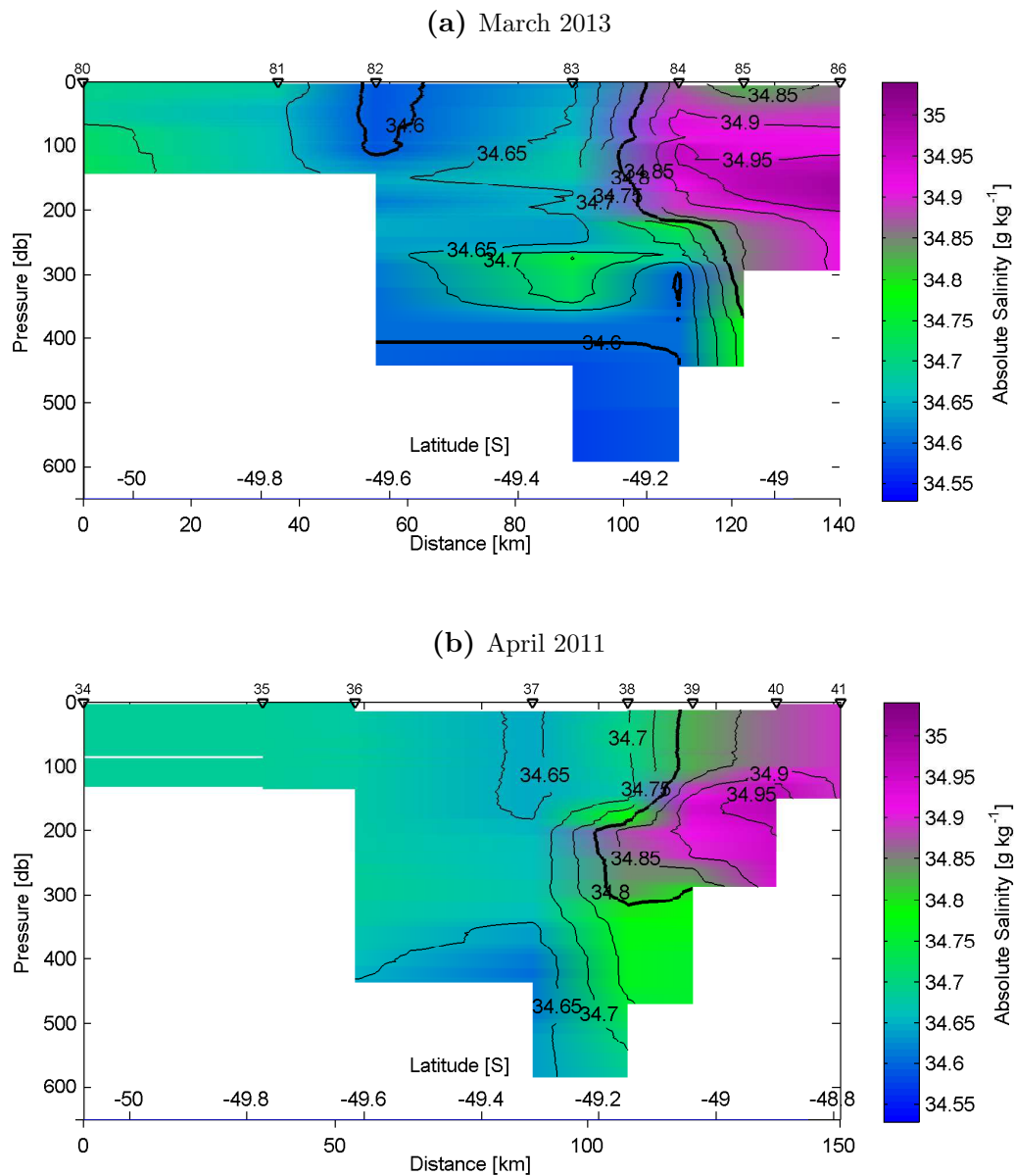


Figure 3.17: Absolute salinity sections across Snares Depression. Labels are above each figure. North to the right side of the figure. Contour interval is 0.05 g kg^{-1} , with bold contours every 0.2 g kg^{-1} . Positions of the stations are marked on the top of the figure. Salinity scale is the same for all the panels.

Campbell Plateau transects

Four transects were taken across the Campbell Plateau during May 1998, December 1998, August 1999 and May 2003. The transects go from the southeast of the New

Zealand coast, across the Campbell Plateau to the Subantarctic Slope (Figure 3.18).

The first three occupied the full transect but the last covered the western end only. The first three transects were first presented by Morris et al. (2001). The timing of the transects helps identify the seasonal structure of the plateau, with transects in late autumn (May), the middle of winter (August) and the beginning of summer (December). The aim of this seasonal sampling is to assess any delayed effects of the previous season in the May and December transects, but also the full effect of winter in the August transect. Interannual variability can also be seen in the two May transects.

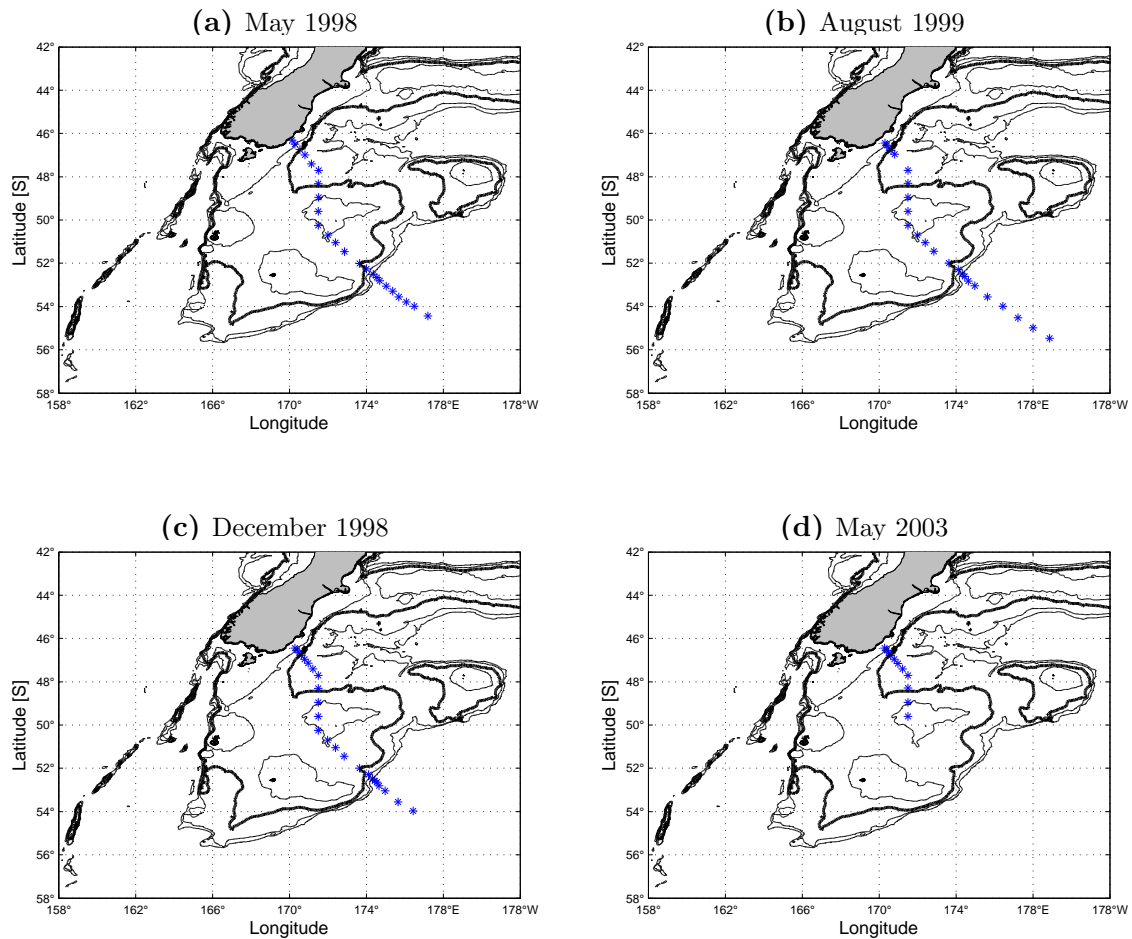


Figure 3.18: Hydrographic stations (blue) for the Campbell Plateau transects, (a) TAN9806, (b) TAN9909, (c) TAN9814 and (d) TAN0307. Contours every 500 m, bold contour show 1000 m isobath.

The northern edge of the May 1998 and December 1998 transects were previously presented by Sutton (2003) to investigate the Southland Current. All cruises show the Southland Front which is the local expression of the STF (e.g., Chiswell, 1996; Sutton, 2003), and the associated strong horizontal gradients in temperature and salinity (Figure 3.19 and Figure 3.20). There is no subsurface high salinity tongue, as seen in the previous upstream transects (Figure 3.11). The signal of the STF reaches approximately 400 m deep.

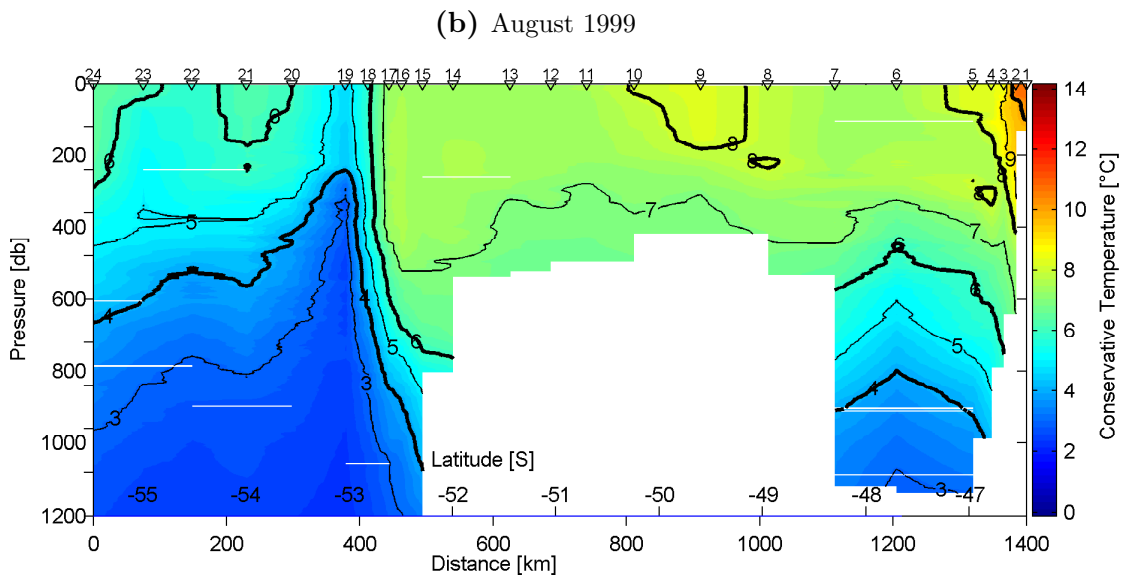
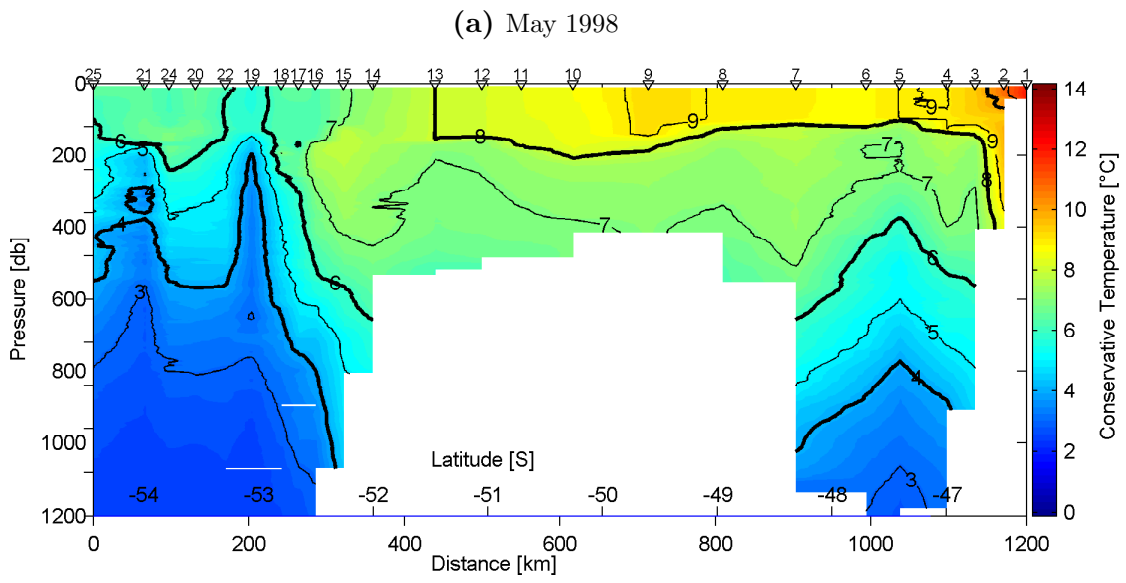
At the southern edge of the plateau only two branches of the SAF can be identified. This is consistent with the idea of the SAF flow being divided into two branches, east of the Campbell Plateau (Orsi et al., 1995; Belkin and Gordon, 1996; Gille, 2003; Stanton and Morris, 2004; Sokolov and Rintoul, 2007a). The May 1998, August 1999 and December 1998 transects were long enough to cross the SAF. In May 1998 the SAF-N is crossed at 52.5°S followed by the SAF-M at 52.9°S. During the December 1998 and August 1999 transects the fronts are so close together they become one. This is noted by stronger gradients in temperature and fresh and colder surface water in the southern extreme of the transects. The SAF was crossed at 52.6°S in December 1998 and at 53.95°S during May 1998. The surface layer starts to homogenise in May, at the end of autumn. A well mixed layer over the plateau is shown in the winter transect (Figure 3.19b). In contrast a stratified surface layer develops at the beginning of summer (Figure 3.19c). The cycle starts again with the mixing of the stratification layer in May 2003 (Figure 3.19d).

LCDW occurs over the southern limit of the transects in the deepest stations. This is characterized by a maximum in salinity given by North Atlantic Deep Water (NADW) (Morris et al., 2001; Sokolov and Rintoul, 2002; Talley et al., 2011). The bottom water seen on the deepest stations on the southern extreme of the transects has the same properties as the water found at the same depth in the northern extreme of the transects.

Over the plateau, from the surface to approximately 500 m, a homogeneous weakly stratified body of water with a temperature of 7°C is found in all the transects. These are values characteristic of SAMW in the Southwest Pacific Basin (Morris et al., 2001).

During summer (December 1998) and autumn (May 1998, May 2003), a surface layer of warmer water forms. This is due to the response of the ocean to the air-sea interaction, with greater insolation and reduced winds. December has a well developed stratified layer (Figure 3.19c) and during the May transects (Figure 3.19a and Figure 3.19d) this layer disappeared with the end of autumn, due to cooling to the atmosphere and increased windiness. In winter this layer disappeared, leaving a well mixed ocean (Figure 3.19c). It is worth noting that May 2003 was warmer than May 1998 (Figure 3.19d and Figure 3.19a), with a surface layer of 10 °C to 11 °C while in May 1998 the layer only reached 8 °C to 9 °C.

The Southland Front is identified by salinity $>34.7 \text{ g kg}^{-1}$ on the coastal side of the transects (Figure 3.20). In most of the plots this water is constrained close to the coast, but in May 2003, this signal was more of a little tongue that extended into the sub-antarctic water. There are some similarities to August 1999. The SAF is identified by vertical isohalines, between 52.5° to 52.8°S, which separate fresher water to the south from the plateau water. This is quite uniform with a salinity subsurface signal of around 34.5 g kg^{-1} , representing SAW.



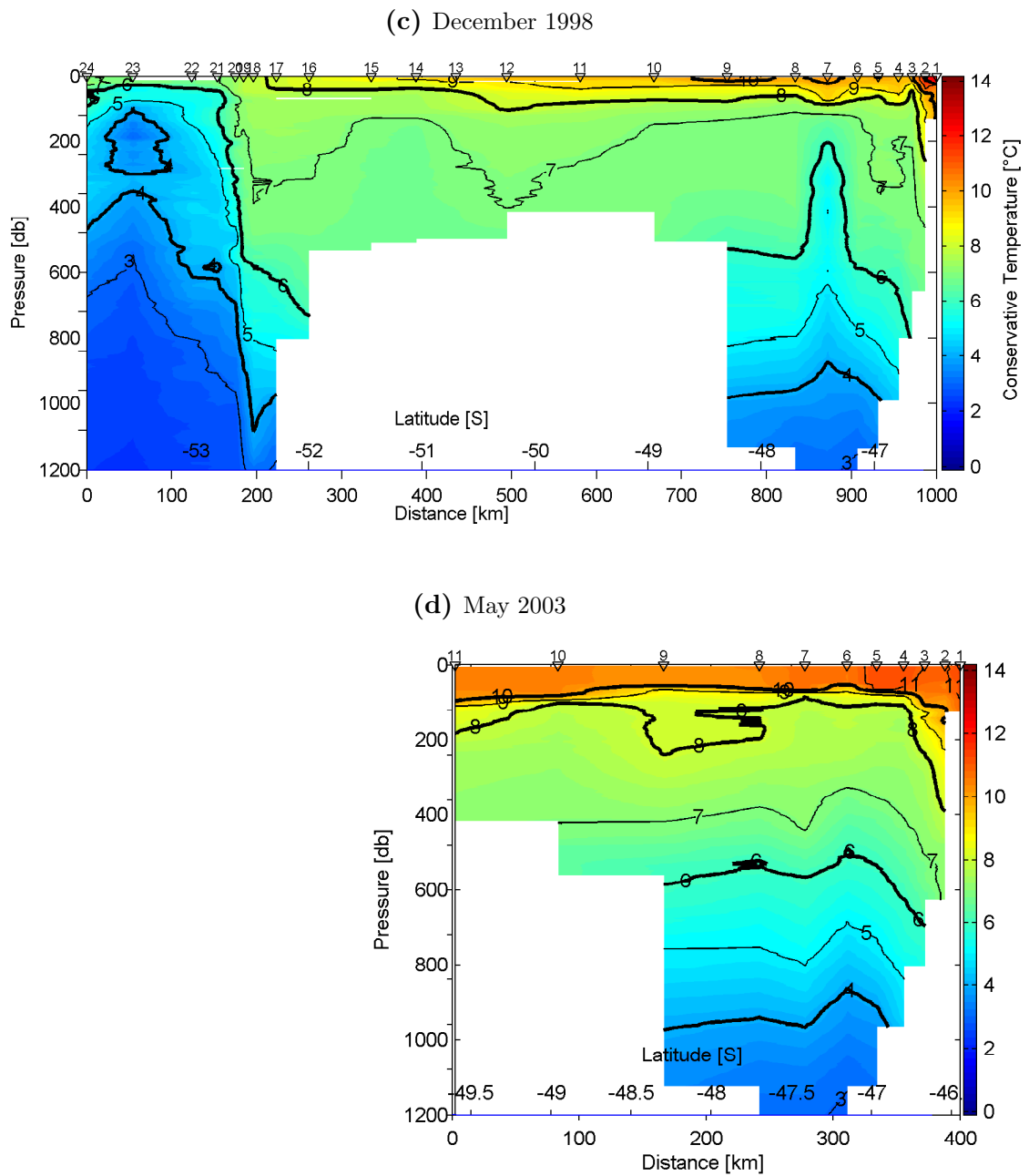
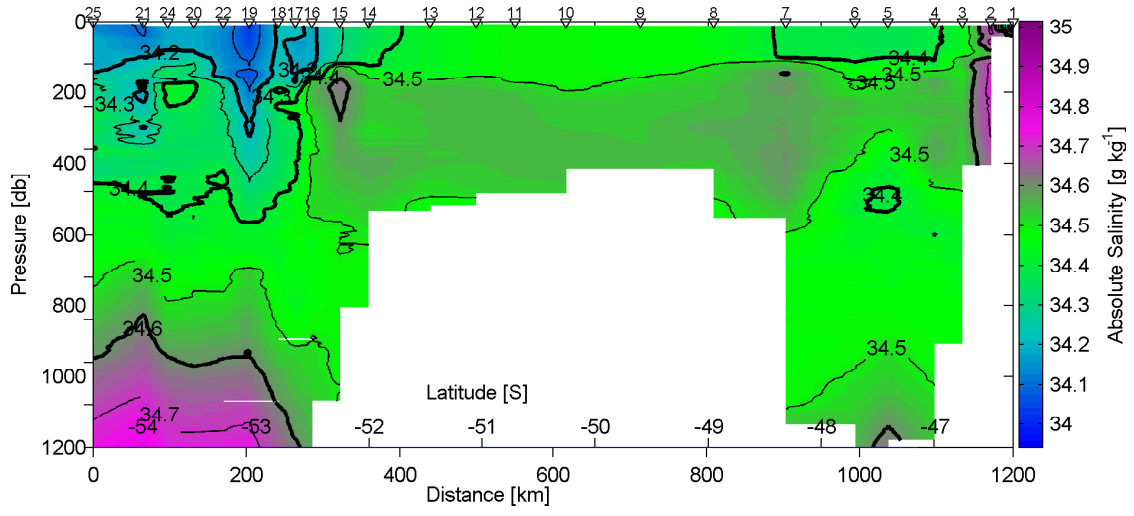
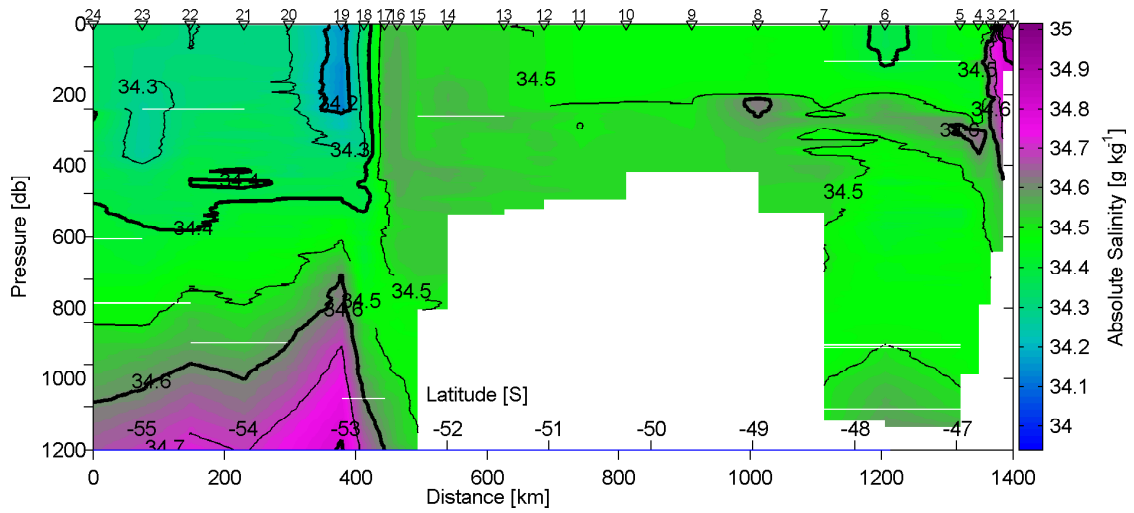


Figure 3.19: Conservative temperature sections over the Campbell Plateau. Labels are above each figure. North to the right side of the figure. Contour interval is $0.5\text{ }^{\circ}\text{C}$, with bold contours every $2\text{ }^{\circ}\text{C}$. Positions of the stations are marked on the top of the figure. Temperature scale is the same for all the panels.

(a) May 1998



(b) August 1999



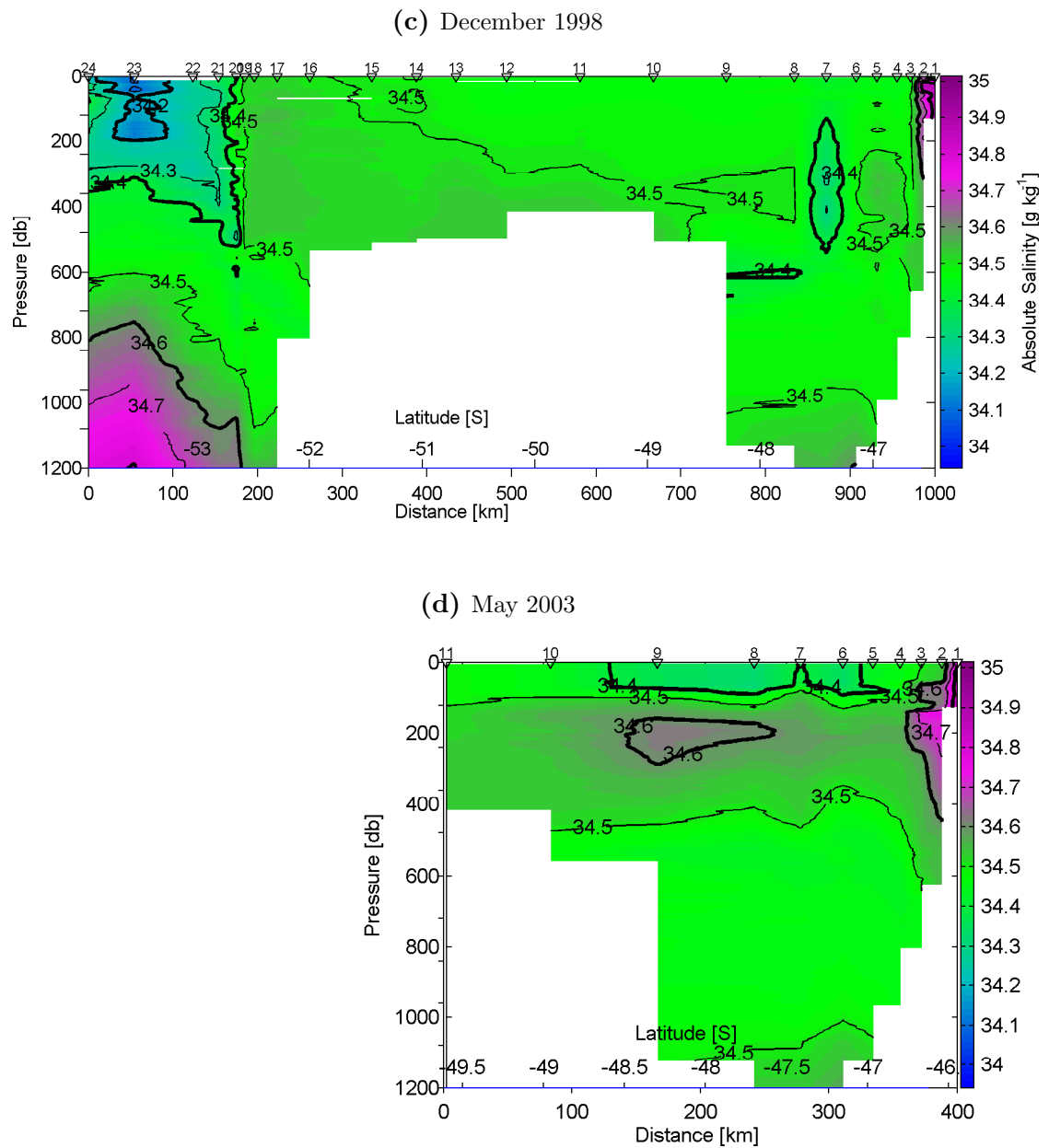


Figure 3.20: Absolute salinity sections along the Campbell Plateau. Labels are above each figure. North to the right side of the figure. Contour interval is 0.1 g kg^{-1} , with bold contours every 0.2 g kg^{-1} . Positions of the stations are marked on the top of the figure. Salinity scale is the same for all the panels.

Pukaki Saddle transect

A transect across the Pukaki Saddle was carried out in May 2003 (Figure 3.21) starting from the Campbell Plateau eastward across Pukaki Saddle and Bounty Plateau towards Bollons Seamount. Parts of this transect were first presented by Griffith et al. (2010) who reported two different types of SAMW, a warmer and saltier type over Pukaki Rise and southeast to the Bounty Plateau and a fresher and colder type in the Pukaki Saddle. However, a different interpretation is made here: the warm surface layer on the western side of the transects is STW on top of the Campbell Plateau, with a layer of SAMW underneath it, lying between the depths of 100 to 500 m over the plateau; the water in the Pukaki Saddle is a weak expression of the SAF, between Stations 39 and 41, which is supported by a layer of colder and fresher SAW between Stations 18 and 41; and the warmer and saltier water found on the eastern transect is possibly related to a warm eddy structure. A similar structure was reported east of the Bollons Seamount by Williams (2004) during June 2001.

A subsurface salinity maximum is, however, found under the fresh and cold water in the Pukaki Saddle (Stations 17 to 26), between 100 and 400 m depth. AAIW and CDW are found in the deeper stations through the gap between the Bounty Plateau and Bollons Seamount.

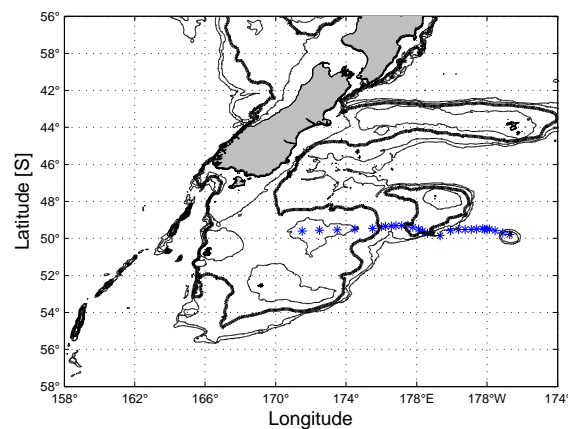


Figure 3.21: Hydrographic stations along the Pukaki Saddle and Bollons Seamount, TAN0307. Contours every 500 m, bold contour show 1000 m isobath.

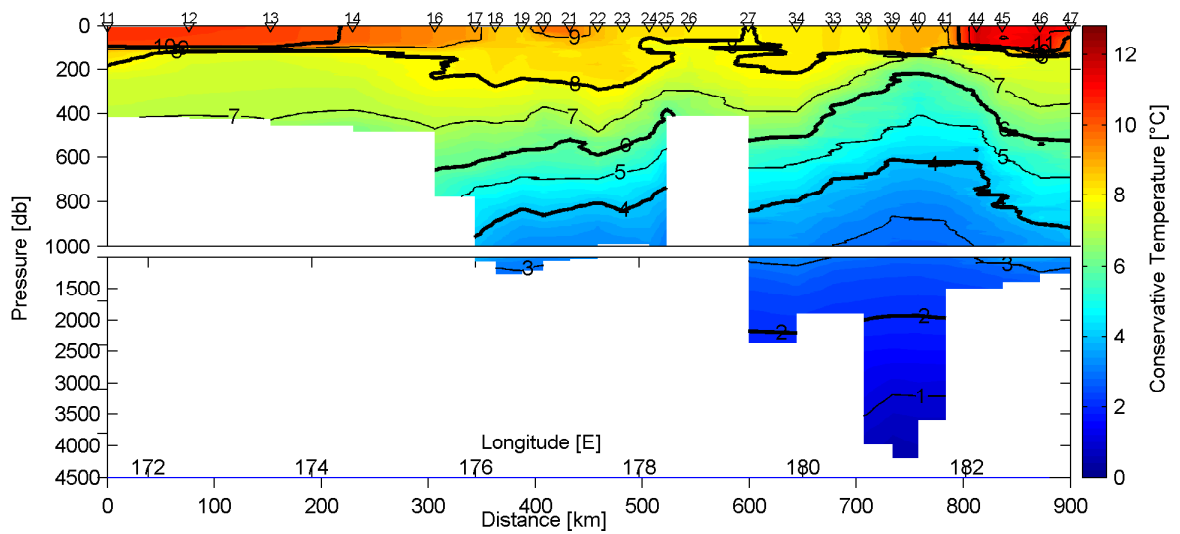


Figure 3.22: Conservative temperature section across the Pukaki Saddle. Contour interval is 1 °C, with bold contours every 2 °C. Positions of the stations are marked on the top of the figure. East to the right of the figure. Top panel shows the top 1000 m of the water column and bottom panel from 1000 to 4000 m.

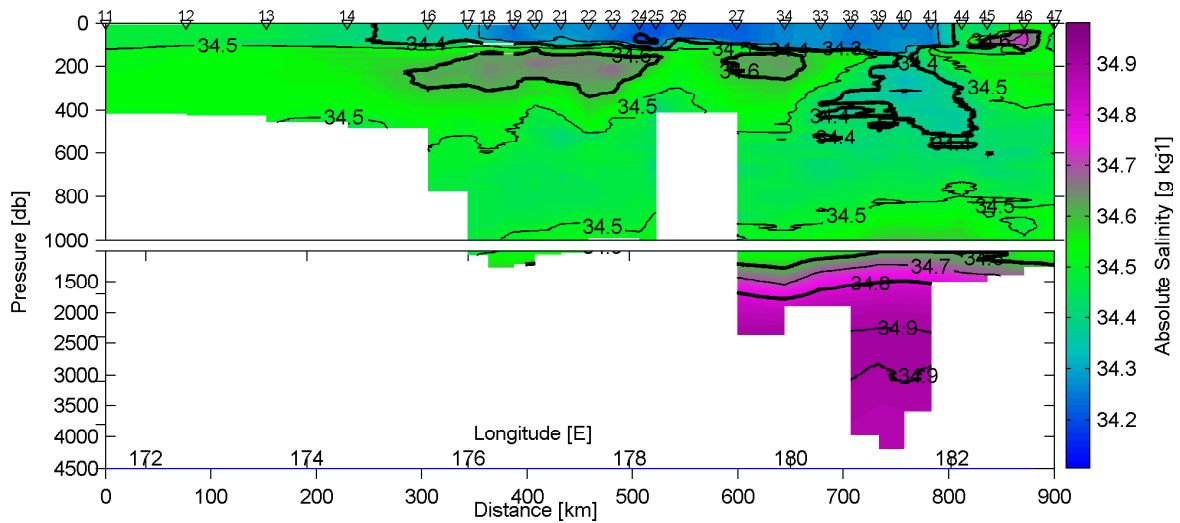


Figure 3.23: Absolute Salinity section across the Pukaki Saddle. Contour interval is 0.1 g kg⁻¹, with bold contours every 0.2 g kg⁻¹. Positions of the stations are marked on the top of the figure. East to the right of the figure. Top panel shows the top 1000 m of the water column and bottom panel from 1000 to 4000 m.

Bounty Trough transects

Transects run southeast across the Bounty Trough from the east coast of the South Island, across the Bounty Plateau and south into the SW Pacific Basin (Figure 3.24). The transects are presented in seasonal order, beginning with the summer (December) then winter (June-August), to show the seasonality. The December and June transects run to approximately 52°S but the August transects extended further south, to 55°S.

The Southland Current is close to the coast and is represented by strong horizontal gradients in temperature and salinity. Stratified warm ($>14^{\circ}\text{C}$) surface water close to the coast in the summer (Figure 3.25a) is followed by a more homogeneous mixed layer in the winter months (Figure 3.25b and 3.25c). A tongue of high salinity water ($>34.6\text{ g kg}^{-1}$) occurs in all the salinity transects from the surface to approximately 500 m. This is similar to those reported by Chiswell (1996).

Two branches of the SAF were crossed in all the transects, between 49.5°S and 50°S, however, the SAF expression in the June 2001 transect is weaker. A fresh and cold surface layer with the characteristics of SASW is seen south of the SAF, and a salinity subsurface maximum is identified in June 2001 in the SAF (Figure 3.26b). During August 1999, in the longest transect, a cold core eddy is found at the southern end of the transect, at 54°S (Figure 3.25c) (this can be confirmed by SSH and geostrophic velocities).

AAIW, UCDW and salty and cold LCDW are found from 900 m depth to the bottom of the water column on both sides of the Bounty Plateau.

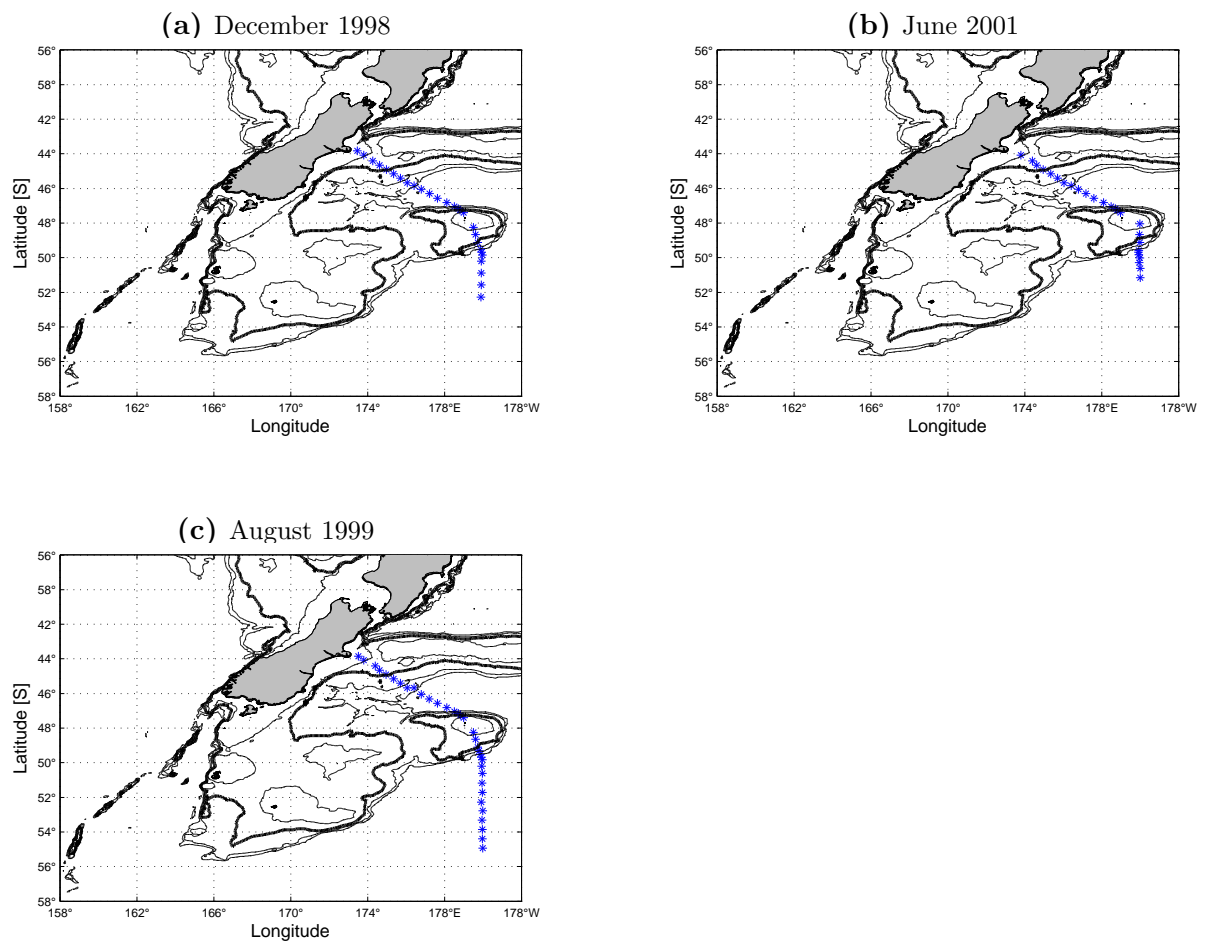


Figure 3.24: Hydrographic stations (blue) for the Bounty Trough transects, (a) TAN9814, (b) TAN0108 and (c) TAN9909. Contours every 500 m, bold contour show 1000 m isobath.

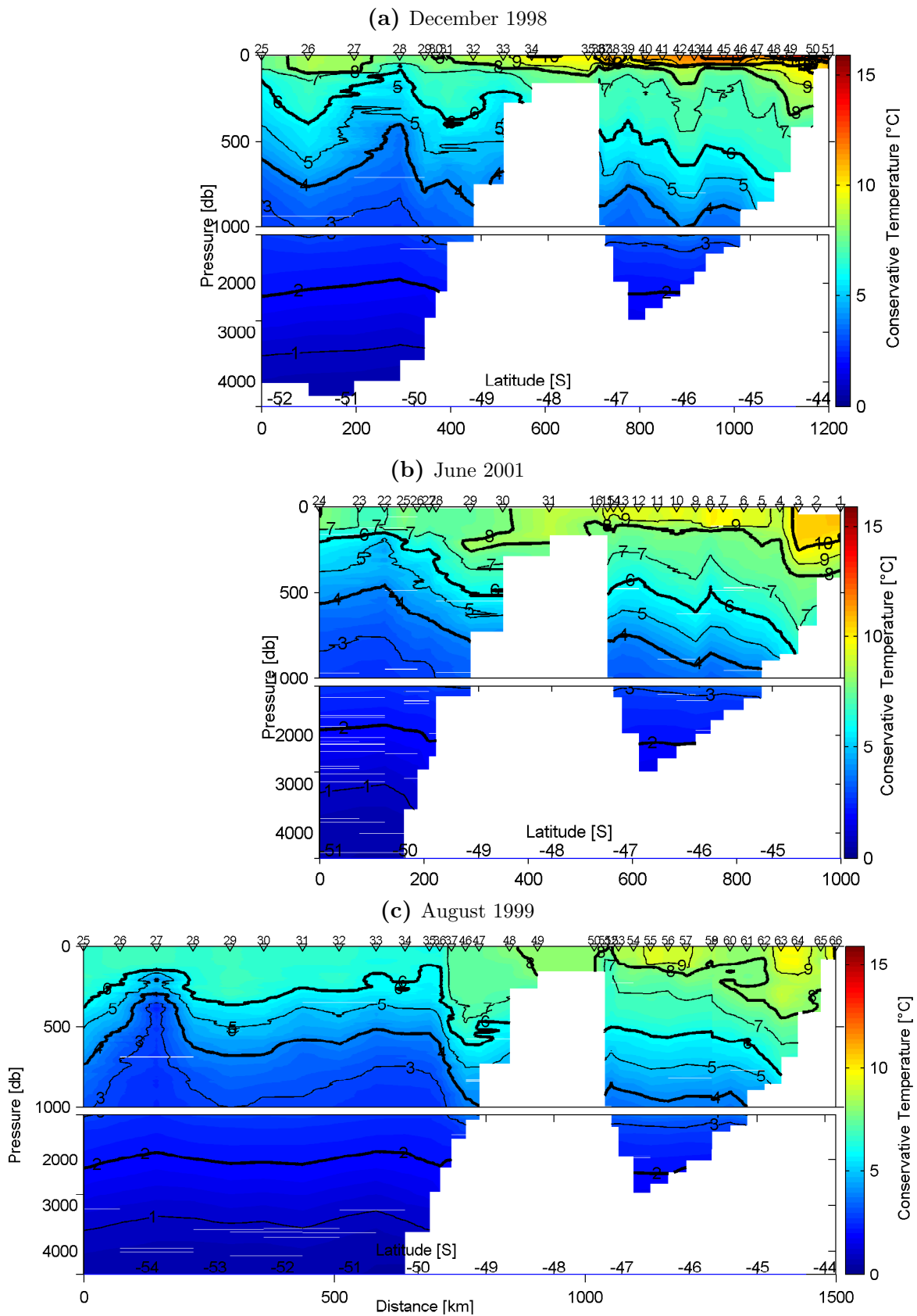


Figure 3.25: Conservative temperature sections over the Bounty Trough. Labels are above each figure. North to the right side of the figure. Contour interval is 1 °C, with bold contours every 2 °C. Positions of the stations are marked on the top of the figure, distance in km on the bottom of the figure. Top panel shows the top 1000 m of the water column and bottom panel from 1000 to 4500 m. Temperature scale is the same for all the panels.

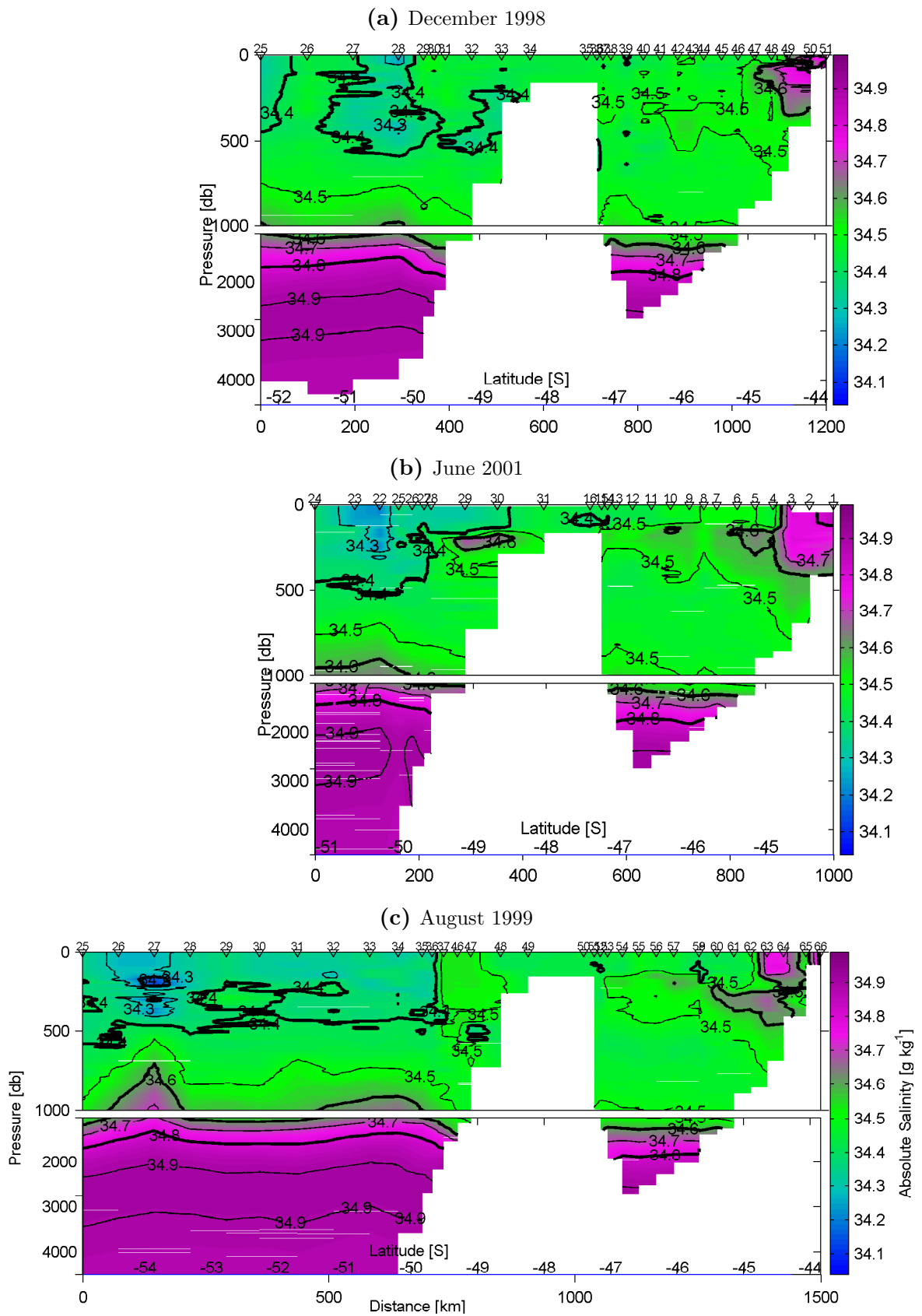


Figure 3.26: Absolute salinity sections along the Bounty Trough. Labels are above each figure. North to the right side of the figure. Contour interval is 0.1 g kg^{-1} , with bold contours every 0.2 g kg^{-1} . Positions of the stations are marked on the top of the figure, distance in km on the bottom of the figure. Top panel shows the top 1000 m of the water column and bottom panel from 1000 to 4500 m. Salinity scale is the same for all panels.

3.2.2 Water mass analysis

As described in Chapter 2, a water mass is a body of water that has a common formation process (e.g., Talley et al., 2011). Θ - S_A (conservative temperature-absolute salinity) diagrams are a useful tool to identify water masses, as they clearly show the different combinations of temperature and salinity properties (e.g., Talley et al., 2011). For the Θ - S_A diagrams the transects were divided into different sections, with each section addressing a particular feature of the area. For example, for the Campbell Plateau and Bounty Trough analysis the different sections were: the Subtropical Front (STF), the Campbell Plateau, the Subantarctic Front (SAF) and Polar Front (PF). The algebraic mean was then calculated over the conservative temperature and absolute salinity of each group of stations. Then Θ - S_A diagrams are shown for selected transects and voyages.

Θ - S_A diagrams are presented as a way of summarizing (i) interannual variability, (ii) seasonal variability between repeated transects and (iii) the overall oceanographic structure of the Campbell Plateau region.

Macquarie Ridge

Θ - S_A diagrams for Macquarie Ridge transects show two distinctive water masses at the surface that merge with depth (Figure 3.27a and Figure 3.27b). Salty ($>35 \text{ g kg}^{-1}$) and warm ($>12^\circ\text{C}$) STW is found at the surface in both years in the northern part of the transects (grey dots). Fresher ($<34.2 \text{ g kg}^{-1}$) and colder, 4°C to 6°C , AASW can be found at the surface of the southern side of the transects (green dots). Below the density layer of 27.5 kg m^{-3} , UCDW and LCDW is found in both profiles, with a temperature of around 2.5°C . The extra leg in March 2007 (purple dots Figure 3.27a) shows very similar properties to the upstream leg (green dots Figure 3.27a), but is colder at the surface and warmer in the bottom part of the profile. Both profiles, March 2007 and April 2008, are similar.

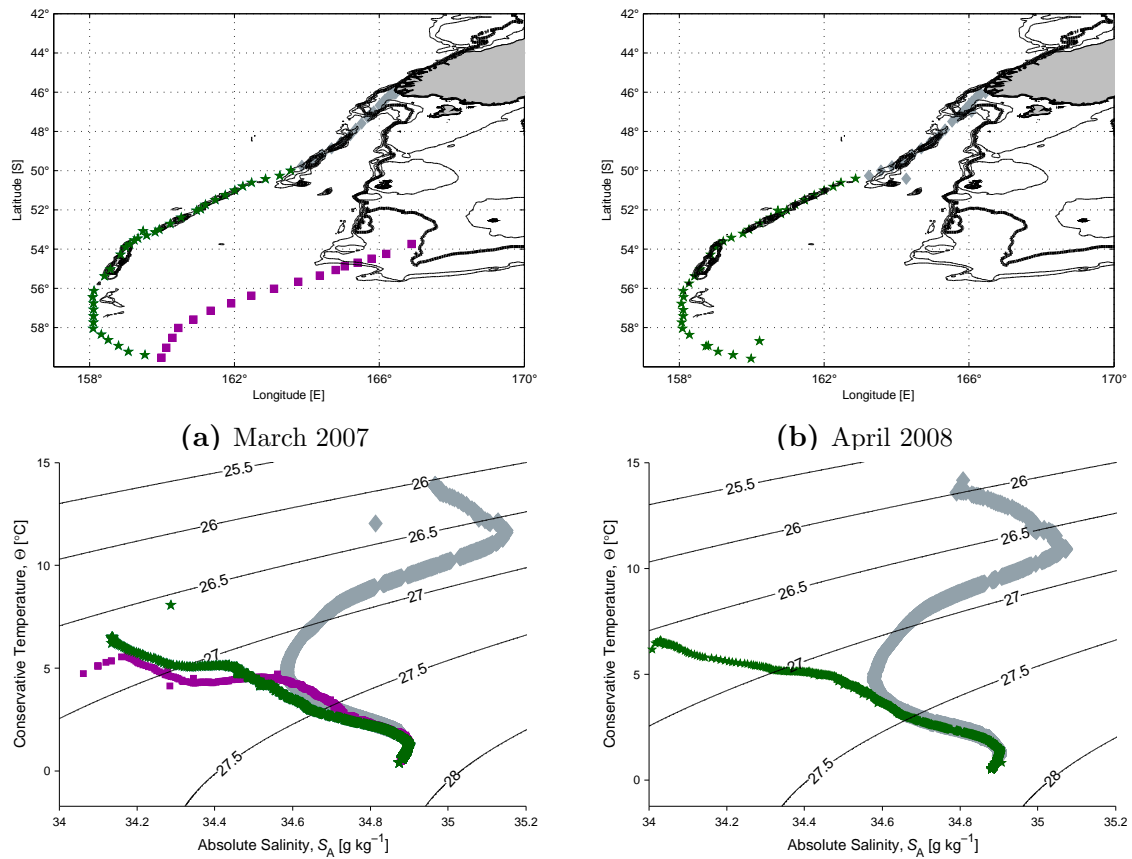


Figure 3.27: (a) Station locations map taken during March 2007 and (b) April 2008. Conservative temperature [°C] versus absolute salinity [g kg⁻¹] for Macquarie Ridge transects, bottom panels. Transects are divided in STF section (grey dots), Macquarie Ridge section (green dots) and downstream section (purple dots). Contours are potential density [kg m⁻³] referenced to 0 dbar

Campbell Plateau and Bounty Trough transects

Two series of transects, across the Campbell Plateau and the Bounty Trough, one at the beginning of summer (December) and the other in mid-winter (August) are presented (Figure 3.28a and Figure 3.28d).

In the summer (Figure 3.28b), the Campbell Plateau transect shows a stratified surface layer in the STF Stations (grey diamonds) and the Campbell Plateau Stations (blue stars). On the STF Stations the water is warmer and saltier at the surface showing the

influence of the STW. The Campbell Plateau stations (blue stars) are confined between the 26.5 kg m^{-3} to 27 kg m^{-3} density layers, and show a salinity maximum (approximately 34.55 g kg^{-1}) at the bottom of the water column. The SAF Stations (orange dots) show cold and fresh SAW at the surface layer. STF and SAF profiles show similar water properties at the bottom of the water column, in water that has properties of CDW.

In the winter (Figure 3.28e), the surface stratification disappears in the STF Stations (grey diamonds) and the subsurface salinity maximum is slightly stronger. The Campbell Plateau stations show a well developed mixed layer with a salinity maximum identified in the summer profile. The SAF Stations show similar characteristics to the summer profile, with the surface layer not as warm as in summer.

During summer on the Bounty transect (Figure 3.28c) a stratified salty and warm surface layer associated with the STW in the Chatham Rise is denoted in the STF stations (grey dots). This is shown by temperatures reaching 15°C and salinities of 34.75 g kg^{-1} . Also, a distinct subsurface salinity maximum of 34.9 g kg^{-1} is associated with the Southland Front. This is similar to those previously reported by Chiswell (1996) and Sutton (2001). The Bounty Stations (blue squares), the Plateau Stations (pink stars) and the SAF Stations (orange stars) of the Bounty transect, show a similar surface structure, with a stratified surface layer, that gets colder and fresher towards the south. These features are similar in the Campbell Plateau transects. All profiles in the Bounty transect show a salinity peak above the 27 kg m^{-3} isopycnal (similar to the one seen in the Campbell Stations (blue stars) in the Campbell Plateau transect). They also show salinity minimums, with AAIW characteristics, that get more obvious towards the south. The bottom part of all the transects show CDW water.

In winter, the stratified layer disappears on the Bounty transect (Figure 3.28f), and the subsurface salinity maximum is weaker in the STF Stations (grey dots). The Bounty Stations (blue squares) and Plateau Stations (pink stars) still show the salinity peak and together with the SAF Stations (orange stars) they show the salinity minimum of the AAIW. In the deeper stations they all share the CDW.

Both transects share some properties within the seasons. Surface layers are modified by the season, with stratified water due to a greater insolation in the summer and developed mixed layer due to air-sea interaction in the winter. SAF Stations (orange dots and stars) in both transects are less variable, not only between transects but also between seasons. The salinity peak above the 27.0 kg m^{-3} density layer in the Campbell Plateau Stations (blue stars) coincides with the salinity maximum in the Bounty Stations (blue dots), suggesting a connection between the two zones. The salinity minimum associated with the AAIW is seen in the SAF Stations (orange), the Plateau Stations (pink), but is weaker in the Bounty Stations (blue squares), suggesting a connection between these areas. All the transects with deep stations share these CDW water properties.

In general, all of the transects show variability at the surface, influenced by the seasonal cycle. This is in contrast to the deeper stations, where water mass properties are very similar.

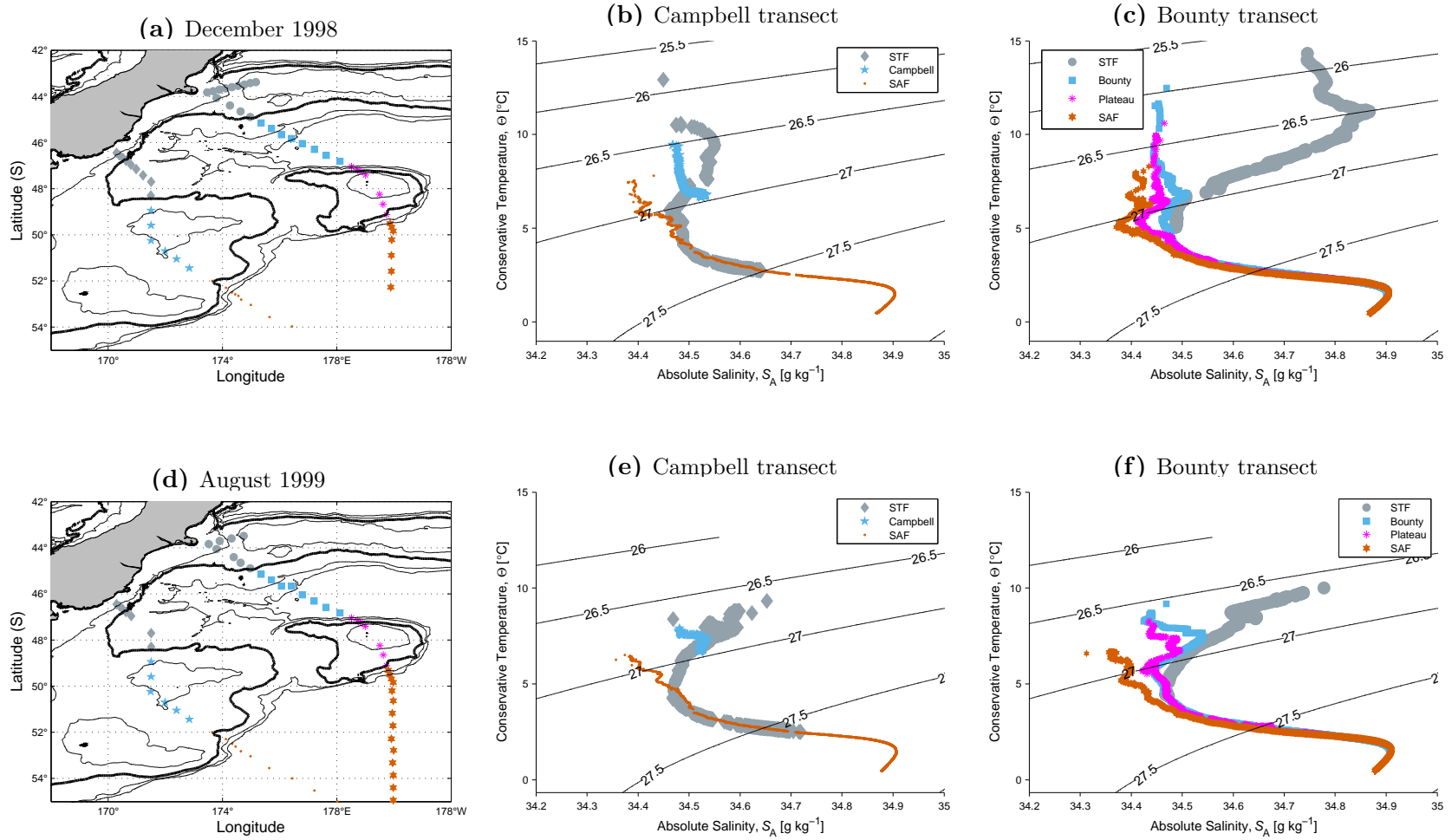


Figure 3.28: (a) Station locations map taken during December and (d) August. Conservative temperature [°C] versus absolute salinity [g kg⁻¹] for (b) and (e) Campbell Plateau transect and (c) and (f) Bounty Trough transects. Transects are divided into STF sections (grey dots), Campbell Plateau and Bounty Trough sections (blue dots), a Bounty Plateau section (pink dots) and a SAF section (orange dots). Contours are potential density [kg m⁻³] referenced to 0 dbar

Campbell Plateau transects

All of the water masses on and surrounding the Campbell Plateau are presented in a Θ - S_A diagram in Figure 3.29. These data are from a single cruise in May 1998 that includes the Solander Trough, Emerald Basin and Campbell Plateau transects, but does not include the Macquarie Ridge.

A nice transition between the different water masses is shown. Surface waters go from the warm and very salty surface water with characteristics of STW found in the Solander Trough section (black triangles) to the cold and fresh AASW ($<5^\circ\text{C}$ and $<34.2\text{ g kg}^{-1}$) south of the SAF (light green dots). The STW is modified when identified in the Southland Front section (green diamonds) due to mixing with SAW. A salinity maximum, associated with the STF occupies the middle section of all the profiles, with the exception of the profiles south of the SAF (orange dots, yellow triangles, blue crosses and light green dots). The two transects crossing the Campbell Plateau (blue stars and pink dots) show similar characteristics at the surface, however, the eastern section (blue stars) is fresher than the western transect (pink dots). Both have the same salinity maximum (around 34.6 g kg^{-1}), but the western section (pink dots) gets colder and saltier at the bottom while the eastern profile gets fresher and warmer at the bottom. This may suggest the different influences of water masses at the bottom of the plateau depending of the position of the stations.

The surface layers are different in the sections south of the SAF (orange dots, yellow triangles, blue crosses and light green dots) to the ones north of the SAF (all the other profiles). Approximately at the 27.0 kg m^{-3} density layer it appears that the differences between the profiles decrease, however, it is noticeable that the profiles between the south of the SAF and north of the SAF are those located north of the Campbell Plateau (green and grey diamonds). This might be due to the influence of the SAW in the Southland Current (Sutton, 2001). The two sections that cross the SAF (purple squares and orange dots) have a similar shape, but the upstream profile is saltier (purple squares), however, the salinity minimum peak related to AAIW is only seen in the eastern SAF

area (orange dots).

The bottom part of the profiles is shared amongst all the transects in CDW, with the exception of the Campbell Plateau, where stations are not deep enough.

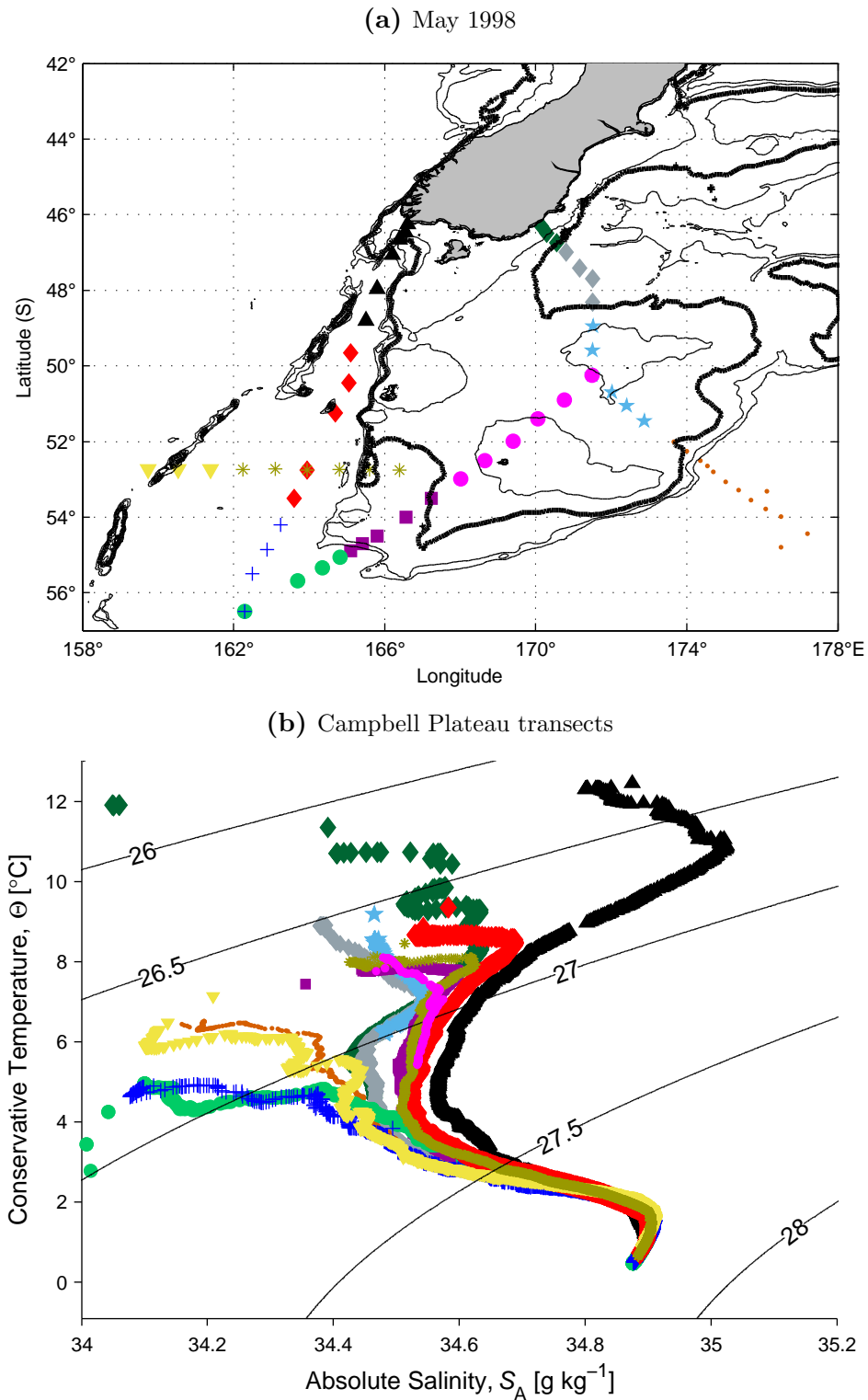


Figure 3.29: (a) distribution of Stations on May 1998. (b) Conservative temperature versus absolute salinity for Campbell Plateau transects. Colours indicate group of stations averaged, Solander Trough STF (black triangles), Solander Trough (red diamonds), Solander Trough SAF (blue crosses), Emerald Basin SAF (yellow triangles), Emerald Basin (brown stars), SAF south Campbell Plateau (green dots), south Campbell Plateau (purple squares), western Campbell Plateau (pink dots), eastern Campbell Plateau (blue stars), eastern SAF (orange dots) and Southland Front north of Campbell Plateau (grey diamonds). Contours are potential density [kg m^{-3}] referenced to 0 dbar.

3.2.3 Geostrophic velocities (general flow)

A general description of the subantarctic regional flow can be addressed by considering geostrophic velocity transects. Only a subset of transects are presented, with those chosen to illustrate the general circulation of the area.

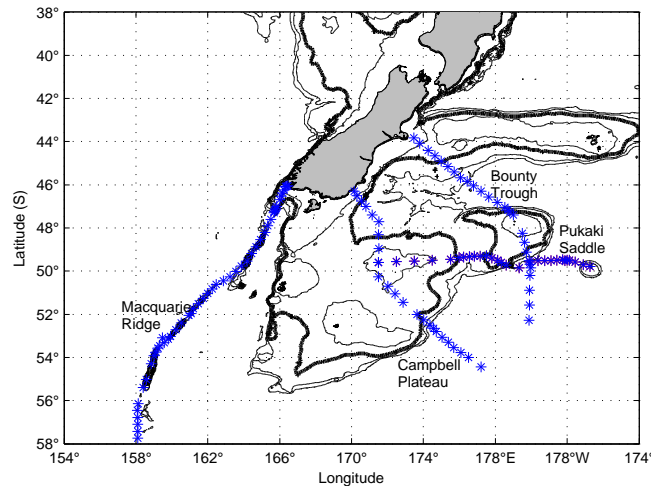


Figure 3.30: Hydrographic stations (blue) for the geostrophic velocity transects, Macquarie Ridge, Campbell Plateau, Pukaki Saddle and Bounty Trough. Contours every 500 m, bold contour show 1000 m isobath.

The stronger currents along the Macquarie Ridge transect occur in the bathymetry gaps as would be expected (Figure 3.31a). This is consistent with the transect in April 2008 (not shown), although in 2008 currents were slightly weaker. Through the 47°S gap the current flows westward through the whole water column. These results agree with those reported in Rintoul et al. (2014).

The Campbell Plateau transect shows the SAF flow as the main feature (Figure 3.31b), with its strong velocity core flowing along the steep Campbell Plateau flanks. This feature is consistent in all four transects, with stronger values in the winter transects (Figure 3.31c). The velocities are stronger close to the slope and weaken eastwards. At the edge of the transect, the current changes direction to a weak southwest flow. The core of the Southland Current bordering the western plateau is also present in all the

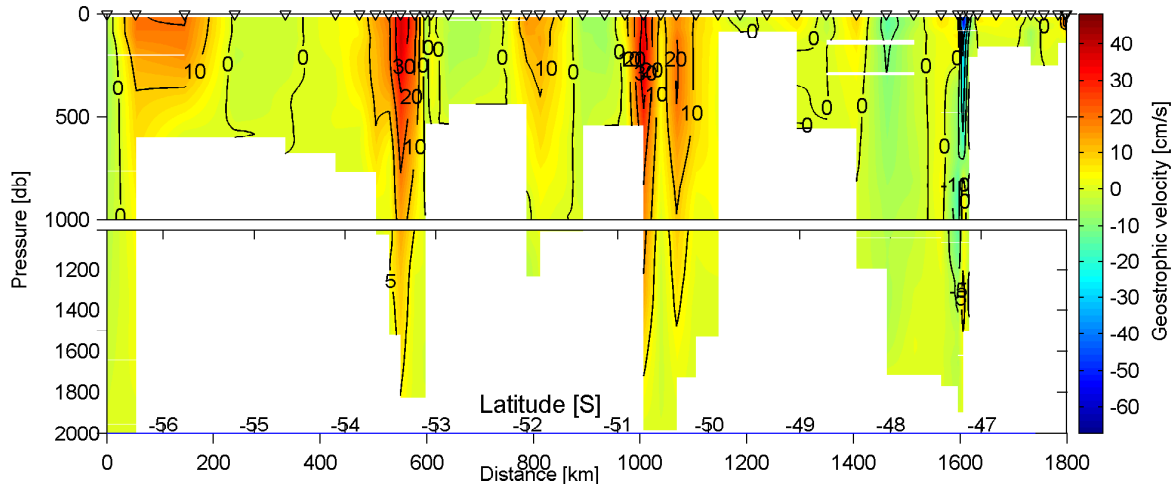
transects with possible recirculation to the south. All these features are consistent with those presented by Morris et al. (2001). There is also a weak current flowing in the opposite direction around 1500 to 2000 m depth that was also captured by the moorings presented by Stanton and Morris (2004).

The southern part of this transect was also documented by Stanton and Morris (2004). They showed a double core structure which is not evident here (Figure 3.31b). The southern edge of the May 1998 transect (not shown) was also presented by Stanton and Morris (2004), who revealed a second weak core further south of the main one, this is consistent with the results shown here. The winter one, August 1999 (Figure 3.31c) has a stronger SAF current and all the features are similar to those seen by Morris et al. (2001).

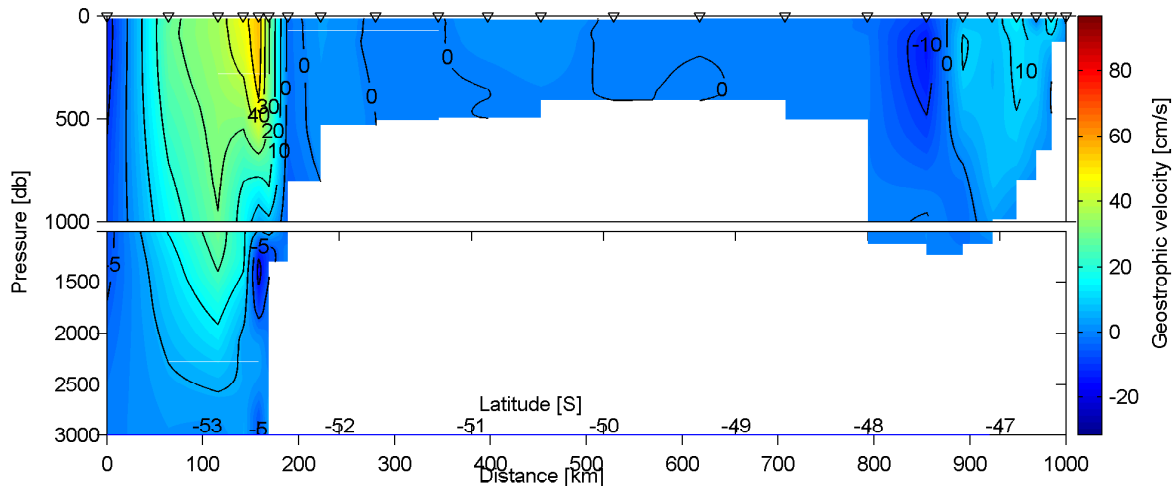
The velocity field in the Pukaki Rise transect has a complex circulation (Figure 3.31d). At the eastern extreme of the transect the cyclonic circulation is likely related to an eddy like structure identified in the temperature and salinity transects in Section 3.2.1 (Figures 3.22 and 3.23). A strong velocity core to the north, associated with the SAF, is found between the Bounty Plateau and Bollons Seamount from 400 m to the bottom of the water column, with the current in the opposite direction at the surface. From the Bounty Plateau towards the west, a group of similar cyclonic and anticyclonic eddy features are identified. This might be a gateway for the SAW to recirculate to the northern edge of the Campbell Plateau.

Velocities along the Bounty Trough transect reveal a strong flow associated with the SAF that follows the Campbell Plateau bathymetry (Figure 3.31e). It shows a weak recirculation with both southwest and northwest flow. On the western side of the transect a triple structure can be seen that is persistent along all the transects (also see Morris et al. (2001)). The strongest currents are again in winter (August 1999; Figure 3.31f) with velocities reaching 50 cm s^{-1} .

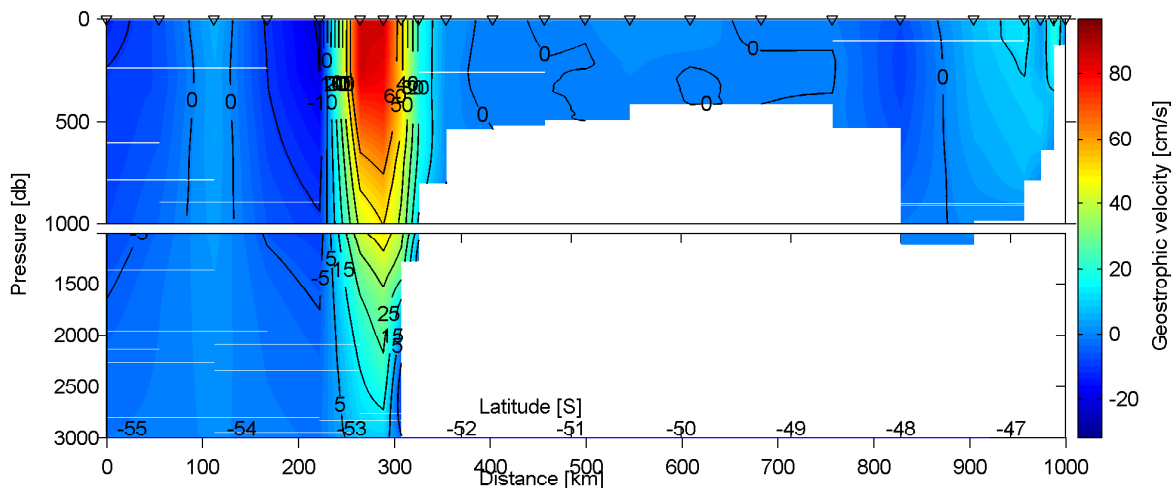
(a) March 2007. Macquarie Ridge



(b) December 1998. Campbell Plateau



(c) August 1999. Campbell Plateau



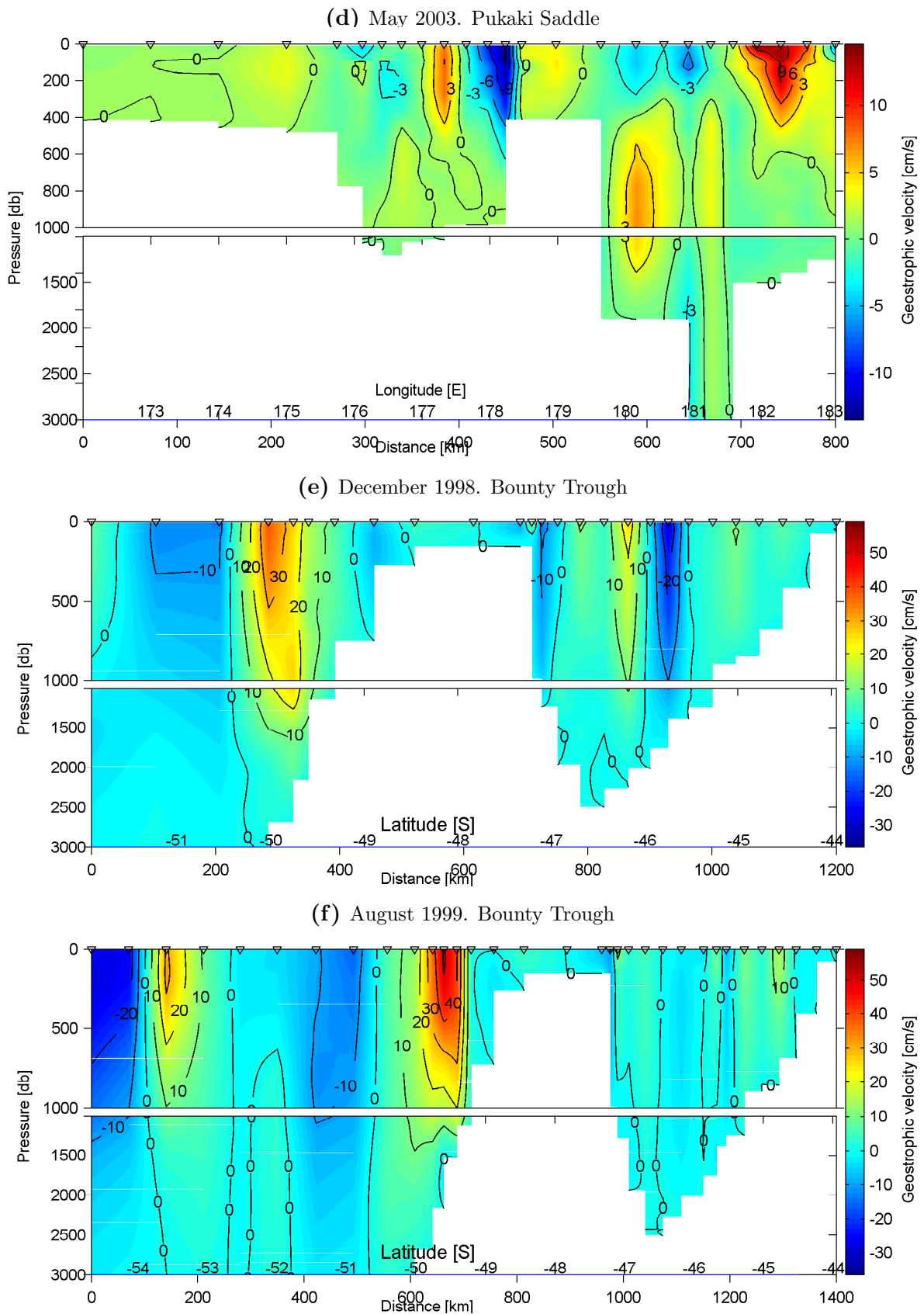


Figure 3.31: Geostrophic velocities on the subantarctic region. (a) Macquarie Ridge, (b and c) Campbell Plateau, (d) Pukaki Saddle and (e and f) Bounty Trough transects. Contours are every 10 cm s^{-1} in (a), (b and c) and (e and f) and every 3 cm s^{-1} in (d). Positive values: to the east in panel (a) northeast in panels (b and c) and (e and f) and north in (d). Velocities are relative to the ocean bottom.

3.3 Discussion

3.3.1 Fronts

The Subtropical Front (STF) to the north and the Subantarctic Front (SAF) to the south mark the oceanographic boundaries of the New Zealand subantarctic region. The position and changes in these fronts were investigated to understand their possible influence on the Campbell Plateau oceanographic structure.

A complete study of the South-STF south of New Zealand was recently presented by Smith et al. (2013), and they found the STF was at approximately 45.6°S in the Tasman Sea (Figure 3.4) and its southern branch at 49.6°S south of New Zealand (Figure 3.7). The STF in the Tasman transect is identified in a similar position to that reported by Sokolov and Rintoul (2002) in the SR3 line which lies south of Tasmania and to the west of the Tasman transect presented in this thesis.

The identification of the different branches of the fronts from hydrography does not always agree with that found from remote sensing data. For example, satellite data show the Antarctic Circumpolar Current (ACC) as a complex structure of different filaments and front branches. Using Sea Surface Height (SSH) it is possible to identify three branches in both the SAF and the Polar Front (PF) (e.g., Sokolov and Rintoul, 2007a, 2009a; Rintoul et al., 2014). However, from hydrography the ACC is usually assumed to have three main Southern Ocean fronts (Orsi et al., 1995; Sokolov and Rintoul, 2007a). This is due to the higher spatial coverage and temporal resolution of the satellite data. It is also easier identifying the different branches of the (ACC) fronts from SSH because those fronts coincide with streamlines of SSH that are well defined in the satellite data (Sokolov and Rintoul, 2007a, 2009a). The position of the three branches of the SAF over Macquarie Ridge (Rintoul et al., 2014), is confirmed by the hydrography presented in this thesis (Figure 3.7a). However, the two branches of the Polar Front reported by Rintoul et al. (2014) were not identified in the transect.

Different studies have indicated that the position of the ACC fronts are strongly in-

fluenced by the bathymetry (e.g., Sokolov and Rintoul, 2007a, 2009a). The branches of the fronts merge and split when encountering important bathymetric features, sometimes resulting in a super front when they are forced to merge. Sokolov and Rintoul (e.g., 2007a) suggested this happens southwest of the Campbell Plateau with the fronts staying together until they diverge again east of the Campbell Plateau. This idea was previously suggested by several authors (e.g., Gordon, 1972; Orsi et al., 1995; Rintoul and Bullister, 1999), and is confirmed in this study, with the three branches of the SAF found merged into one strong frontal feature south of the Campbell Plateau (Figure 3.12). However, Sokolov and Rintoul (e.g., 2007a) suggest that east of the Campbell Plateau, the northern branch follows the Campbell Plateau bathymetry and the middle and southern fronts turn to the southeast at approximately 165°E , while in this study the northern and middle branches of the SAF appear to follow the bathymetry. The southern branch of the SAF could not be identified as the transect did not cross it, presumably because the branch was further south (Figure 3.19).

3.3.2 Water masses

The range of the New Zealand subantarctic water mass structure is driven by the influence of three oceanographic regions: north of the STF, where warm and salty Subtropical Water (STW) is found; south of the SAF, where the southern polar regimes are; and in between, the subantarctic region, where cold and fresh Subantarctic Water (SAW) is found (e.g., Orsi et al., 1995; Belkin and Gordon, 1996; Williams, 2004). A general description of the water masses in the subantarctic region is summarized in Figure 3.32 and it was previously presented in Section 3.2.2 (Figure 3.27a). This Θ - S_A (conservative temperature-absolute salinity) diagram shows the mean profiles from two transects, one along the Macquarie Ridge (black dots) and the other to the east of Macquarie Ridge (green dots) (Figure 3.6a). Here, they are representative of the unmixed water masses in the New Zealand subantarctic region. However, a new complete description of the late autumn New Zealand subantarctic region is shown in Figure 3.29b. That figure shows the transition and distribution of water masses between profiles in the reference Θ - S_A diagram. The influence of the different regions, the STF region, the subantarctic region

and south of the SAF region, previously described can also be seen in Figure 3.29b. The change in surface water masses depends on the region. It can also be appreciated how the properties change between regions due to mixing. The figure also shows how homogeneous the water is at depth regardless of the region.

A subsurface high salinity tongue of STW associated with the STF is found south of the South Island, for example, in the transects west of the Campbell Plateau (Figure 3.10). The tongue disappears in the transects crossing the Southland Current (Figure 3.19), where the STW is modified due to mixing with SAW (e.g., Chiswell, 1996; Morris et al., 2001; Sutton, 2003). The subsurface tongue appears again further north, off the east coast of the South Island in the Bounty Trough transects, showing less modified STW (Figure 3.26). Finding the subsurface tongue in those transects might be related to the idea of the STF over Chatham Rise being a region of formation of the subsurface salinity tongue (e.g., Heath, 1976; Sutton, 2001).

Off the Campbell Plateau and below 1400 m temperature and salinity are those of Circumpolar Deep Water (CDW). CDW is commonly divided in two types: Upper Circumpolar Deep Water (UCDW) and Lower Circumpolar Deep Water (LCDW). The LCDW has a salinity maximum that is derived from the influence of the North Atlantic Deep Water (NADW) (e.g., Talley et al., 2011). Morris et al. (2001) had previously indicated that NADW was found south of the SAF, especially in the Emerald Basin (their Figure 4 top panel and Figure 3.10a in this work). Here, this is identified as LCDW. The revised description of the water masses used in this thesis (Table 3.2) now identifies the water previously considered as NADW as LCDW. Morris et al. (2001) also suggested that the Macquarie Ridge was blocking the NADW (LCDW), so that it did not appear in their zonal transect (their Figure 4, second panel from the top), however, it is observed here deeper than 1000 m. The likely reason they did not report it is because they focused on the first 1000 m and the AAIW is found below 1000 m.

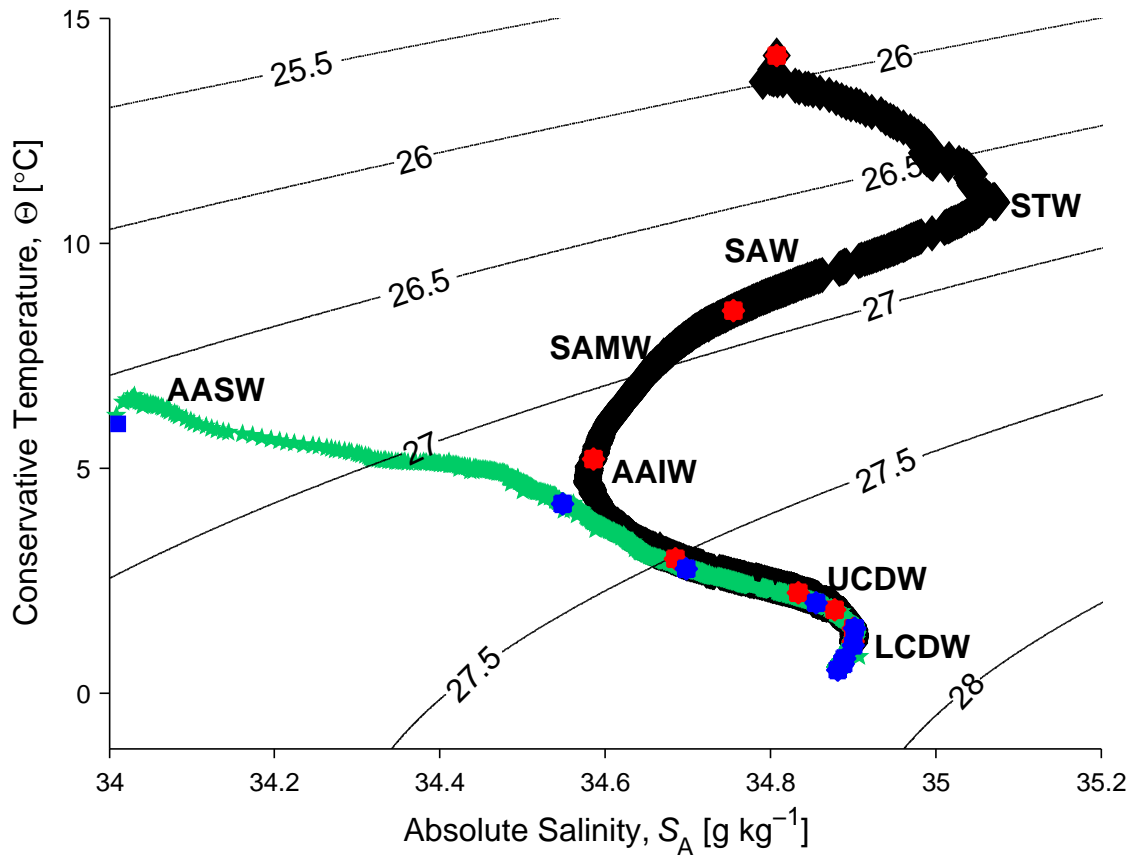


Figure 3.32: General Θ - S_A diagram for the subantarctic region. Black dots are averaged along the Macquarie Ridge transect and green dots east to the Macquarie Ridge as described in Section 3.2.2. Red and blue dots mark depth every 500 m. Contours are potential density referenced to 0 dbar.

These intermediate and deep water masses (AAIW, LCDW and UCDW) are found in all of the transects analysed in this work, from the Macquarie Ridge (Figure 3.27), around the Campbell Plateau (Figure 3.29b) and in the Bountry Trough (e.g., Figure 3.28c), where the transects are deep enough to capture these water masses. The distribution of these water masses to the north of the plateau, was previously reported by several authors (e.g., Mccave and Carter, 1997; Chiswell and Sutton, 1998). Mccave and Carter (1997) suggested that the AAIW is partially blocked by the Chatham Rise in its flow towards the north, and would flow into the South Pacific Gyre. That flow pattern could be an explanation for the differences types of AAIW found north and south of the Chatham

Rise: to the north, it is more saline (34.56 g kg^{-1}), and has travelled within the Gyre; to the south, less saline (34.46 g kg^{-1}) which would be closer to its source (e.g., Chiswell and Sutton, 1998; Bostock et al., 2013).

Focusing on the water mass structure and seasonality on the Campbell Plateau and in the Bounty Trough (Figure 3.28), it is noted that the structure found on the plateau (blue dots in Figure 3.28b and Figure 3.28e) is similar to the Bounty Trough profile (blue dots in Figure 3.28c and Figure 3.28f) in the same density range (26.5 to 27 kg m^{-3}). The salinity maximum at the bottom of the profiles (above the 27 kg m^{-3} isopycnal) in the December transect is also similar in both transects. Both August transects, not only show the same salinity maximum, but also show a freshening at the bottom of the profile. These similarities suggest a connection between water on and off the plateau. Inspecting the general circulation in that area (Figure 3.30), one explanation could be the cyclonic flow in the Bounty Trough, previously suggested by Morris et al. (2001), which could transport AAIW to the northern edge of the Campbell Plateau.

The water masses found in the Pukaki Saddle (Figure 3.22 and 3.23) were previously reported as being two different types of SAMW by Griffith et al. (2010). One fresher and colder occurring in the Pukaki Saddle, and the other saltier and warmer, over the Campbell Plateau and east to the Bounty Plateau. However, a different interpretation was given here. The saltier and warmer water they found over the Campbell Plateau is a stratified surface layer similar to that described in Figure 3.19d. The stations where this stratified layer is found were sampled in May 2003, a warm year preceded by a warm December 2002 (see Section 4.2.4). May 2003 was warmer than May 1998 (Section 3.2.1). Underneath this warm layer, a well mixed layer of SAMW occupies the rest of the water column. In the Pukaki Saddle, the fresh and cold water is SAW, and occupies the surface layer on the Pukaki Saddle towards the east until approximately 178°W . In the Pukaki Saddle, AAIW occupied the bottom part of the transect (Figure 4.15d). The last three stations of the transect (on the eastern end) show a blob of warm and salty water. This feature could be identified as a STW eddy. The proximity of the STF (e.g., Sutton, 2003) and the eddy activity reported in this area (e.g., Bryden and Heath, 1985; Stanton

and Morris, 2004; Fernandez et al., 2014) supports this explanation. A similar feature, namely a warm core eddy, was previously reported by Williams (2004). That eddy was found on approximately the same latitude, but further east.

3.3.3 Circulation

The general flow around the Campbell Plateau is summarized in Figure 3.33. A weak flow is associated with the STF to the south of the South Island, with a stronger flow associated with the Southland Current to the east of the South Island. There is a persistent cyclonic circulation along the northern edge of the plateau and the western corner of the Bounty Trough (Morris et al., 2001). A strong flow associated with the SAF crosses Macquarie Ridge and flows around the eastern edge of the plateau. When the current associated with the SAF encounters the Pukaki Saddle and the Bounty Plateau, the circulation becomes more complex, with part of the current flowing through the Pukaki Saddle and along the northern edge of the plateau, and the remaining flow continuing around the Bounty Plateau.

The speed of the currents found in this study (Section 3.2.3) have a seasonal variability, with stronger currents during winter. This seasonality was previously suggested by Morris et al. (2001) and Stanton and Morris (2004), who also noted this seasonality in the transport. Seasonal variability in wind stress (stronger in winter) would force faster currents in the flow associated with the SAF. However, more recent studies suggest that stronger westerly winds appear to enhance ACC turbulence through eddy activity (Böning et al., 2008). Further work would be necessary to determine the effect of the wind stress on the currents investigated in this study.

Although the geostrophic current structure calculated in this study in general coincide with those presented by Morris et al. (2001) and Stanton and Morris (2004) (as expected since the same data sets were used), the double velocity core structure that they described in their work (Figure 5 in Stanton and Morris (2004)) is not found in this thesis (Figure 3.31e). One reason could be the different methods used to interpolate

the data. Stanton and Morris (2004) horizontally interpolated the data to have equally distant stations. However, those used in this study were not interpolated. Because of this it is suggested that there is not a double velocity core in that transect.

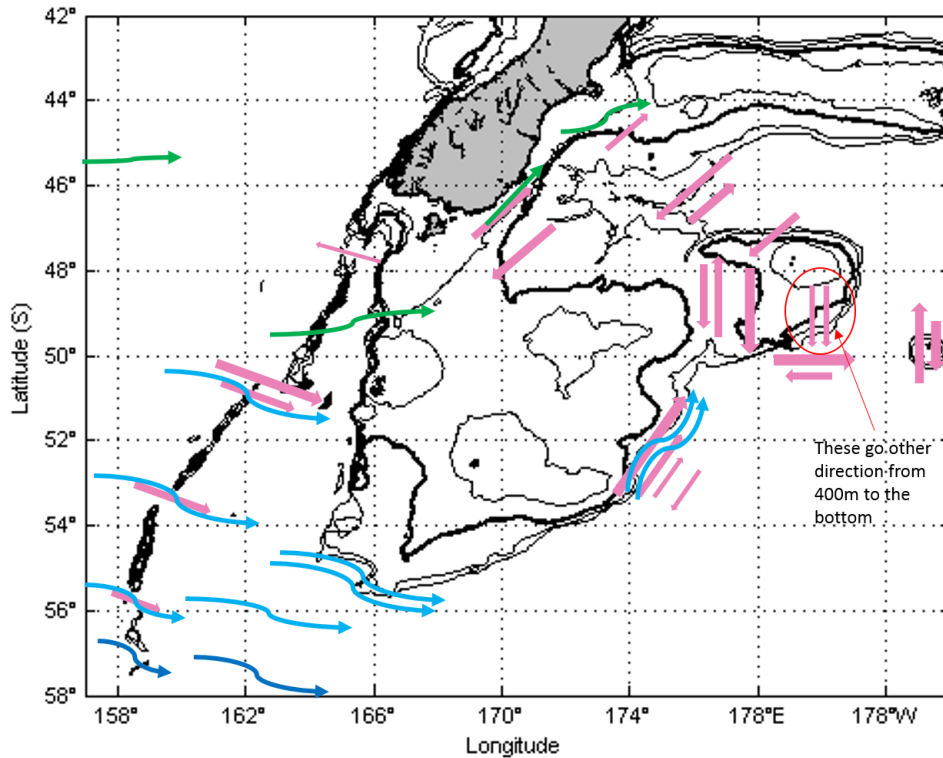


Figure 3.33: Front positions and geostrophic velocity flow summary. STF (green arrows), SAF (light blue) and Polar Front (dark blue). The pink arrows show the direction of the flow and the size of the arrows show the strength of the flow. Contours every 500 m, bold contours show the 1000 m isobath.

In the water mass analysis (Section 3.2.2) the subantarctic region appeared to be very sensitive to the 1000 m isobath, with the shape of the mean Θ - S_A profile changing depending on whether stations deeper than 1000 m were included. This isobath is, for example, the depth where AAIW encounters the Campbell Plateau. In their study, Stanton and Morris (2004) suggested that the limit of the SAF influence was the 1000 m isobath, as flow associated with the SAF in the Subantarctic Slope is found at 1000 m depth or deeper. This is supported by sensitivity of the water mass analysis to station

selection around 1000 m, as it appears to be the isobath where the Campbell Plateau meets the deeper ocean.

3.4 Summary of the chapter

This chapter illustrates the oceanography of the New Zealand subantarctic region, focusing on the region south of the STF, and describes the ocean structure of the Campbell Plateau. It also gives some background to investigating the spatial variability on the Campbell Plateau and discussing of seasonal variability over the plateau.

The STF at the northern end of the western transects is associated with a subsurface high salinity tongue. In the northern end of the eastern transects, this subsurface tongue has disappeared but the strong horizontal gradients remain, showing the position of the Southland Front, the local expression of the STF (e.g., Chiswell, 1996; Sutton, 2003). Further north, in the Bounty Trough, the subsurface tongue is present again.

The three branches of the SAF are identified in the Macquarie Ridge transect through the natural gates along the Ridge. The three branches of the Polar Front are difficult to identify with hydrography, and just the northern branch of the Polar Front was found. The medium branch of the Polar Front is not clear from the hydrography although it is shown by SSH in Rintoul et al. (2014). The position of the branches of the SAF look quite steady with time along the Macquarie Ridge, confirming the idea suggested by Sokolov and Rintoul (2007a) and Rintoul et al. (2014) that the bathymetry stabilizes the flow and minimizes meandering of the SAF across the Ridge. The three branches of the SAF along the southern edge of the Campbell Plateau become unclear, as they are forced to merge where they pass south of the Campbell Plateau, making it difficult to differentiate one from another. The Polar Front keeps its position not being affected by bathymetry. Along the transects downstream of the Campbell Plateau, only two branches of the SAF are found, confirming the idea that the SAF splits in two. The north and medium branches follow the bathymetry of the Campbell Plateau and the southern branch turns sharply to the south east at about 164°E (Orsi et al., 1995;

Belkin and Gordon, 1996; Gille, 2003; Stanton and Morris, 2004; Sokolov and Rintoul, 2007a).

The Θ - S_A diagrams show a general view of the structure of the water masses in the New Zealand subantarctic region and specifically on the Campbell Plateau. The top part (surface) of the profiles analysed on the Θ - S_A diagrams changes properties depending on the position of the stations and the oceanographic regime they are related to. They also change depending on the season in which they were sampled. At the northern ends of the transects, STW is being modified from west (the STF) to east (the Southland Front) due to the mixing of SAW. AASW is found at the surface of the southernmost ends, and SAW is found at the surface of the Campbell Plateau and Bounty Trough transects. During summer the top part of the profiles is more stratified and becomes a well developed mixed layer in winter.

The bottom part of the profiles, from approximately 1000 m to the bottom of the water column is shared amongst all the transects in CDW. There are two types of CDW, UCDW which is shallower and not that salty and LCDW, which is deeper, colder and saltier. These two types of water are found all around the plateau in the transects and stations that are deep enough to accommodate this water.

SAMW, SAW and STW are the main water masses on the structure of the plateau (depth shallower than 1000 m depth) but there are different influences at the surface and bottom in the eastern and western sides of the plateau. The profiles on the western side of the plateau close to the southern edge of the plateau show a salinity minimum with AAIW properties that are not seen on the eastern side of the plateau. The eastern side has a salinity peak at approximately 700 m that is not seen in the northern transects.

The general flow around the Campbell Plateau and within the plateau coincides with those presented by Morris et al. (2001) and Stanton and Morris (2004), which is expected as the data used are the same. The reversing of the flow at approximately 1500 m depth that was shown in the Stanton and Morris (2004) moorings is also seen in the

summer transect in this thesis (Figure 3.31b). However, the double velocity core that they showed in their work (their Figure 5b) is not seen in this transect (Figure 3.31b). In their study, Mooring number 3, at 1000 m depth on the Subantarctic Slope, showed stronger currents than those on the plateau, suggesting that this location was already being influenced by the SAF.

The direction of the flow around and on the Campbell Plateau, especially the flow associated with the SAF, looks consistent over seasons, however, a strengthening during winter is noted. The differences in velocities between the different voyages and seasons suggest a seasonality in the SAF agreeing with Morris et al. (2001). A summary of the positions of the fronts and the geostrophic velocities is shown in Figure 3.33.

Chapter 4

Interannual variability of the Campbell Plateau

A low resolution Conductivity Temperature and Depth (CTD) data set is presented with the aim of determining the variability of the oceanographic structure on the Campbell Plateau. This low vertical resolution data set consists of eight years of CTD hydrographic profiles scattered over the Campbell Plateau, sampled during December in each year. The distribution of the profiles allows identification not only of the vertical structure but also the spatial structure of the plateau. The timing of sampling allows for assessment of any interannual variability in December. This data set gives a new insight into the interannual variability of the Campbell Plateau where other products, such as Argo buoys, cannot be used, because the plateau is too shallow.

4.1 Data and methods

Low resolution CTD hydrographic profiles were collected in December each year from 2002 to 2009. The profiles were sampled as part of regular fisheries research cruises on board RV Tangaroa (Table 4.1). The hydrographic profiles were sampled with a Sea-Bird Electronics SBE 37-SM MicroCAT attached to one of the warps (trawl tow lines) during fishing trawls.

Table 4.1: Dates of the Fisheries cruises and number of casts sampled on each cruise

| Name of cruise | Year | Sampled period | Number of casts |
|----------------|------|------------------|-----------------|
| Tan0219 | 2002 | 25 Nov to 20 Dec | 87 |
| Tan0317 | 2003 | 14 Nov to 09 Dec | 70 |
| Tan0414 | 2004 | 28 Nov to 20 Dec | 70 |
| Tan0515 | 2005 | 26 Nov to 19 Dec | 81 |
| Tan0617 | 2006 | 27 Nov to 21 Dec | 72 |
| Tan0714 | 2007 | 27 Nov to 21 Dec | 86 |
| Tan0813 | 2008 | 27 Nov to 20 Dec | 79 |
| Tan0911 | 2009 | 27 Nov to 21 Dec | 78 |

Table 4.2: Number of casts reaching specified depth in each year

| depth [m] | 2002 | 2003 | 2004 | 2005 | 2006 | 2007 | 2008 | 2009 |
|-----------|------|------|------|------|------|------|------|------|
| 0 | 87 | 70 | 70 | 81 | 72 | 86 | 80 | 78 |
| 100 | 87 | 70 | 70 | 81 | 72 | 86 | 80 | 78 |
| 200 | 87 | 70 | 70 | 81 | 72 | 86 | 80 | 78 |
| 300 | 87 | 70 | 70 | 80 | 72 | 86 | 80 | 78 |
| 400 | 85 | 69 | 64 | 58 | 68 | 81 | 74 | 76 |
| 500 | 73 | 56 | 54 | 54 | 59 | 68 | 64 | 68 |
| 600 | 45 | 37 | 35 | 43 | 40 | 43 | 46 | 47 |
| 700 | 22 | 18 | 18 | 21 | 13 | 20 | 31 | 24 |
| 800 | 11 | 9 | 6 | 10 | 8 | 10 | 12 | 10 |
| 900 | 6 | 4 | 1 | 6 | 2 | 8 | 4 | 4 |

The hydrographic profiles were sampled from the surface to the sea floor where possible (Table 4.2). The distribution of stations was designed for fisheries stock assessment and monitoring purposes, and were randomly distributed with a weighting towards the main fishing regions (Francis et al., 2002). An examination of the data distribution in Figure 4.1, shows that all the casts fall within the 1000 m isobath: for this reason, the 1000 m isobath will define the limits of the Campbell Plateau in this study. Although not originally intended to evaluate oceanographic variability, these data provide the first spatially extensive time series which allows the subsurface variability to be investigated.

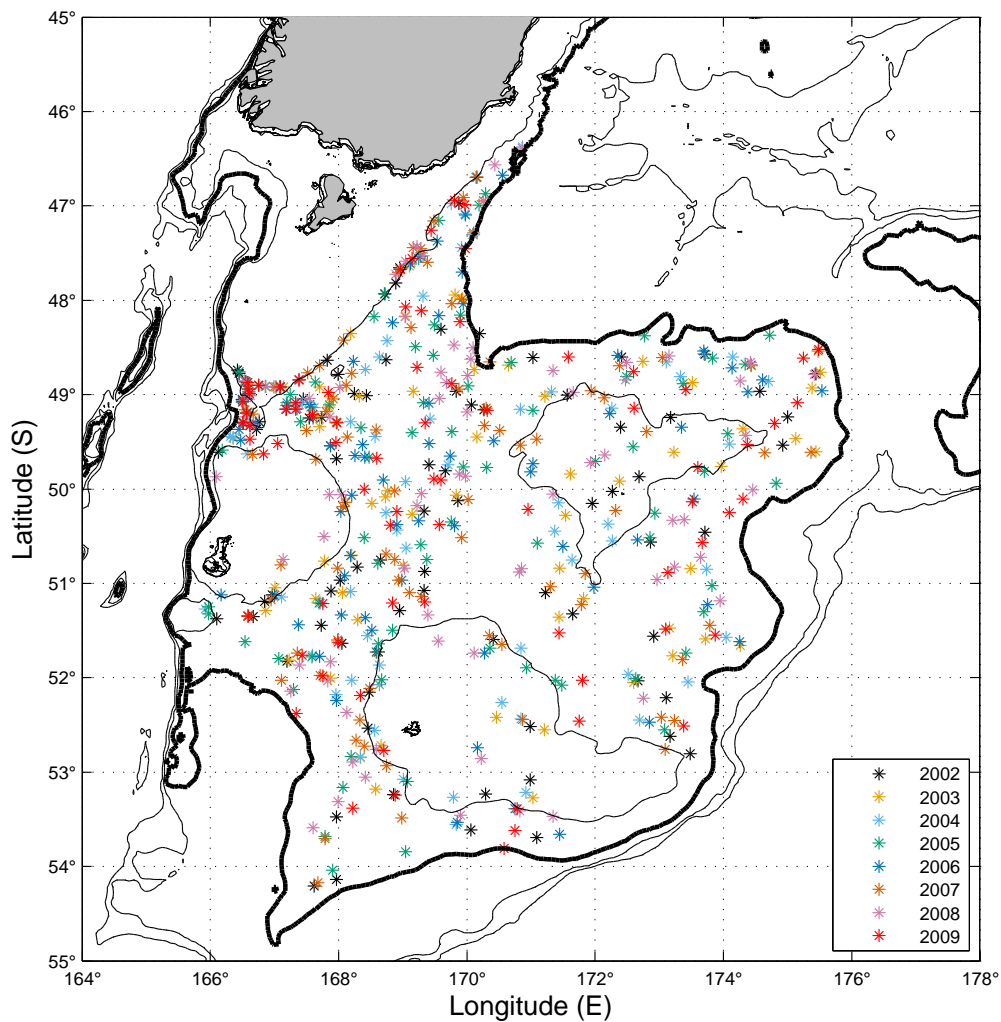


Figure 4.1: Distribution of low resolution CTD profiles over the Campbell Plateau. Contours every 500 m, bold contour show 1000 m isobath.

4.1.1 Low resolution data processing

The first processing step for this data was to calculate the conservative temperature (Θ) and absolute salinity (S_A) with the new TEOS-10 routines from the *in situ* temperature and salinity (for more information about TEOS-10 see Appendix A). This was followed by a quality check of the data, and it was found that the newly converted data had several outliers. As a first way of filtering the data, values saltier than 35.16 g kg^{-1} (salinity of 35) and fresher than 34.36 g kg^{-1} (salinity of 34.2) were removed as values outside that range were not previously reported in the Campbell Plateau literature. To remove the remaining outliers, a $3\text{-}\sigma$ outliers detection method was used (e.g., Emery and Thomson, 2001). This method identifies outliers as any value that exceeds ± 3 standard deviations from the mean, being the mean calculated over all the profiles for a given year. If either the temperature or salinity was defined as an outlier, then both were removed to maintain consistent coverage. The salinity in 2005 was found to be significantly fresher than in other years of the data set with a range of 33.2 to 33.95 g kg^{-1} . After checking the calibration history of the CTD equipment it was not possible to identify a cause for the problem. It is possible that the error was caused by some sort of biofouling for which no appropriate correction can be made, thus salinity for 2005 has been excluded from the analysis.

The slow sampling rate of a MicroCAT (from 2 to 3 m to 10 m sampling interval) and the variable descent rates in each profile, due to the primary focus on fisheries, mean the vertical data are unevenly and coarsely spaced. Hence, traditional processing techniques such as binning the data are not possible. This is why these data are considered low resolution in opposition to the data set used in Chapter 3. Also, some data at the top of the water column are missing due to the method of data collection (Table 4.3), i.e., the CTD is attached to the trawl warp during the deployment of the trawl net so the first metres are the ones that have the most missing data. For example, in 2002 54% of the profiles have surface data, reaching 95% of the profiles at 40 m depth. In 2009, 66.7% of the profiles having surface data and 93.6% at 40 m depth. 2005 has 70.4% of the profiles with surface data and 93.8% at 40 m depth. 2007 reaches 93% of usable

profiles at 20 m depth and all the other years have more than 90% of the data at depths shallower than 10 m depth, with 2003 having a complete data set, and 2006 has just one data point missing at the surface. Despite the missing data in the first few metres of the water column, the distribution of the profiles over the plateau provides a good coverage for this analysis (Figure 4.2).

Table 4.3: Number of data missing in the first 80 m of the water column.

| depth [m]/year | 2002 | 2003 | 2004 | 2005 | 2006 | 2007 | 2008 | 2009 |
|----------------|------|------|------|------|------|------|------|------|
| surface | 40 | - | 7 | 24 | 1 | 15 | 12 | 26 |
| 10 | 38 | - | 7 | 22 | - | 11 | 7 | 20 |
| 20 | 23 | - | 4 | 14 | - | 6 | 4 | 15 |
| 30 | 12 | - | 2 | 9 | - | 4 | 3 | 11 |
| 40 | 4 | - | 2 | 5 | - | 1 | 3 | 5 |
| 50 | - | - | - | 4 | - | 1 | 1 | 4 |
| 60 | - | - | - | 2 | - | 1 | - | 1 |
| 70 | - | - | - | 2 | - | 1 | - | 1 |
| 80 | - | - | - | 1 | - | 1 | - | - |

To generate a regular grid from the different vertical distributions in each profile the data were vertically interpolated onto a 10 m regular vertical grid, from the surface to the maximum depth of each cast. For the vertical interpolation every 10 m the interpolation method used was the “linear interpolation”. This method finds values at intermediate points, of a one dimensional function $f(x)$ that underlies the data. The profiles were then linearly horizontally interpolated onto a $0.25^\circ \times 0.25^\circ$ regular grid using all available data at each depth. An example of the resulting surface is shown in Figure 4.3. This interpolation method, linearly fills missing data gaps, and allows a regular grid to be made that reveals the spatial oceanographic structure of the Campbell Plateau, with the Subtropical Front (STF) to the north and northwest and the Subantarctic Front (SAF) around the southern and eastern edges of the plateau. Towards the bottom, the number of profiles decline, with 280 m the maximum common depth for all the years. For this reason, the interpolated area obtained for each depth varies from 280 m to the bottom

of the water column.

For a clearer understanding of the different approaches, each method used to investigate the variability will be explained at the beginning of each section.

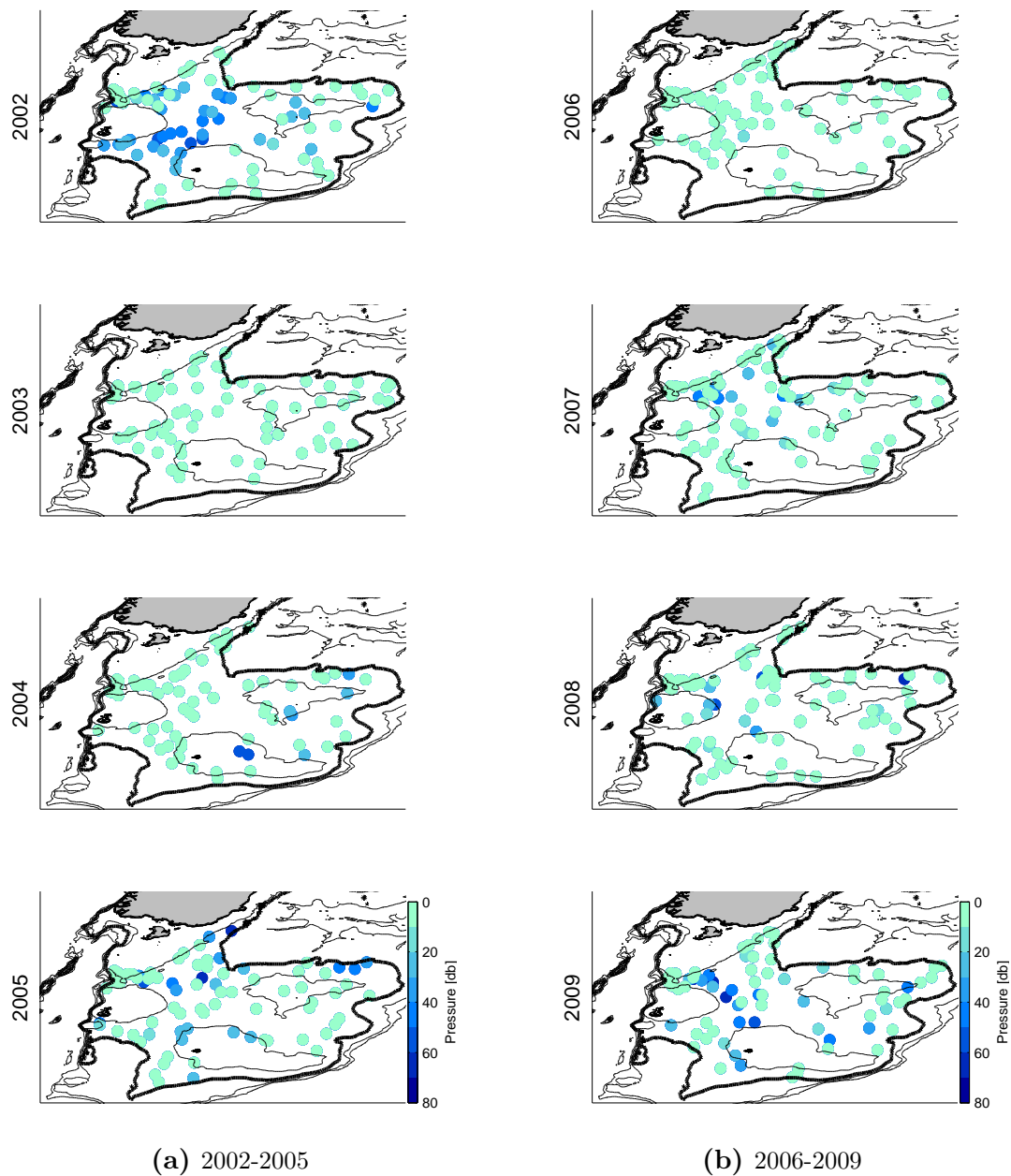


Figure 4.2: Depth distribution of the low resolution data set coloured by the depth of the shallowest data point. 80 m is the deepest depth with missing data. Colourbar to the right of the bottom panels. Contours every 500 m, bold contours show the 1000 m isobath

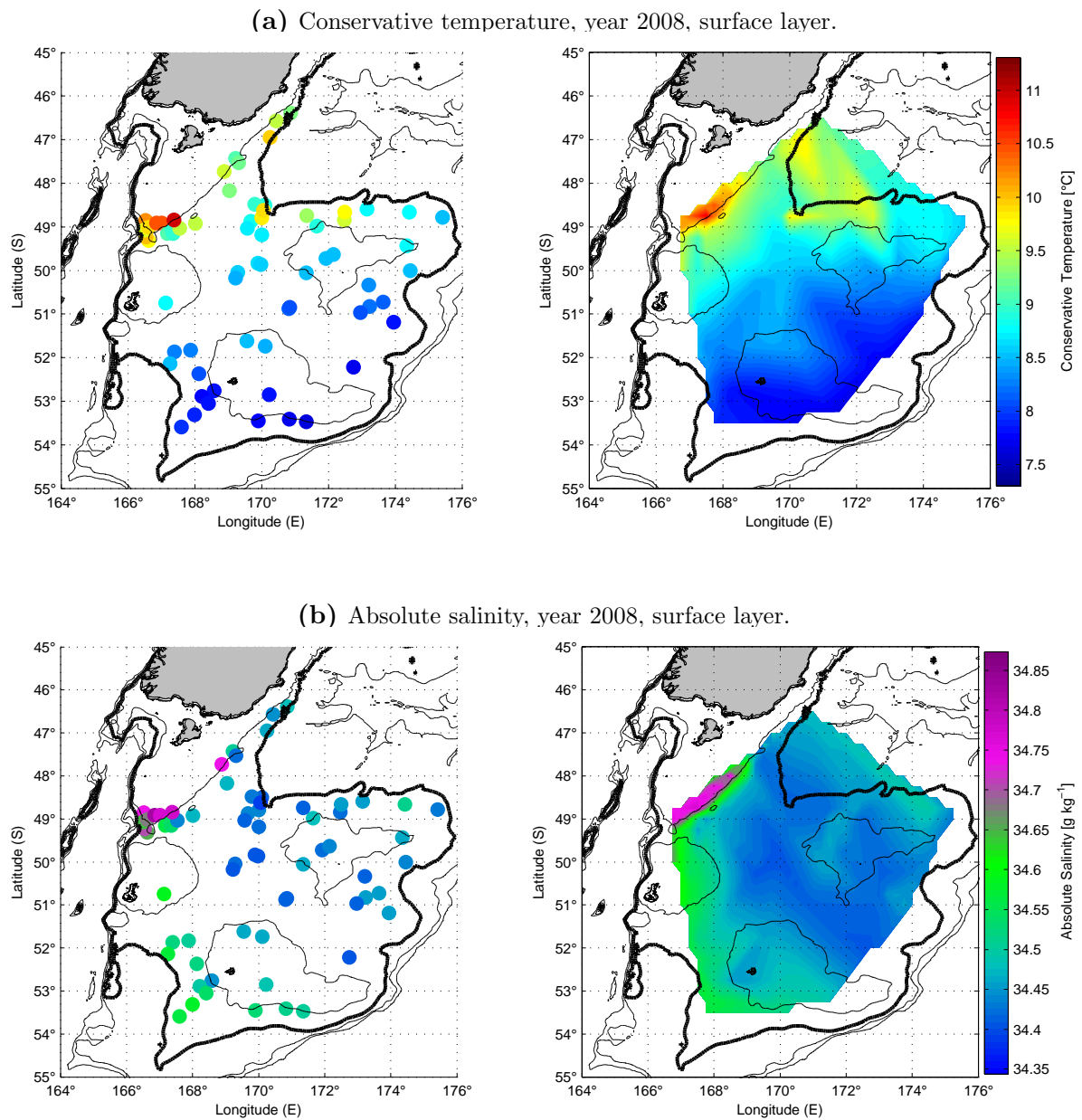


Figure 4.3: Conservative temperature (top panel), raw data to the left and interpolated data to the right. Absolute salinity (bottom panel), raw data to the left and interpolated data to the right. Both for year 2008 and for the surface layer.

4.1.2 Water mass identification criteria

In Chapter 3 a summary of the water masses in the New Zealand subantarctic region was presented. In this chapter a more focused description of the Campbell Plateau water masses is presented focusing on the spatial and temporal variability of water masses found within the 1000 m isobath.

Temperature and salinity ranges for the water masses found in the Campbell Plateau are converted to TEOS-10 from the description of the water masses found in the literature (Table 4.4). The water masses definition is the same as those in Chapter 3. Here, the original T-S signature appears to reflect the mixing of the different water masses. The Θ - S_A diagram shows the different combination of the water masses and the transition between them (Figure 4.4).

Table 4.4: Campbell Plateau water masses from Table 3.2. ¹ McCartney (1977), ² Sutton (2001), ³ Morris et al. (2001), ⁴ Sokolov and Rintoul (2002) and ⁵ Talley et al. (2011). The acronyms for the water masses are: Antarctic Intermediate Water (AAIW); Subantarctic Mode Water (SAMW); Subantarctic Water (SAW) and Subtropical Water (STW).

| | Temperature [°C] | Salinity [g kg ⁻¹] | Density [kg m ⁻³] | Depth [m] | Other features |
|---------------------|--------------------------|--------------------------------|-------------------------------|-----------|---|
| AAIW ^{4,5} | 4-6 | <34.46 | 27.1-27.3 | 600-1200 | salinity minimum core |
| SAMW ^{1,3} | 7 | 34.41-34.65 | | 200-500 | weak stratification minimum in potential vorticity |
| SAW ^{2,5} | <10 winter <14 summer | <34.76 | | up to 500 | north of SAF |
| STW ² | >18 summer >14 winter | >35.26 | | | high salinity subsurface tongue |

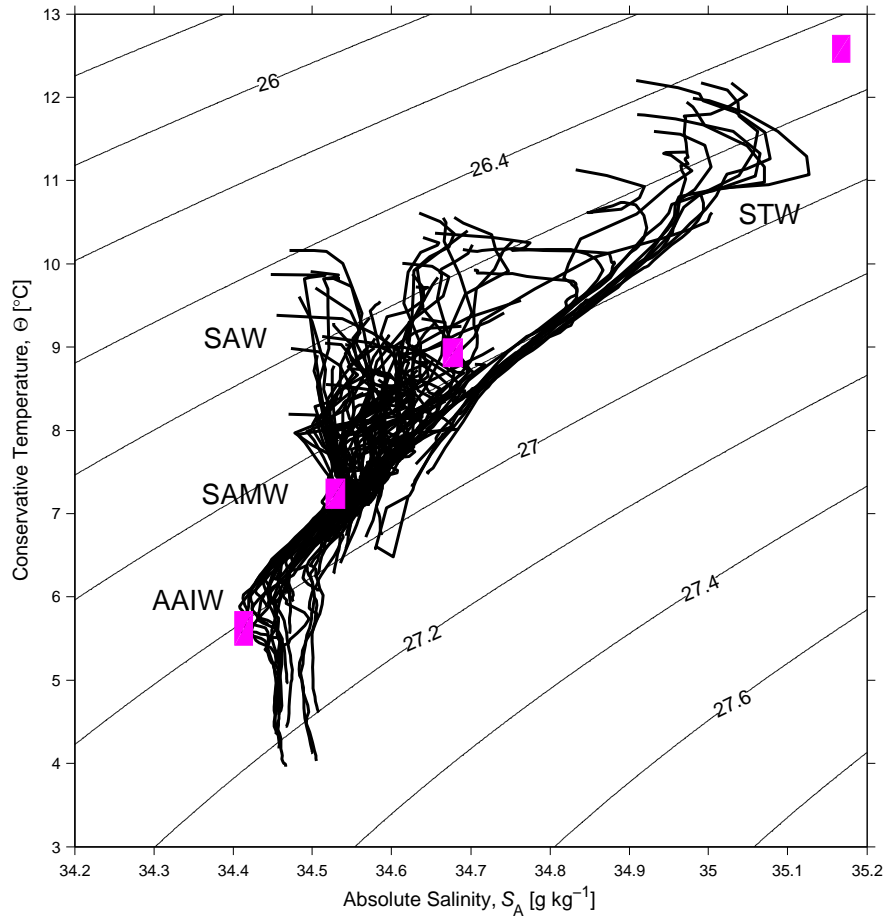


Figure 4.4: Θ - S_A diagram for year 2002 from the low resolution data set, profiles have a 30 m running mean applied. Pink squares mark the approximate position of the water masses defined in Table 4.4. Contours are potential density [kg m⁻³] referenced to 0 dbar.

4.2 Results

4.2.1 Spatial variability over the Campbell Plateau

To investigate the spatial structure a mean for the whole time period, excluding 2005, was calculated for each depth. To calculate the mean, the regular grid resulting from the previous interpolation was used. The area from the surface to 280 m is similar. The common area at 350 m depth is slightly smaller but still reveals some structure.

At the surface, the STF is identified by its strong temperature gradient, with temperatures between 9.5 °C and 10.5 °C. It can be seen near the Snares Shelf to the northeast and then following the 500 m isobath. The influence of STW related with the STF reaches waters east and south of the Auckland Islands. The signal of the STW can also be recognized in salinity, corresponding to the temperature signal, with saltier water following the 500 m isobath, the Auckland Islands and the southwest edge of the plateau. Temperature decreases and salinity freshens towards the eastern edge of the plateau due to the influence of subantarctic waters coming around the plateau with the SAF (Chapter 3) (Figure 4.5). At 150 m and 250 m, the STW influence is still persistent, but the temperature has decreased to 7.7 °C. A homogeneous distribution of 7 - 7.5 °C water, characteristic of SAMW, remains over the eastern side of the plateau. Salinity from the STF influences not only the north edge of the plateau, but also the Auckland Islands and to the southwest edge of the plateau. At 350 m depth, the signal of the STF is still present, with the western side of the plateau being saltier than the eastern side. However, cold and fresh SAW dominates almost the whole spatial structure of the plateau.

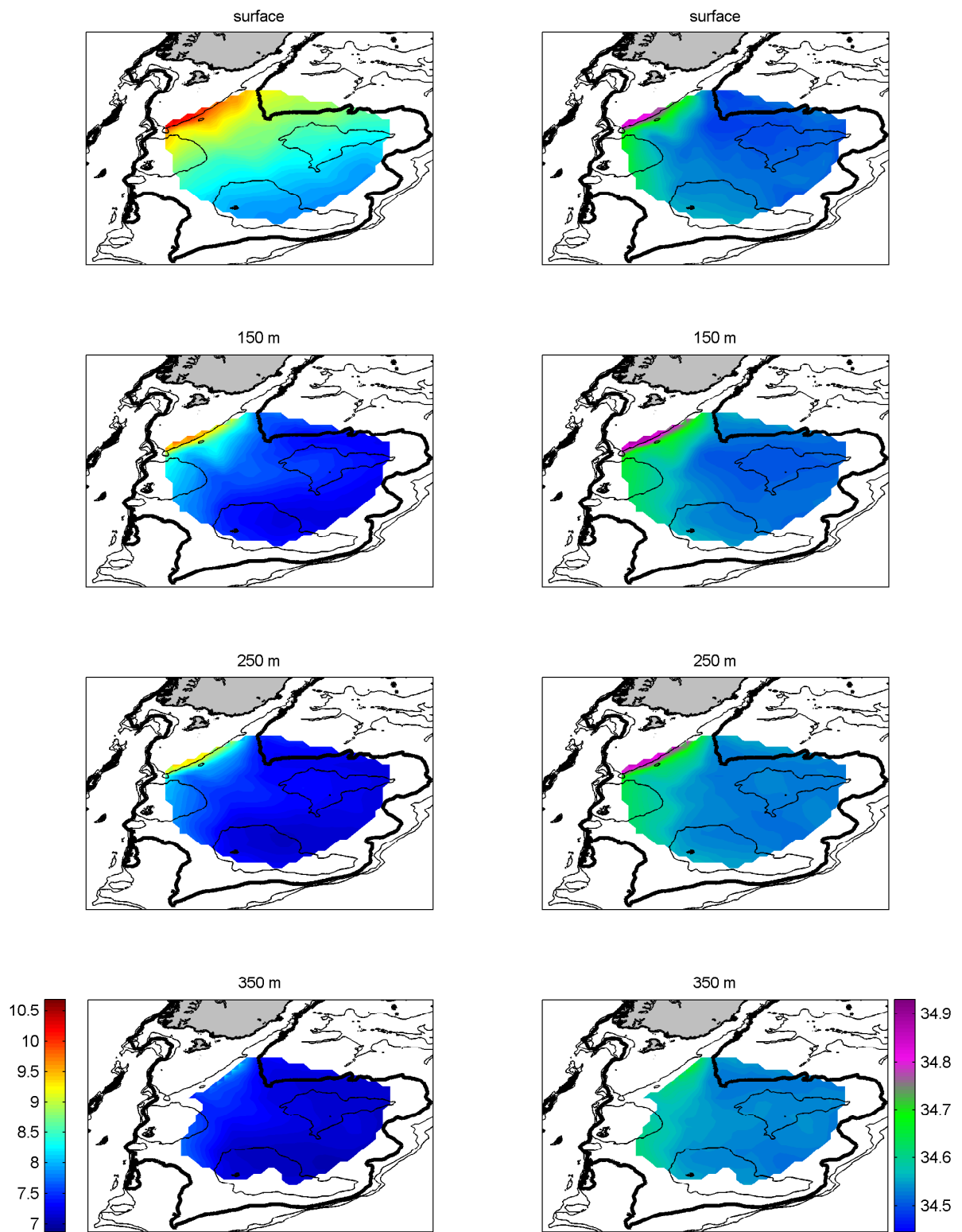


Figure 4.5: Seven year mean conservative temperature to the left [$^{\circ}\text{C}$] and mean absolute salinity to the right [g kg^{-1}] for the surface, 150 m, 250 m and 350 m depth. Colour scales are beside the bottom figures. Thick black line shows the 1000 m isobath.

4.2.2 Vertical variability over the Campbell Plateau

To investigate the vertical structure and interannual variability through the water column over the Campbell Plateau, a spatial mean was calculated for each year, every 10 m from the surface to the bottom of the water column. To do that, the previously interpolated regular grid was used for each individual year. This way, vertical temperature and salinity profiles show the structure of the water column. The spatial means were then used to plot Θ - S_A diagrams (conservative temperature vs absolute salinity) to investigate the distribution and variability of water masses through time. Between the surface and 280 m the area that this spatial mean covers is the same. From 280 to 350 m the area is reduced, but is still common to those depths. From 350 m to the bottom of the water column the area varies depending on the year and the depth.

Mean vertical profiles of conservative temperature and absolute salinity summarize the vertical variability on the Campbell Plateau (Figure 4.6). The first 100 m of the water column are highly variable, in both temperature and salinity. A difference of 1.2 °C, from 8.1 °C to 9.3 °C, between the coldest year, 2009, and the warmest, 2002 is identified at the surface (Figure 4.6a). From 100 to 350 m, the depth where the areas are still common, the water column cools homogeneously to a conservative temperature of 7.1 °C to 7.5 °C. However, 2007 remains 0.2 °C colder than the other years. From 350 to 500 m, the water column is still very homogeneous, and has decreased to a temperature range between 6.7 °C and 7.2 °C. This homogeneous part of the water column has the temperature and salinity properties of SAMW and also sits at the depth range that would be expected. From 500 m depth to the bottom of the water column (between 820 and 930 m depth), the water column temperature decreases and variability increases, with 2002 much colder than the other years. 2002 gets almost the same temperature at 850 m depth than 2007 at 930 m, which is 4.4 °C. The variability in the deepest part of the water column might be due to the position of the original casts over the Campbell Plateau. Because the number of casts is reduced the deeper the sampling goes, this variability might be weighted by where the profile was sampled, thus biasing variability in the deeper water mass structure.

High variability is also seen at the top and bottom of the salinity profiles (Figure 4.6b). A range of 0.1 g kg^{-1} between the freshest year, 2008, and the saltiest, 2002 is seen at the surface. In the first 100 m of the water column, all the profiles have a relative salinity maximum above a salinity minimum, except in 2003 when waters remained homogeneous. The layer from 100 to 300 m is very homogeneous with all profiles getting slightly saltier with depth. Below 300 m the salinity starts decreasing towards 500 m where the salinity range between different years is smaller. Salinity keeps decreasing from 500 m to the ocean bottom albeit in an irregular manner, with 2002 and 2007 as fresher years and 2003 and 2009 as the most saline with a range of 0.03 g kg^{-1} .

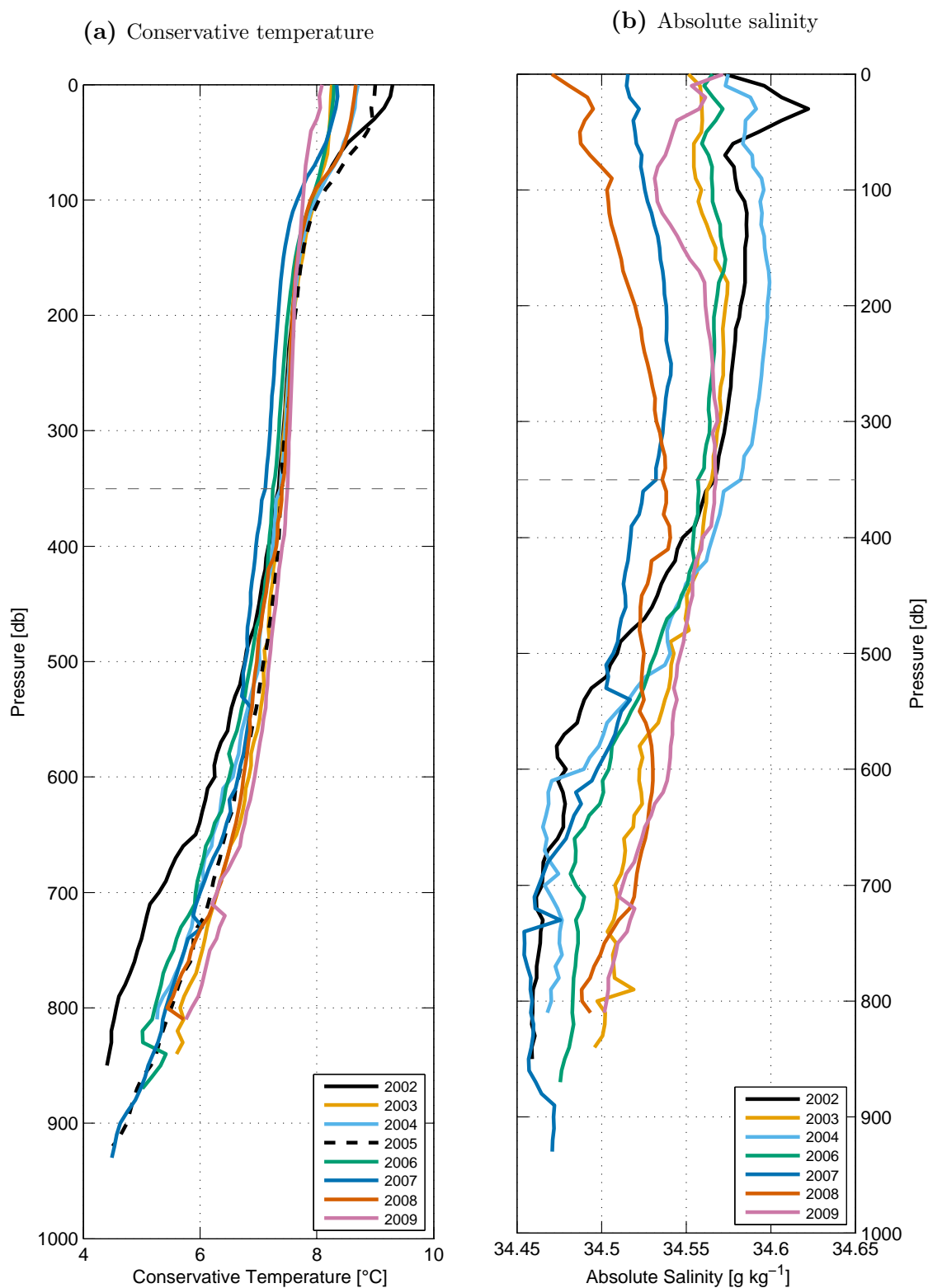


Figure 4.6: Conservative temperature (left) and absolute salinity (right) means from the gridded data. The dashed line marks the depth where the spatial mean is common to all the years. Note the change on range scales between temperature and salinity.

4.2.3 Water mass variability

To assess the water mass variability a Θ - S_A diagram with mean values for every 10 m of the water column is presented in Figure 4.7. Surface waters are warmer and saltier due to the influence of STW. 2002 is the warmest and saltiest and 2008 is the warmest and freshest, both have the lightest surface waters. 2007 is more similar to 2008 while the rest of the years have more similarities to 2002. All the years come together between a temperature range of 6.5 °C and 7 °C, here identified as SAMW. At the bottom of the profiles (from 600 m depth) there is also high variability, with two groups of years; the fresher and colder (2002, 2004 and 2007) and the saltier and warmer (2003, 2008 and 2009). 2006 sits between the two groups.

At the surface, 2002 is warmer and saltier than 2008, but they share the same density range (just below 26.6 kg m⁻³). At the bottom, 2002 is fresher and deeper than 2007, however, both are equally dense, which suggests that temperature is controlling the density. 2002 is fresher and colder than 2003, but they are almost the same depth. However 2002 is much more dense than 2003.

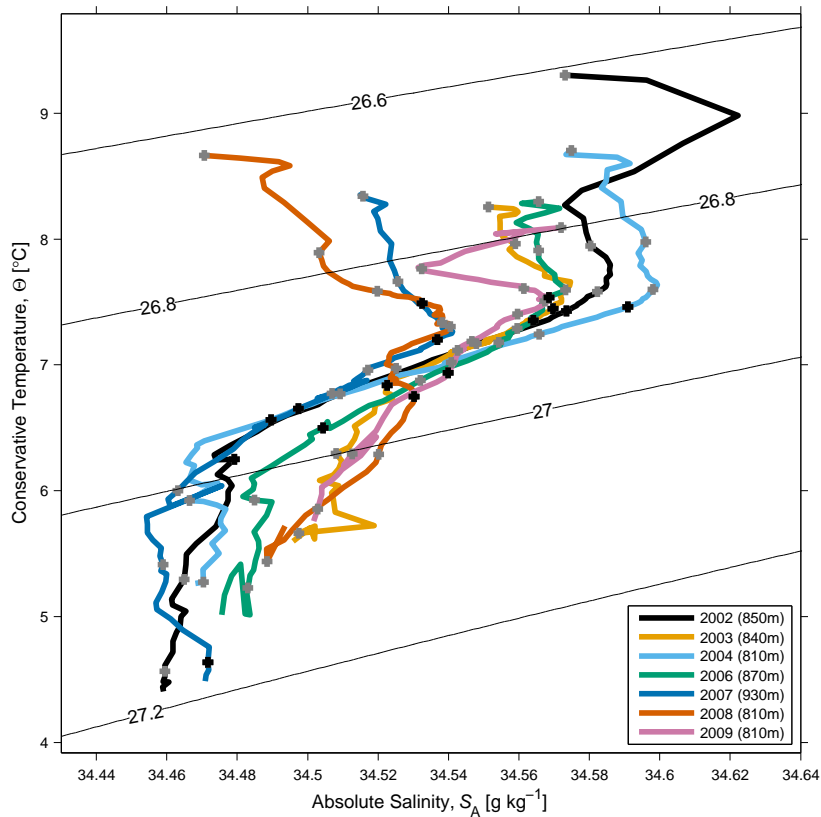


Figure 4.7: Θ - S_A (conservative temperature vs absolute salinity) diagram from mean values for December of the years shown. Grey dots represent depth every 100 m and black dots every 300 m. Contours are potential density [kg m^{-3}] referenced to 0 dbar. The bottom depth of each profile is by the year in the legend.

4.2.4 Interannual variability on the Campbell Plateau

To investigate the interannual variability over the Campbell Plateau, three different methods are used depending on the depth being investigated. Anomalies were calculated for the surface and 250 m depth (Figure 4.8 and Figure 4.9). Anomalies were calculated by subtracting the seven year mean from each year and depth. For the layer at 450 m depth (Figure 4.10), the common area was too small to calculate anomalies, instead, the interpolated data for each year is used to show the spatial structure and variability. For depths deeper than 450 m the distribution of the interpolated data is insufficient to describe the structure at that depth.

The third method used is to examine Θ - S_A diagrams from the original data and for all available years (Figure 4.11). Salinity observations for 2005 are not shown in the figures as they were previously excluded from the analysis. For the Θ - S_A diagrams, the CTD profiles that were previously vertically interpolated onto a 10 m regular vertical grid, were smoothed to reduce profile noise using a vertical 30 m running mean.

Most of the time, temperature and salinity anomalies change together, with positive anomalies warmer and saltier, and negative anomalies colder and fresher. This relationship suggests a change in water mass. If the changes are seen only in one of the variables, it could be due to other mechanisms such as evaporation, rain or heat fluxes. Changes in depth are not affected by air-sea interaction, hence, deeper changes may be related with changing in flows, i.e., water masses change variability.

The largest range of anomalies occurs at the surface, with a temperature range of 4.2 °C (−1.4 °C to 2.8 °C) and a salinity range of 0.5 g kg^{−1} (−0.21 g kg^{−1} to 0.33 g kg^{−1}). 2002 is the most consistently warm year. 2005 is similar but with cooling on the southeast flank of the plateau. 2009 is the coldest year with a very strong negative anomaly (cold) to the north side of the plateau. 2003, 2006 and 2007 are also cold years, but with some patches of warm anomalies. 2003 has a strong cold anomaly over the STF and a weak warm anomaly over the northern edge of the plateau. 2006 is cold in general, with two strong cold patches over the STF and the north edge of the plateau, but it also has a warm spot in the centre of the plateau. 2007 is cold in general but with a warm anomaly over the STF.

Salinity anomalies are more variable, normally corresponding with temperature, with fresh anomalies corresponding to colder waters. However, there are years that this relation is unclear. For example, 2008 is the freshest year of the whole period, but is not the coldest year, although there is a strong negative (fresh) signal that extends from the STF through the centre of the plateau to the eastern edge of it that has a weak negative anomaly (cold) in the temperature map. 2007 is divided between a salty STF and a fresh east side of the plateau. 2002, 2003, 2004, 2006 and 2009 have in general saltier

anomalies, with small patches of fresh anomalies, which normally coincide with colder waters.

In general, surface signals are coherent with those observed at 250 m, although the gradients at 250 m are weaker, with an anomaly temperature range of 2.6 °C (−1.2 °C to 1.4 °C) and 0.39 g kg^{−1} (−0.17 g kg^{−1} to 0.22 g kg^{−1}). The 250 m anomaly maps have more variability than the surface ones, but also more zones with no changes (anomaly = 0) (Figure 4.9). 2002 which was the warmest year at the surface, shows a colder signal at 250 m depth. 2005, was also a warm year at surface, and also shows some cold anomalies at 250 m depth. 2009, was the coldest year at surface, and shows a very warm distribution at 250 m depth. 2007 (cold at surface), however, kept its cold distribution, with the only change due to confining the warm anomaly to the STF. The rest of the years have an irregular distribution of temperature anomalies.

Regarding salinity anomalies, the period from 2002 to 2004 is saltier than the 2006 to 2009 period, with 2008 the freshest year, preceded by a fresh 2007 with a salty STF. This signal was already identified at the surface layers, with 2007 less homogeneous (is the fresh water coming from the deep?). The saltiest anomalies, however, are over the STF and the north edge of the plateau.

Although there is not a significant trend for the anomalies, it looks like these are coming from the edges of the plateau. It appears that the anomalies on the northern and eastern side of the plateau come from the STF, with years where the anomaly affects the whole plateau, e.g., 2003, 2006, 2009 and years where the anomalies over the STF are confined to the 500 m isobath, such in 2007. It appears that the western side of the plateau is more influenced by the SAF.

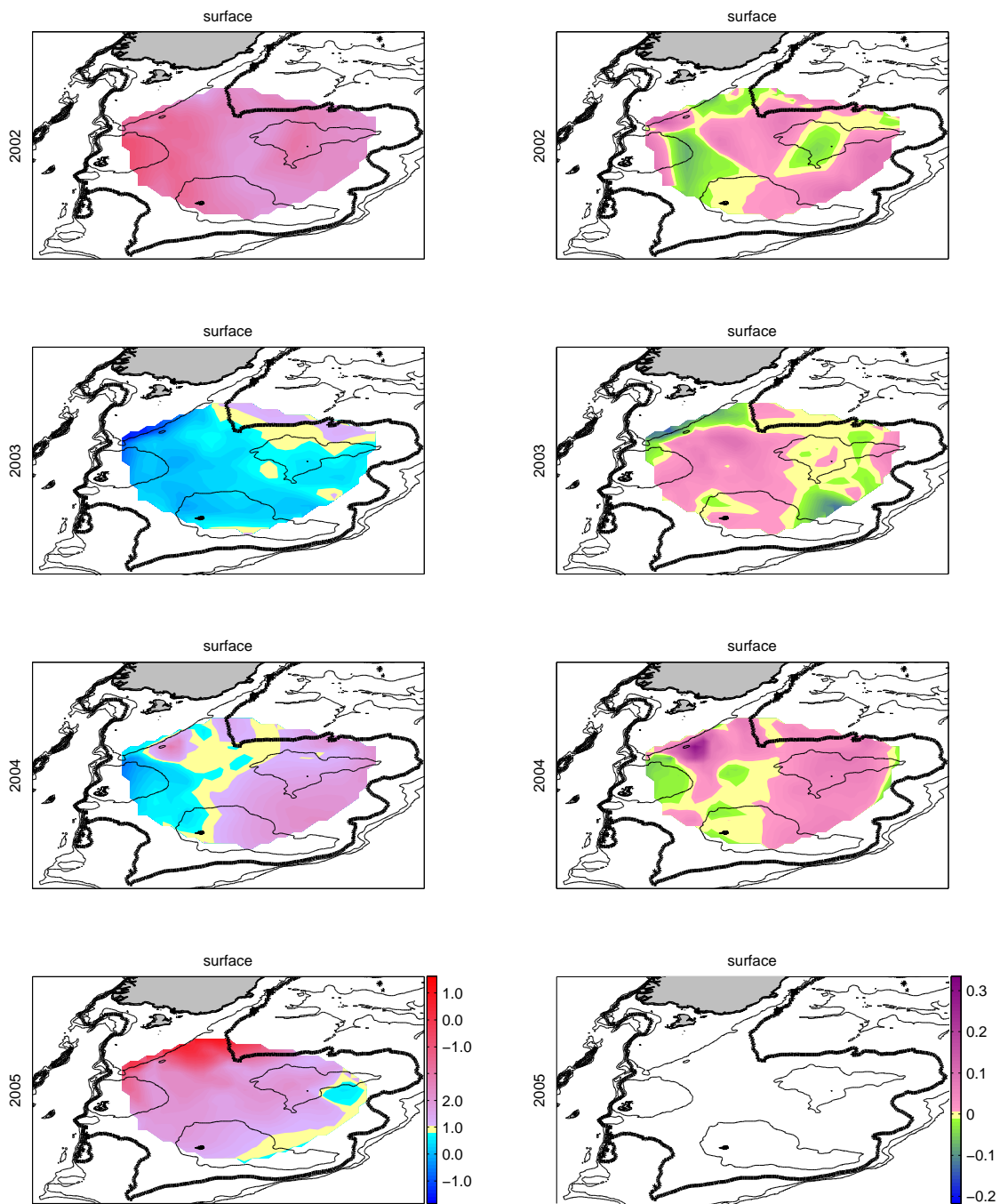
The 450 m maps cover less area due to the bathymetry (Figure 4.10). They show some signals propagate through the whole water column. They are also useful to identify any weakening of the STF with depth. Temperature ranges at 450 m are still noticeable, with a range of 3.3 °C (5.7 °C to 9 °C), while salinity ranges are smaller, with a range

of 0.38 g kg^{-1} (34.4 g kg^{-1} to 34.78 g kg^{-1}). The presence of SAMW at this depth during the whole period is defined by temperature its (7 to $7.5 \text{ }^\circ\text{C}$). However, the influence of the STF is still noticeable, with warmer and saltier water on the western side of the plateau, e.g., 2003, 2006 and 2009. 2002 shows a cold patch of water to the north of the plateau. 2003, 2004 and 2006 have cold water influence from the eastern edges of the plateau. 2003, 2006 and 2009 also have warm water on the western flank of the plateau.

Θ - S_A diagrams of all the data available over the whole period give an insight to the whole water mass structure and its variability (Figure 4.11). The range of water masses introduced in Figure 4.4 is shown in all the years. It appears 2002 and 2007 are the years that have more influence of STW, and also the years that have waters above the 26.6 kg m^{-3} density layer. The middle parts of the profiles are homogeneous with water that has characteristics of SAMW (temperature around $7 \text{ }^\circ\text{C}$ and salinity around 34.5 g kg^{-1}). Variability deeper than 600 m strongly depends on the distribution of the CTD casts. The structure at deeper layers show a common salinity minimum at the density layer of 27 kg m^{-3} which has the characteristics of AAIW (salinity $<34.5 \text{ g kg}^{-1}$ and temperature between 4 and $6 \text{ }^\circ\text{C}$). The only year that does not show this feature is 2008. All deep profiles have temperatures colder than $6 \text{ }^\circ\text{C}$ and salinities between 34.4 and 34.5 g kg^{-1} . 2002 and 2007 show a double structure at the bottom of the profiles, with the same temperature but two different salinity ranges.

(a) Conservative temperature anomaly

(b) Absolute salinity anomaly



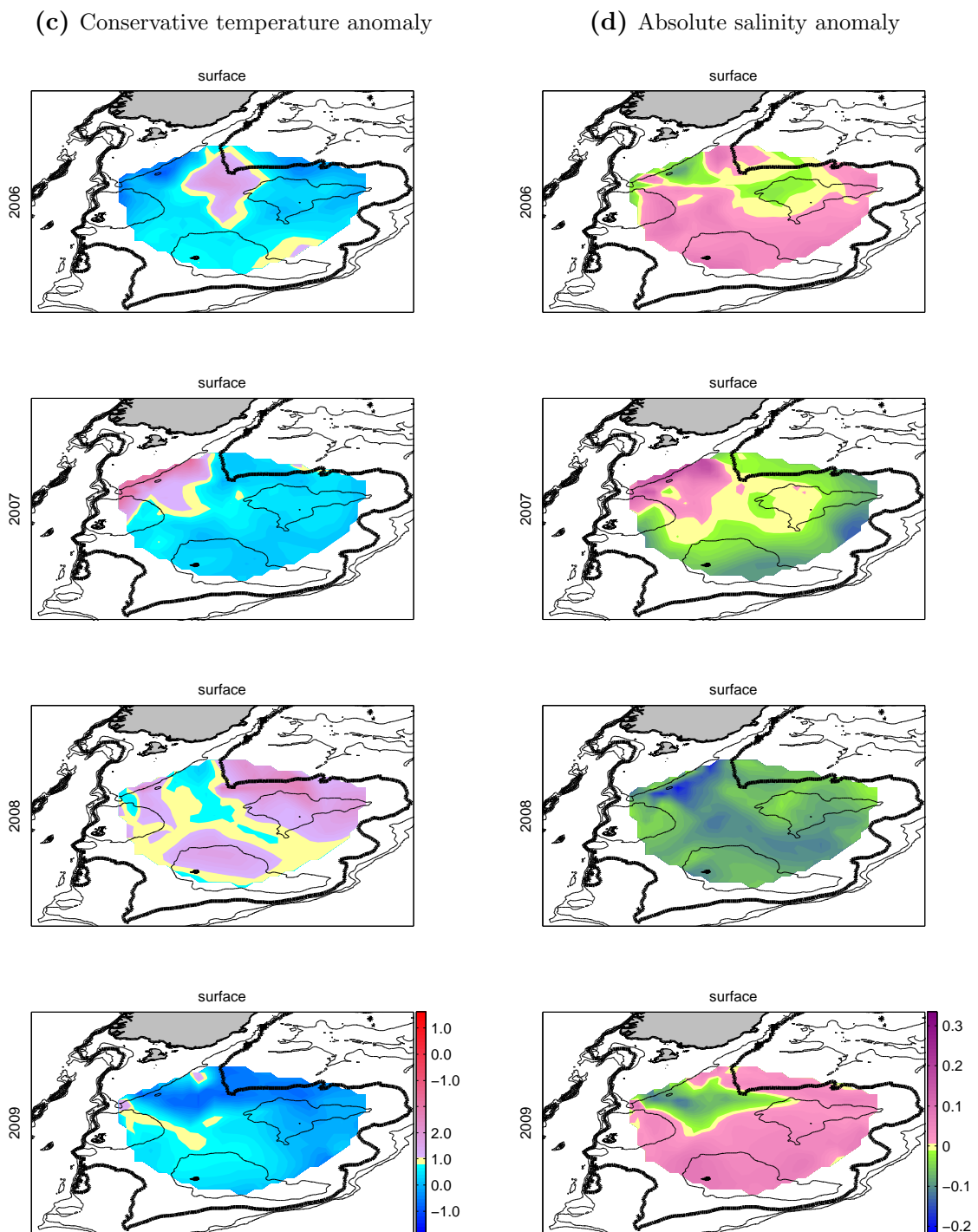
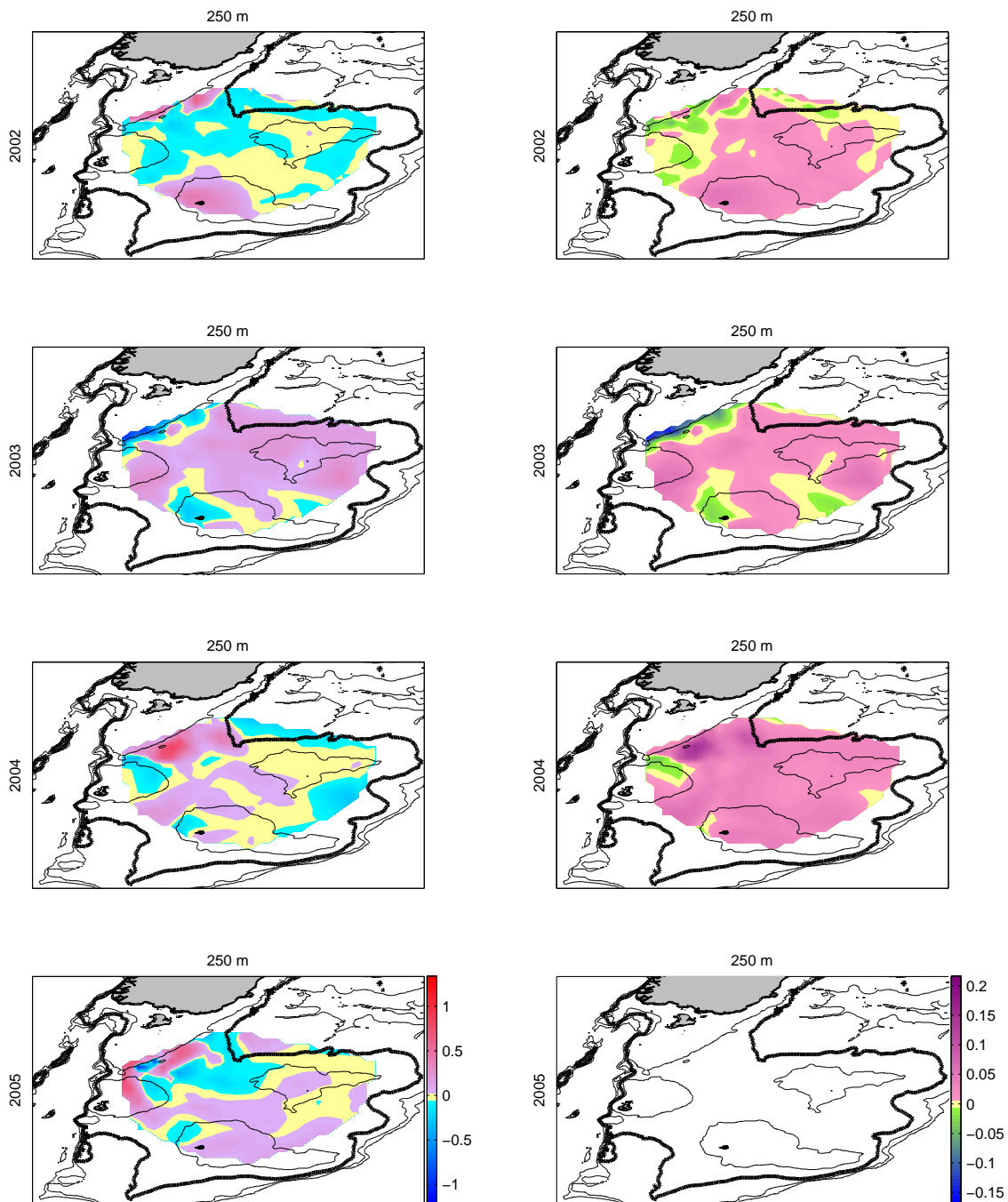


Figure 4.8: Conservative temperature anomalies, to the right, and salinity anomalies, to the left, at surface layer. Pale yellow shows anomalies equals zero. Temperature [$^{\circ}\text{C}$] and salinity [g kg^{-1}] colourbar to the right of the bottom figure in each panel. Thick contour shows the 1000 m isobath.

(a) Conservative temperature anomaly

(b) Absolute salinity anomaly



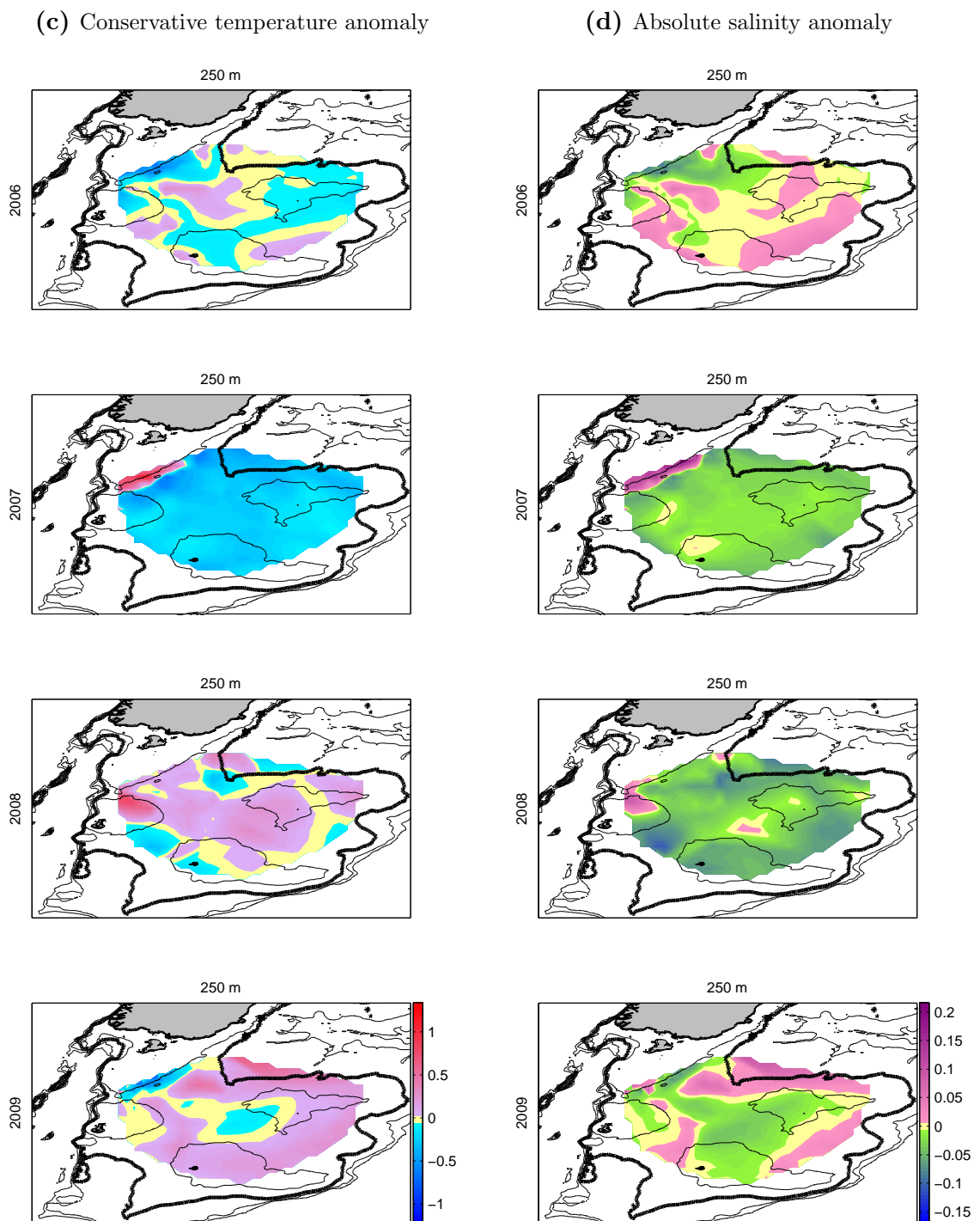
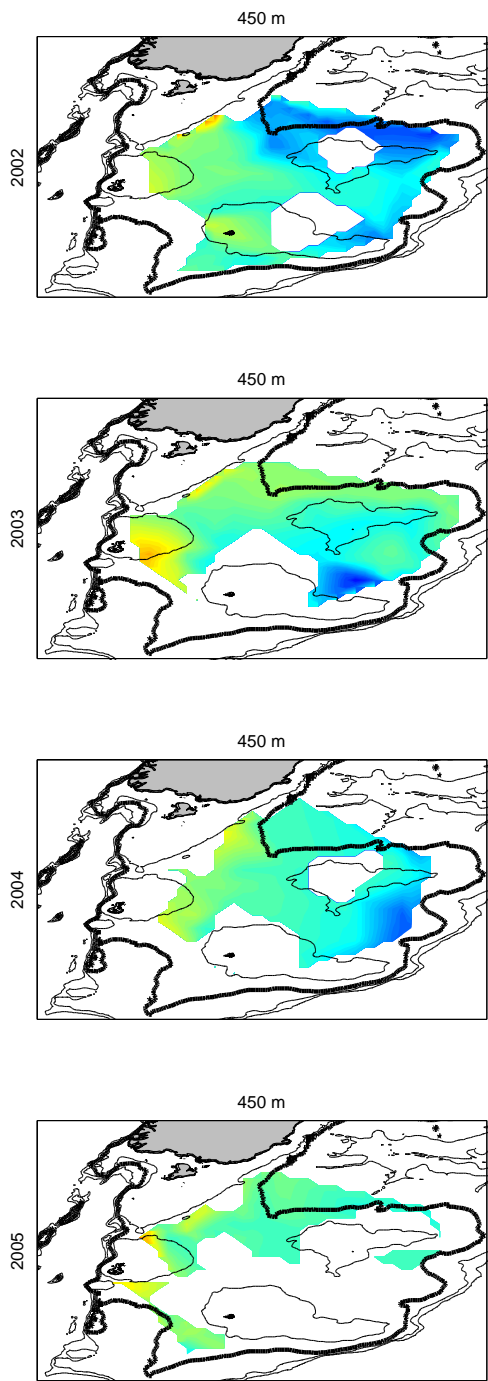
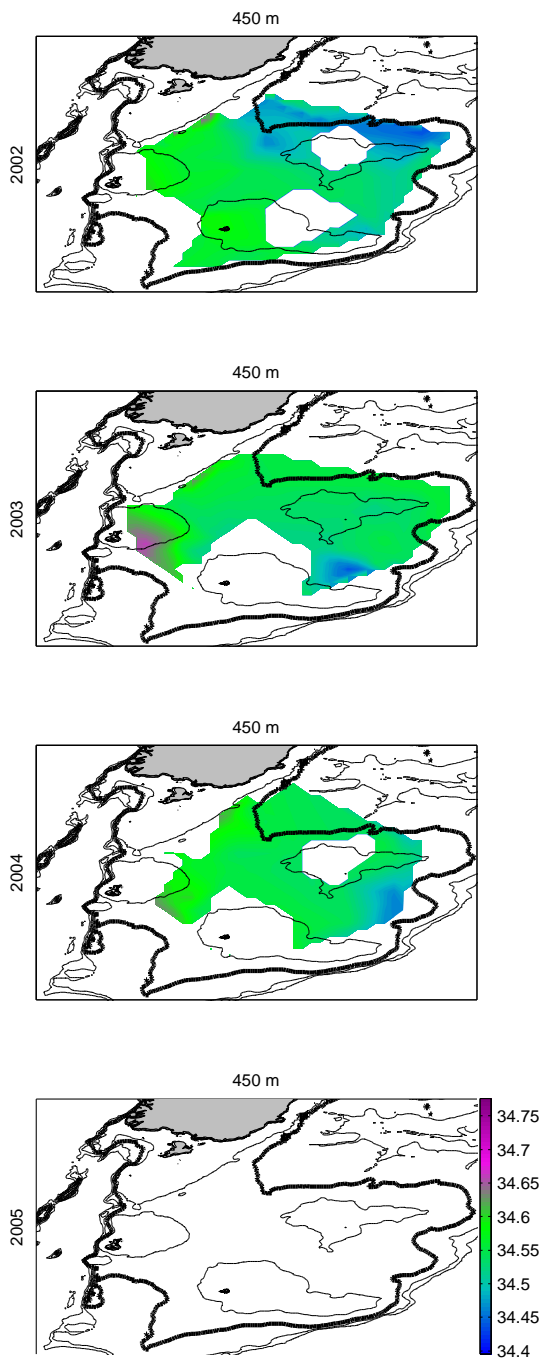


Figure 4.9: Conservative temperature anomalies, to the right, and salinity anomalies, to the left, at 250 m layer. Pale yellow shows anomalies equals zero. Temperature [$^{\circ}\text{C}$] and salinity [g kg^{-1}] colourbar to the right of the bottom figure in each panel. Thick contour shows the 1000 m isobath.

(a) Conservative temperature



(b) Absolute salinity



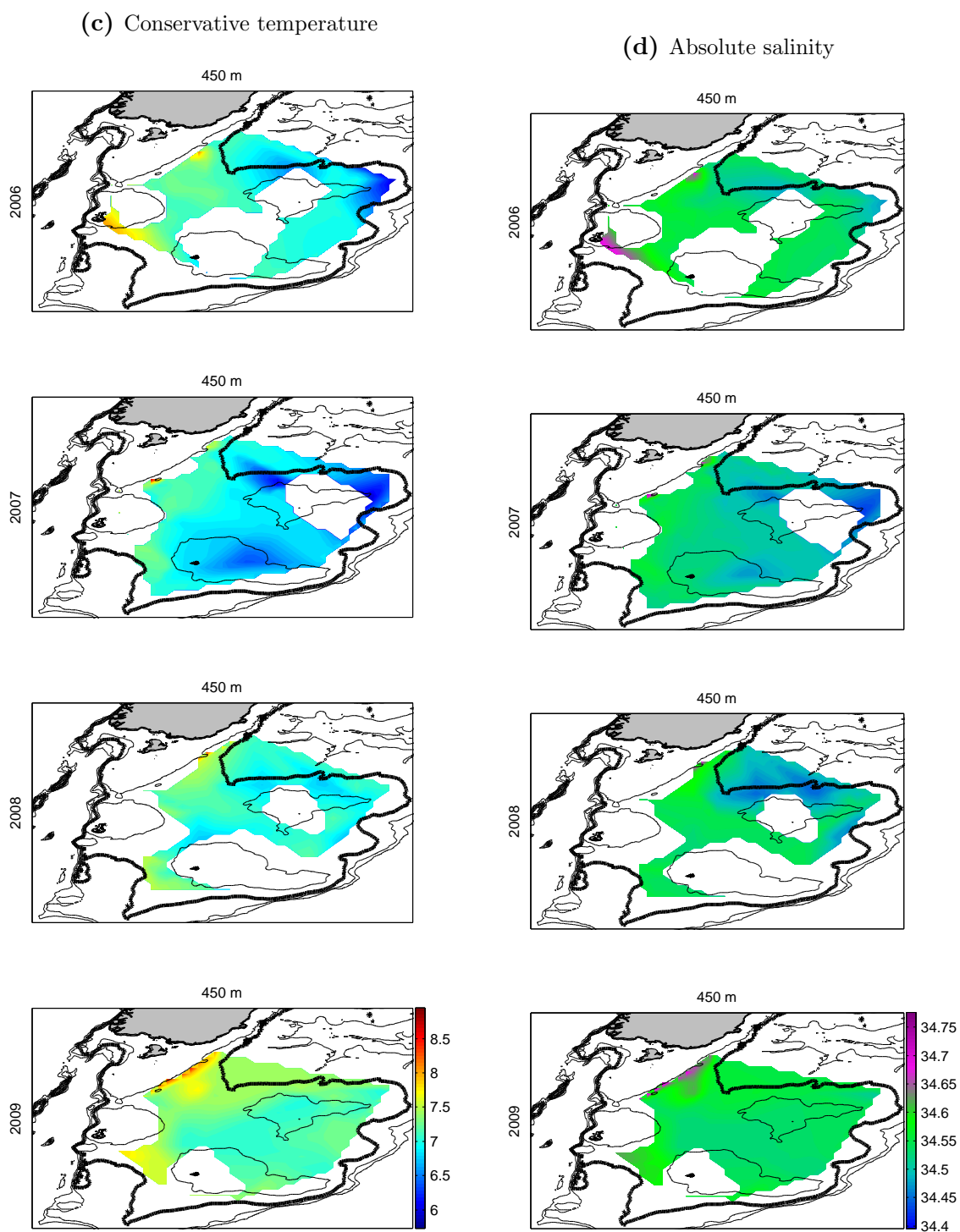


Figure 4.10: Conservative temperature, to the right, and salinity, to the left, at 450 m layer. Temperature [$^{\circ}\text{C}$] and salinity [g kg^{-1}] colourbar to the right of the bottom figure in each panel. Thick contour shows the 1000 m isobath.

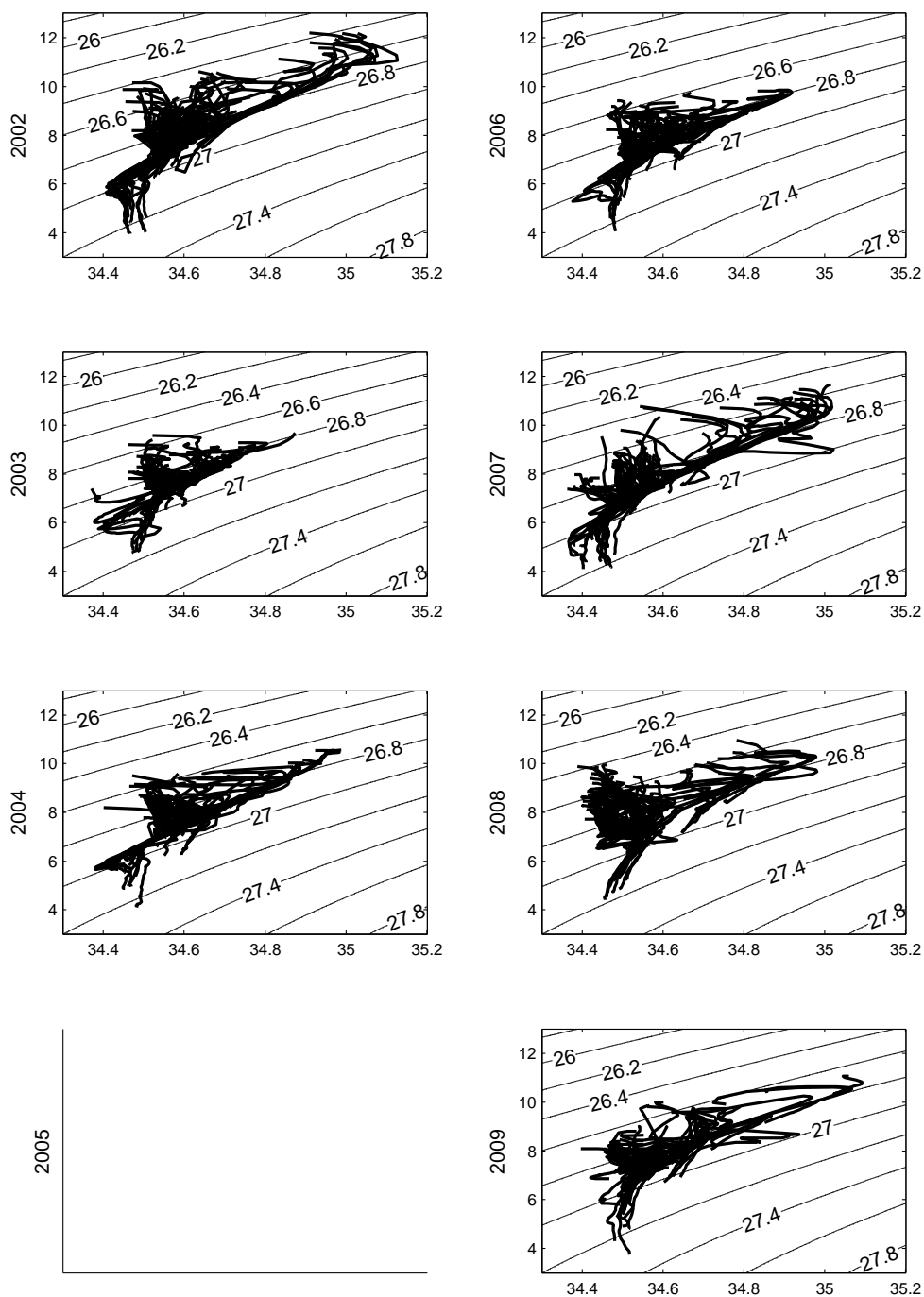


Figure 4.11: Θ - S_A (conservative temperature (x-axis [$^{\circ}\text{C}$]) vs absolute salinity y-axis [g kg^{-1}]) diagram for all the years. Profiles have a 30 m running mean to avoid noise. Contours are potential density [kg m^{-3}] referenced to 0 dbar.

4.2.5 Steric height

Steric height determines the distance, or depth difference, between two surfaces of constant pressure. It is defined as:

$$h(z_1, z_2) = \int_{z_1}^{z_2} \delta(T, S, p) \rho_0 dx \quad (4.1)$$

where h is steric height, (m); z_1 and z_2 are the depths of the pressure surfaces, (m); δ is the specific volume anomaly, ($\text{m}^3 \text{kg}^{-1}$); T is temperature, ($^{\circ}\text{C}$); S is salinity, (g kg^{-1}); p is pressure, (dbar) and ρ_0 is reference density of sea water, (1028 kg m^{-3}).

Steric height has the dimension of height and is expressed in m. The specific volume anomaly is the difference in volume between a unit mass of water at temperature T and salinity S and a unit mass of standard salinity $S = 35.0$ and $T = 0^{\circ}\text{C}$. Another term related to steric height is dynamic height D or dynamic topography, and is defined as hg , the product of gravity and steric height. The “dynamic metre” as a unit of D is $\text{m}^2 \text{s}^{-2}$ as opposed to units of steric height that are units of length (Tomczak and Godfrey, 2001).

Steric height was calculated over the Campbell Plateau from the common grid for each individual year. The shallowest common depth for all years (280 m) was chosen as the reference level to integrate up the steric height through the water column. Because salinity for 2005 could not be used, the mean salinity in the other years was combined with the 2005 temperature to calculate steric height in 2005. As steric height is expected to be dominated by temperature, this gives a reasonable approximation. Accordingly, the mean over the whole period was calculated leaving 2005 out.

Steric height maps at one surface relative to another provide the relative streamfunction for the geostrophic flow. In the streamfunction the currents flow along the contours of steric height with the high height to the left of the flow in the Southern Hemisphere (e.g., Talley et al., 2011), with the speed proportional to the gradient of the slope at that point.

The mean steric height map for the upper 280 m shows a flow along the gradient of the STF (Figure 4.12) following the contours. It also shows a flow on the western side of the plateau, flowing across the plateau and getting weaker towards the north edge of the plateau.

A strong gradient is identified where the STF is located, with the flow towards the northeast as part as the Southland Current (Figure 4.13). The STF gradient changes between the years, with a strong gradient during 2002, which disappears in 2003 and 2004, and builds up in 2005. 2006 is weaker than the other years, but in 2007 the gradient associated with the STF appears again. 2006 has an anticyclonic recirculation on the north edge of the plateau that coincides with the signal in the temperature and salinity anomalies described previously. This feature appears to weaken in 2007 and change into two smaller recirculation cores in 2008. However, this recirculation seems to be consistent over the years, sometimes developing into a stronger pattern. Over the southern plateau, the flow is consistently eastward, with another recirculation feature near the southern part of the plateau, with 2002 and 2005 presenting similar features in the same spot.

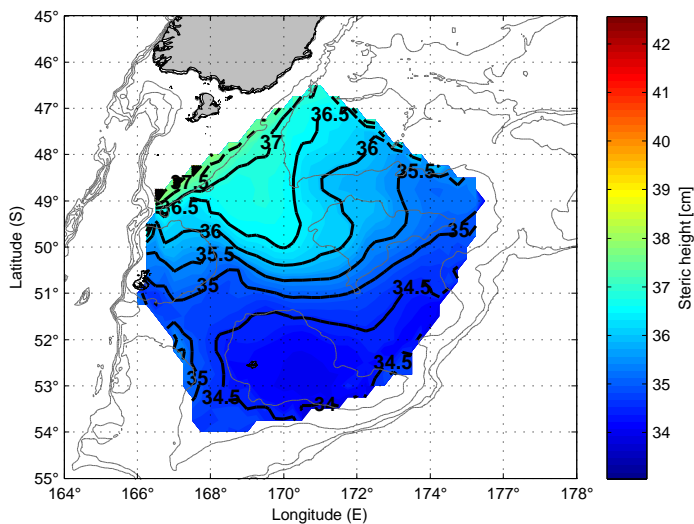


Figure 4.12: Steric height mean for the low resolution data from 2002 to 2009 (except 2005). Contours every 0.5 cm. Grey contours show bathymetry with contours every 500 m.

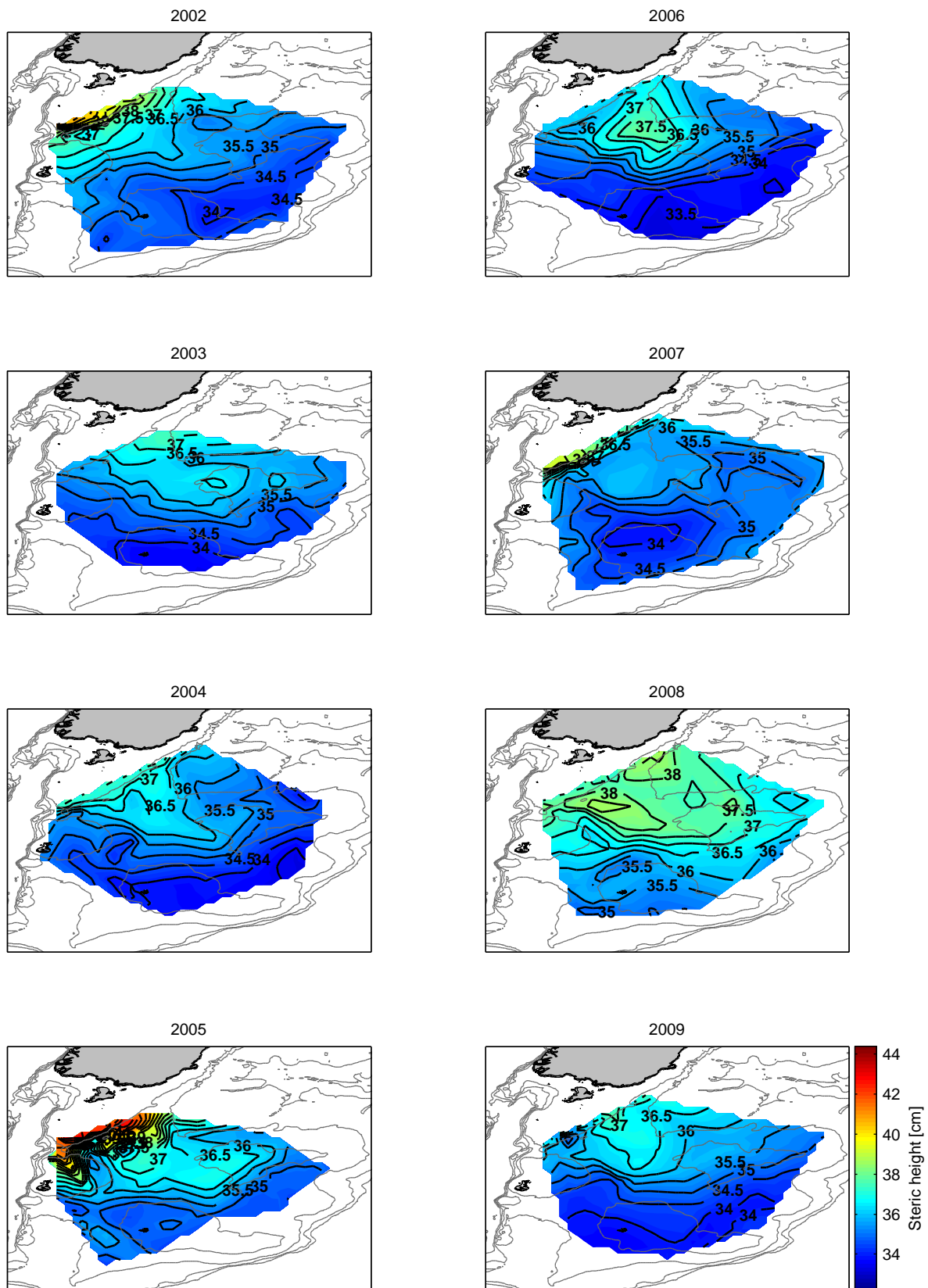


Figure 4.13: Steric height maps for the period 2002 to 2009 for a water column of 280 m. Contours every 0.5 cm. Grey contours show bathymetry with contours every 500 m.

4.3 Discussion

4.3.1 Water masses

For the first time Antarctic Intermediate Water (AAIW) has been reported in the deeper parts of the Campbell Plateau, between 600 and 900 m, underneath the SAMW layer (Figure 4.11). This AAIW has a temperature between 4°C and 6°C, salinity $<34.55 \text{ g kg}^{-1}$ and a density anomaly between 27.1 and 27.3 kg m^{-3} . These characteristics are similar to the Southern Ocean AAIW type reported by Bostock et al. (2013). AAIW was detected in every year except 2005, which was previously excluded because of unexplained salinity values. The occurrence of AAIW is shown in Figure 4.14.

To gain another perspective on AAIW on the plateau, and some insight into how it gets onto the plateau, a group of stations from the high resolution data set (Chapter 3) have been selected from where AAIW was found in the low resolution casts (Figure 4.15a). Two transects are to the southwest and southeast of the Campbell Plateau (May 1998), and the other is a longitudinal transect across the Pukaki Saddle (May 2003) (all these transects have been previously presented in Section 3.2.1). The variables (conservative temperature, absolute salinity and potential density anomaly) are again presented here (Figure 4.15) but with the range of Southern Ocean AAIW properties highlighted (temperature and density ranges are shown through the isolines and salinity is shown by the colour scale). AAIW can be seen on the edge of the Campbell Plateau in all the transects between 600 and 900 m. It appears that it is coming from further south (Figure 4.15b) and it does not go deeper due to the shallower bathymetry of the Campbell Plateau.

Two more transects, on the northern edge of the plateau and across the Bounty Trough from December 1998, were also investigated (Figure 3.18c and Figure 3.24a). In these, AAIW was also found between 800 and 1100 m. This suggests that AAIW follows the bathymetry around the Campbell Plateau from the south to the east before flowing through the Pukaki Saddle and continues along the northern edge of the plateau into the Bounty Trough.

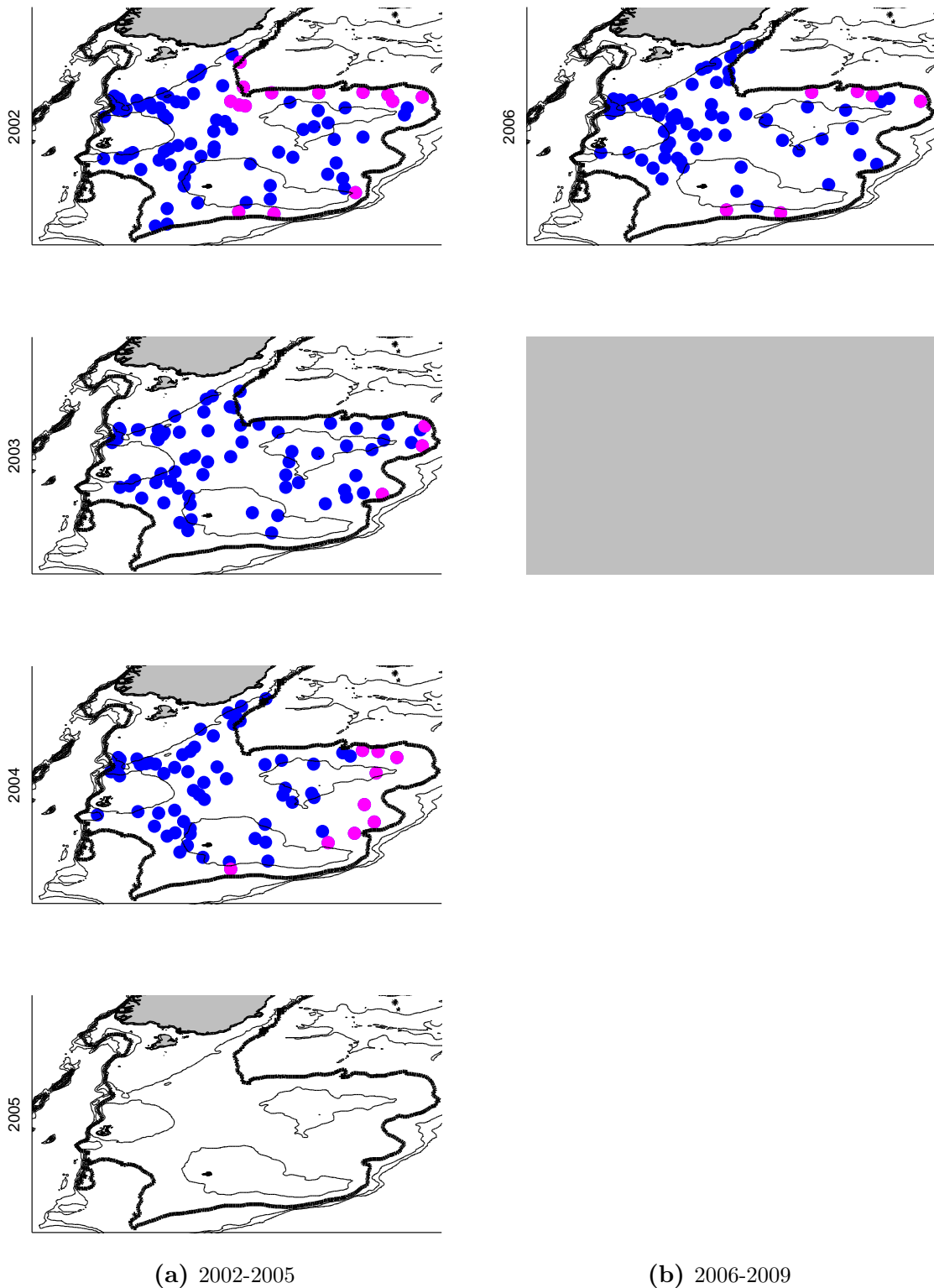
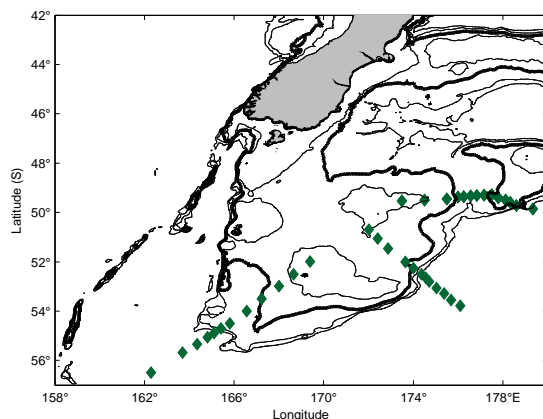
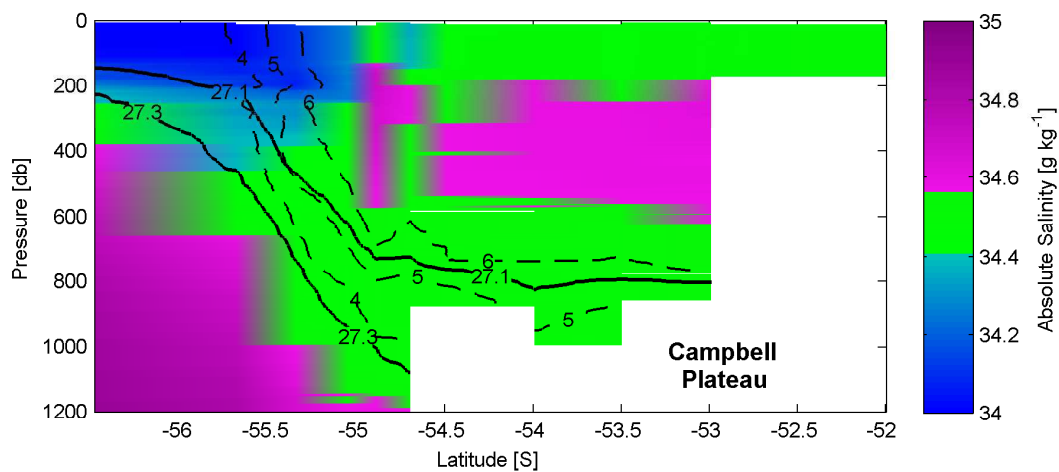


Figure 4.14: Pink dots show the distribution for the low resolution casts where AAIW has been found at the bottom of the profile, between 600 and 900 m, blue dots the distribution for the all the casts. 2005 salinity values were excluded from the analysis in Chapter 4. Contours every 500 m, bold contours show the 1000 m isobath

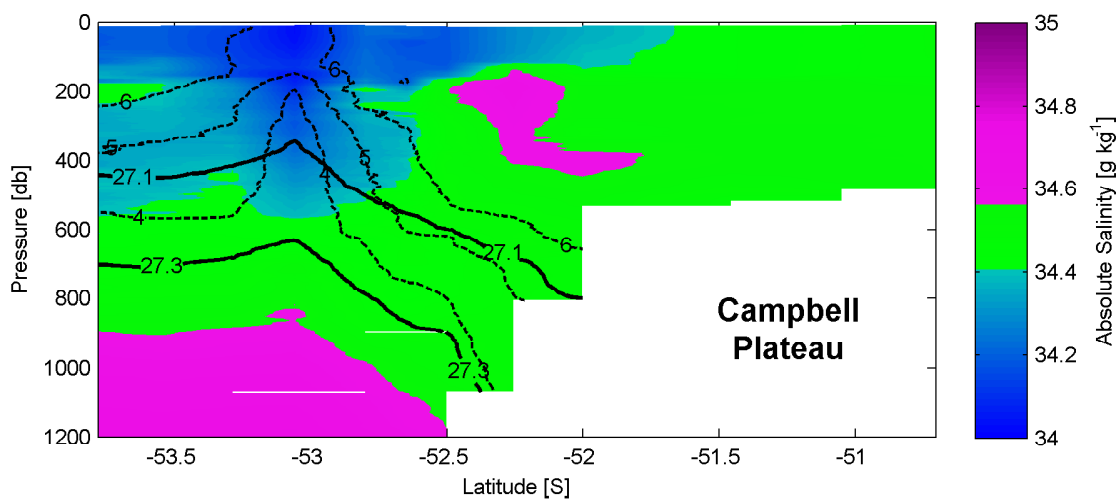
(a) Hydrographic stations for AAIW



(b) Western Campbell Plateau transect



(c) Eastern Campbell Plateau transect



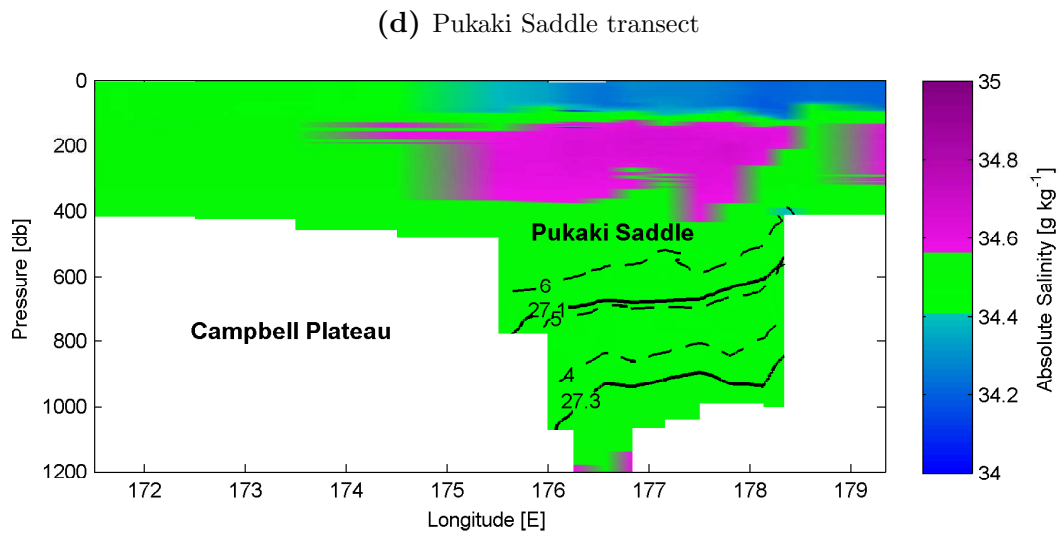


Figure 4.15: (a) Hydrographic stations (green) on the Campbell Plateau. Contours every 500 m, bold contour show 1000 m isobath. (b) Western transect showing AAIW, (c) Eastern transect and (d) Pukaki Saddle showing AAIW. North to the right side of (b) and (c) and East to the right side on (d). Colour code is absolute salinity, the green code is the salinity range for AAIW. Dashed lines are conservative temperature, °C, on AAIW range. Solid lines are potential density anomaly, kg m^{-3} , on AAIW range.

The idea of SAMW leaking onto the plateau is not confirmed by this study. However, due to the distribution of AAIW around the edges, it is apparent that, AAIW is leaking onto the plateau where it meets the deeper ocean. Still, the question of the region of SAMW formation remains unclear.

4.3.2 Circulation

Steric height calculated over the first 280 m of the water column over the Campbell Plateau (Figure 4.13) shows the first picture of the variability in the flow on the Campbell Plateau. Despite the interannual variability it looks like there is a constant flow to the east over the central plateau and towards the north on the northern edge of the plateau. This flow appears to divide the plateau into two parts; the northern part, where in some years an anticyclonic flow develops, such as 2006, and the southern part, where in

some years a cyclonic flow develops, such as 2007. In years where these features do not develop, such as 2009, the flow in the north appears to be towards the northeast and in the south towards the west.

4.3.3 Spatial and interannual variability

The Campbell Plateau is influenced by the STF and SAF. Interannual variability of the ocean properties during December from 2002 to 2008 shows spatial and vertical changes with no specific trend over time. However, the influence of the STF on the western side of the plateau and the SAF on the eastern side is observed in the mean conservative temperature and absolute salinity mean maps (Figure 4.5), and these influences are consistent with depth. This is also seen in the distribution of the anomalies which suggest spatial variability driven by the STF on the northwest of the plateau, for example, 2003, 2006, 2007 and 2009 (Figure 4.8). Smith et al. (2013) traced the S-STF south of the South Island as far south as 49.6°S with it then turning north around the Snares Shelf (their Figure 11). This position is consistent with the influence of the STF on the northwest side of the plateau. Interannual variability in the top 100 m, is mainly linked to air-sea interaction, however, it appears that the variability driven by the SAF comes from deeper layers on the eastern edge of the plateau, for example, 2003, 2004, 2006 and 2007 at 450 m depth (Figure 4.10). As previously suggested, it appears that the 1000 m isobath is the depth at which the SAF starts influencing the Campbell Plateau (Stanton and Morris, 2004). An explanation for this variability could be linked to the variability in the SAF, i.e., strength or position, although this cannot be confirmed here. Further work on SAF flow using altimetry data would be needed to link both variabilities.

Subantarctic Mode Water (SAMW) has been found over the Campbell Plateau, as a homogeneous thick layer of 7°C water, in the high resolution data set (Figure 3.19). In the low resolution data sets SAMW is found between 100 and 500 m (Figure 4.6). This layer is very homogeneous through time, although the thickness of this layer varies with season. The seasonal variations are consistent with the SAMW seasonality described in the high resolution transects across the Campbell Plateau in Section 3.2.1. The presence

of SAMW on the Campbell Plateau was expected as it had been reported in previous studies (Morris et al., 2001) where it was suggested that SAMW may leak onto the deeper parts of the plateau along its flanks.

4.4 Summary of the Chapter

In this chapter the December interannual variability on the Campbell Plateau is investigated. The spatial and vertical variability is revealed through the CTD profiles distributed over the plateau. The water mass structure of the Campbell Plateau shallower than 1000 m deep is described and the surface flow related to the first 280 m of the water column reported through steric height.

The mean conservative temperature and absolute salinity show the Campbell Plateau being influenced by the STF and the SAF regimes. The STF influence extends along the 500 m isobath to the northwest of the plateau, to the south over the Auckland Islands and further south. The SAF influence covers all the eastern side of the plateau with a very homogeneous distribution. This suggests dividing the plateau in two parts, the western part with a major influence of the STF and the eastern part with a major influence of the SAF.

Vertical mean profiles reveal a highly variable surface layer to 100 m in conservative temperature and absolute salinity. This variability shows no specific trend, with warm years followed by cold years. This variation is likely due to air-sea interaction. A very homogeneous layer with SAMW properties is found from 100 to 500 m. A highly variable bottom of the water column suggests different water masses are being sampled in the deeper stations. The mean Θ - S_A diagram confirms the vertical profile results and shows the different water masses distribution and composition.

Conservative temperature and absolute salinity anomalies are spatially coherent in most of the cases. These anomalies are also coherent with depth. The distribution of the anomalies with depth suggests a stronger source of variability coming from the STF to

the north edge of the plateau, and from the SAF to the southeast of the plateau in the deeper maps.

The water mass structure of the Campbell Plateau has been identified with connections to the surrounding oceans. STW and SAW are found on the surface of the plateau. SAMW is found through the middle depths of the plateau, and for the first time, AAIW has been reported at the deeper casts around the edges of the plateau.

The surface flow related to the first 280 m of the water column reveals a consistent flow across the Campbell Plateau. Some recirculation features to the south of the plateau appear to vary between years.

Chapter 5

Long-term variability on the Campbell Plateau

To study the ocean's long-term, seasonal to interdecadal variability, extended data records are needed. The most suitable satellite-observed Sea Level Anomalies (SLA) and Sea Surface Temperature (SST) records are analysed here. Such data have spatial and temporal resolution that ship-borne hydrographic observations are unable to capture, so provide the opportunity to study long-term changes over the water column. They also bring high resolution temporal sampling that better identifies variability on seasonal and longer time scales. To help understand the variability over the Campbell Plateau other information is also used in the analysis. Products such as the "Gravity Recovery and Climate Experiment (GRACE)" which provides ocean mass estimates from satellite measurements, are used to assist the evaluation of sea level changes over the Campbell Plateau. Other long-term continuous observations, preferably through the water column, are needed to compare and validate the interpretations of the satellite data and to identify any long-term variability of the ocean's vertical structure. For this reason, Argo based interpolated and gridded data are used to calculate steric height. Winds from the National Center for Environmental Prediction/National Center for Atmospheric Research (NCEP/NCAR) reanalysis are also analysed to determine if they are a likely forcing mechanism of the variability over the plateau.

Atmospheric climate indices are used to identify any link between long-term variability observed over the Campbell Plateau and equatorial variations and mid-latitude westerlies. The Southern Oscillation Index (SOI) is related to changes in the strength of the Trade Winds and SST anomalies in the tropical Pacific Ocean (e.g., Philander, 1983). Here it is used to find any connection between equatorial variations and the Campbell Plateau. The Southern Annular Mode (SAM) is a pattern of variability that can be used to indicate changes in the position and strength of the westerlies around Antarctica that is extended to the latitudes of New Zealand (e.g., Renwick and Thompson, 2006; Sallée et al., 2008). Here it is used to find if there is any connection between variations in the strength of the westerly winds over the Southern Ocean and Campbell Plateau's long-term variability.

5.1 Data and Methods

Different periods of time were analysed depending on the available lengths and temporal overlaps of different data sets. The AVHRR SST data set goes from January 1982 till December 2013; SLA from January 1993 to December 2012; satellite ocean mass from August 2002 to October 2013; steric height from January 2002 to December 2012 and the wind records from January 1948 till December 2012. Both SOI and SAM records are long enough to be compared with the other data sets.

The first part of this section discusses the methods used to construct the time series followed by the statistical processing and significance of the results. In the second part, the data used in this chapter are described. This includes showing an initial description of the general trends of the time series.

5.1.1 Time series processing methods

In order to analyse local fluctuations, sources of variation and to compare different time series, each record's mean, trend and seasonal cycle were removed. Some of these components, such as the trend and the seasonal cycle, were also analysed. The time

series $y(t)$ analysed can be modelled using this form:

$$y'(t) = y(t) - \overline{y(t)} \quad (5.1)$$

where:

$$\overline{y(t)} = y_0 + \alpha t \quad (5.2)$$

and y_0 is the mean value and αt is the linear trend over time t where α is constant. The trend $\overline{y(t)}$ is then defined as “a long-term change in the mean level” and was subtracted from the data (e.g., Emery and Thomson, 2001; Chatfield, 2004).

The seasonal cycle was removed from each time series by calculating the twelve monthly averages (seasonal cycle) and then subtracting from the appropriate month (e.g., whole period mean of February (n = number of years) minus February each year and so on) (Thompson et al., 1985; Emery and Thomson, 2001; Chatfield, 2004).

A 13-month running mean was applied to all of the anomalies (after removing the seasonal cycle) to suppress high-frequency variability (e.g., von Storch and Zwiers, 1999). Note that smoothing the time series shortens the time series by seven points at each end.

Even though all of the time series were de-trended for analysis, particularly when determining correlations, trends have been added back when the times series are plotted, as it can be useful to examine the total long-term variability of the data.

5.1.2 Statistical methods

The *standard deviation* σ was calculated from the *variance*, σ^2 , (e.g., Emery and Thomson, 2001)

$$\sigma^2 = \frac{1}{N-1} \sum_{i=1}^N (x_i - \bar{x})^2 \quad (5.3)$$

The *standard error*, S_ϵ is related to the *standard deviation* (Equation 5.4), (e.g., Talley et al., 2011),

$$S_\epsilon = \frac{\sigma}{\sqrt{N}} \quad (5.4)$$

Assuming x and y are stationary processes the cross-covariance function was used to study the relationship between two time series in the time domain (e.g., Emery and Thomson, 2001; Chatfield, 2004), and was calculated as follows:

$$C_{xy}(\tau) = \frac{1}{N-k} \sum_{i=1}^{N-k} [y_i - \bar{y}][x_{i+k} - \bar{x}] \quad (5.5)$$

where $\tau = \tau_k = k\Delta t$ ($k = 0, \dots, M$) is the lag time for k sampling time increments, of duration Δt , and $M \ll N$.

The cross-correlation function is then defined as:

$$r_{xy}(\tau) \equiv \frac{C_{xy}(\tau)}{\sigma_x \sigma_y} \quad (5.6)$$

where σ_x and σ_y are the standard deviations for each time series (e.g., Emery and Thomson, 2001; Chatfield, 2004).

Consecutive data values within a time series might not be independent. For this reason and to determine the confidence limits of the correlations, the Effective Number of Degrees of Freedom (EDOF) is determined. This gives a measurement of the true independence of the data (e.g., Emery and Thomson, 2001). The EDOF are defined as

$$EDOF = \frac{N\Delta t}{T} \quad (5.7)$$

where $N\Delta t$ is the total length of the time series and T is the decorrelation time of the time series, i.e., the time lag for which the data become uncorrelated. The EDOF is calculated based on knowledge of the auto-covariance function, C_{yy} , which is a lagged correlation of the time series with itself, estimated by:

$$C_{yy}(\tau) = \frac{1}{N-k} \sum_{i=1}^{N-k} [y_i - \bar{y}][y_{i+k} - \bar{y}] \quad (5.8)$$

where the auto-correlation coefficient is given by:

$$r_{yy}(\tau) \equiv \frac{C_{yy}(\tau)}{(\sigma)^2} \quad (5.9)$$

At lag = 0 $r = 1$, but with longer lags the auto-correlation decreases approaching zero. The decorrelation time, T , is approximated by the time lag for the first zero crossing of the auto-correlation function, (e.g., Emery and Thomson, 2001; Talley et al., 2011). The auto-correlation functions for SST averaged over the Campbell Plateau and SOI can be seen in Figure 5.1, from this the first zero crossing is used to calculate the EDOF. Here, for example, the zero crossing is 14 months for SOI and 38 months for SST, so the EDOF are respectively 27 and 10.

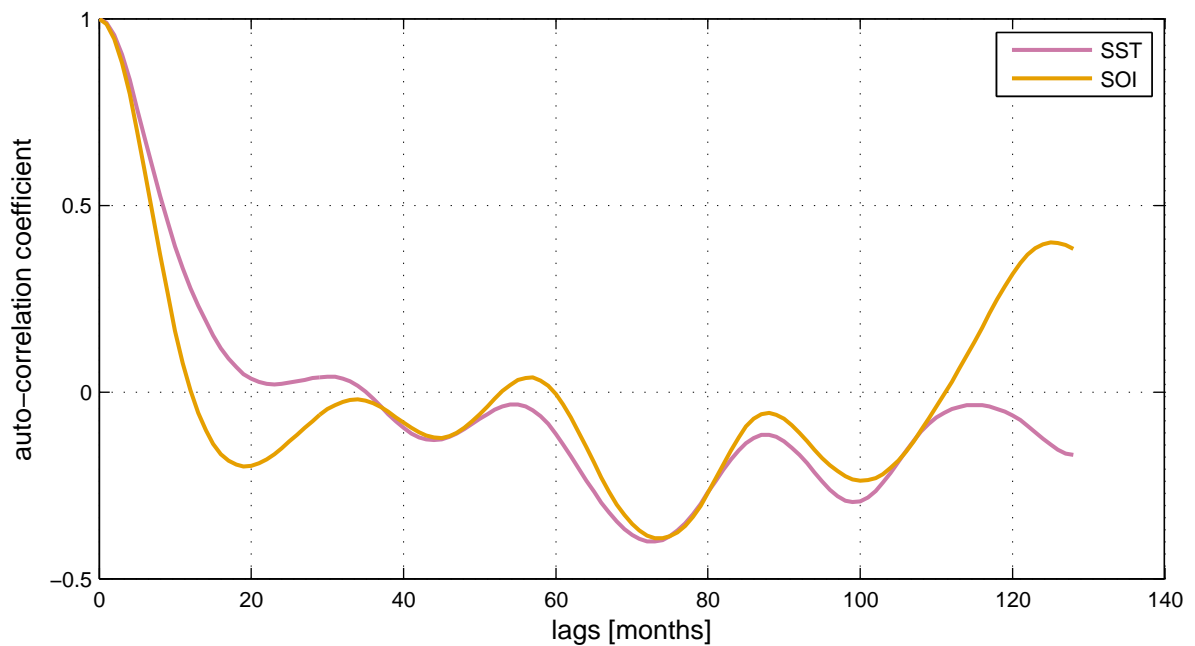


Figure 5.1: Auto-correlation function for SST (solid pink) and for SOI (solid orange).

To determine the significance of the correlations, r was converted into a t -value using the smallest EDOF of the two time series through Equation 5.10, (e.g., von Storch and

Zwiers, 1999),

$$t = |r_{xy}(k)| \sqrt{\frac{EDOF}{1 - r_{xy}(k)^2}} \quad (5.10)$$

The correlation coefficients r , are presented with the EDOF and the level of significance, p -value, for testing the hypothesis of no correlation. Each p -value is the probability of getting a correlation as large as the observed value by random chance, when the true correlation is zero. When testing for statistical significance a p -value of less than 0.1 is considered significant. The confidence level is calculated in each case by $100 \times (1 - \alpha)\%$, α being the confidence coefficient through the t -Student test.

5.1.3 Maps of Sea Level Anomalies

SLA (or Δ Sea Surface Height (Δ SSH)) came from the Mapped Sea Level Anomalies (MSLA) product which is based on satellite altimeter data. These data were retrieved from the AVISO (Archiving, Validation and Interpretation of Satellite data in Oceanography; <http://www.aviso.oceanobs.com/en/>) database. Global Merged MSLA products were used. The data set is a suite of high resolution maps that use observations from up to four available missions to provide a homogeneous, inter-calibrated and highly accurate time series of SLA and MSLA altimeter data. The data set has a global geographic coverage weekly product, re-sampled to a regular $0.25^\circ \times 0.25^\circ$ regular grid (Dibarboure et al., 2008), and is a product that can be used for both signal analysis and comparison with *in situ* data (Ducet et al., 2000).

Close to the coast, altimetric observations often have lower accuracy or are not interpretable due to several factors, including land/shallow seabed contamination in the footprint (altimeter and radiometer), inaccurate tidal corrections and incorrect removal of atmospheric (wind and pressure) effects at the sea surface (e.g., Vignudelli, 2005; Cipollini et al., 2009; Roblou et al., 2011). The Campbell Plateau has several bathymetric features emerging to the surface, and so a topographic mask has been applied to the data to avoid possible land/shallow seabed contamination for water depths shallower than 200 m. Figure 5.2a shows the bathymetric mask applied to the area. The 1000 m

depth was used to approximate the limit of the Campbell Plateau for this study, as most of the plateau is within that depth range. This is consistent with the definition used in Chapter 4.

The sea level anomalies retrieved from the AVISO website are calculated relative to a seven year mean (1993-1999). The mean used to calculate the anomalies is the CNES-CLS09 Mean Dynamic Topography (MDT). This mean is an estimate of the ocean sea surface above the geoid for 1993-1999, with a resolution of 0.25° (Rio et al., 2011). Because the period covered by this study is longer than the referenced mean, ΔSSH needs to be referenced for the whole period, i.e., 1993 to 2012. To do this the SLA referenced to the 1993-1999 period is used to re-calculate the MDT for the whole period (Rio et al., 2011), by referencing the mean:

$$MDT_{93-12} = MDT_{93-99} + (\overline{SLA}_{93-99})_{93-12} \quad (5.11)$$

where MDT_{93-12} is the new mean referenced to 1993-2012, MDT_{93-99} is the mean referenced to seven years (1993-1999) and $(\overline{SLA}_{93-12})_{93-12}$ is the mean of the SLA for 1993-2012. With the new mean, the anomalies were re-calculated.

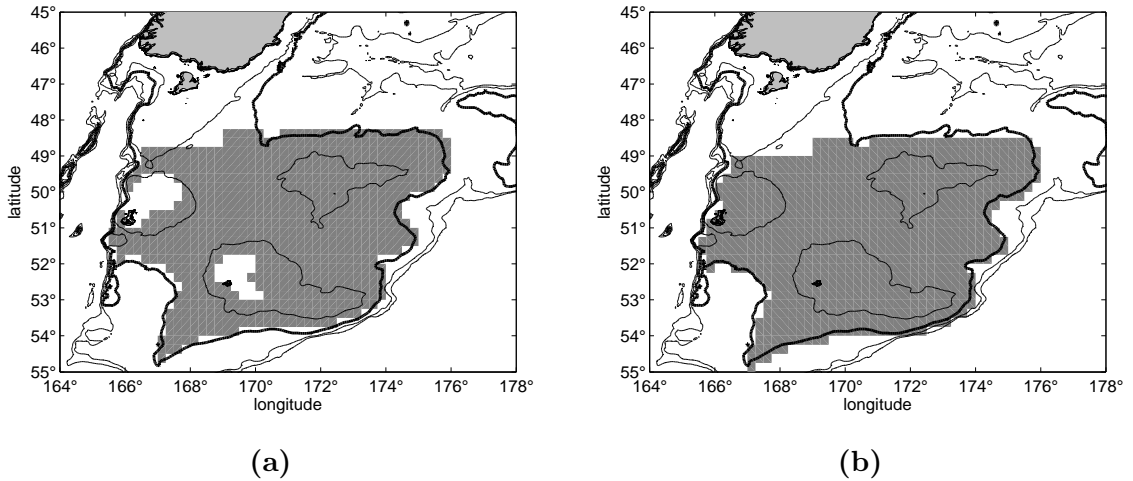


Figure 5.2: Masks applied to data set. Thick contour shows 1000 m isobath.
 (a) SSH, blank patches over the plateau represent depths shallower than 200 m
 (b) SST.

A monthly mean was calculated from the weekly data at each point of the grid; then an

average for the whole plateau was computed to obtain the time series.

The monthly SLA for 1993-2012 shows a positive trend along the whole record, with an increase of about $5.2 \text{ cm decade}^{-1}$ (Figure 5.3). Between 1993 and 1999 the values are below zero with a positive trend. From 1999 to mid 2005, anomalies oscillate around zero but with a weak trend. This is followed by a positive trend and positive anomaly values till 2012. Some year to year variability can be seen, e.g., the large high that lasted from late 1998 to early 2002. When calculating the full SSH a constant value of the mean is seen over the plateau.

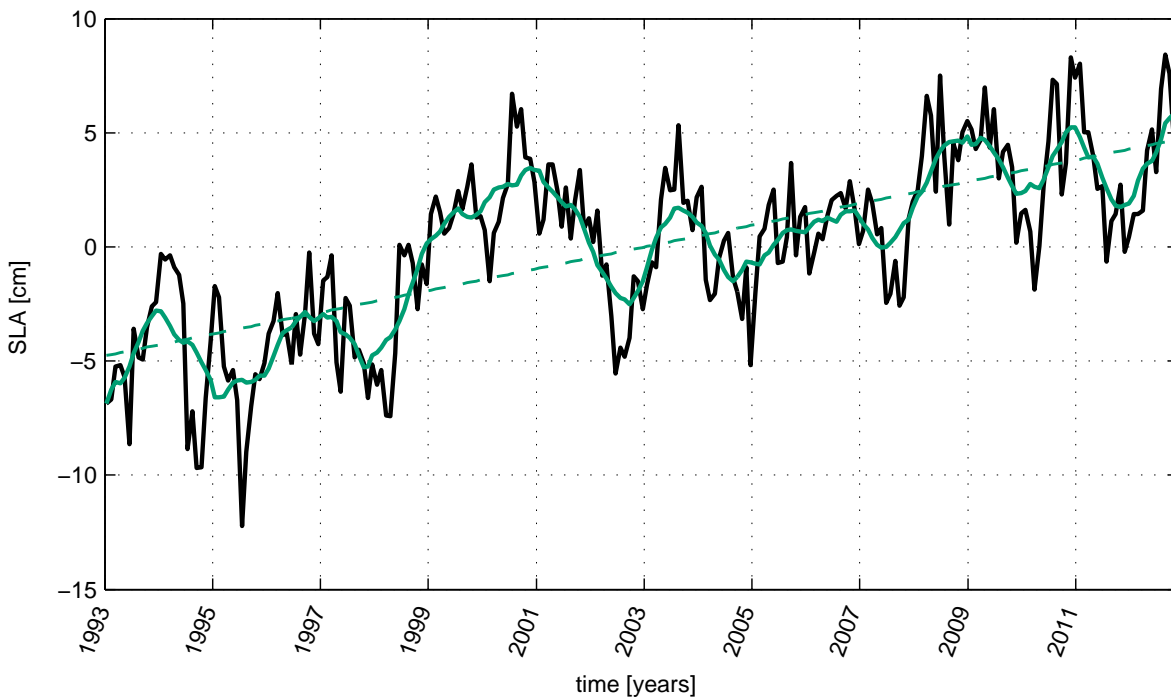


Figure 5.3: Monthly SLA data averaged over the Campbell Plateau (solid black). SLA with the seasonal cycle removed and a 13-month running mean applied (solid green). Dashed line shows the overall trend. Tick labels are at the beginning of the year.

5.1.4 Sea Surface Temperature

For the Sea Surface Temperature (SST) data the National Oceanic and Atmospheric Administration (NOAA) Optimum Interpolation (OI) SST version 2 (V2) product was used (<http://www.esrl.noaa.gov/psd/>), from January 1982 to December 2013. The data are available to the public after the following processing. Monthly fields are derived by a linear interpolation of the weekly optimum interpolation (OI V2) fields to daily fields. These daily fields are then averaged for each month. The weekly product, from which the monthly mean was calculated, was produced from *in situ* and satellite data. It has a resolution of 1° in latitude and longitude. Contamination by clouds gives the SST data a negative bias, i.e., underestimates temperatures as cloud temperatures are colder than the SSTs, for this reason a cloud-clearing algorithm is applied to the data set to minimise the contamination problem and after this, *in situ* data are used for final bias correction (Reynolds and Rayner, 2002).

To compare SST with the Δ SSH data set, SST data were interpolated onto a 0.25° regular grid and a mask was then applied to remove waters deeper than the 1000 m depth (Figure 5.2b). A spatial mean over the whole plateau was then calculated for each month to obtain a time series. The anomalies were calculated by removing the mean for the whole period, then the seasonal cycle was removed. The trend was also removed from the time series for the correlation analysis.

For the SST data, two record lengths were analysed, the shorter record covers January 1993 to December 2012 to match the SLA record; the longer record comprises the whole SST data set, from January 1982 to December 2013, and was used for the comparisons with the climate indices SOI and SAM. The different periods of time are noted on the figures.

A slightly negative trend is seen on the long record (1982-2013) of SST anomalies whereas the shorter record (1993-2012) has a slightly positive trend (Figure 5.4), hence longer periods are needed to be confident with the trend. This caution has to be taken with all

the time series, however it is pointed out here because of the difference between the two time periods.

There are two major anomaly peaks ($>0.6\text{ }^{\circ}\text{C}$) that are followed by sharp declines. The first decline of almost $1\text{ }^{\circ}\text{C}$ occurs between 1987 and early 1988; the second cooling of almost $0.8\text{ }^{\circ}\text{C}$ occupies 2002-2003. Also, there is high inter-annual variability larger in amplitude than the trends observed in the time series. After 2006, the time series has a strong positive trend, but this might be emphasized by the very low value registered in 2007. This behaviour is not particularly unusual as 1983-1987 and 1998-2002 also have big upward trends.

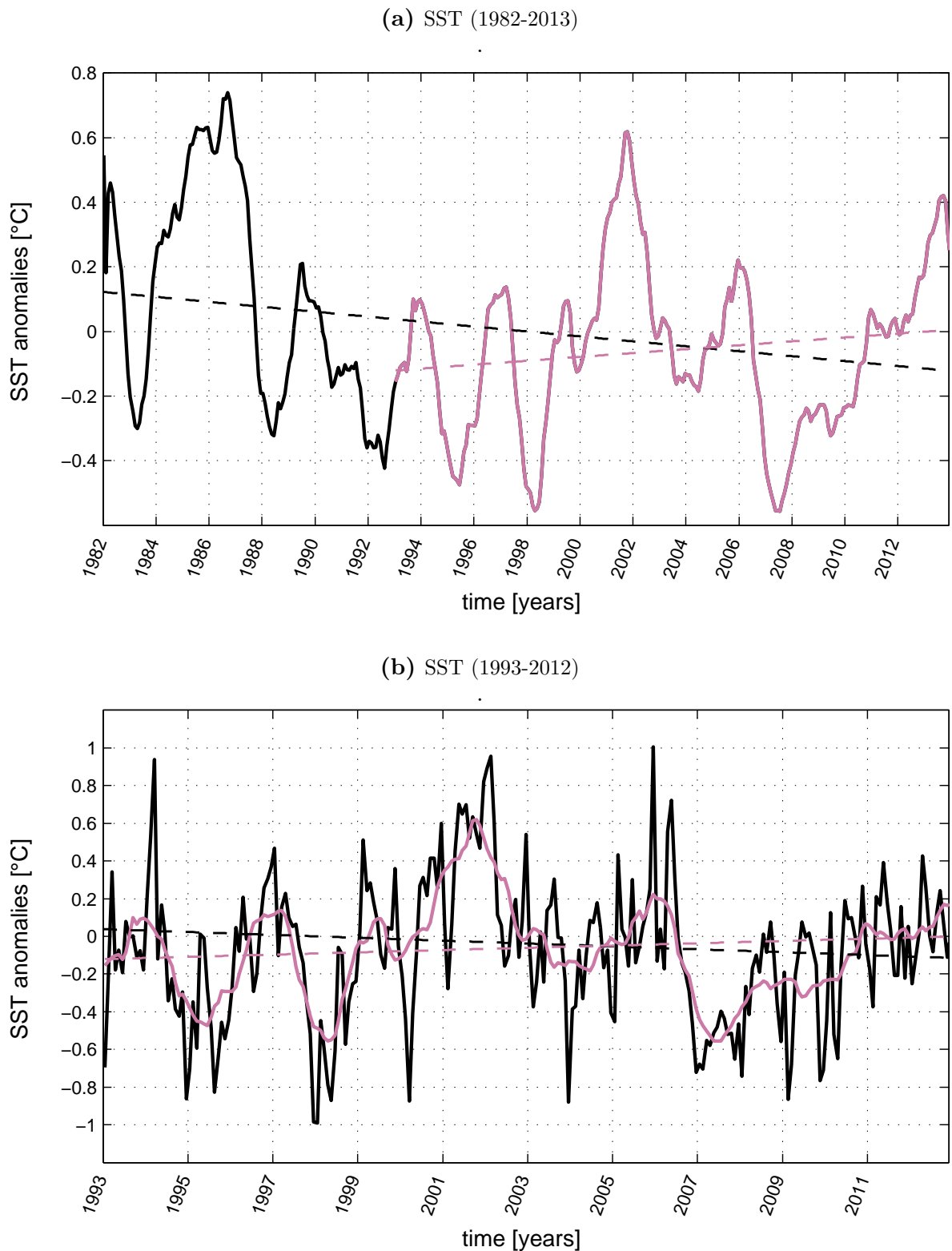


Figure 5.4: (a) Short SST anomalies (1993-2012) (solid pink) and the extension to the long record (1982-2013) (solid black). Both have a 13-month running mean applied. Dashed lines show the trends. (b) Monthly SST anomalies for the short period (1993-2012) (solid black) and with a 13-month running mean applied (solid pink). Dashed lines show the respective trends in either the long or short record. For both figures tick labels are at the beginning of the year.

5.1.5 Climate Indices

The Southern Oscillation Index (SOI) is based on the difference in sea level pressure between Tahiti, French Polynesia and Darwin, Australia (Trenberth, 1984). Because this index is closely related with El Niño events, the full climate phenomenon is often referred to as El Niño - Southern Oscillation (ENSO), with El Niño events associated with negative SOI and La Niña with positive SOI (Talley et al., 2011). During El Niño events, the Trade Winds get weaker over most of the equatorial Pacific Ocean leading to anomalously warm SST over the eastern Pacific Ocean (Philander, 1983). ENSO events are associated with local variations such as changes in winds and SST (e.g., Morrow et al., 2010; Holbrook et al., 2011). Although it has origins in the tropics, ENSO generates atmospheric Rossby waves that propagate their signal to higher latitudes (Karoly, 1989). El Niño events, for example, are associated with colder SST around New Zealand (Mullan, 1998). SOI data were retrieved from <http://www.cgd.ucar.edu/cas/catalog/climind/soi.html>.

The Southern Annular Mode (SAM), also known as the Antarctic Oscillation (AAO) (Gong and Wang, 1999), refers to an oscillation of atmospheric mass around Antarctica that extends from middle to higher latitudes of the Southern Hemisphere (e.g., Gong and Wang, 1999; Limpasuvan and Hartmann, 1999; Marshall, 2003; Sallée, Speer, Rintoul, and Wijffels, 2010). Originally called “High Latitude Mode” (HLM) (e.g., Kidson, 1975, 1988b,a) it describes the north-south movement of the westerly wind belt that circles Antarctica. For example, westerly winds are weaker over the Southern Ocean in the negative phase of SAM when the pressures over Antarctica are higher than normal (Renwick and Thompson, 2006). The SAM is associated with changes in patterns of precipitation, wind fields and storm activity in the New Zealand region (Ummenhofer and England, 2007). Relatively light winds, warm and dry conditions over New Zealand and intensified westerlies and storms further south in the Southern Ocean are associated with the positive phase of SAM which has been dominant for the last few decades (e.g., Thompson et al., 2000; Renwick and Thompson, 2006; Gillett et al., 2006). The numerical definition of the SAM is as follows:

$$SAM = P_{40S}^* - P_{65S}^* \quad (5.12)$$

where P_{40S}^* and P_{65S}^* are the normalized monthly zonal MSLP at 40°S and 65°S (Gong and Wang, 1999; Marshall, 2003). The SAM index was downloaded from: <http://www.antarctica.ac.uk/met/gjma/sam.html>.

5.1.6 Steric Height

Steric Height data were retrieved from the Roemmich-Gilson Argo Climatology, using nine years of Argo data from January 2004 to December 2012. The climatology is described in Roemmich and Gilson (2009), and the data were selected from the Global Marine Argo Atlas (http://www.argo.ucsd.edu/Marine_Atlas.html). The pressure reference to calculate steric height was 400 dbar and the limits of the area are 48.5° to 55°S and 165° to 176°E. The data retrieved are already a monthly time series, so anomalies were calculated and the seasonal cycle removed. Data over the Campbell Plateau are an interpolation from nearby Argo floats, as the plateau is too shallow for the floats to sample (Professor Dean Roemmich, Scripps Institute of Oceanography, personal communication). Steric height determines the distance, or depth difference, between two surfaces of constant pressure. A full description of how steric height is calculated is given in Section 4.2.5

Figure 5.5 shows steric height anomalies calculated over the first 400 m of the water column with a slight positive overall trend. The first period 2004-2008 has the most negative anomalies, followed by a positive period of 3 years up till 2011 and then it becomes negative again before returning to positive values midway through 2012.

5.1.7 Ocean mass

Ocean mass data were retrieved from the Gravity Recovery and Climate Experiment (GRACE) *Tellus* website at the NASA Jet Propulsion Laboratory (JPL), <http://grace.jpl.nasa.gov/>. The data set is presented as “equivalent water thickness” and units are cm of equivalent-water-thickness. The product used here is Release-05 (RL05.DSTvDPC1401) and is constructed as monthly values on a 1° x 1° regular grid. More information about

the data processing and accuracy can be found in Chambers and Bonin (2012). The data set covers August 2002 to October 2013. Anomalies were calculated and the seasonal cycle removed.

Overall there appears to be a downward trend, however care must be taken in interpreting the trend due to the short length of the time series (Figure 5.6).

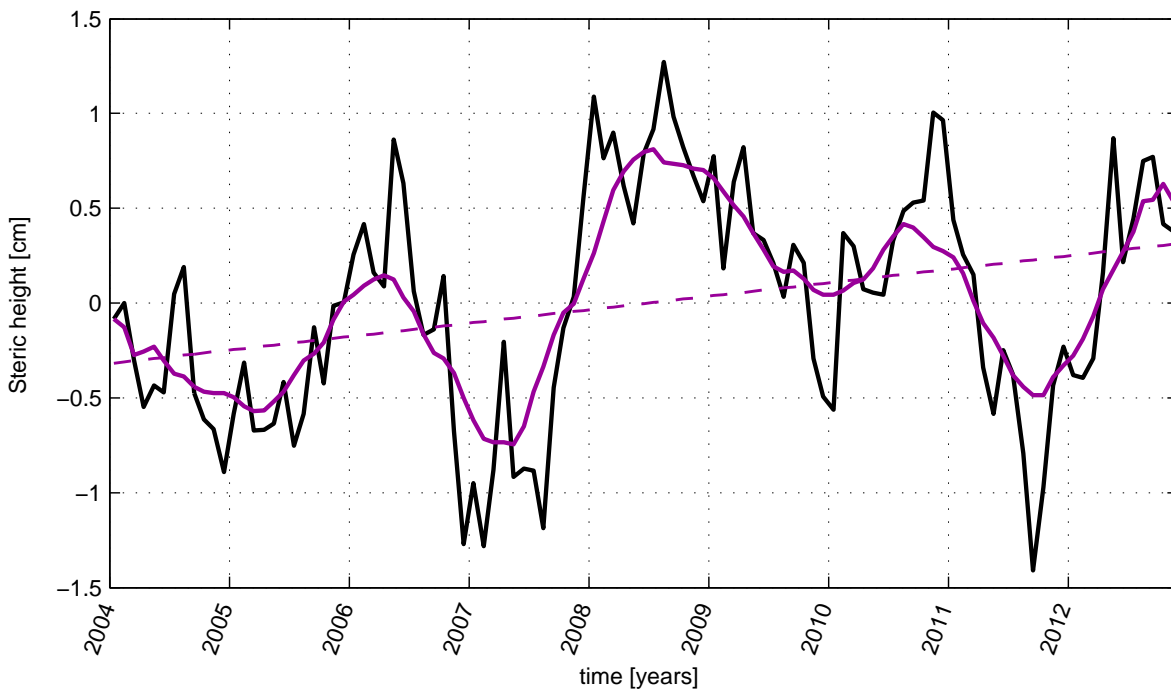


Figure 5.5: Monthly steric height anomalies (solid black) with a 13-month running mean (solid purple). Dashed line shows the overall trend. Tick labels are at the beginning of the year.

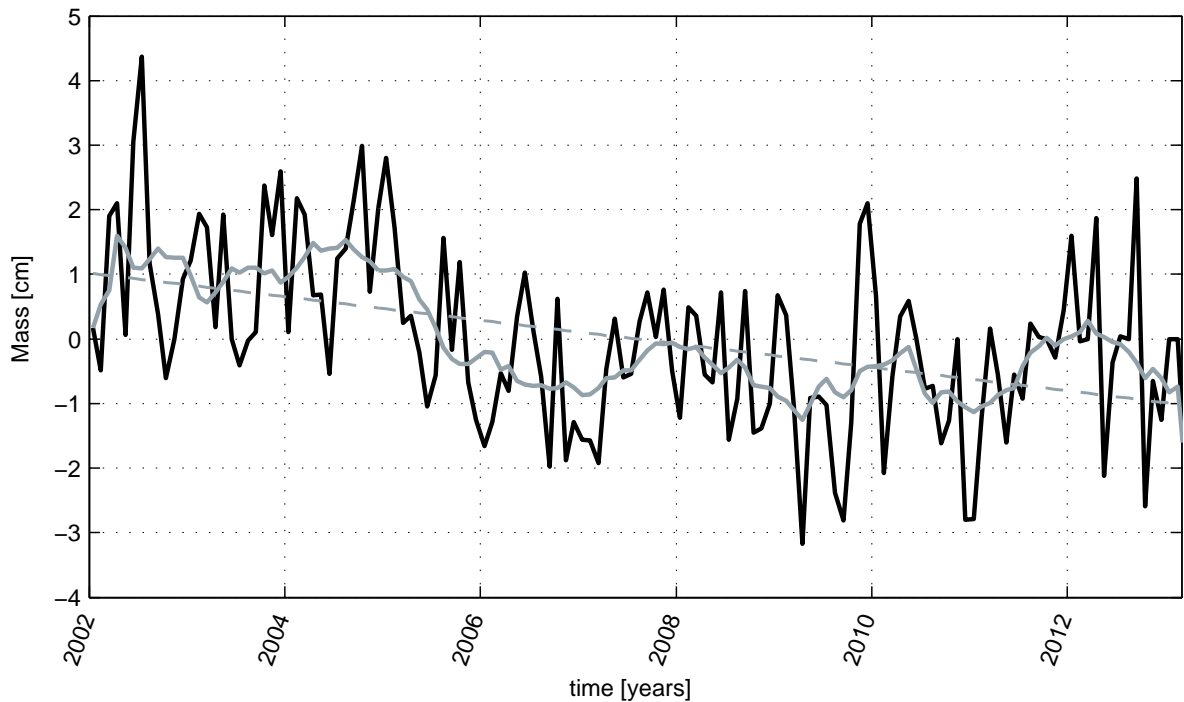


Figure 5.6: Monthly ocean mass anomalies (solid black) with a 13-month running mean applied (solid grey). Dashed line shows the overall trend. Tick labels are at the beginning of the year.

5.1.8 Wind

Monthly averaged wind stress data were retrieved from the National Center for Environmental Prediction/National Center for Atmospheric Research (NCEP/NCAR) website <http://www.esrl.noaa.gov>. The NCEP/NCAR Reanalysis uses *in situ* and remote sensed observations to produce a record of 65 years of global analyses of atmospheric fields (Kalnay and Kanamitsu, 1996; Kistler et al., 2001). Data are linearly interpolated into a $0.5^\circ \times 0.5^\circ$ regular grid, with monthly means from January 1948 to December 2012. The same mask as used for SST was applied to the wind stress data (Figure 5.2b). This focuses the analysis on local forcing. Anomalies were then calculated and the seasonal cycle removed.

The anomalies for the wind stress magnitude for 1982 to 2013 show a small increase in wind stress (Figure 5.7). When the analysis is made for both components, the east-

west component is the larger component of the stress (Figure 5.8).

The wind stress magnitude reveals a strong seasonality with the lowest stress during summer and midwinter (Figure 5.9), and stress maxima around the equinoxes.

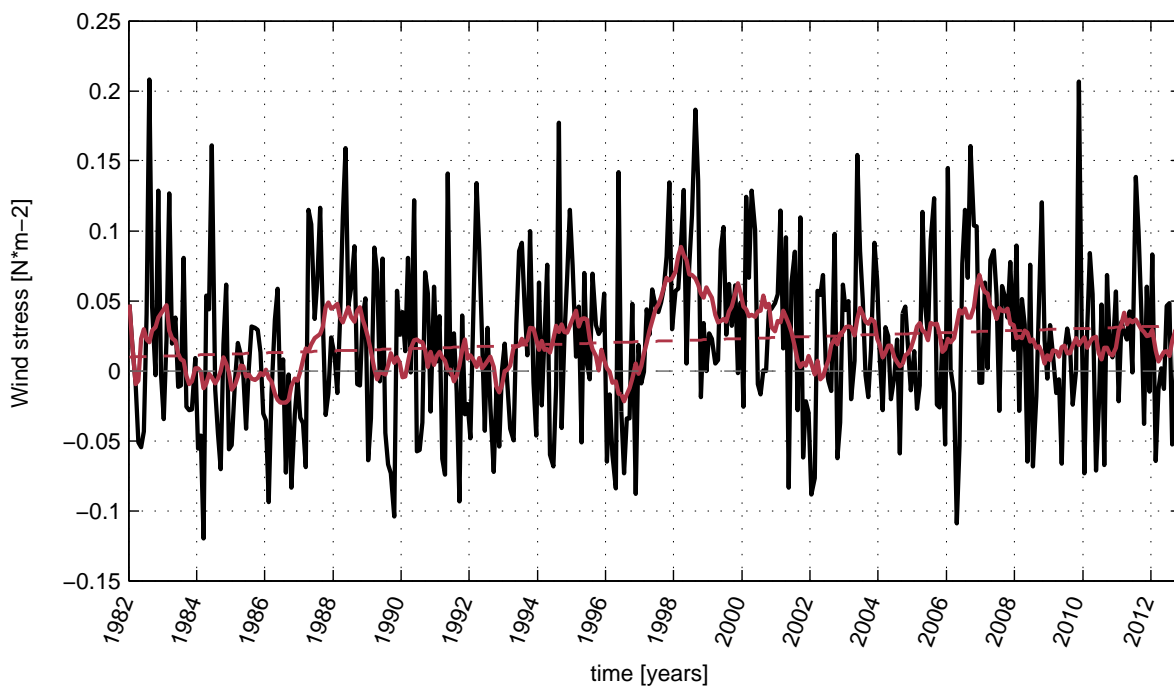


Figure 5.7: Monthly wind anomalies of the wind stress magnitude (solid black) and with a 13-month running mean applied (solid red). Dashed line shows the trend. Tick labels are at the beginning of the year.

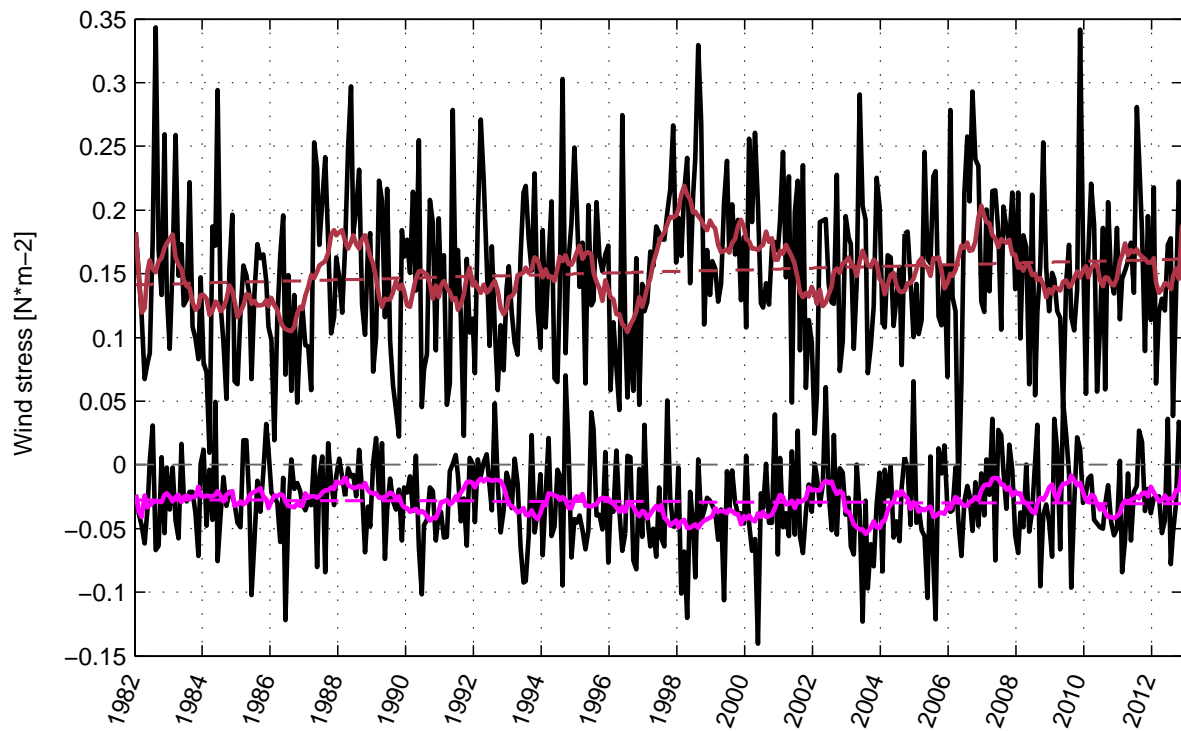


Figure 5.8: Monthly anomalies for both components of the wind stress (solid black). With a 13-month running mean applied, (east-west) u-component (solid red), (north-south) v-component (solid magenta). Dashed line show the overall trends. Tick labels are at the beginning of the year.

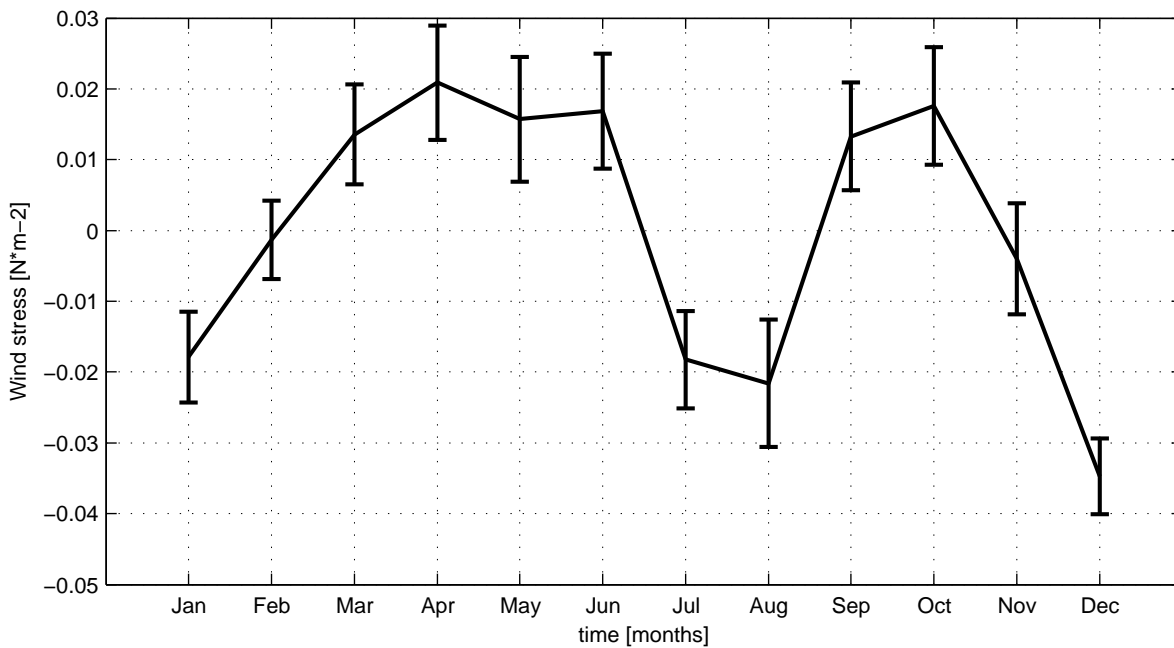


Figure 5.9: Wind stress anomalies seasonal cycle and ± 1 standard error, calculated for 1948-2012.

5.2 Results

5.2.1 Sea Level Anomaly

Records for SLA and SOI (Figure 5.10) have a correlation coefficient of $r = 0.54$ ($EDOF=7$; $p = 0.06$). A maximum cross-correlation of $r = 0.58$ with $EDOF=7$ and a $p = 0.05$ is obtained, which was considered to be significant. The peak of the correlation is when SOI leads SLA by two months.

In the case of SLA and SAM (Figure 5.11a) the correlation coefficient is $r = 0.34$, ($EDOF = 7$; $p = 0.18$), i.e. it is not significant. The last five years co-vary more strongly than the rest of the record. When the cross-correlation was applied, it was found with $r = 0.44$, ($EDOF = 7$; $p = 0.11$) when SAM leads SLA by 22 months. This lead might be due to a periodicity of around two years in the data. This means that shifting the time series by 22 months is aligning the time series with the next oscillation.

No relationship is found between SLA and local winds (Figure 5.11b) when there is no lag ($r = 0.07$; $EDOF = 6$; $p = 0.27$). However, a maximum cross-correlation of $r = 0.57$, ($EDOF = 6$; $p = 0.07$), is found when winds lead SLA by 17 months.

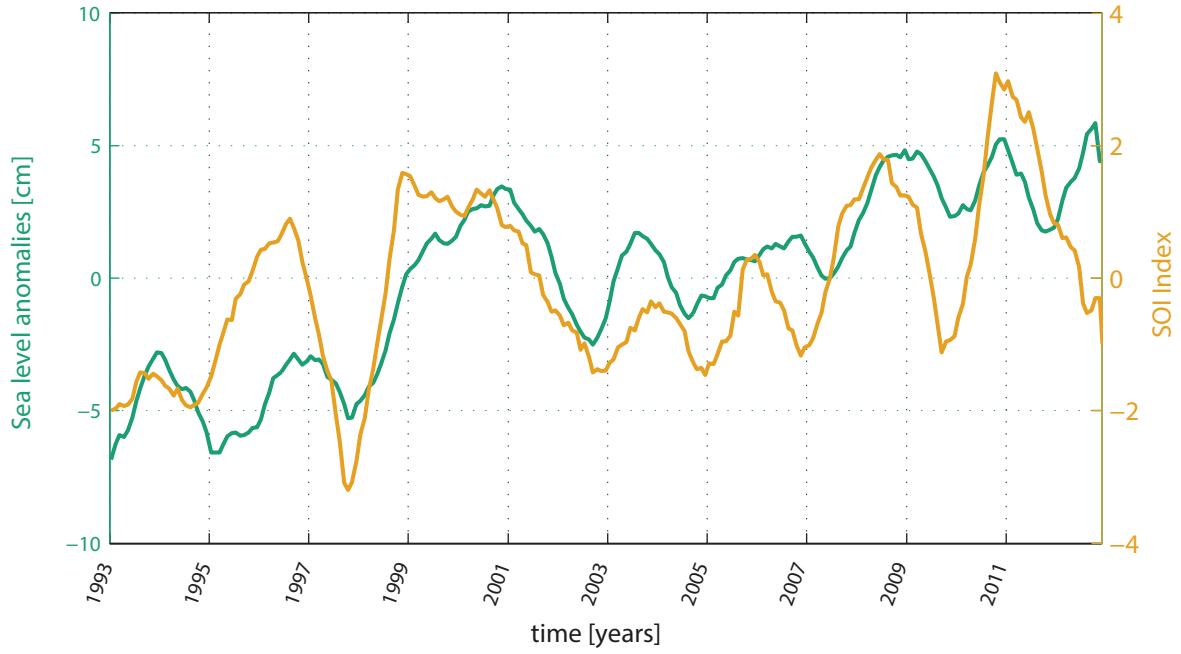


Figure 5.10: SLA (solid green) and SOI (solid orange) for 1993-2012, with a 13-month running mean applied. Tick labels are at the beginning of the year.

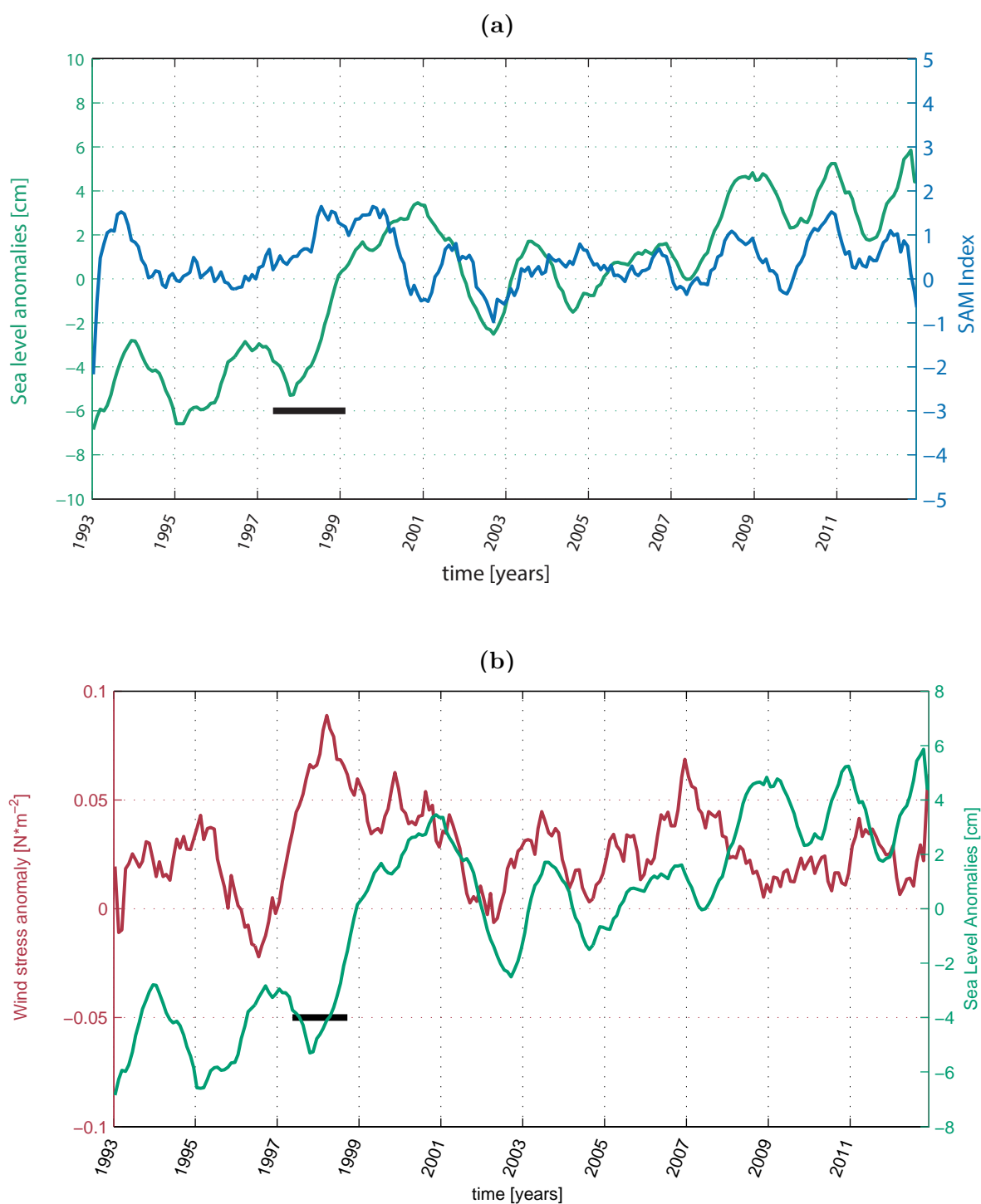


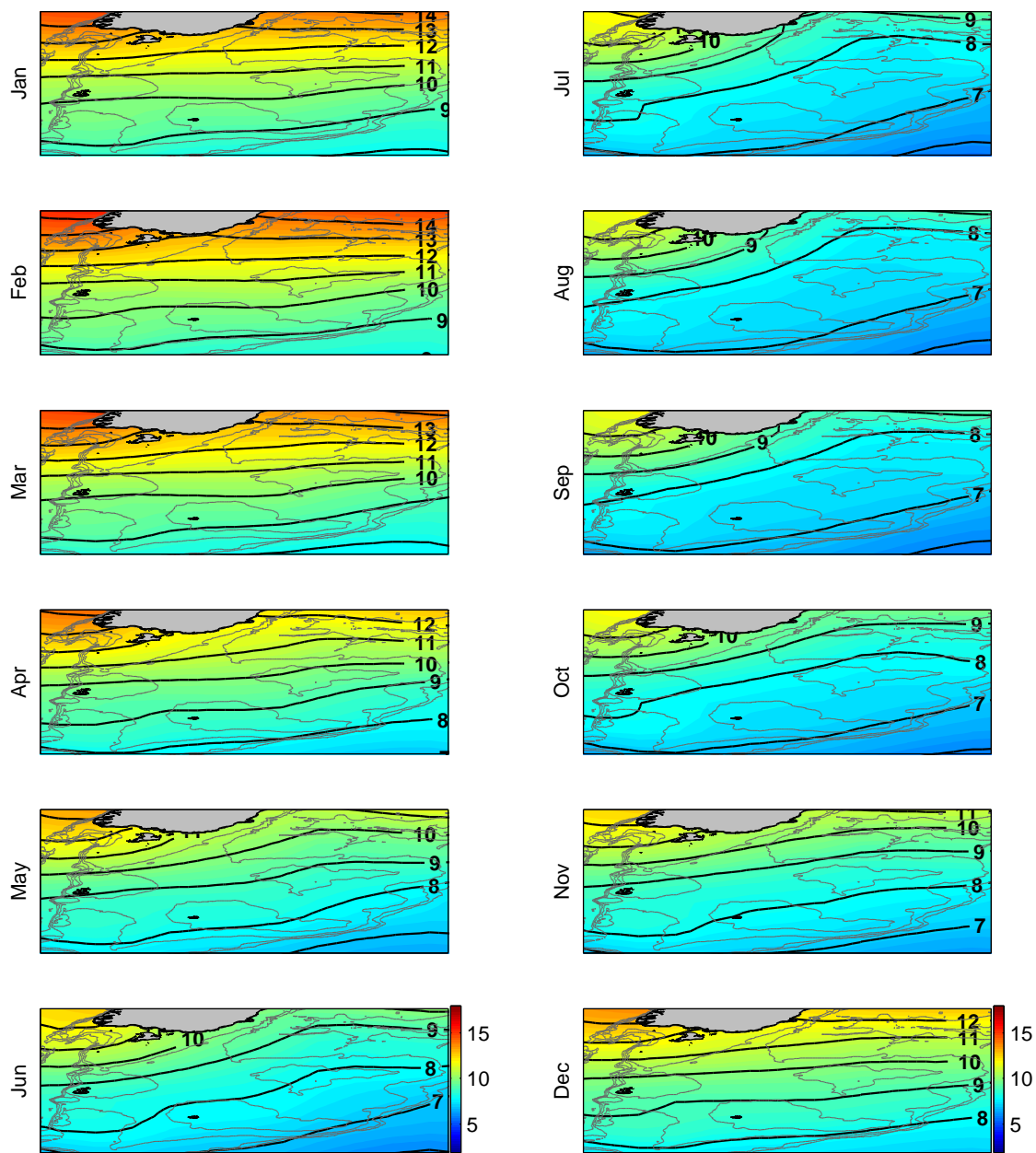
Figure 5.11: (a) SLA (solid green) and SAM (solid blue) for 1993-2012, both have a 13-month running mean applied. (b) SLA (solid green) and wind stress anomaly (solid brown), both have a 13-month running mean applied. Black solid bars in both figures represent 22 and 17 months, the respective lags. Tick labels are at the beginning of the year.

5.2.2 Sea Surface Temperature

Figure 5.12 summarizes the spatial pattern of the SST seasonal cycle over the Campbell Plateau. The spring month of October marks the start of the surface ocean seasonal warming. This leads to a strengthening of temperature gradients towards the northern side of the region. This is noticeable by the southward shift of the 9 °C contour from the northern plateau in October to the southern plateau in January. The peak of the temperature gradient is reached in February when temperatures range from 9 °C to 14 °C from the north to south over the plateau. The lowest gradient occurs in September with an almost homogeneous SST across the plateau, ranging from 7 °C in the north to 9 °C in the south.

The de-seasoned and smoothed SST anomalies over the Campbell Plateau at each point in time is shown with a $\pm 1 \sigma$ *standard deviation* around it. This shows interannual variability in the spatial nature of SST on the plateau (Figure 5.13). When the *standard deviation* SST across the plateau is more homogeneous it means a smaller temperature gradient as all the values are closer to the mean.

SST anomalies and the SOI (Figure 5.14a) have a correlation coefficient of $r = 0.18$, ($EDOF = 10$; $p = 0.28$), when the time lag is zero, which is not significant. However, a maximum cross-correlation of $r = 0.43$, ($p < 0.08$) when the SOI leads SST by seven months, which is significant, may suggest a relation with changes in the equatorial region. Although it appears that cold SST anomalies vary with periods of a negative SOI, for example in the strong El Niño events in 1982 and 1998, there are similar cold SST anomalies that are not related to SOI variations. After 2006 the two profiles separate and SST starts warming again to co-vary with the SOI at the end of the record.



(a) January - June

(b) July - December

Figure 5.12: Seasonal SST structure over the Campbell Plateau, calculated for 1982-2013. Black contours show temperature intervals of 1 °C, grey contours show bathymetry contours, colourbars show temperature scale in °C.

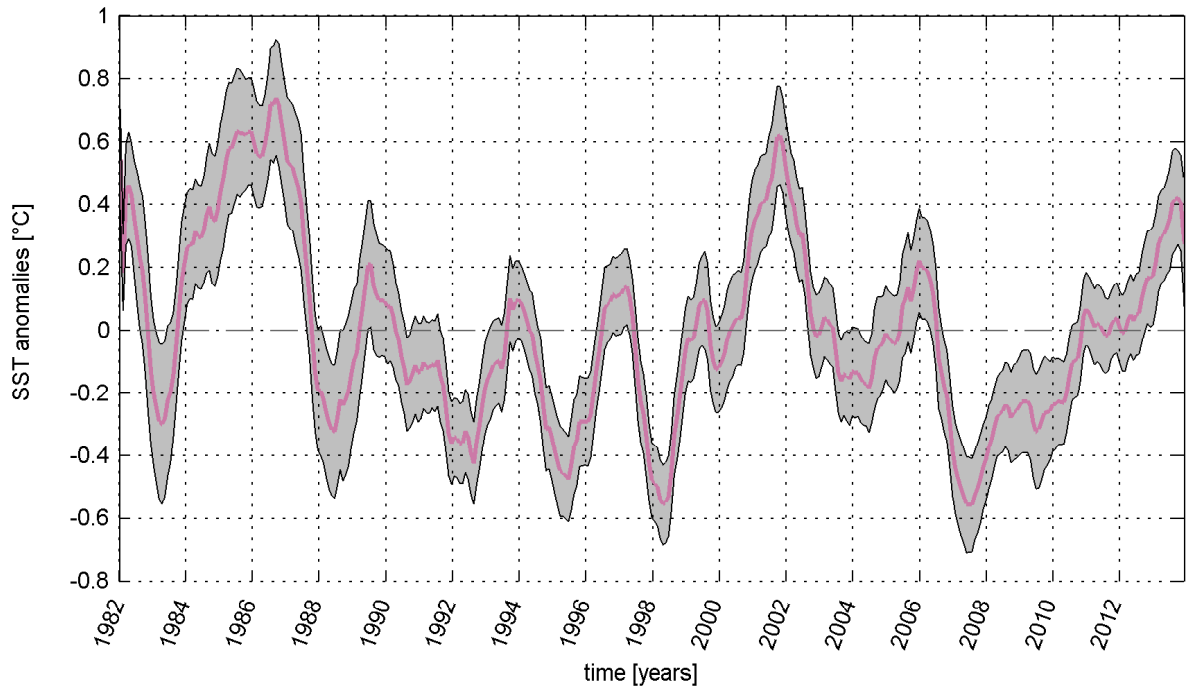


Figure 5.13: SST anomalies time series. The gray shading shows $\pm 1 \sigma$, 13-month running mean applied. Tick labels are at the beginning of the year.

Records of SST anomalies and SAM (Figure 5.14b) with a time lag of zero months, have a correlation coefficient of $r = 0.02$, ($EDOF = 10$; $p = 0.46$), which shows that they are not correlated. No significant cross-correlations were found for SST anomalies leading or lagging SAM by up to 24 months.

An anti-correlation relationship between SST and local winds (Figure 5.15) is revealed by an r of -0.47 , ($EDOF = 12$; $p = 0.06$). A maximum of $r = -0.48$ is found when winds lead SST by two months, the $p = 0.04$ reveals a significant relationship. This relationship might be a result of wind stirring at the ocean surface. When the winds are weaker, it is easier to warm the surface of the ocean, as opposed to stronger winds that will mix the upper water column and result in colder surface waters.

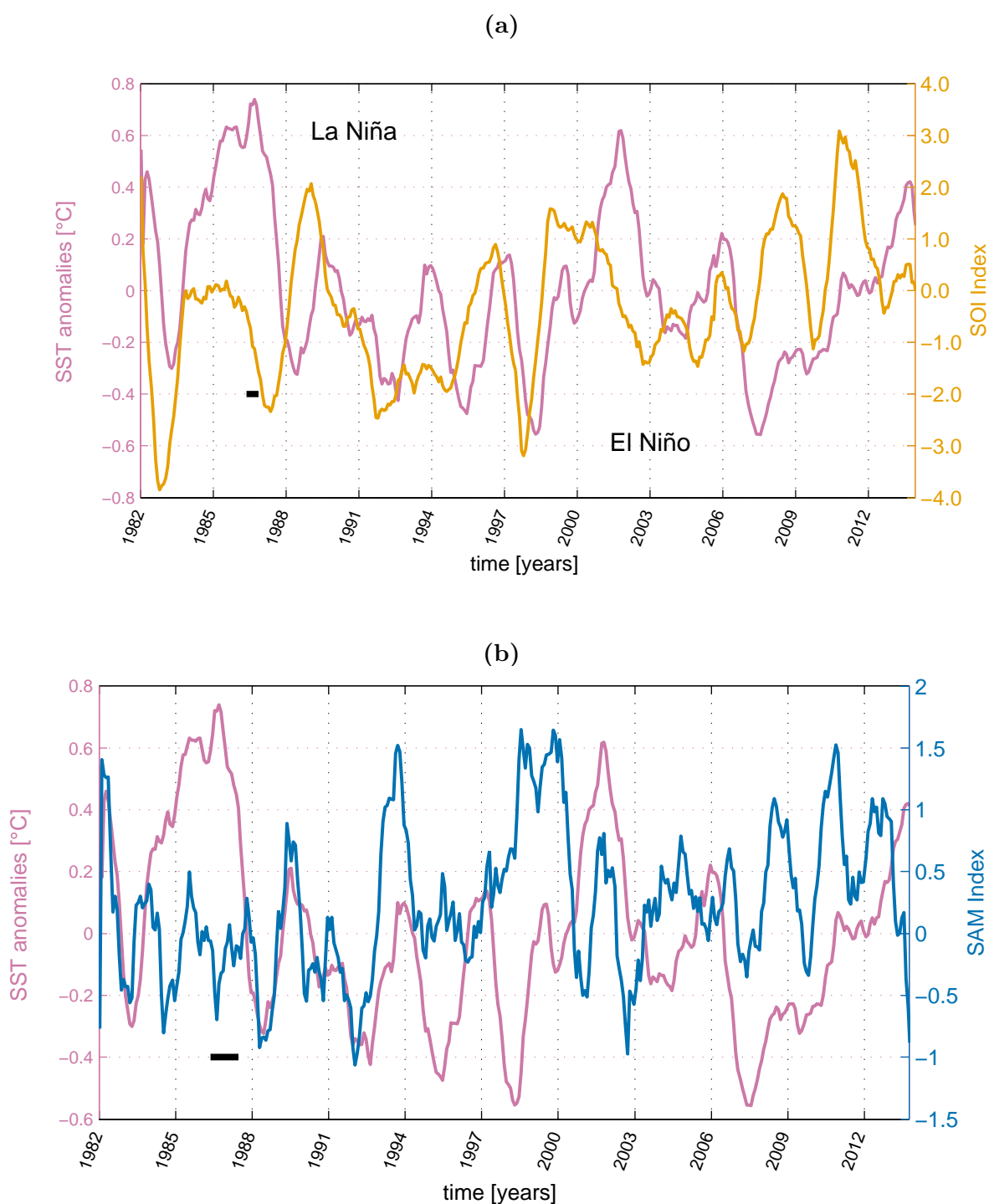


Figure 5.14: (a) SST anomalies (solid pink) and the SOI (solid orange) for 1982-2013, both have a 13-month running mean applied. (b) SST anomalies (solid pink) and SAM (solid blue), both with a 13-month running mean applied. Tick labels are at the beginning of the year. Black solid bars in both figures represent 7 and 14 months, lags periods respectively.

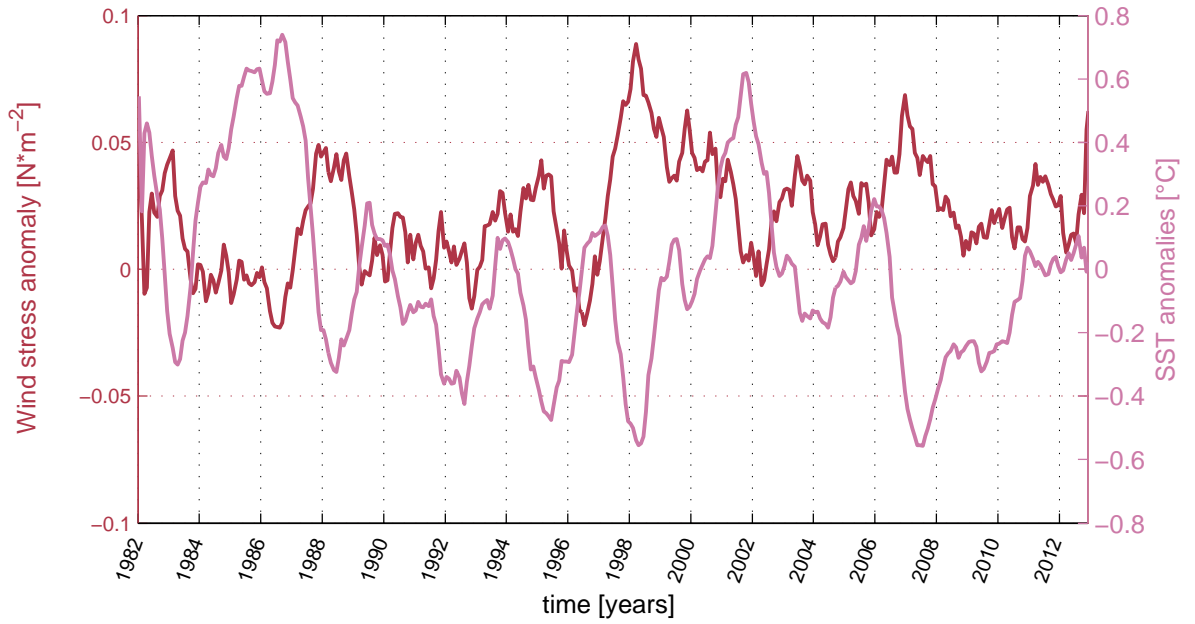


Figure 5.15: Wind stress magnitude anomalies (solid brown) and SST anomalies (solid pink) for 1982-2012, both have a 13-month running mean applied. Tick labels are at the beginning of the year.

5.2.3 Sea Surface Temperature vs Sea Level Anomalies

SST and SLA time series over their common period of 1993-2012 (Figure 5.16) have a correlation coefficient of $r = 0.43$, ($EDOF = 7$; $p = 0.12$). A maximum cross-correlation of $r = 0.55$ ($p = 0.06$), when SLA leads SST by 29 months.

Both time series co-vary together in the first part of the record, with a similar increase after the 1998 El Niño event until 2006. In 2006 there is a major decline in temperature of almost $0.8\text{ }^{\circ}\text{C}$ and a minor decline of SLA, which is followed by a slow recovery of SST and a larger increase in SLA. This poses the question of how much temperature would be needed to explain the SLA trend by thermal expansion. The warming needed can be estimated by (Equation 5.13) (e.g., Kundu and Cohen, 2008):

$$\partial T = \frac{\partial SLA}{\alpha H} \quad (5.13)$$

where ∂T is the trend in SST anomalies, °C; ∂SLA is the trend in SLA, 0.104 m in two decades; $\alpha = 1.7 \times 10^{-4} \text{ K}^{-1}$ is the thermal expansion coefficient and H is the depth of the water column over which warming is occurring, here assumed to be 1000 m. This gives a result of:

$$\partial T = 0.61 \text{ }^\circ\text{C}$$

This result means that it would be necessary for a trend in SST anomalies of $0.61 \text{ }^\circ\text{C}$ over two decades to raise the sea level 10.4 cm, which is not observed in the SST time series (Figure 5.16).

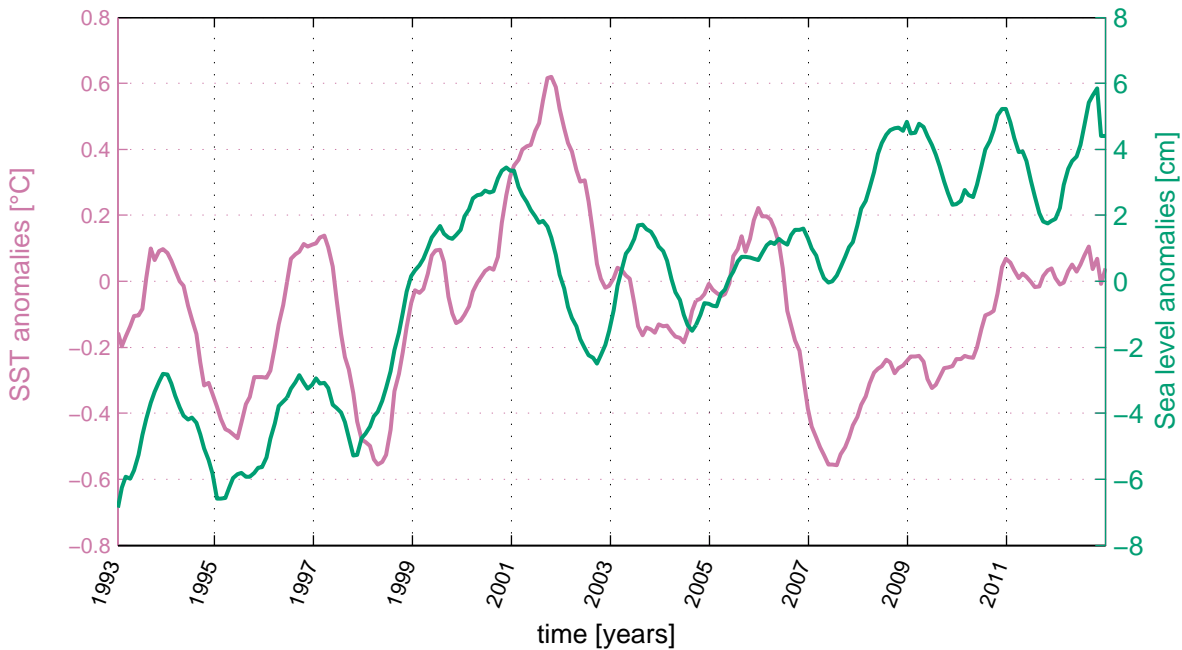


Figure 5.16: SST anomalies (solid pink) and SLA (solid green) for 1993-2012 with a 13-month running mean applied. Ticks are at the beginning of the year.

5.2.4 Campbell Plateau sea level budget

Long-term global sea level changes are due to two major processes: (i) steric sea-level changes due to variations in the total heat content and salinity that affect density (steric) changes and (ii) mass variations through the exchange of water between the oceans and other reservoirs (Emery and Thomson, 2001; Leuliette and Miller, 2009). Global sea

level changes can be expressed in terms of these processes (Equation 5.14):

$$SL_{total} = SL_{steric} + SL_{mass}, \quad (5.14)$$

where SL_{total} is the total sea level, SL_{steric} is the steric component and SL_{mass} is the ocean mass component (Leuliette and Miller, 2009). The steric sea-level changes arise without changes in mass and are driven by thermal expansion (heating) or contraction (cooling) (Emery and Thomson, 2001). The mass variations can be driven by the melting or accumulation of land-based ice and snow in the major sheets in Antarctica and Greenland, as well as mountain glaciers (Emery and Thomson, 2001; Leuliette and Miller, 2009). Changes in ocean mass can also be driven by the modification of world-wide precipitation patterns, that involves the temporary shifting of water mass from the ocean to land (Boening et al., 2012). These can be closely related to El Niño-La Niña events. Also, local changes in mass can occur through changes in large-scale ocean circulation (Roemmich et al., 2007).

SSH data provide the SL_{total} , steric height data gives SL_{steric} , and the satellite mass data closes the sea level budget providing the SL_{mass} component (Willis et al., 2008; Leuliette and Miller, 2009).

Seasonal cycle anomalies for steric height, SSH, ocean mass, the sum of steric height and ocean mass and SST for the Campbell Plateau are presented in Figure 5.17. The seasonal cycle anomaly for each variable was calculated by computing the twelve monthly averages (seasonal cycle) and then subtracting them from the appropriate month as previously described. The maximums of each variable are at different times of the year. SST is first in February, steric height in March, followed by SSH in April-May and mass in August. Assuming changes only come from solar insolation, SST peaks first because it is shallower, as a response to the summer warming, since it takes a shorter time to warm the surface of the ocean. Steric height lags because it takes longer for the heat to mix deeper into the ocean, and this also happens with Δ SSH. The ocean mass signal peaks in August, which coincides with the Boreal summer when the global seasonal freshwater exchange reaches its maximum. In a global average, this comes from the inland water

(ice and snow) that melts on a seasonal basis in the Northern Hemisphere (Willis et al., 2008; Leuliette and Miller, 2009). As the seasonal behaviour of the ocean mass in the Campbell Plateau was similar to the global signal, it was assumed, as a first approach, that the change in ocean mass on a seasonal scale on the Campbell Plateau was globally driven.

SSH responds to both solar insolation and seasonal freshwater exchange, but on a global scale changes in steric height normally dominate the SSH signal, so it would be expected that steric height and SSH would have similar seasonal cycles (Roemmich and Gilson, 2009). This happens because the steric height signal is typically much larger than the mass signal, hence the latter can be neglected. In this region, however, steric height needs to be added to the mass to match the SSH signal, because on the Campbell Plateau, the steric height signal is approximately the same magnitude as the mass signal, so both terms are needed to account for the complete change in sea level. In this case combining the steric height and ocean mass signals match up well with the SSH signal.

To investigate the behaviour of interannual fluctuations of the different components of the sea level change, the estimation of each component is presented in the next section. Equation 5.14 has been used to calculate each component from the other two components, i.e., the inferred steric height is calculated by subtracting the ocean mass to the SLA, and the inferred ocean mass by subtracting the steric component to the SLA. Each component has been retrieved from a different source, i.e., they are independent data sets (SLA from satellite (AVISO), steric height from Argo floats, and ocean mass from satellite (GRACE)), so this analysis gives an insight of the consistency between data sources. When the time series are compared with the seasonal cycle, the strong seasonality of the steric height (over 400 m) is observed (Figure 5.18). In this case, the inferred variables agree reasonably well in the centre of the time series, between 2006 and 2008. When the seasonal cycle is removed (Figure 5.19), the steric height contribution decreases considerably. Years between 2006 and 2008 are still in good agreement, but steric height does not match that well. When the trend is also removed (Figure 5.20), both SLA and ocean mass agree reasonably well, but the steric height is still not being

accurately inferred by the other two. This last figure suggests two things, i) that there is a trend that is influencing the time series, ii) there is something in steric height that is being missed when calculated from the other two components. This might be related to the depth of the steric height, as it was calculated only over the top 400 m of the water column.

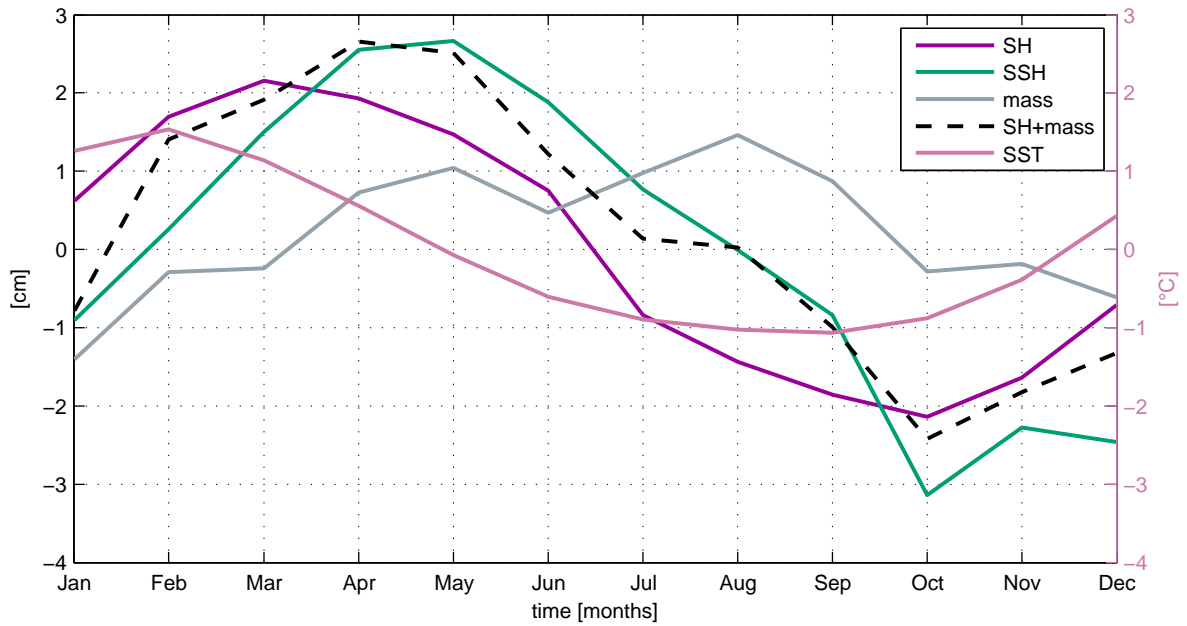


Figure 5.17: Steric height (solid purple), SSH (solid green), ocean mass (solid grey), steric height + ocean mass (dashed black) and SST (solid pink) seasonal cycle anomalies. SST is °C and the rest of the variables are cm.

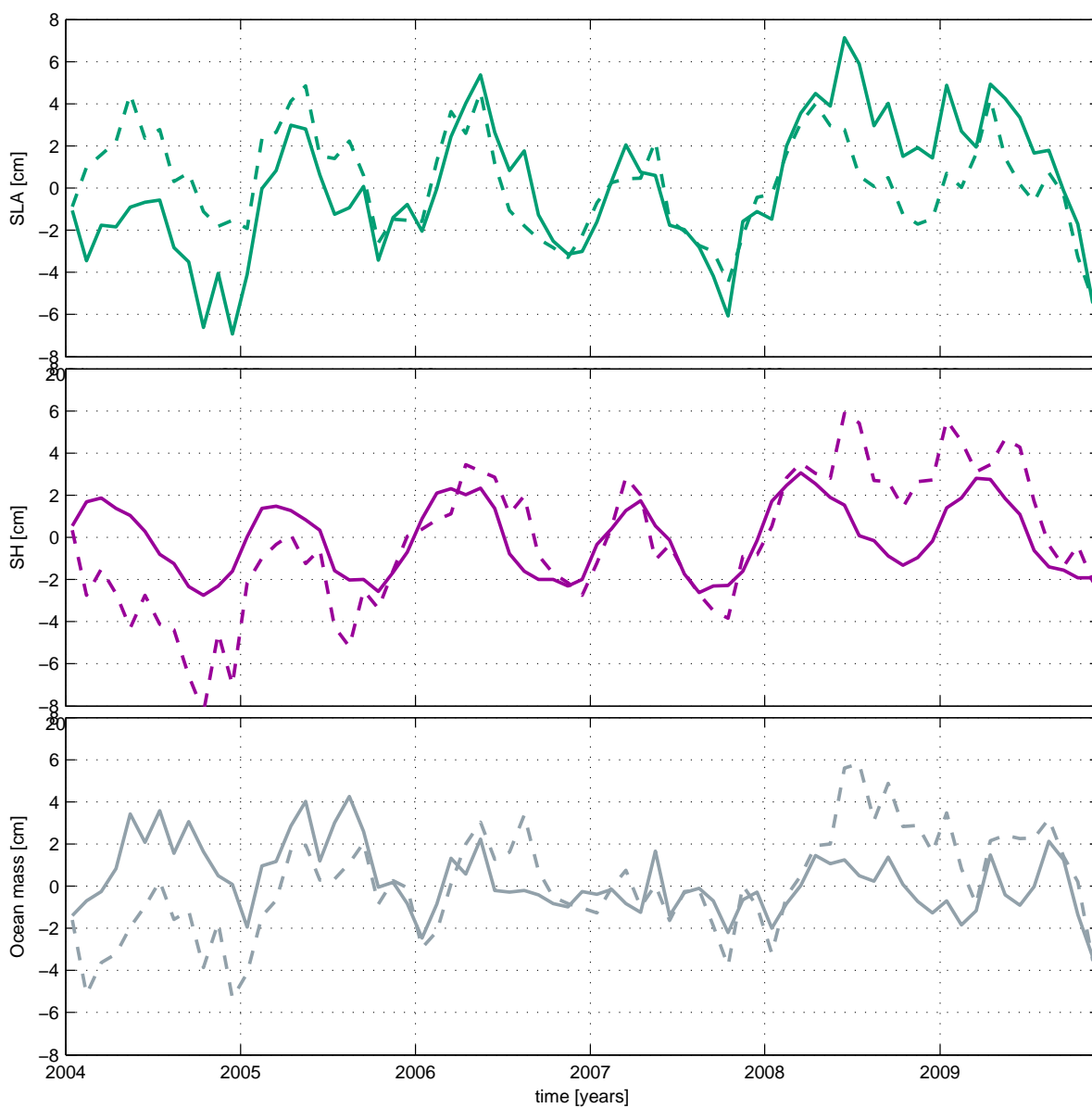


Figure 5.18: Campbell Plateau mean sea level variability and its components. (Top) SLA (solid green), (middle) steric height (solid purple), (bottom) ocean mass (solid grey). Gray lines show the inferred variables computed from Equation 5.14.

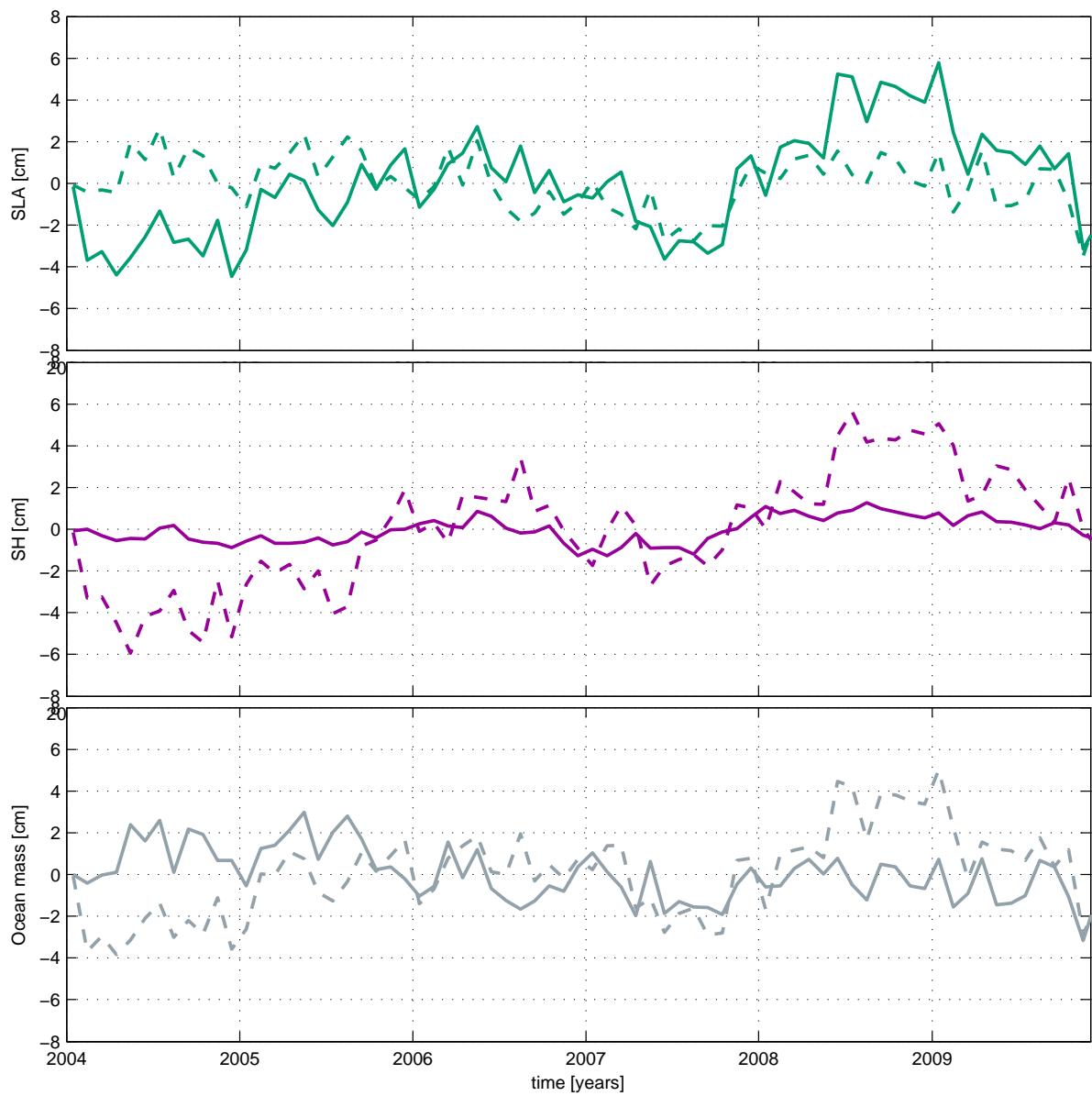


Figure 5.19: The same as Figure 5.18 with the seasonal cycle removed.

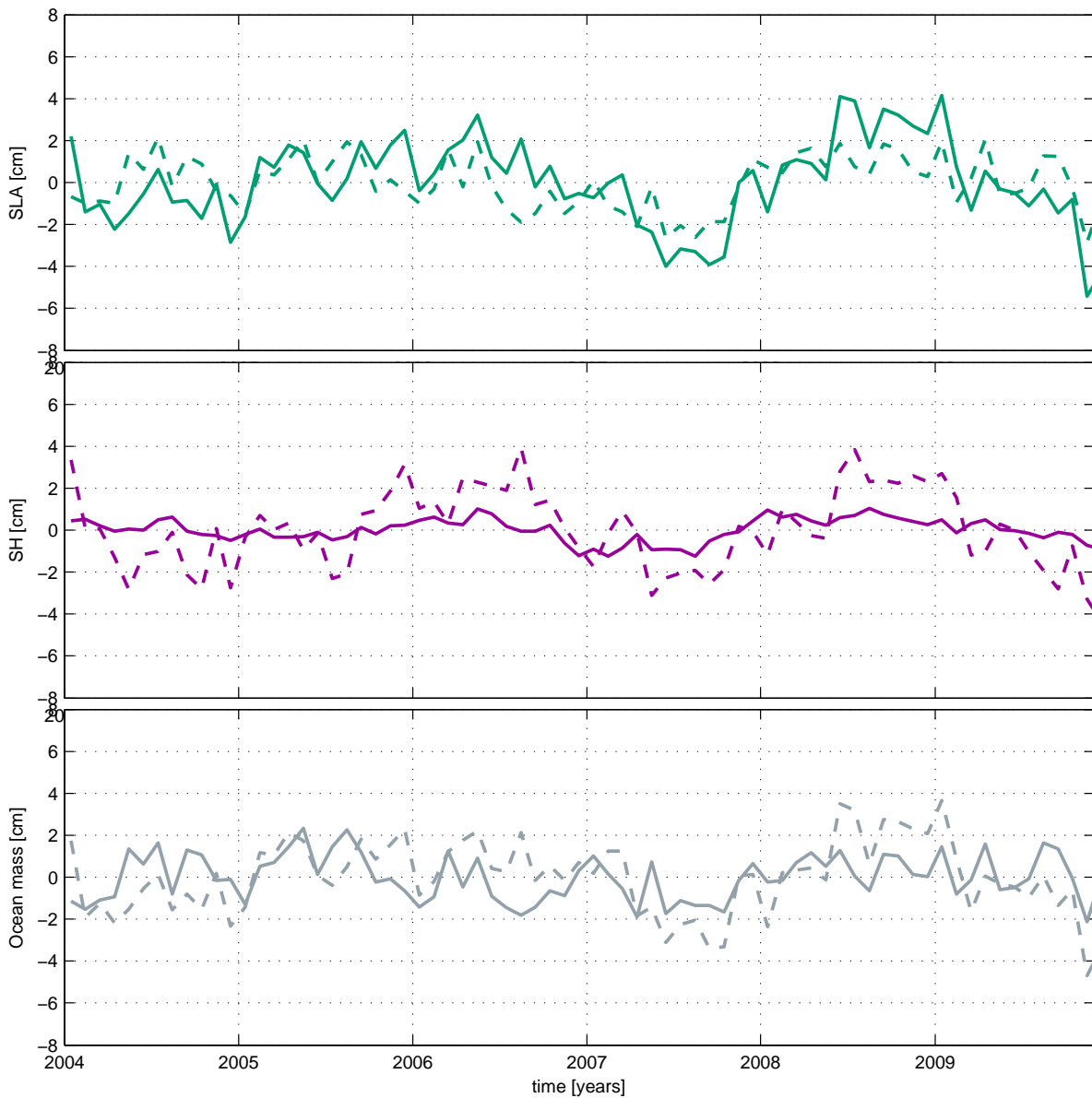


Figure 5.20: The same as Figure 5.19 with the seasonal cycle and the trend removed.

5.3 Discussion

5.3.1 Sea surface temperature

The Campbell Plateau SST is strongly dominated by seasonality. This is most noticeable towards the STF side of the plateau, with temperature gradients across the STF during

summer are approximately 4 °C (Figure 5.12). Seasonality in SST is driven by heat-fluxes from incoming solar radiation, in summer, the insolation is greater, the ocean surface is warmer and stratification increases. In the winter, insolation is smaller and the ocean loses heat to the atmosphere. SST anomalies reveal a high interannual variability up to 1 °C in some cases (Figure 5.4a). One mechanism that could explain this variability is the wind mixing the upper ocean. The wind stress magnitude is significantly anticorrelated with the SST (Figure 5.15). When the winds are weaker, there is less mixing of cold water from depth. In contrast, stronger winds will mix more cold water from depth into the water at the surface. Further work needs to be done to investigate the heat-flux relation with SST anomalies variability.

In Chapter 4 was suggested that interannual variability in the top 100 m is mainly linked to air-sea interaction. In Section 5.2.2 this link was suggested by the interaction between wind and SST, where colder SST was associated with a stronger wind stress magnitude (Figure 5.15). To investigate if that relation can be extended to the different data sets analysed in this study, a comparison between SST over the Campbell Plateau and *in-situ* surface temperatures averaged during the different voyages is shown in Figure 5.21. In this figure, three independent data sets (SST, high resolution and low resolution CTD) agree on the temperature at the surface confirming that the signal is real, and hence, some of the surface variability described for the different data sets could be related to air-sea interaction. The low resolution surface temperature (December from 2002 to 2009) was averaged over the whole plateau (Section 4.2.2). The high resolution temperatures were averaged over the CTD cast within the 1000 m isobath (Figure 3.18). The low resolution temperature shows better agreement with the SST than the high resolution probably due to the distribution of the data, it being more similar to the distribution of SST measurements.

However, other mechanisms such as heat-flux interactions or the influence of precipitation on the ocean surface layer would be necessary to fully understand the air-sea interaction.

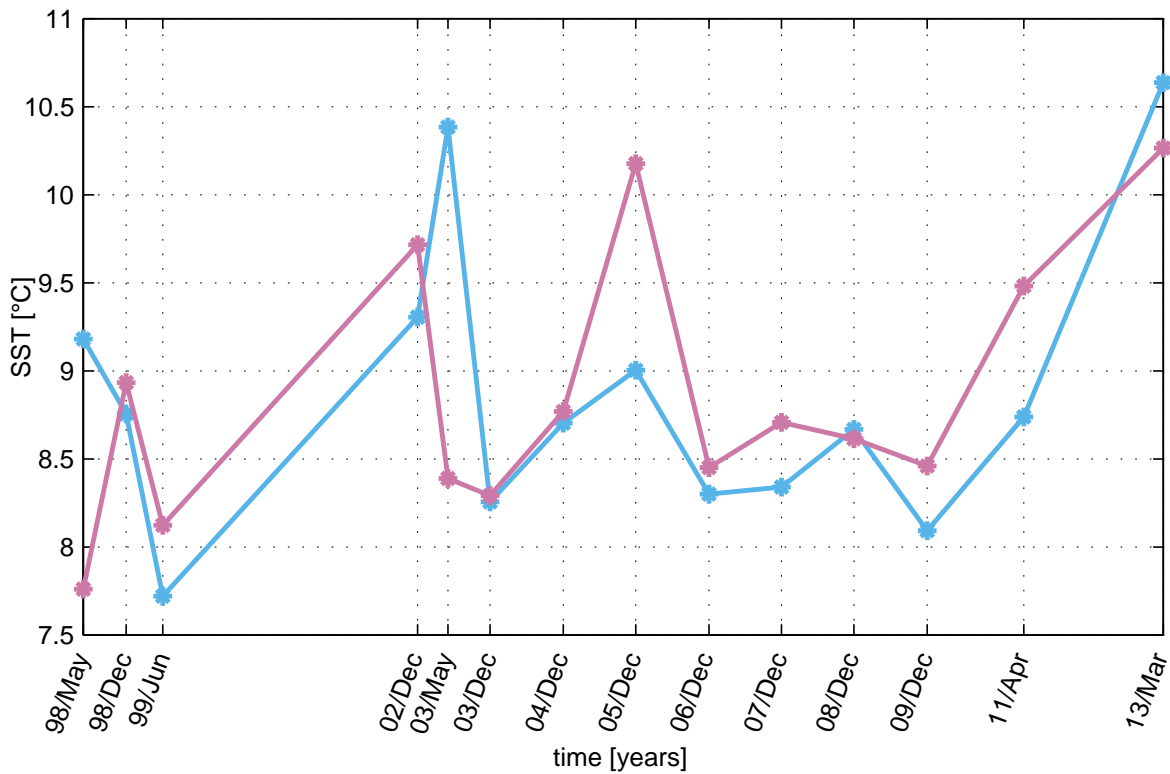


Figure 5.21: SST mean averaged over the Campbell Plateau (solid pink) and *in-situ* surface temperature CTD observations in low and high resolution data sets (solid blue).

A significant correlation was found between SOI and SST with SOI leading SST by seven months (Figure 5.14a). This positive relationship has been previously reported around New Zealand by several studies, for example Hopkins et al. (2010), observed that “El Niño Southern Oscillation (ENSO) indices lead changes in the fronts temperature by up to six months”, which is a similar lag to that found here. This relationship is consistent with those found between ENSO and global mean temperatures, for example (Foster et al., 2010) Stronger and colder southerly winds would increase air-sea heat-flux interactions during El Niño events, which would lead to colder SST (e.g., Gordon, 1986; Basher and Thompson, 1996; Mullan, 1998). Hence, the connecting mechanism between El Niño and SST anomalies is a combination of air-sea interaction and Ekman transport due to stronger winds. This explanation, the increase of heat fluxes due to stronger winds cooling the surface of the ocean, is one explanation for the link between SOI and SST

variability over the Campbell Plateau. However, further work is needed to understand which mechanisms will take part in SST variability, for example, southerly winds also generate more northward Ekman transport which would bring colder waters and increase heat-flux interaction.

There is no notable trend over the whole period, with any trend dependent on the period of time selected. There is a slightly negative trend from 1982 to 2013 but a slightly positive trend from 1992 to 2013 (Figure 5.4a). This variability is consistent (although of much less magnitude) to the one found in the northeast (downstream) of the Campbell Plateau in STW by Fernandez et al. (2014).

5.3.2 Sea level anomalies

The time series of the sea level anomalies (SLA) over Campbell Plateau shows a positive trend of $5.2 \text{ cm decade}^{-1}$ (Figure 5.3). Different mechanisms may be causing this trend and it maybe a result of both local and large scale processes. It has been estimated that SST anomalies would require a trend of $0.61 \text{ }^\circ\text{C}$ per two decades to induce the observed increase through expansion of sea level due to local warming (Section 5.2.3), but no such temperature trend has been seen. However, there may still be some periods where the SST trend contributes to the SLA trend, for example, from 1993 to 1998 (Figure 5.16).

The significant correlation of SLA on the Campbell Plateau with SOI (Figure 5.10) suggests that variability of the SLA may also be linked to variations in the equatorial regions, but further investigation is needed to relate these to the actual mechanisms creating the change, for example changes derived from variations in wind stress curl in the South Pacific (e.g. Holbrook and Bindoff, 1999; Hill et al., 2008).

Local wind stress curl may also force sea level changes by causing convergences and divergences of water through Ekman pumping. Ekman pumping was calculated follow-

ing Equation 5.15 (e.g. Talley et al., 2011; Cushman-Roisin and Beckers, 2011):

$$w_{Ek} = \frac{1}{\rho_0} \left[\frac{\partial}{\partial x} \left(\frac{\tau^y}{f} \right) - \frac{\partial}{\partial y} \left(\frac{\tau^x}{f} \right) \right] \quad (5.15)$$

where w_{Ek} is the Ekman pumping (vertical velocity), (m s^{-1}); ρ_0 is reference density of sea water, (1028 kg m^{-3}); τ^y and τ^x are the wind stress components in x - and y -directions, (N m^{-2}); and f is the Coriolis parameter. In the Southern Hemisphere a clockwise (cyclonic) wind pattern (negative curl) generates divergence (upwelling), and a counter-clockwise (anticyclonic) wind pattern (positive curl) causes convergence (downwelling) (e.g. Cushman-Roisin and Beckers, 2011). This means that positive Ekman pumping causes the sea level to rise (convergence).

Changes in SLA appear to be related with Ekman pumping (Figure 5.22). The time series appear to have a similar behaviour, both with an increasing trend along the whole period. However, both time series have a better match in the second part of the record, from 2000 onward. The time series have a correlation coefficient of $r = 0.14$ ($EDOF=6$; $p = 0.03$). A maximum cross-correlation of $r = 0.56$ ($EDOF=6$; $p = 0.07$) is obtained, which was considered to be significant. The peak of the correlation is when Ekman pumping leads SLA by 20 months. However, a full description of how winds force sea level on the plateau would have to include the propagation of sea level anomalies on and off the plateau. Nevertheless, the correspondence suggests this is a mechanism that should be investigated further.

Sea level on the Campbell Plateau was studied by investigating the different components of the sea level anomalies, including estimates of the steric component and the ocean mass component (Section 5.2.4). The ocean mass appears to be an important component on the Campbell Plateau, as it has to be added to the steric component (over 400 m deep) to match the SLA (Figure 5.17). However, it is not clear what mechanism is causing the sea level to change. It could be through Ekman pumping with the wind stress curl driving the water to pile up on a seasonal basis (Figure 5.23). Here, it appears that Ekman pumping is contributing to part of the sea level change in the first

months (Jan-Jul), but after that the seasonal signal does not match with the sea level variability. Further investigation might need to investigate not only local wind forcing but also look for large-scale connections, since it has been previously suggested that local changes in mass can occur through changes, for example, in large-scale ocean circulation (Roemmich et al., 2007).



Figure 5.22: Ekman pumping anomalies (solid brown) and SLA (solid green). Convergence is shown when Ekman pumping is positive. Monthly data.

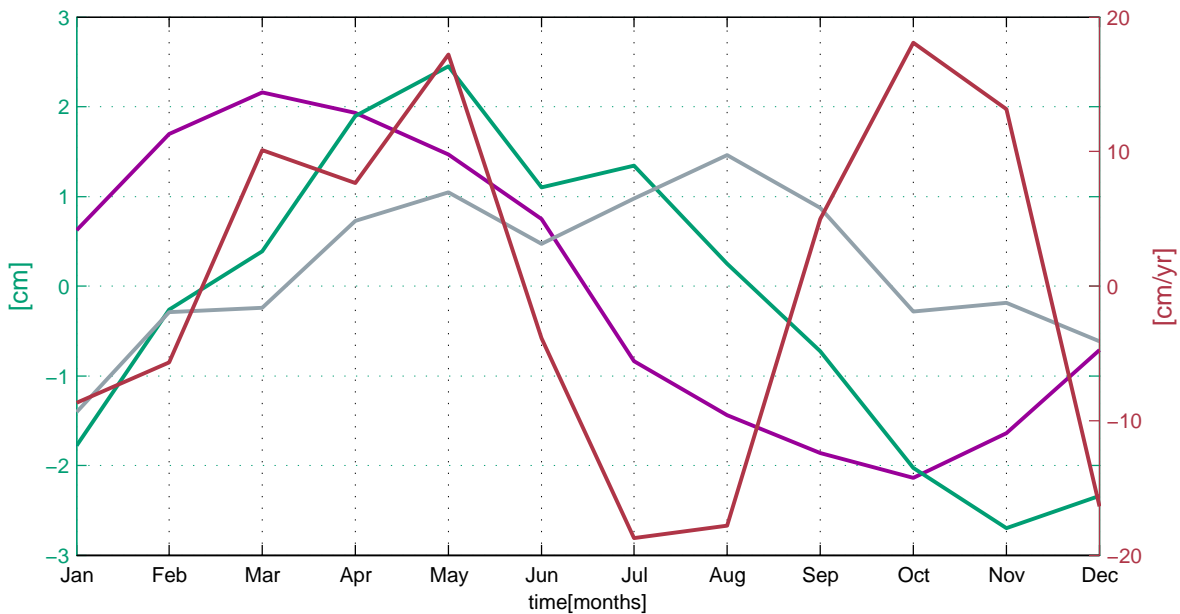


Figure 5.23: Seasonal cycles anomalies of the different components of the sea level budget: SLA (solid green), steric height (solid purple), ocean mass (solid grey); and Ekman pumping seasonal cycle anomalies (solid brown).

Interannually, the steric component (over 400 m) is always the one that differs the most from the other two components (Figure 5.18 to Figure 5.20). One reason for the difference may be due to the contribution of steric height from deeper levels around the plateau. To investigate the steric height component from a deeper level, steric height was calculated over 2000 m from Argo floats, from the Global Marine Argo Atlas (<http://www.argo.ucsd.edu/MarineAtlas.html>), in different places around the Campbell Plateau (Figure 5.24). The trends between steric height and SLA in the three different boxes (Figure 5.25, 5.26 and 5.27) match closely, in contrast to those on the Campbell Plateau. It appears that the trend observed in the Tasman Sea in steric height, 4 cm in nine years (Figure 5.27a), and SLA, 7 cm in seven years (Figure 5.27b), is similar to the trend in SLA observed in the Campbell Plateau, which was 5.2 cm decade⁻¹. The SAF boxes do not show any trend (Figure 5.25 and 5.26).

The similarity between the trend of the Tasman Sea and the Campbell Plateau suggests that the behaviour of the Campbell Plateau is similar to the Tasman Sea, and that

much of that rise in SLA is due to a trend in steric height. There may be different reasons to explain why the steric height in the Campbell Plateau is not showing the same trend as the SLA. One explanation could be related to the depth of the water column used to calculate the steric height. In the Campbell Plateau, the steric height was integrated over the top 400 m of the water column, hence the bottom part of the water column is not contributing to the trend. Another reason could be related to the origin of the data. The steric height data was retrieved from Argo floats, and as previously described in Section 5.1.6 the Argo data over the Campbell Plateau are an interpolation from nearby Argo floats, as the Campbell Plateau is not deep enough for the floats to sample. It might happen that the interpolation made over the Campbell Plateau is made from floats in the subantarctic region. If that was the case, the Campbell Plateau steric height trend would be more similar to the subantarctic region one. However, further work is needed to fully understand the contribution of the steric height to the SLA variability.

As stated at the beginning of the Section, different mechanisms may be causing the SLA trend observed on the Campbell Plateau as a result of both local and large scale processes. Cazenave and Llovel (2010) suggested that local sea level trend patterns are influenced by ocean warming and cooling, freshwater exchange with the atmosphere, redistribution of mass via ocean advection and the response of the ocean to wind stress curl. Some of those have been investigated here, but further work is needed to complete the picture of the SLA variability in the Campbell Plateau.

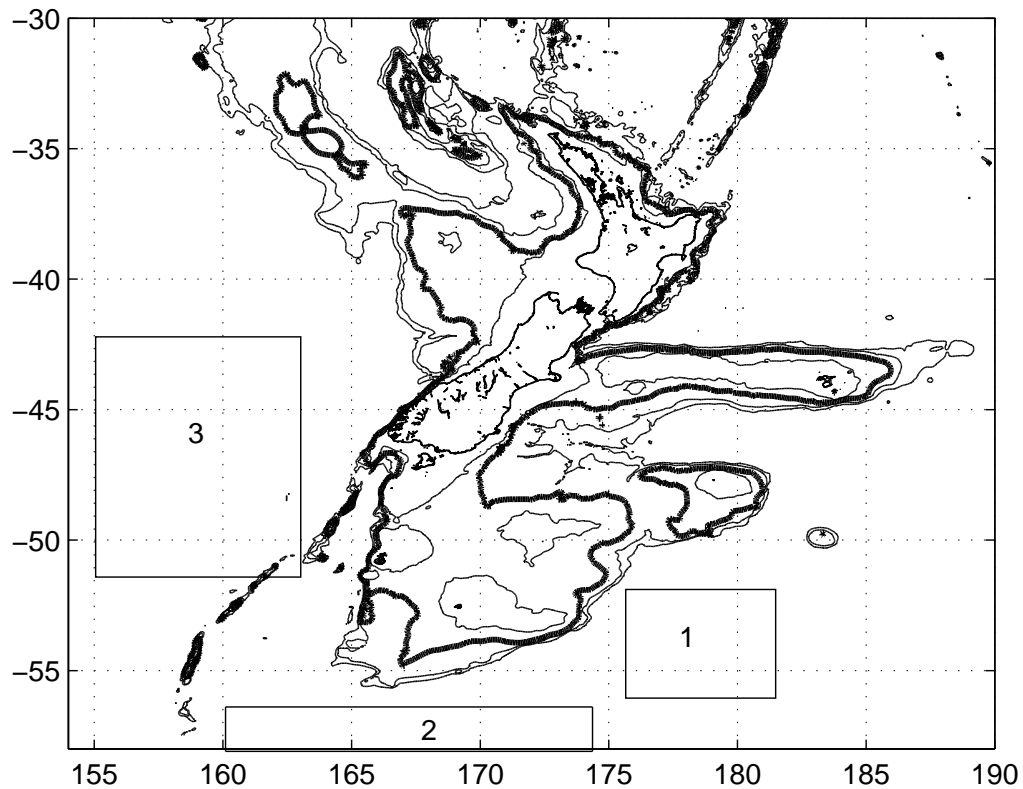
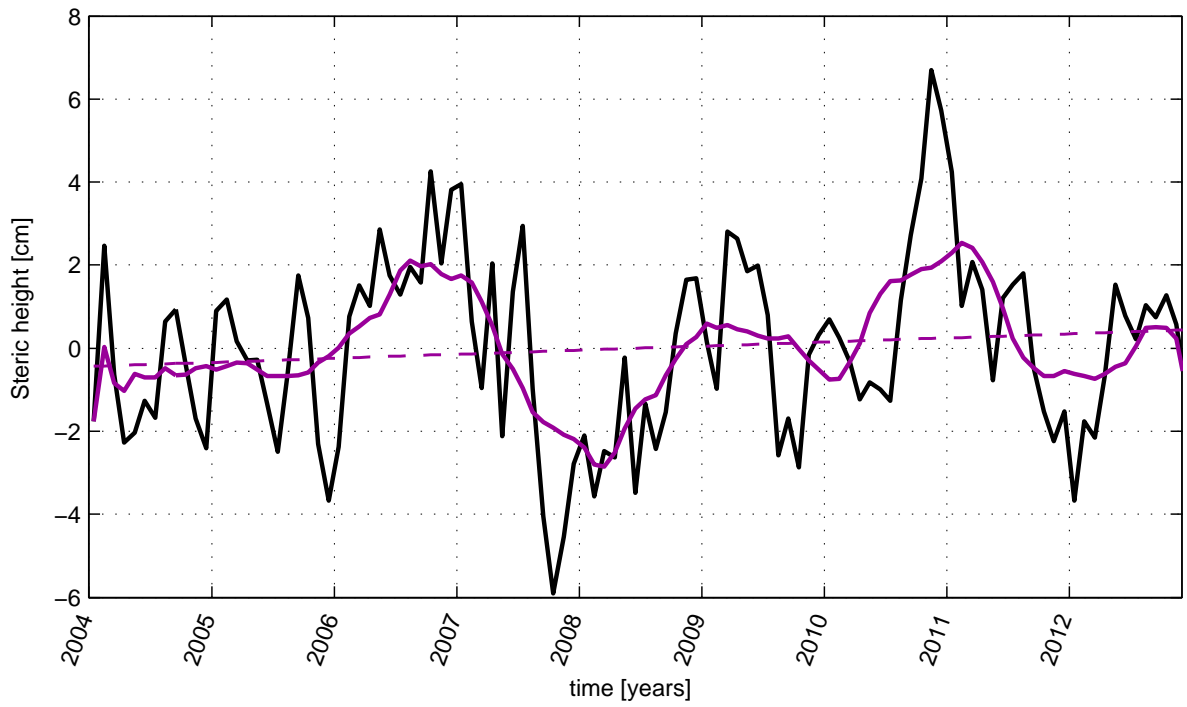


Figure 5.24: Areas where the steric height and SSH have been averaged.

(a) Box 1 steric height



(b) Box 1 SSH

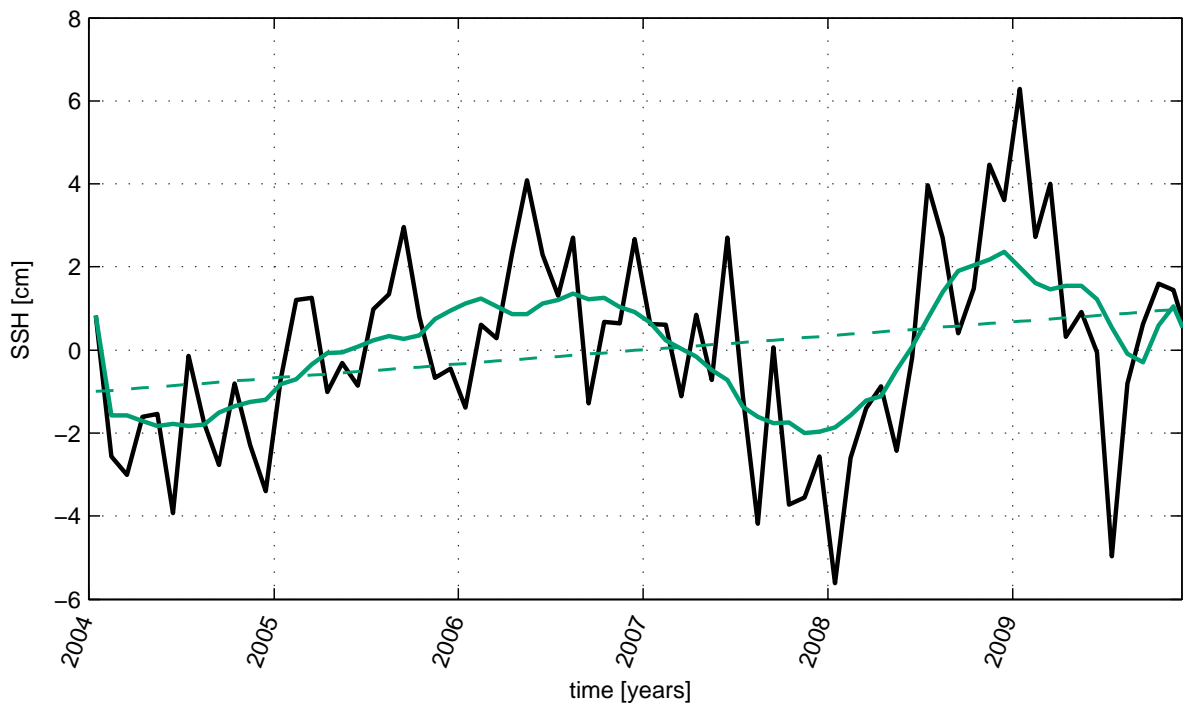


Figure 5.25: (a) Steric height over 2000 m. Coordinates 52 to 56°S, and 176°E 178°W. (b) SSH over same area.

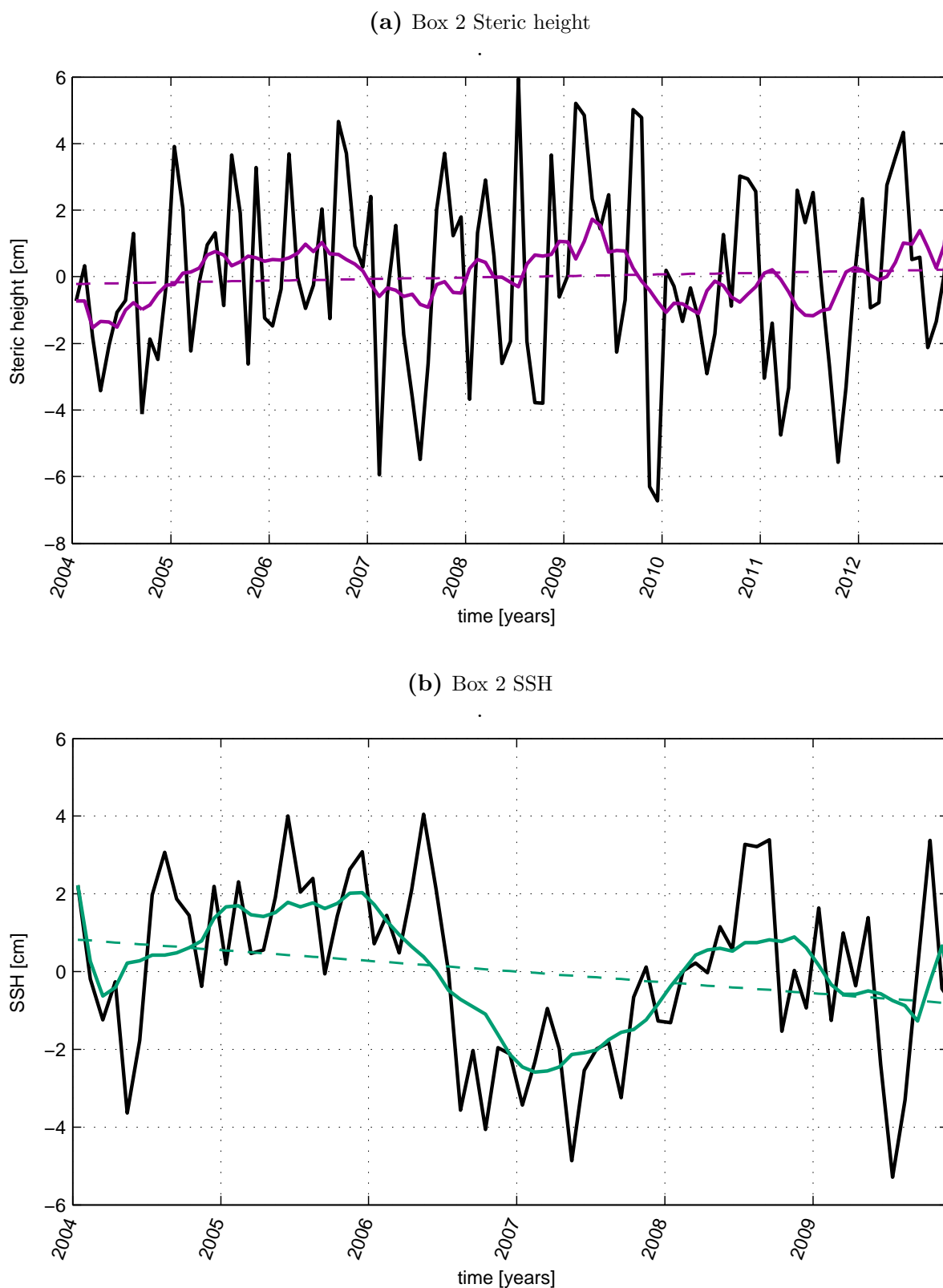
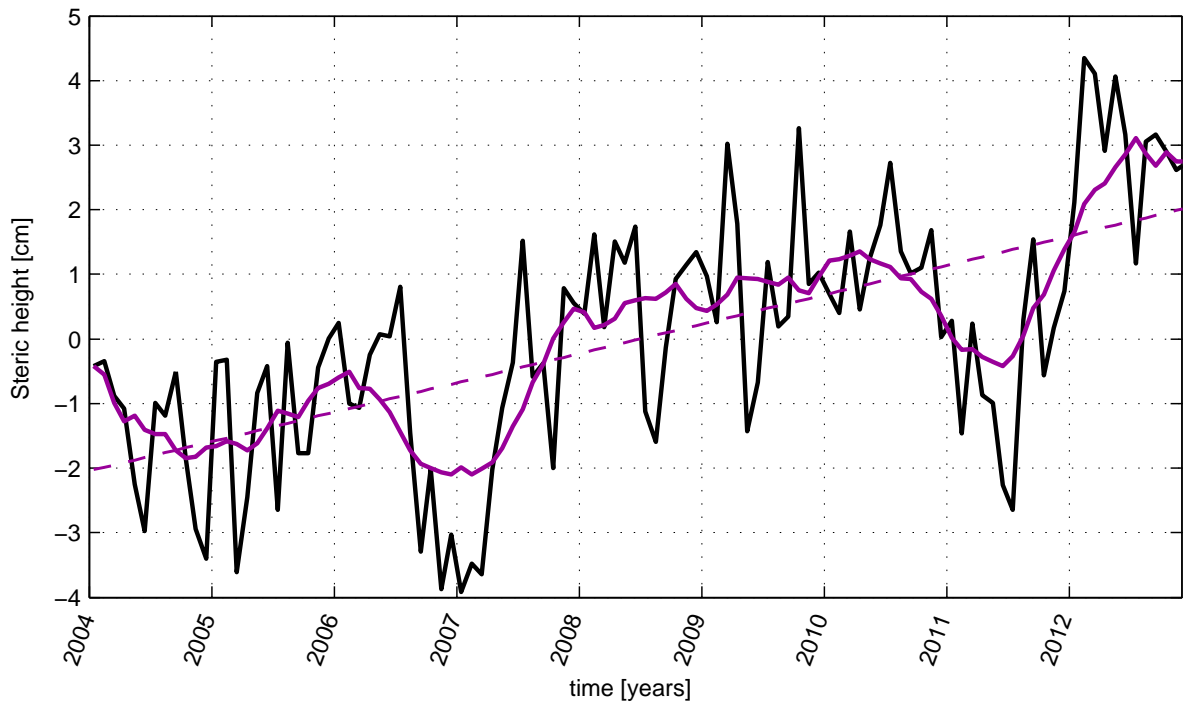


Figure 5.26: (a) Steric height over 2000 m. Coordinates 56 to 60°S, and 160 to 174°E. (b) SSH over same area.

(a) Box 3 Steric height



(b) Box 3 SSH

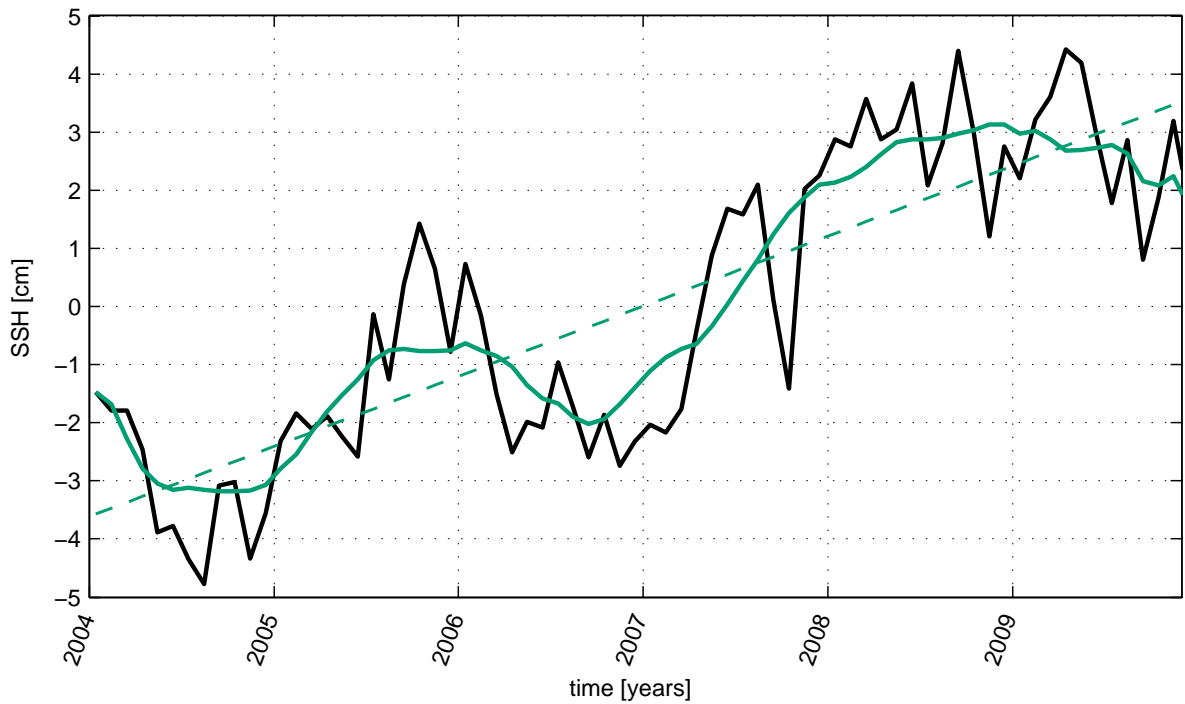


Figure 5.27: (a) Steric height over 2000 m. Box 3. Coordinates 44 to 52°S, and 155 162°E (b) SSH over the same area.

5.4 Summary of the Chapter

This chapter analyses the long-term variability of the Campbell Plateau using remote sensing data. Climate indices are used to find relationships, if any, between variability and large-scale atmospheric changes. Local forcing mechanisms are also investigated. Some of the explanation of the physical mechanisms involved in the long-term variability have also been discussed.

A summary of the correlation results is shown in Table 5.1. It shows the poor correlation of SAM with SLA and SST anomalies, all failing to reach the 90% confidence level. SOI correlates well with SLA and SST anomalies with two and seven month lags, respectively. SLA and SST anomalies are well correlated with SST leading SLA by 27 months. Wind is anti-correlated with SST wind leading by two months. Wind is well correlated with SLA when leading by 17 months.

Table 5.1: Correlation results for the different variables. Positive lag show Climate Indices, wind leading and Ekman pumping. Between SLA and SST, positive lag shows SST leading. Negative r shows anti-correlation.

| | SLA | | | | SST | | | |
|---------------|-------------|------------|----------|-------------|--------------|------------|-----------|-------------|
| | r | lag(month) | EDOF | p-value | r | lag(month) | EDOF | p-value |
| SOI | 0.54 | 0 | 7 | 0.06 | 0.18 | 0 | 10 | 0.0003 |
| | 0.58 | 2 | 7 | 0.07 | 0.43 | 7 | 10 | 0.08 |
| SAM | 0.34 | 0 | 7 | 0.18 | 0.03 | 0 | 10 | not sig |
| | 0.45 | 22 | 7 | 0.11 | -0.38 | -14 | 10 | not sig |
| Wind | 0.07 | 0 | 6 | not sig | -0.43 | 0 | 12 | 0.06 |
| | 0.57 | 17 | 6 | 0.07 | -0.48 | 2 | 12 | 0.04 |
| Ekman pumping | 0.14 | 0 | 6 | 0.03 | | | | |
| | 0.56 | 22 | 6 | 0.07 | | | | |
| SST | 0.44 | 0 | 7 | 0.13 | | | | |
| | 0.55 | 27 | 7 | 0.06 | | | | |

The trend in SST anomalies varies with the time period selected, suggesting neither trend is robust. SST shows a strong seasonality with more pronounced gradients (4°C) towards the north of the region. Despite that, it appears that the whole plateau has a homogeneous spatial behaviour. It shows a strong interannual variability with, in some cases up to 1°C difference. Some of this variability could be explained by local forcing such as wind stress, with a significant anti-correlation of -0.48 when wind leads the SST anomalies by two months. A significant correlation ($r = 0.43$; $p < 0.08$) with the SOI indicates that there might be a connection with large-scale changes in winds associated with the SOI, i.e., changes in wind patterns that would lead to changes in air-sea interaction.

ΔSSH shows a positive trend of $5.2\text{ cm decade}^{-1}$ in the last two decades. This variability might be explained by a combination of local and large-scale processes. SST anomalies show a relationship with SLA and a significant correlation of 0.43 , however, a trend in SST of 0.61°C over two decades would be needed to cause the sea level to rise due to SST warming, which is not the case. A significant correlation with the SOI, might indicate a connection with large-scale changes in winds associated with the SOI. Local wind stress curl may also force sea level changes by causing convergences and divergences of water through Ekman pumping, but further analysis is needed to fully understand the relationship of the local winds and SLA. It appears that ocean mass and steric height are important contributions to the sea level change, but the cause of the poor agreement remains unclear.

Although it has been previously reported that SAM is one of the main forcing mechanisms of this region (e.g., Marshall, 2003; Morrow et al., 2010; Sallée, Speer, and Rintoul, 2010) this analysis does not show the significant relationship between SAM and SST or SLA on the Campbell Plateau.

The sea level budget of the Campbell Plateau is well described on a seasonal scale through the different components with the steric component added to the ocean mass component to match the total component. The SST seasonal cycle also matches the bud-

get as one of the contributions to the steric component. Although the SST, steric height and SLA show a local signal linked to the averaged region (the Campbell Plateau), the ocean mass seasonal cycle responds to a global signal, i.e., the peak of the ocean mass is in August responding to the melting and run off contribution in the Northern Hemisphere summer. However, the contribution of local forcing, such as Ekman pumping, to ocean mass redistribution and associated sea level changes needs further investigation to see if it has a role in the seasonal sea level budget.

The analysis of the different components of the sea level budget on an interannual scale suggests: i) there may be a trend that is dominating the time series, ii) the steric component may be lacking some information due to being referenced to the top 400 m of the water column, iii) ocean mass might also be forced locally and not just be a response to a global signal.

Chapter 6

Conclusions

The aim of this thesis was to describe the oceanography of the Campbell Plateau, understand its variability at different time and space scales and determine the driving mechanisms.

This study provides a new and more complete description of the water mass structure of the New Zealand subantarctic and the Campbell Plateau, confirms the presence of Subantarctic Mode Water (SAMW) and shows, for the first time, the presence of Antarctic Intermediate Water (AAIW) in the deeper regions of the plateau. It also links long-term variability to local and large scale mechanisms. A mix of *in-situ* and satellite measurements have been used in the process to build a picture of the oceanography of the Campbell Plateau.

The Campbell Plateau is surrounded by a heterogeneous water mass structure, with a variety of water masses associated with the Subtropical Front to the north, and associated with the Antarctic Circumpolar Current (ACC) and the Subantarctic Front (SAF) to the south. On the Campbell Plateau, some of these waters meet and get modified by mixing. Here, Subtropical Water (SAW) mixes with Subantarctic Water (SAW) in the upper water column of the Campbell Plateau, influenced by seasonality. The middle part of the water column on the Campbell Plateau is occupied by Subantarctic Mode Water (SAMW), from 200 m to the bottom of the plateau. This SAMW layer also varies

according to a seasonal cycle. For the first time, Antarctic Intermediate Water (AAIW) is found between 700 and 1000 m, around the perimeter of the plateau where the deep ocean encounters the plateau bathymetry. It appears that the AAIW may be moving onto the plateau from the deeper ocean. Off the plateau, in the deeper ocean, Upper Circumpolar Deep Water (UCDW) and Lower Circumpolar Deep Water (LCDW) are also found around the edges of the plateau.

Water structure on the Campbell Plateau is similar to the water masses structure of the top 700 m of the Bounty Trough. This similarity suggests a connection with both regions either sharing the same source regions, or there being strong and frequent exchange between the two.

No trend, but significant variability of the ocean properties on the Campbell Plateau was found. It appears that the western side of the plateau is more influenced by the STF and the eastern part by the SAF, except for the upper water column which is influenced by air-sea interaction. SAMW is found in the middle part of the water column, which is largely homogeneous with time. The bottom part of the Campbell Plateau, from 700 to 900 m depth, shows high variability, with up to 0.7°C variability, sometimes in consecutive years. Although this might be due to the spatial sampling of the data, it might also suggest some advection on the deeper parts of the plateau, likely related to changes associated with the SAF.

For the first time, variability of the surface flow in the upper 280 m of the water column has been described from steric height. A constant flow across the middle plateau towards the east is described. Also, two circulation features are found; one on the northern side of the plateau, and another on the southern side. It appears that the stronger variability comes from the STF.

The Sea Surface Temperature (SST) spatial distribution on the Campbell Plateau is strongly influenced by seasonality, however, it appears that the plateau responds homogeneously to the variability. SST anomalies have high interannual variability of up to

1 °C, which may be partially driven by local wind stress mixing. Significant correlation with SOI indicates that changes may be influenced by changes in the winds related to El Niño events. However, the influence of other local mechanisms such as the local heat-flux interaction have yet to be investigated.

SLA has a strong positive trend over the last two decades. This variability is likely driven by a combination of both local and large scale mechanisms. SST changes are not contributing to most of the SSH trend but may be responsible for some of the SSH variability. Local wind stress curl may contribute over the second half of the period through local Ekman pumping. Significant correlation with SOI indicates that SLA variability may be linked to variations in the equatorial region. Similar SSH and steric height trends in the Tasman Sea suggest that the Campbell Plateau is behaving more like the subtropics than the other subantarctic regions.

Ocean variability in the Campbell Plateau is influenced by local forcing mechanisms like the air-sea interaction and local winds. Also, the Campbell Plateau is influenced by global oceanographic features such as the Subtropical and the Subantarctic Fronts. From the correlation with SOI, the Campbell Plateau appears to be influenced by changes in the equatorial and mid-latitude, which are related to changes derived from variations in wind stress curl in the South Pacific, although the exact mechanisms by which this may be occurring are yet to be determined.

Simpson and Sharples (2012) split the ocean depths between shelf (surface to 500 m depth), slope (500 to 2500 m depth) and abyssal (2500 to 6000 m depth). They define shelf seas as highly dynamic regions, with a number of different forcing mechanisms such as winds, large inputs of solar radiation increasing air-sea interactions or precipitation. Because of the topographic structure of the Campbell Plateau, it is tempting to classify it as a shelf ocean. However, due to the influence of the surrounding oceans and the mechanisms influencing its variability, it can be said that the Campbell Plateau brings together characteristics of a continental marginal sea and a fully open ocean setting.

Within this study, some of the initial research questions have been answered. These questions were:

1. What is the oceanographic structure of the New Zealand subantarctic region and the Campbell Plateau?
2. What is the seasonal, interannual and long-term variability of the ocean properties on the Campbell Plateau?
3. What physical mechanisms, local or large scale, are driving these changes?

This study has analysed a completely new set of observations to describe the oceanography of the Campbell Plateau. Although a more advanced picture has been developed, there are still a number of limitations inherent to the data. Temporal and spatial limitation on the *in-situ* measurements makes it hard to describe the full seasonality of the Campbell Plateau, water mass formation, air-sea heat-fluxes and actual seasonal steric height. Spatial sampling limits our understanding of some regions of the plateau, in particular it does not capture all of the plateau perimeter where the plateau water is interacting with the surrounding ocean.

A number of priorities for future work have been identified, in Chapter 3 these were identifying where, and how the SAMW and AAIW found on the Campbell Plateau, form, mix and vary. In Chapter 4 investigating the influence of the fronts positions in the interannual variability of the Campbell Plateau. In Chapter 5 investigating how do local and large-scale forcing mechanisms influence the Campbell Plateau, whether these be variations derived from El Niño - Southern Oscillation (ENSO) events, or changes in atmospheric heat-fluxes, or Ekman pumping. Continuing to develop our understanding of the Campbell Plateau is important, because ocean variability here both influences New Zealand climate, and is important for marine mammal, sea bird and fisheries populations on the plateau itself. With larger climate changes expected in future than we have already seen in the past record, understanding how the Campbell Plateau responds will be important.

Bibliography

- Basher, R. E., and Thompson, C. S. (1996). Relationship of air temperatures in New Zealand to regional anomalies in Sea-surface temperature and atmospheric circulation. *International Journal of Climatology*, 16(4), 405–425.
- Belkin, I., and Gordon, A. (1996). Southern Ocean fronts from the Greenwich meridian to Tasmania. *Journal of Geophysical Research*, 101(C2), 3675–3696.
- Boening, C., Willis, J. K., Landerer, F. W., Nerem, R. S., and Fasullo, J. (2012). The 2011 La Niña: So strong, the oceans fell. *Geophysical Research Letters*, 39(19), L19602. doi: 10.1029/2012GL053055
- Böning, C. W., Dispert, A., Visbeck, M., Rintoul, S. R., and Schwarzkopf, F. U. (2008). The response of the Antarctic Circumpolar Current to recent climate change. *Nature Geoscience*, 1(12), 864–869. doi: 10.1038/ngeo362
- Bostock, H. C. (2011). *Voyage Report TAN1106, Solander Trough* (Tech. Rep. No. May). Wellington: National Institute of Water and Atmospheric Research (NIWA).
- Bostock, H. C., Sutton, P. J., Williams, M. J., and Opdyke, B. N. (2013). Reviewing the circulation and mixing of Antarctic Intermediate Water in the South Pacific using evidence from geochemical tracers and Argo float trajectories. *Deep Sea Research Part I: Oceanographic Research Papers*, 73, 84–98. doi: 10.1016/j.dsr.2012.11.007
- Bradford-Grieve, J. M., Probert, P., Nodder, S. D., Thompson, D., Hall, J., Hanchet, S., ... Wilkinson, I. (2003). Pilot trophic model for subantarctic water over the Southern Plateau, New Zealand: a low biomass, high transfer efficiency sys-

- tem. *Journal of Experimental Marine Biology and Ecology*, 289(2), 223–262. doi: 10.1016/S0022-0981(03)00045-5
- Brown, E., Colling, A., Park, D., Phillips, J., Rothery, D., and Wright, J. (2001). *Ocean Circulation* (Second ed.). Oxford: Butterworth-Heinemann Elsevier.
- Bryden, H. L., and Heath, R. A. (1985). Energetic eddies at the Northern edge of the Antarctic Circumpolar Current in the Southwest Pacific. *Progress in Oceanography*, 14, 65–87. doi: 10.1016/0079-6611(85)90006-0
- Burling, R. W. (1961). *Hydrology of circumpolar waters south of New Zealand*. R.E. Owen, Government Printer.
- Butler, E., and Butt, J. (1992). Oceanography of the subtropical convergence zone around southern New Zealand. *New Zealand Journal of Marine and Freshwater Research*, 26(2), 131–154.
- Carter, L., McCave, I., and Williams, M. (2008). Circulation and water masses of the Southern Ocean: A review. *Developments in Earth and Environmental Sciences*, 8, 85–114. doi: 10.1016/S1571-9197(08)00004-9
- Cazenave, A., and Llovel, W. (2010). Contemporary sea level rise. *Annual Review of Marine Science*, 2, 145–173. doi: 10.1146/annurev-marine-120308-081105
- Chambers, D. P., and Bonin, J. A. (2012). Evaluation of Release-05 GRACE time-variable gravity coefficients over the ocean. *Ocean Science*, 8(5), 859–868. doi: 10.5194/os-8-859-2012
- Chatfield, C. (2004). *The Analysis of Time Series, An Introduction* (Sixth ed.). New York: Chapman and Hall.
- Chiswell, S. M. (1996). Variability in the Southland Current, New Zealand. *New Zealand Journal of Marine and Freshwater Research*, 30(1), 1–17.
- Chiswell, S. M., and Sutton, P. J. H. (1998). Deep eddy in the Antarctic Intermediate Water north of the Chatham Rise. *American Meteorological Society*, 28(3), 535–540.

- Cipollini, P., Gommenginger, C., Coelho, H., Fernandes, J., Gomez-Enri, J., Martin-Puig, C., ... Benveniste, J. (2009). Progress in Coastal Altimetry: the experience of the COASTALT Project. *EGU General Assembly Conference Abstracts*, 11, 12862.
- Cortese, G., Dunbar, G. B., Carter, L., Scott, G., Bostock, H., Bowen, M., ... Sturm, A. (2013). Southwest Pacific Ocean response to a warmer world: Insights from Marine Isotope Stage 5e. *Paleoceanography*, 28(3), 585–598. doi: 10.1002/palo.20052
- Currie, K. I., and Hunter, K. A. (1998). Surface water carbon dioxide in the waters associated with the subtropical convergence, east of New Zealand. *Deep Sea Research Part I: Oceanographic Research Papers*, 45(10), 1765–1777. doi: 10.1016/S0967-0637(98)00041-7
- Currie, K. I., and Hunter, K. A. (1999). Seasonal variation of surface water CO₂ partial pressure in the Southland Current, east of New Zealand. *Marine and Freshwater Research*, 50(5), 375. doi: 10.1071/MF98115
- Currie, K. I., Reid, M. R., and Hunter, K. a. (2011, August). Interannual variability of carbon dioxide drawdown by subantarctic surface water near New Zealand. *Biogeochemistry*, 104(1-3), 23–34. doi: 10.1007/s10533-009-9355-3
- Cushman-Roisin, B., and Beckers, J.-M. (2011). *Introduction to Geophysical Fluid Dynamics, Volume 101, Second Edition: Physical and Numerical Aspects*. Academic Press.
- Deacon, G. (1937). The hydrology of the Southern Ocean. In *Discovery reports, number xv*. (pp. 56–63). Cambridge University Press.
- Deacon, G. (1982, January). Physical and biological zonation in the Southern Ocean. *Deep Sea Research Part A. Oceanographic Research Papers*, 29(1), 1–15. doi: 10.1016/0198-0149(82)90058-9
- Dibarboure, G., Lauret, O., and Mertz, F. (2008). SSALTO/DUACS user handbook:(M) SLA and (M) ADT near-real time and delayed time products. *Rep. CLS-DOS-NT(M)*.

- Ducet, N., Le Traon, P. Y., and Reverdin, G. (2000). Global high-resolution mapping of ocean circulation from TOPEX/Poseidon and ERS-1 and -2. *Journal of Geophysical Research*, *105*, 19,419–477,498.
- Emery, W., and Thomson, R. (2001). *Data Analysis Methods in Physical Oceanography* (Second ed.). Amsterdam: Elsevier B.V.
- Fernandez, D., Bowen, M., and Carter, L. (2014). Intensification and variability of the confluence of subtropical and subantarctic boundary currents east of New Zealand. *Journal of Geophysical Research: Oceans*, *119*(2), 1146–1160. doi: 10.1002/2013JC009153
- Foster, G., Annan, J. D., Jones, P. D., Mann, M. E., Mullan, B., Renwick, J., ... Trenberth, K. E. (2010). Comment on Influence of the Southern Oscillation on tropospheric temperature by J. D. McLean, C. R. de Freitas, and R. M. Carter. *Journal of Geophysical Research*, *115*(D9), D09110. doi: 10.1029/2009JD012960
- Francis, M. P., Hurst, R. J., and McArdle, B. H. (2002). New Zealand demersal fish assemblages. *Environmental Biology of Fishes*, *65*(1998), 215–234.
- Garner, D. M. (1959). The sub-tropical convergence in New Zealand surface waters. *New Zealand Journal of Geology and Geophysics*, *2*(2), 315–337. doi: 10.1080/00288306.1959.10417650
- Gille, S. T. (2003). Float observations of the Southern Ocean. Part I: Estimating mean fields, bottom velocities, and topographic steering. *Journal of Physical Oceanography*, *33*(6), 1167–1181.
- Gillett, N. P., Kell, T. D., and Jones, P. D. (2006). Regional climate impacts of the Southern Annular Mode. *Geophysical Research Letters*, *33*(23), L23704. doi: 10.1029/2006GL027721
- Gnanadesikan, A., and Hallberg, R. W. (2000). On the Relationship of the Circumpolar Current to Southern Hemisphere Winds in Coarse-Resolution Ocean Models. *Journal of Physical Oceanography*, *30*(8), 2013–2034.

- Gong, D., and Wang, S. (1999). Definition of Antarctic Oscillation index. *Geophysical Research Letters*, 26(4), 459–462. doi: 10.1029/1999GL900003
- Gordon, A. L. (1966). Potential temperature, oxygen and circulation of bottom water in the Southern Ocean. *Deep Sea Research and Oceanographic Abstracts*(966).
- Gordon, A. L. (1972). On the interaction of the Antarctic Circumpolar Current and the Macquarie Ridge. *Antarctic Research Series*, 19, 71–78.
- Gordon, A. L. (1975). An Antarctic oceanographic section along 170 E. *Deep Sea Research and Oceanographic Abstracts*, 22(2178).
- Gordon, N. D. (1986). The southern oscillation and New Zealand weather. *Monthly weather review*.
- Graham, R. M., and De Boer, A. M. (2013). The Dynamical Subtropical Front. *Journal of Geophysical Research: Oceans*, 118(10), 5676–5685. doi: 10.1002/jgrc.20408
- Grieg, M. (1999). *Voyage Report, TAN9909, Campbell Plateau* (Tech. Rep.). Wellington: National Institute of Water and Atmospheric Research (NIWA).
- Griffith, G. P., Vennell, R., and Williams, M. J. M. (2010). An algal photoprotection index and vertical mixing in the Southern Ocean. *Journal of Plankton Research*, 32(4), 515–527. doi: 10.1093/plankt/fbq003
- Hamilton, L. (2006). Structure of the Subtropical Front in the Tasman Sea. *Deep Sea Research Part I: Oceanographic Research Papers*, 53(12), 1989–2009. doi: 10.1016/j.dsr.2006.08.013
- Hanawa, K., and Talley, L. (2001). Mode Waters. In G. Siedler and J. Church (Eds.), *Ocean circulation and climate* (Second ed., pp. 373–386). Academic Press.
- Hanchet, S., and Bradford, J. (2002). Understanding ecosystems: a key to managing fisheries? *Water and Atmosphere (NIWA)*, 10(4), 16–17.
- Hartin, C. A., Fine, R. A., Sloyan, B. M., Talley, L. D., Chereskin, T. K., and Happell, J. (2011). Formation rates of Subantarctic Mode Water and Antarctic Intermediate

- Water within the South Pacific. *Deep Sea Research Part I Oceanographic Research Papers*, 58(5), 524–534.
- Hasson, A., Koch-Larrouy, A., and Morrow, R. (2011). The origin and fate of mode water in the southern Pacific Ocean. *Ocean Dynamics*, 62(3), 335–354. doi: 10.1007/s10236-011-0507-3
- Heath, R. A. (1972). The southland current. *New Zealand Journal of Marine and Freshwater Research*, 6(4), 497–533. doi: 10.1080/00288330.1972.9515444
- Heath, R. A. (1976). Models of the diffusive advective balance at the subtropical convergence. *Deep Sea Research and Oceanographic Abstracts*, 23(12), 1153–1164. doi: 10.1016/0011-7471(76)90891-3
- Heath, R. A. (1981). Oceanic fronts around southern New Zealand. *Deep Sea Research Part A. Oceanographic Research Papers*, 28(6), 547–560.
- Heath, R. A. (1985). A review of the physical oceanography of the seas around New Zealand - 1982. *New Zealand Journal of Marine and Freshwater Research*, 19(1), 79–124. doi: 10.1080/00288330.1985.9516077
- Herraiz-Borreguero, L., and Rintoul, S. R. (2011). Subantarctic Mode Water: distribution and circulation. *Ocean Dynamics*, 61(1), 103–126.
- Hill, K. L., Rintoul, S. R., Coleman, R., and Ridgway, K. R. (2008). Wind forced low frequency variability of the East Australia Current. *Geophysical Research Letters*, 35(8), L08602. doi: 10.1029/2007GL032912
- Hill, K. L., Rintoul, S. R., Oke, P. R., and Ridgway, K. (2010). Rapid response of the East Australian Current to remote wind forcing: The role of barotropic-baroclinic interactions. *Journal of Marine Research*, 68(3), 413–431. doi: 10.1357/002224010794657218
- Holbrook, N. J., and Bindoff, N. L. (1999). Seasonal Temperature Variability in the Upper Southwest Pacific Ocean. *Journal of Physical Oceanography*, 29(3), 366–381.

- Holbrook, N. J., Goodwin, I. D., McGregor, S., Molina, E., and Power, S. B. (2011). ENSO to multi-decadal time scale changes in East Australian Current transports and Fort Denison sea level: Oceanic Rossby waves as the connecting mechanism. *Deep Sea Research Part II: Topical Studies in Oceanography*, 58(5), 547–558. doi: 10.1016/j.dsr2.2010.06.007
- Holte, J. W., Talley, L. D., Chereskin, T. K., and Sloyan, B. M. (2012). The role of air-sea fluxes in Subantarctic Mode Water formation. *Journal of Geophysical Research*, 117, C03040. doi: 10.1029/2011JC007798
- Hopkins, J., Shaw, A. G. P., and Challenor, P. (2010). The Southland Front, New Zealand: Variability and ENSO correlations. *Continental Shelf Research*, 30(14), 1535–1548. doi: 10.1016/j.csr.2010.05.016
- IOC, SCOR, and IAPSO. (2010). The international thermodynamic equation of seawater 2010: Calculation and use of thermodynamic properties. *Intergovernmental Oceanographic Commission, Manuals and Guides*(56), 220.
- Jillett, J. B. (1969). Seasonal hydrology of waters off the Otago peninsula, South Eastern New Zealand. *New Zealand Journal of Marine and Freshwater Research*, 3(3), 349–375. doi: 10.1080/00288330.1969.9515303
- Kalnay, E., and Kanamitsu, M. (1996). The NCEP/NCAR 40-year reanalysis project. *Bulletin of the American Meteorological Society*.
- Karoly, D. J. (1989). Southern Hemisphere Circulation Features Associated with El Niño-Southern Oscillation Events. *Journal of Climate*, 2(11), 1239–1252. doi: 10.1175/1520-0442
- Kidson, J. W. (1975). Eigenvector Analysis of Monthly Mean Surface Data. *Monthly Weather Review*, 103(3), 177–186.
- Kidson, J. W. (1988a). Indices of the Southern Hemisphere Zonal Wind. *Journal of Climate*, 1(2), 183–194.

- Kidson, J. W. (1988b). Interannual Variations in the Southern Hemisphere Circulation. *Journal of Climate*, 1(12), 939–953. doi: 10.1175/1520-0442(1988)001<1177:IVITSH>2.0.CO;2
- Kistler, R., Collins, W., and Saha, S. (2001). The NCEP-NCAR 50-year reanalysis: Monthly means CD-ROM and documentation. *Bulletin of the American Meteorological Society*, 82(2), 247–268.
- Kundu, P. K., and Cohen, I. M. (2008). *Fluid Mechanics* (Fourth ed.). Oxford: Elsevier Inc.
- LaCasce, J., and Isachsen, P. (2010). The linear models of the ACC. *Progress in Oceanography*, 84(3-4), 139–157. doi: 10.1016/j.pocean.2009.11.002
- Leuliette, E. W., and Miller, L. (2009). Closing the sea level rise budget with altimetry, Argo, and GRACE. *Geophysical Research Letters*, 36(4), L04608. doi: 10.1029/2008GL036010
- Limpasuvan, V., and Hartmann, D. L. (1999). Eddies and the annular modes of climate variability. *Geophysical Research Letters*, 26(20), 3133–3136. doi: 10.1029/1999GL010478
- Marshall, G. J. (2003). Trends in the Southern Annular Mode from observations and reanalyses. *Journal of Climate*, 16(1999), 4134–4143. doi: 10.1175/1520-0442
- Marshall, G. J., and Speer, K. (2012). Closure of the meridional overturning circulation through Southern Ocean upwelling. *Nature Geoscience*, 5(3), 171–180. doi: 10.1038/ngeo1391
- McCartney, M. S. (1977). Subantarctic Mode Water. In M. Angel (Ed.), *A voyage of discovery george deacon 70th anniversary volume* (p. 712). Pergamon Press.
- McCartney, M. S. (1982). The subtropical recirculation of mode waters. *Journal of Marine Research*, 24, 427–464.

- Mccave, I., and Carter, L. (1997). Recent sedimentation beneath the Deep Western Boundary Current off northern New Zealand. *Deep Sea Research Part I: Oceanographic Research Papers*, 44(7), 1203–1237. doi: 10.1016/S0967-0637(97)00011-3
- McDougall, T. J., and Barker, P. (2011). *Getting started with TEOS-10 and the Gibbs Seawater (GSW)* (No. May). SCOR/IAPSO WG127.
- McDougall, T. J., Jackett, D. R., Millero, F. J., Pawlowicz, R., and Barker, P. M. (2012). A global algorithm for estimating Absolute Salinity. *Ocean Science*, 8(6), 1123–1134. doi: doi:10.5194/os-8-1123-2012
- Millero, F. J., Feistel, R., Wright, D. G., and McDougall, T. J. (2008). The composition of Standard Seawater and the definition of the Reference-Composition Salinity Scale. *Deep Sea Research Part I: Oceanographic Research Papers*, 55(1), 50–72. doi: 10.1016/j.dsr.2007.10.001
- Mitchell, J., Mackay, K., Neil, H. L., Mackay, E., Pallentin, A., and Notman, P. (2012). *Undersea New Zealand, NIWA Chart, Miscellaneous Series no 92*. Wellington: National Institute of Water and Atmospheric Research.
- Moore, J. K., and Abbott, M. R. (2000). Phytoplankton chlorophyll distributions and primary production in the Southern Ocean. *Journal of Geophysical Research*, 105(C12), 28709. doi: 10.1029/1999JC000043
- Moore, J. K., Abbott, M. R., and Richman, J. G. (1999). Location and dynamics of the Antarctic Polar Front from satellite sea surface temperature data. *Journal Of Geophysical Research*, 104(C2), 3059–3073.
- Morris, M., Stanton, B., and Neil, H. (2001). Subantarctic oceanography around New Zealand: Preliminary results from an ongoing survey. *New Zealand Journal of Marine and Freshwater Research*, 35(3), 499–519.
- Morrison, A. K., Hogg, A. M., and Ward, M. L. (2011). Sensitivity of the Southern Ocean overturning circulation to surface buoyancy forcing. *Geophysical Research Letters*, 38, L14602, 1–5. doi: 10.1029/2011GL048031

- Morrow, R., Coleman, R., Church, J., and Chelton, D. (1994). Surface Eddy Momentum Flux and Velocity Variances in the Southern Ocean from Geosat Altimetry. *Journal of Physical Oceanography*, 24(10), 2050–2071. doi: 10.1175/1520-0485
- Morrow, R., Ward, M. L., Hogg, A. A. M., and Pasquet, S. (2010). Eddy response to Southern Ocean climate modes. *Journal of Geophysical Research*, 115(C10), C10030, 1–12. doi: 10.1029/2009JC005894
- Mullan, A. B. (1998). Southern hemisphere sea-surface temperatures and their contemporary and lag association with New Zealand temperature and precipitation. *International Journal of Climatology*, 18(8), 817–840.
- Murphy, R. J., Pinkerton, M. H., Richardson, K. M., BradfordGrieve, J. M., and Boyd, P. W. (2001). Phytoplankton distributions around New Zealand derived from SeaWiFS remotely-sensed ocean colour data. *New Zealand Journal of Marine and Freshwater Research*, 35(2), 343–362. doi: 10.1080/00288330.2001.9517005
- Naveira-Garabato, A. C., Jullion, L., Stevens, D. P., Heywood, K. J., and King, B. A. (2009). Variability of Subantarctic Mode Water and Antarctic Intermediate Water in the Drake Passage during the Late-Twentieth and Early-Twenty-First Centuries. *Journal of Climate*, 22(13), 3661–3688. doi: 10.1175/2009JCLI2621.1
- Neil, H. L. (1998). *Voyage Report, TAN9814, Campbell Plateau* (Tech. Rep.). Wellington: National Institute of Water and Atmospheric Research (NIWA).
- Neil, H. L. (2001). *Voyage Report, TAN0108, Campbell Plateau* (Tech. Rep.). Wellington: National Institute of Water and Atmospheric Research (NIWA).
- Neil, H. L. (2003). *Voyage Report, TAN0307, Campbell Plateau* (Tech. Rep.). Wellington: National Institute of Water and Atmospheric Research (NIWA).
- Neil, H. L., Carter, L., and Morris, M. Y. (2004). Thermal isolation of Campbell Plateau, New Zealand, by the Antarctic Circumpolar Current over the past 130 kyr. *Paleoceanography*, 19(4), PA4008. doi: 10.1029/2003PA000975

-
- Olson, D., and Emery, W. (1978). Eddies and ridges in the thermal structure south of New Zealand. *Antarctic Journal of the United States*, 13(4), 79–81.
- Orsi, A., Whitworth, T., and Nowlin, W. (1995). On the meridional extent and fronts of the Antarctic Circumpolar Current. *Deep Sea Research Part I: Oceanographic Research Papers*, 42(5), 641–673.
- Pawlowicz, R. (2010). *What every oceanographer needs to know about TEOS-10 (the TEOS-10 Primer)*. unpublished manuscript.
- Philander, S. G. H. (1983). El Niño Southern Oscillation phenomena. *Nature*, 302(5906), 295–301. doi: 10.1038/302295a0
- Pickard, G. L., and Emery, W. J. (1990). *Descriptive Physical Oceanography: An Introduction* (Vol. 7). Oxford: Elsevier.
- Qiu, B., and Chen, S. (2006). Decadal Variability in the Large-Scale Sea Surface Height Field of the South Pacific Ocean: Observations and Causes. *Journal of Physical Oceanography*, 36(9), 1751–1762. doi: 10.1175/JPO2943.1
- Renwick, J., and Thompson, D. (2006). The Southern Annular Mode and New Zealand climate. *Water and Atmosphere (NIWA)*, 14(2), 24–25.
- Reynolds, R., and Rayner, N. (2002). An improved in situ and satellite SST analysis for climate. *Journal of Climate*, 15, 1609–1625.
- Rintoul, S. R., and Bullister, J. L. (1999). A late winter hydrographic section from Tasmania to Antarctica. *Deep Sea Research Part I: Oceanographic Research Papers*, 46(8), 1417–1454.
- Rintoul, S. R., Sokolov, S., Williams, M. J. M., Peña Molino, B., Rosenberg, M., Bindoff, N. L., and Peña Molino, B. (2014). Antarctic Circumpolar Current transport and barotropic transition at Macquarie Ridge. *Geophysical Research Letters*, xx(xx), submitted. doi: 10.1002/2014GL061880

- Rintoul, S. R., and Trull, T. W. (2001). Seasonal evolution of the mixed layer in the Subantarctic zone south of Australia. *Journal of Geophysical Research*, 106(C12), 31447. doi: 10.1029/2000JC000329
- Rio, M. H., Guinehut, S., and Larnicol, G. (2011). New CNES-CLS09 global mean dynamic topography computed from the combination of GRACE data, altimetry, and in situ measurements. *Journal of Geophysical Research*, 116(C7), C07018. doi: 10.1029/2010JC006505
- Robertson, B. C., and Chilvers, B. L. (2011). The population decline of the New Zealand sea lion *Phocarcos hookeri*: a review of possible causes. *Mammal Review*, 41(4), 253–275. doi: 10.1111/j.1365-2907.2011.00186.x
- Roblou, L., Lamouroux, J., Bouffard, J., Lyard, F., Henaff, M. L., Lombard, A., ... Birol, F. (2011). Post-processing Altimeter Data Towards Coastal Applications and Integration into Coastal Models. In S. Vignudelli, A. G. Kostianoy, P. Cipollini, and J. Benveniste (Eds.), *Coastal altimetry* (pp. 217–246). Berlin, Heidelberg: Springer Berlin Heidelberg.
- Roemmich, D., and Gilson, J. (2009). The 2004-2008 mean and annual cycle of temperature, salinity, and steric height in the global ocean from the Argo Program. *Progress in Oceanography*, 82(2), 81–100. doi: 10.1016/j.pocean.2009.03.004
- Roemmich, D., Gilson, J., Davis, R., Sutton, P. J. H., Wijffels, S., and Riser, S. (2007). Decadal Spinup of the South Pacific Subtropical Gyre. *Journal of Physical Oceanography*, 37(2), 162–173. doi: 10.1175/JPO3004.1
- Rowden, A. A. (2008). *Voyage Report, TAN0803, Macquarie Ridge* (Tech. Rep. No. June). Wellington: National Institute of Water and Atmospheric Research (NIWA).
- Sabine, C. L., Feely, R. a., Key, R. M., Bullister, J. L., Millero, F. J., Lee, K., ... Wong, C. S. (2002). Distribution of anthropogenic CO₂ in the Pacific Ocean. *Global Biogeochemical Cycles*, 16(4), 30–1–30–17. doi: 10.1029/2001GB001639

- Sallée, J. B., Speer, K., and Morrow, R. (2008). Response of the Antarctic Circumpolar Current to Atmospheric Variability. *Journal of Climate*, *21*(12), 3020–3039. doi: 10.1175/2007JCLI1702.1
- Sallée, J.-B., Speer, K., Rintoul, S., and Wijffels, S. (2010). Southern Ocean Thermocline Ventilation. *Journal of Physical Oceanography*, *40*(3), 509–529. doi: 10.1175/2009JPO4291.1
- Sallée, J. B., Speer, K. G., and Rintoul, S. R. (2010). Zonally asymmetric response of the Southern Ocean mixed-layer depth to the Southern Annular Mode. *Nature Geoscience*, *3*(4), 273–279. doi: 10.1038/ngeo812
- Schulz, E. W., Josey, S. a., and Verein, R. (2012). First air-sea flux mooring measurements in the Southern Ocean. *Geophysical Research Letters*, *39*(16), 1–8. doi: 10.1029/2012GL052290
- Simpson, J. H., and Sharples, J. (2012). *Introduction to the Physical And Biological Oceanography of Shelf Seas* (First ed.). New York: Cambridge University Press.
- Sloyan, B. M., and Rintoul, S. R. (2001). Circulation, Renewal, and Modification of Antarctic Mode and Intermediate Water. *Journal of Physical Oceanography*, *31*(4), 1005–1030. doi: 10.1175/1520-0485
- Smith, R. O., Vennell, R., Bostock, H. C., and Williams, M. J. (2013). Interaction of the subtropical front with topography around southern New Zealand. *Deep Sea Research Part I: Oceanographic Research Papers*, *76*, 13–26.
- Sokolov, S., and Rintoul, S. R. (2002). Structure of Southern Ocean fronts at 140 E. *Journal of Marine Systems*, *37*, 151–184.
- Sokolov, S., and Rintoul, S. R. (2007a). Multiple Jets of the Antarctic Circumpolar Current South of Australia. *Journal of Physical Oceanography*, *37*(5), 1394–1412. doi: 10.1175/JPO3111.1

- Sokolov, S., and Rintoul, S. R. (2007b). On the relationship between fronts of the Antarctic Circumpolar Current and surface chlorophyll concentrations in the Southern Ocean. *Journal of Geophysical Research*, *112*(C7), C07030. doi: 10.1029/2006JC004072
- Sokolov, S., and Rintoul, S. R. (2009a). Circumpolar structure and distribution of the Antarctic Circumpolar Current fronts: 1. Mean circumpolar paths. *Journal of Geophysical Research*, *114*, C11018, 1–19.
- Sokolov, S., and Rintoul, S. R. (2009b). Circumpolar structure and distribution of the Antarctic Circumpolar Current fronts: 2. Variability and relationship to sea surface height. *Journal of Geophysical Research*, *114*, C11019, 1–15.
- Speer, K., Rintoul, S. R., and Sloyan, B. (2000). The Diabatic Deacon Cell. *Journal of Physical Oceanography*, *30*(12), 3212–3222. doi: 10.1175/1520-0485
- Stanton, B. R. (1998). *Voyage Report, TAN9806, Campbell Plateau* (Tech. Rep.). Wellington: National Institute of Water and Atmospheric Research (NIWA).
- Stanton, B. R., and Morris, M. Y. (2004). Direct velocity measurements in the Subantarctic Front and over Campbell Plateau, southeast of New Zealand. *Journal of geophysical research*, *109*, C01028–11pp.
- Stewart, R. H. (2008). *Introduction to Physical Oceanography* (September ed.). online. Retrieved from http://oceanworld.tamu.edu/home/course_book.htm
- Sutton, P. J. H. (2001). Detailed structure of the Subtropical Front over Chatham Rise, east of New Zealand. *Journal of Geophysical Research*, *106*(C12), 31045. doi: 10.1029/2000JC000562
- Sutton, P. J. H. (2003). The Southland Current: a subantarctic current. *New Zealand Journal of Marine and Freshwater Research*, *37*, 645–652.
- Sutton, P. J. H. (2006). *Voyage Report TAN0609, Tasman Boundary* (Tech. Rep.). Wellington: National Institute of Water and Atmospheric Research (NIWA).

- Sutton, P. J. H., Bowen, M. M., and Roemmich, D. (2005). Decadal temperature changes in the Tasman Sea. *New Zealand Journal of Marine and Freshwater Research*, 39(6), 1321–1329. doi: 10.1080/00288330.2005.9517396
- Talley, L. D., Pickard, G. L., Emery, W. J., and Swift, J. H. (2011). *Descriptive Physical Oceanography: An Introduction*. Academic Press.
- Thompson, D. W. J., Wallace, J. M., and Hegerl, G. C. (2000). Annular Modes in the Extratropical Circulation. Part II: Trends. *Journal of Climate*, 13(689), 1018–1036. doi: 10.1175/1520-0442
- Thompson, R. E., Tabata, S., and Ramsden, D. (1985). Comparison of sea level variability on the Caribbean and the Pacific coasts and the Panama canal. *Time Series of Ocean Measurements*, 2, 33–37.
- Tomczak, M., and Godfrey, J. S. (2001). *Regional Oceanography: an introduction* (1.0 ed.). on line.
- Tomczak, M., and Liefvink, S. (2005). Interannual variations of water mass volumes in the Southern Ocean. *Journal of Atmospheric & Ocean Science*, 10(1), 31–42. doi: 10.1080/17417530500062838
- Trenberth, K. E. (1984). Signal Versus Noise in the Southern Oscillation. *Monthly Weather Review*, 112(2), 326–332. doi: 10.1175/1520-0493
- Ummenhofer, C. C., and England, M. H. (2007). Interannual Extremes in New Zealand Precipitation Linked to Modes of Southern Hemisphere Climate Variability. *Journal of Climate*, 20(21), 5418–5440. doi: 10.1175/2007JCLI1430.1
- Vignudelli, S. (2005). Improved satellite altimetry in coastal systems: Case study of the Corsica Channel (Mediterranean Sea). *Geophysical Research Letters*, 32(7), L07608. doi: 10.1029/2005GL022602
- von Storch, H., and Zwiers, F. (1999). *Statistical Analysis Climate Research*. United Kingdom: Cambridge University Press.

- Williams, M. J. (2004). Analysis of quasi-synoptic eddy observations in the New Zealand subantarctic. *New Zealand Journal of Marine and Freshwater Research*, 38(1), 183–194. doi: 10.1080/00288330.2004.9517227
- Williams, M. J. (2013). *Voyage Report TAN1302, Mertz Polynya* (Tech. Rep.). Wellington: National Institute of Water and Atmospheric Research (NIWA).
- Williams, M. J. M. (2007). *Voyage Report, TAN0704, Macquarie Ridge* (Tech. Rep. No. March). Wellington: National Institute of Water and Atmospheric Research (NIWA).
- Willis, J. K., Chambers, D. P., and Nerem, R. S. (2008). Assessing the globally averaged sea level budget on seasonal to interannual timescales. *Journal of Geophysical Research*, 113(C6), C06015. doi: 10.1029/2007JC004517

Appendix A

The International Thermodynamic Equation of Seawater - 2010 (TEOS-10)

The Intergovernmental Oceanographic Commission (IOC), International Association for the Physical Sciences of the Oceans (IAPSO) and the Scientific Committee on Oceanic Research (SCOR) have defined a new standard for the calculation of the thermodynamic properties of seawater. The new standard, named the International Thermodynamic Equation of Seawater-2010, TEOS-10, has been adopted for use by oceanographers in place of the International Equation Of State-1980 (EOS-80), (IOC et al., 2010; Pawlowicz, 2010).

The biggest difference compared to EOS-80 is the introduction of Absolute Salinity S_A to replace Practical Salinity S_P (PSS-78). The conversion is shown in equation A.1. Thermodynamic properties of seawater are directly influenced by the ratio of the mass of all dissolved constituents in seawater to the mass of sea water, expressed as either kg kg^{-1} or g kg^{-1} . With the new TEOS-10, Absolute Salinity S_A returns to the original definition of salinity defined as the mass fraction of dissolved material in seawater. S_A is preferred over Practical Salinity S_P , as Practical Salinity it is calculated only from the electrical conductivity of seawater. Absolute Salinity S_A is measured in SI units (Millero

et al., 2008; IOC et al., 2010; McDougall et al., 2012).

$$S_A = (35.16504 \text{g kg}^{-1}/35)S_P + \delta S_A(x, y, p) \quad (\text{A.1})$$

Conservative temperature Θ replaces potential temperature θ in TEOS-10. Conservative temperature has the advantage over θ of representing more accurately the “heat content” of seawater and it is approximately two orders of magnitude more conservative compared with θ , (McDougall et al., 2012; IOC et al., 2010).

Under TEOS-10 all the thermodynamic properties are functions of absolute salinity the first step when using TEOS-10 is to calculate Absolute Salinity S_A , which is a function of Practical Salinity, pressure, longitude and latitude (McDougall and Barker, 2011). This recognizes that the composition of the sea water varies around the world ocean in particular their effect on the density of seawater. Then, Conservative Temperature is evaluated with units of °C. With these new variables, water masses are analysed on a S_A - Θ diagram, and potential density anomaly σ^Θ contours are drawn on the diagram (IOC et al., 2010). Table A.1 shows a list of the variables used through the development of this work. The MatLab routine toolbox used in this thesis (Gibbs SeaWater (GSW) Oceanographic Toolbox Version 3.02) is available in the Seawater-Ice-Air (SIA) software library on the TEOS-10 website, <http://www.teos-10.org/index.htm>.

Table A.1: List of nomenclature

| Variable | Symbol | Units |
|----------------------------|-----------------|--------------------|
| Practical Salinity | S_P | Unitless |
| Absolute Salinity | S_A | g kg^{-1} |
| <i>in situ</i> Temperature | T | °C |
| Conservative Temperature | Θ | °C |
| Potential Temperature | θ | °C |
| Pressure | p | dbar |
| Potential density anomaly | σ^Θ | kg m^{-3} |